Synthèse unifiée de commandes robustes pour la chaine d'air des moteurs à combustion interne

Chao Deng

THÈSE PRESENTÉE A L'UNIVERSITÉ D'ORLÉANS
POUR OBTENIR LE GRADE DE
DOCTEUR DE L'UNIVERSITÉ D'ORLÉANS

PAR

CHAO DENG

ÉCOLE DOCTORALE SCIENCES ET TECHNOLOGIES
Laboratoire PRISME

Discipline : Sciences et technologies industrielles

Synthèse Unifiée de Commandes Robustes pour la Chaine d'Air des Moteurs à Combustion Interne

Soutenue le: 14/06/2013

MEMBRES DU JURY :

Pr. A. El Hajjaji	*Rapporteur*	*Université de Picardie Jules Verne*
Dr. N. Langlois	*Rapporteur*	*ESIGELEC*
Pr. F. Kratz	*Examinateur*	*ENSIB*
Pr. J.R. Zhang	*Examinateur*	*Beijing Institute of Technology*
Dr. Y. Zou	*Examinateur*	*Beijing Institute of Technology*
Dr. G. Colin	*Co-Encadrant*	*Université d'Orléans*
Dr. D. Nelson-Gruel	*Co-Encadrant*	*Université d'Orléans*
Pr. Y. Chamaillard	*Directeur de thèse*	*Université d'Orléans*

Table des matières

CHAPTER 3 Application: Air path control of a gasoline engine

CHAPTER 4 Application: Air path control of a diesel engine

À mon père

Remerciements

Ce travail est proposé par mon superviseur et directeur de thèse Yann Chamaillard ainsi que mon encadrant Guillaume Colin. Ainsi, je donne mes grands mercis à eux. Grace à leur abondance de soutiens et de guides, j'ai eu l'occasion de me plonger dans ce domaine très intéressant, que je n'avais jamais touché avant de venir en France.

Certes, c'est mon grand plaisir d'obtenir de nombreuses aides de mon deuxième encadrant, Dominique Nelson-Gruel, en raison de sa faveur que je peux finir ma thèse, et remercie aussi bien pour ses discussions très intéressantes et ses propositions. Par ailleurs, je dois les remercier encore une fois surtout quand je me suis senti décourager heureusement, ils m'ont motivé d'aller plus loin. En outre, ce travail est financé par les Council Scholarship Chinois (CSC) et l'axe thématique Energie Combustion Moteur (ECM) du laboratoire PRISME de l'Université d'Orléans basé dans les locaux de Polytech Orléans, donc merci beaucoup au CSC et à ECM qui soutiennent ma vie en recherche en France.

Ensuite, c'était un temps grand et important où j'ai passé trois ans et demi avec mes collègues aimables. Abdellah Louzimi, qui est le premier collègue à qui je tiens à exprimer mes remerciements. Grâce aux discussions agréables et encourageantes, nous avions passé cette période qui était très difficile. Ensuite, je dois remercier mon ancien collègue Andrej Ivanco, il m'a montré toute l'impression de la période de la vie de doctorant dans notre laboratoire.

Les remerciements sont aussi offerts à mes collègues Kristan Gillet, Pascal Brejaud, Toni Tahtouh, Jérémie Dernotte, Jianxi Zhou, Maxime Debert, Sergio Avila, Guillaume Broustail, Nicolas Bordet, Jamil El Hadef, Abderrahim Lamara, Amine Va Dreed, Bénédicte Galmiche, …, et en raison de leurs discussions agréables et encourageantes, j'ai passé une période inoubliable dans notre laboratoire.

Ensuite, je donne mes grandes appréciations à l'équipe technique ECM, qui comprend entre autre Benoît Bellicaud, Julien Lemaire, Bruno Moreau ..., grâce à leurs supports, j'ai terminé toutes mes expériences au banc moteur.

Par conséquent, je remercie bien le groupe ECM, PRISME, Polytech Orléans, qui me soutient pendant tout mon temps de doctorat. En outre, je me souviens encore que chaque Noël, j'ai passé du temps très agréable avec notre groupe. J'aime surtout la cuisine française, le fromage et le vin, nous avons eu plusieurs dîners très délicieux à Saran, je ne peux absolument pas oublier la compétition de Karting et de bowling.

Je tiens remercier à mes amis religieux Landry Bangake, Louis-Marie Lemofac, Samuel Schott, Ifeoluwa Oloruntoba, Gaëtan Vaille-Bunet, Xavier Voyau... pour m'offrir de nombreuses

préoccupations, les encouragements à moi et ma thèse. Eh bien, je dois aussi remercier à mes autres amis qui m'ont aidé dans mon travail et ma vie.

Merci à mes parents, ma grande sœur, frère et toute ma famille, si je suis toujours encouragé, ils m'ont motivé et m'ont soutenu toujours dans ma vie. Cependant, ma grande culpabilité va aller à mon père, qui est décédé le 19 Octobre 2011, je ne suis pas rentré à la maison même si je savais que c'est la plus pire des nouvelles de ma vie!!

Je tiens également à remercier mes amis que je n'ai pas mentionnés ci-dessus, mais ils ont donné leurs mains vers moi pour surmonter mon temps difficile et de faire avancer mon travail de doctorat.

A la fin, je vais garder tous mes appréciations et les esprits pour mon avenir, et je crois que l'homme véritable doit se battre contre lui-même et conserver toujours la pensée, ne jamais cesser d'avancer!

Orléans, France

11, Avril, 2013

Chao DENG

Introduction générale

Depuis la création des moteurs à combustion interne, les recherches sur l'optimisation du fonctionnement des moteurs essence et diesel se sont développées indépendamment. Afin de réduire les temps et les coûts de développement d'un moteur, une approche unifiée de conception serait intéressante. Dans ce cadre, le contrôle et la mise au point des moteurs à combustion interne pourrait être la première étape de cette unification. Bien évidemment, ce contrôle doit être stable, robuste vis-à-vis des disparités de fabrication, comme de fonctionnement. Cette thèse propose alors, une démarche unifiée pour les moteurs essence comme pour les moteurs diesel, afin d'obtenir un contrôle robuste de la chaîne d'air du moteur. La chaîne d'air du moteur contient les éléments permettant de contrôler la quantité et les proportions d'air et de gaz neutres dans le cylindre (Recirculation des gaz d'échappement, papillon d'admission, turbocompresseur). Cette démarche unifiée de commande, permettant de contrôler les systèmes monovariables, tout comme multivariables non carrés (nombre d'entrées différent du nombre de sorties), contient plusieurs étapes : identification d'un modèle du système, analyse du système permettant d'en déduire une structure de contrôle, synthèse d'un contrôleur autour d'un nominal, vérification de la robustesse en stabilité, tests du contrôle. Le couplage des entrées vers les sorties, les non linéarités sont pris en compte lors de la synthèse du contrôleur. Cette méthode de conception a été validée sur plusieurs applications dont un moteur essence et un moteur diesel. Des résultats expérimentaux sur un banc moteur diesel haute dynamique ont montrés que la commande multivariable permettait de réduire les émissions d'oxydes d'azote.

La présentation de cette thèse suit alors la logique ci-dessus, et est donc présentée en quatre chapitres, résumés ici:

Le chapitre 1 présente le contexte de cette thèse. Depuis la révolution des moteurs à combustion interne, le turbocompresseur est l'une des solutions les plus intéressantes pour satisfaire de nombreuses exigences dans les moteurs. Ces exigences sont une haute performance, satisfaire la législation sur les émissions polluantes et une consommation réduite de carburant. En outre, et en comparaison avec des solutions de post-traitement, la commande de la combustion est une solution moins chère pour réduire les émissions polluantes. Afin de réaliser une combustion optimale, l'air dans le cylindre doit être contrôlé avec précision. Par conséquent, de nombreux actionneurs sont introduits dans les moteurs modernes avec comme objectif une commande rapide et précise. Les principes généraux du contrôle moteur sont détaillés à la fin de ce chapitre.

Le chapitre 2 présente une nouvelle méthodologie qui contient la modélisation, l'identification fréquentielle, l'analyse du système, la synthèse de la commande robuste et sa validation, nommée méthodologie séquentielle de conception d'une commande robuste. Cette méthodologie est utilisée pour réaliser la régulation de la chaîne d'air dans les moteurs à combustion interne. A ce titre, plusieurs

outils d'aide à la conception sont introduits pour comprendre sa contrôlabilité et les interactions entrées/sorties. Le rapport de performance entre le domaine temporel et le domaine fréquentiel sont aussi discutés dans ce chapitre.

Le chapitre 3 exécute la méthodologie présentée dans le chapitre 2 pour le contrôle de la chaîne d'air d'un moteur essence turbocompressé (Smart). Le simulateur utilisé est un modèle 0D moyen créé au laboratoire PRISME à Orléans, France. Le défi de ce moteur essence est la consommation de carburant et le contrôle en couple puisque les émissions polluantes sont bien maîtrisées avec le catalyseur trois voies et un rapport air carburant bien contrôlé à la stœchiométrie. La consommation de carburant dépend alors de la masse d'air enfermée dans le cylindre. Par conséquent, il est régi par la chaîne d'air. Pour ce faire, les capteurs à notre disposition sont les mesures de pression dans le collecteur d'admission et après le compresseur. Les actionneurs disponibles sont le papillon d'admission et la vanne de décharge du turbocompresseur. La première étape de notre méthodologie a consistée à modéliser notre système d'étude par deux modèles : le premier est un modèle boite grise basse fréquence utilisé pour comprendre le système et surtout pour valider notre loi de commande ; le deuxième est un modèle boîte noire permettant de concevoir notre régulateur et de valider sa robustesse. Il est prouvé dans ce chapitre que notre stratégie appliquée au contrôle de la chaîne d'air du moteur essence permet bien d'obtenir un régulateur multi-SISO robuste aux incertitudes non-paramétriques du système. Les résultats montrent des performances satisfaisantes et respectant les spécifications faite lors de la conception du régulateur en termes de dépassement et de robustesse vis-à-vis des temps de montées.

Le chapitre 4 exécute la méthodologie présentée dans le chapitre 2 pour le contrôle de la chaîne d'air d'un moteur diesel turbocompressé avec recirculation des gaz d'échappement. Comme les émissions polluantes ne sont pas réglées facilement sur un moteur diesel, une solution populaire est d'employer une vanne d'EGR pour réduire les NOx. D'abord la stratégie de commande robuste unifiée est d'abord appliquée à un système ayant 2 entrées (vanne de recirculation des gaz brûlés et vanne de décharge du turbo) et 2 sorties (débit d'air et pression de suralimentation). L'objectif de cette première application, réalisée en simulation, est de maîtriser la quantité d'air entrant dans le cylindre et de maîtriser la consommation du moteur. Dans la deuxième partie de ce chapitre, la stratégie est cette fois appliquée à un système augmentée d'un actionneur (papillon d'admission). L'objectif, cette fois ci, est d'aller plus loin dans le compromis NOx et consommation, à l'aide d'un degré de liberté supplémentaire. La validité de ces deux applications est prouvée par un grand nombre d'essais sur simulateur mais aussi sur banc d'essai où les quantités de NOx sont abaissé durant les transitoires de couple et de régime.

CHAPTER 1 The internal combustion engines: Pre-requisites

Contents

1.1 Résumé

Le rendement des moteurs à combustion interne est limité par la quantité de gaz entrant dans le cylindre. Le turbocompresseur peut augmenter cette quantité et c'est pour cette raison qu'ils sont maintenant couramment utilisés. Souvent utilisé en combinaison avec d'autres composants (waste-gate par exemple) ces systèmes présentent l'inconvénient de ralentir la dynamique de remplissage du cylindre. Les stratégies de contrôles associés doivent exploiter pleinement toute la dynamique de ce système complexe afin d'assurer la demande de couple du conducteur. Cette thèse propose une stratégie de contrôle unifiée permettant de résoudre le problème de contrôle de la chaîne d'air des moteurs essence et diesel turbocompressés. Ce chapitre présente de manière générale le moteur à combustion interne et les défis à relever lors de la calibration d'un moteur. Ces défis sont généralement liés aux exigences législatives concernant les niveaux de polluants, la consommation de carburant et les performances. En raison des caractéristiques physiques différentes des moteurs essence et diesel, ces défis doivent être traités différemment. L'objectif de cette thèse est d'employer la même méthodologie de conception du régulateur pour la chaîne d'air d'un moteur essence et d'un moteur diesel.

1.2 Introduction

Due to the evolution and the development of electronics and embedded computers, the interaction between the engine and the driver has become more complicated. The improvement and miniaturization of electronics has allowed increasing sensor accuracy, lower actuator cost and above all a number of possible calculations in the electronic control unit (ECU). Linked to this improvement, the number of variables and control actuators in automotive applications has increased tenfold. In addition, research has been done on combustion which leads to the apparition of new types of combustion, such as **L**ow **T**emperature **C**ombustion (LTC), **P**re-mixed **C**harge **C**ompression **I**gnition (PCCI) or **H**omogeneous **C**harge **C**ompressions **I**gnition (HCCI). Through these advancements, pollutant emissions have been reduced significantly. All of these technologies have led to a more and more optimized Internal Combustion Engine (ICE).

However, because of environmental concerns linked to the regulation of pollutant emission and non-infinite energy resources (natural gas, oil), some governments implement laws on allowed level of pollutants products hoping that these laws reduce negative effects on the climate (acid rain) and on the environment (greenhouse effect). Additionally, the drivability (performance) and comfort need to meet various demands of consumers. All of this challenges the engineers and researchers from the ICE department every day. The internal combustion engines can be stored in two main families, which are gasoline engines and diesel engines. In the automobile industry, vehicles equipped only with gasoline engine or diesel engine are the two main vehicles that are sold in the marketing (99% in 2009 in France). Vehicles equipped with internal combustion engine are still the absolute types of vehicles that

people buy. This situation is going to last for some years as it is depicted in Fig.1. 1. These two engine families have different combustion modes and operate in totally different ways, and consequently separate control methods are usually designed. It consumes much time for designing different methods for different engines. Thus it is necessary and interesting to propose one unified control methodology that can be applied in these different ICE, i.e. diesel engines and gasoline engines.

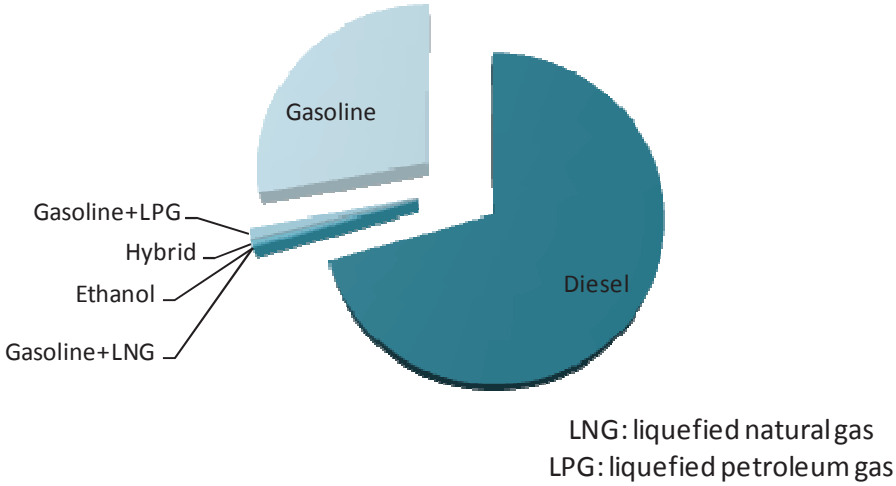

Fig.1.1 The shares of sale for private vehicle in France in 2009 (source: ADEME)

As stringent legislation on pollutant emissions emerges, many more actuators or/and sensors are employed to control ICE in order to respect legislation. The main objective of this thesis is to realize an optimization between lower pollutant emissions and lower fuel consumption while maintaining drivability. This objective has to be combined with air charging and mechanism of emissions post treatment. The main goal of engine control is to control precisely in the cylinder the timing and the quantity of fresh and burned gases (Air path) and of fuel (Fuelpath). Air path and fuel path are the two main resources required to produce an efficient combustion. Note that the quantity of air introduced in the cylinder is one of the key points to control engine-out emissions [Shen, et al., 2009].

1.3 Automatic control background

If a system has one input and one output, it is called a SISO (Single-Input-Single-Output) system; otherwise this system is called Multi-Input-Multi-Output (MIMO) system. A MIMO system is characterized by coupling phenomena that is expressed by the fact that an output is not affected by only one input but by all inputs. The corresponding plant is not represented by a single transfer function but by a matrix of mxn transfer functions for a system with m inputs and n outputs. In this thesis, the particular case where the MIMO system have the same number of inputs than outputs, and one more input than outputs are considered; in other words, plants represented by matrices with mxm and nxm ($n \neq m$)transfer functions [Wang, et al., 2011].

For systems without coupling, which are easier to analyze and control, SISO classical control theory can be used to design a controller. For example, Ziegler-Nicols, Chien-Hrones-Reswick, Cohen-Coon,

Broïda, frequential empirical tuning can be used. A way to choose the good method is to solve the tradeoff between time consuming by adjusting the parameters and the performances of the closed loop system. PID control, which can be calibrated on-line, is commonly employed in the industry because of its simplicity. If the synthesis is only based on a nominal, the closed loop system can be unstable especially for uncertain systems [Horowitz, 1982]. Quantitative Feedback Theory (QFT) is a frequency domain control design method, which designs a robust controller that considers uncertainties of the system, but the controller is not always easy to design [Tan, et al., 2003]. Model-based Predictive Control (MPC) and Internal Model Control (IMC) use an explicit model of the process directly in the controller. This type of control design is very sensitive to the model of system like feed-forward control [Doyle and Stein, 1981].

Some of the control design methods cited above cannot be used directly to control MIMO plants due to matrix representation. Doyle and Stein in [Jain and Alleyne, 2009, Bakule, 2008, Skogestad and Postlethwaite, 2007] are first concerned by the question of how to achieve benefits of feedback in the presence of unstructured uncertainty and matrix transfer function. They showed that classical SISO control ideas of feedback design could be generalized to multivariable systems using singular value description of matrix transfer function.

Sensitivity function, Complementary sensitivity function, disturbance rejection at plant input function and control effort function are given in the Fig.1.2.

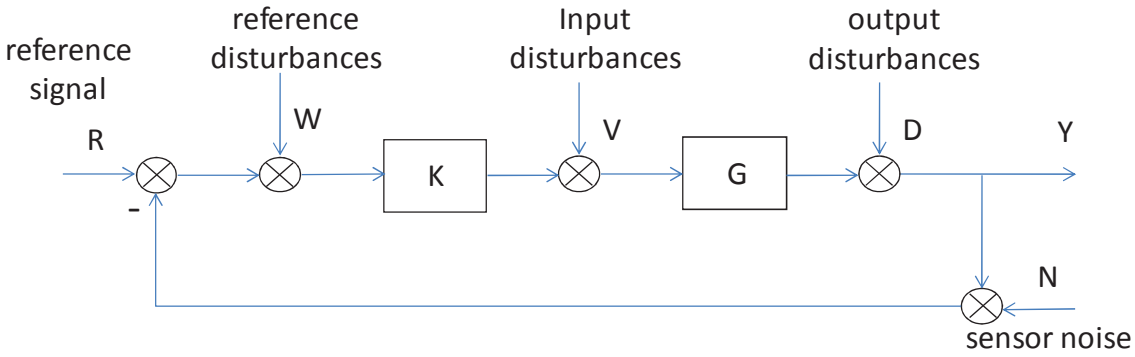

Fig.1.2 Scheme of classical SISO feedback with disturbances and noises signals

$$S = \frac{1}{1+KG} \qquad (1.1)$$

$$T = \frac{KG}{1+KG} \qquad (1.2)$$

$$KS = \frac{K}{1+KG} \qquad (1.3)$$

$$GS = \frac{G}{1+KG} \qquad (1.4)$$

Hence, all SISO closed-loops requirements on S,T, KS and GS can be transformed to MIMO closed-loops requirements on the singular values of matrix transfer function S,T, KS and GS. The main

problem that appears is that stability problem simply solved with Bode's work for SISO systems (stability related to open-loop gain and phase near the crossover frequency ω_c where $GK(j\omega_c) = 1$ will be transformed in a difficult problem on magnitude of the eigenvalues of GK. Direct links between shaping singular values of GK and the place of the magnitude of eigenvalues of the same matrix do not exist. Hence, few MIMO control design methods oriented transfer function shaping are proposed in the literature [Procházka, 2003]. For example, Linear Quadratic Gaussian (LQG) is an easy MIMO control method to use, but it lacks robustness to system uncertainty and the control system has degraded performance [Zames, 1981, Eitelberg, 2007]. The second example is H_2 and H_∞ control. These methodologies are frequency domain control methods, which design the control with overall MIMO systems, but it is not also sensitive for the uncertainty, which means it can increase the error via the wrong model identification, and the saturation of the system cannot be well-handed by them [Chughtai, et al., 2005]. Besides, they often find some very high-order controllers which are difficult to execute in reality.

Furthermore, in order to deal with the coupling problem of MIMO systems and continuing to use the SISO control methods, an idea is to classify MIMO systems into two types: small and closely coupled. For small coupled MIMO system, decentralized control, detuning factor methods [Deng, et al., 2012], sequential loop turning methods [Huang, et al., 2003, Xiong and Cai, 2006], equivalent transfer methods [Colin, et al., 2011], multi-SISO methods [Tham, 1999] can be employed. These control methods design one loop by one loop while considering the coupling. For closely coupled MIMO systems, decoupling control must be employed. It means that the MIMO system is decoupled into individual loops, and afterwards, each control loop can be designed separately with ideal decoupling [Shen, et al., 2010, Cai, et al., 2008], normalized decoupling [Vázquez and Morilla, 2002], simplified decoupling [Stotsky and Kolmanovsky, 2002, Andersson, 2005], etc.

Decentralized and decoupled methods are used to employ SISO control methods on MIMO systems, while the coupling is post-treated or prior-treated. Because the broadly use of PID control in industry, this thesis is focused on decentralized control methods and pole-placement PID to control the air path of internal combustion engines. MIMO and SISO control have been studied for new technologies of combustion (HCCI, LTC and PCCI concepts) [Chauvin, et al., 2008, Guzzella and Onder, 2009].

1.4 Application motivations

For the automobile industry, legislation concerning the pollutant emissions of gasoline and diesel vehicles is more restrictive than never before. Due to improvements of air path [Bordet, 2011] and fuel path control, pollutant emissions can be regulated up to the requirement of the legislation, with the use of a **T**hree-**W**ay (HC, CO and NOx) **C**atalytic (TWC) for gasoline engine. However, for a diesel engine, in order to meet the legislation only a Two Way (HC and CO) Catalytic converter can be used because of lean operation of diesel engine (λ<1). Hence, a diesel engine generates more NOx than

gasoline engine. Moreover, particle matters (PM) are more important for diesel engines than for indirect injection gasoline engines. Consequently, a pollutant emissions reduction solution has to be introduced for diesel engines and researchers and engineers are challenged to solve this problem. EGR valve is a good low cost solution to reduce NOx [Colin, 2006] while Selective Catalytic Reduction (SCR) is a very high efficiency device to decrease NOx but it is more expensive. Moreover, diesel particle filters, diesel oxidation catalysts (DOC) [Heywood, 1988] or lowering density and distillation characteristics of the diesel fuel are used to restrict PM [Yildiz, et al., 2010].

Table.1.1 illustrates the amount of each pollutant emissions for gasoline and diesel passenger vehicles. From this table, the emission regulation for Gasoline engine does not change between Euro 5 and Euro 6 contrary to Diesel emissions regulation. To satisfy emissions levels of Euro 6 new Diesel engines must emit 30% less for HC+NOx and 56% less for CO.

Tab.1 EU Emission Standards for Passenger Cars (Category M_1*)

Emissions Laws	Date	CO (g/km)		HC(g/km)		HC+NOx(g/km)		NOx(g/km)		PM(g/km)	
		(Gasoline)	*(Diesel)*	*(Gasoline)*	*(Diesel)*	*(Gasoline)*	*(Diesel)*	*(Gasoline)*	*(Diesel)*	*(Gasoline)*	*(Diesel)*
Euro 1†	1992.08	2.72 (3.16)	2.72 (3.16)	-	-	0.97 (1.13)	0.97 (1.13)	-	-	-	0.14 (0.18)
Euro 2, IDI	1996.02	2.2	1.0	-	-	0.5	0.7	-	-	-	0.08
Euro 3	2000.02	2.30	0.64	0.20	-	-	0.56	0.15	0.50	-	0.05
Euro 4	2005.02	1.0	0.50	0.10	-	-	0.30	0.08	0.25	-	0.025
Euro 5b	2009.09[b]	1.0	0.50	0.10[d]	-	-	0.23	0.06	0.18	0.005[e,f]	0.005[f]
Euro 6	2014.10	1.0	0.50	0.10[d]	-	-	0.17	0.06	0.08	0.005[e,f]	0.005[f]

† Values in brackets are conformity of production (COP) limits

b. 2011.01 for all models

d. and NMHC = 0.068 g/km

e. applicable only to vehicles using DI engines

f. 0.0045 g/km using the PMP measurement procedure

g. 6.0×10^{12} 1/km within first three years from Euro 6 effective dates

Table.1.1 The trend of European Pollutant Emissions Standards (Source: Emission standard, Cars and light trucks, 2012)

From this table we can see that the emission limits for gasoline and diesel cars have been a challenge to manufacturers since 1992, the implementation of the first Emissions Standard. Facing to this challenge, lots of advanced technologies have been studied and implemented in engines, such as injectors, turbocharger, EGR valve, variable intake and exhaust valve timing and common rail. Due to improvements of electronic technologies, more actuators and sensors are chosen to regulate these complex systems. Moreover, there are two ways to reduce the pollutant emissions, optimization of the combustion process and post-treatment, their relative cost and the effect of reduction is shown in Fig.1.3 [Bordet, 2011].

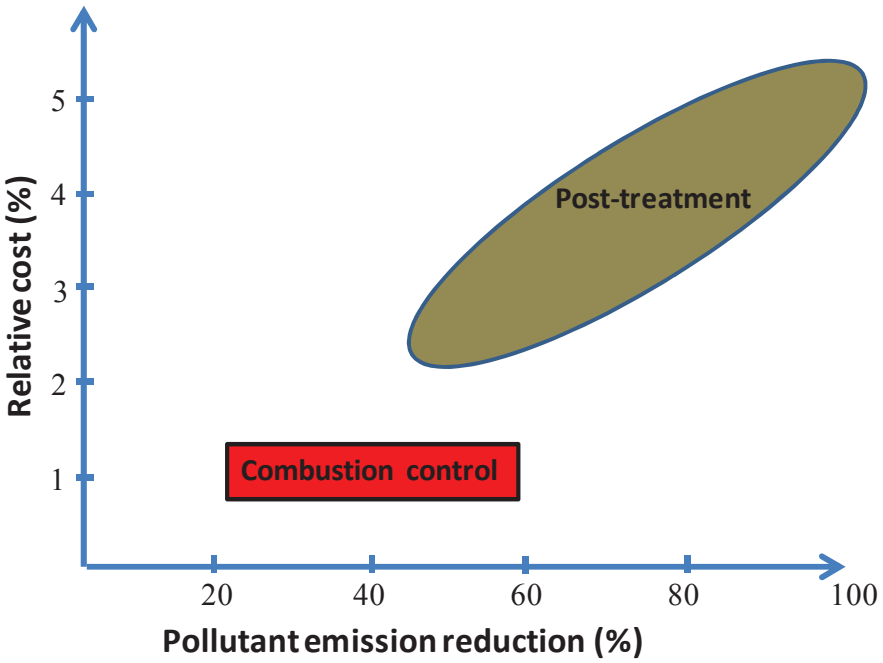

Fig.1.3 Relative cost for different reduction solutions in internal combustion engines

Fig.1.3 shows that comparing to the post-treatment, combustion control costs less and can realize until 60% pollutant emission reduction. Post-treatment can achieve up to 100% of reduction, but it costs much more than combustion control. In order to meet the pollutant emissions standard, both of them needs to be combined and compromised together in order to optimize the relative cost.

Much of the world's resources of fossil fuels were consumed in less than two centuries. According to the American Petroleum Institute, the remaining fossil petroleum will not last for more than 50 years at the present consumption speed. A solution to this problem is to lower fuel consumption (Fig.1.4) and to find some other energy to replace this resource.

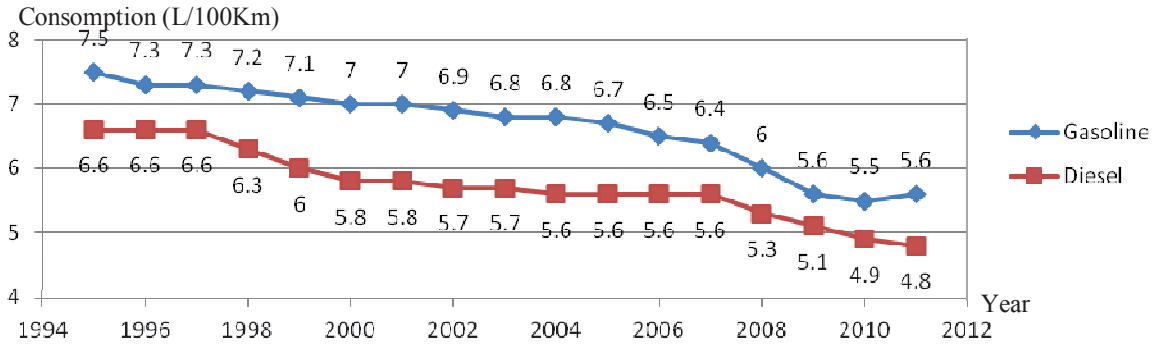

Fig.1.4 Fuel consumption for Diesel and Gasoline engines versus years according to ACEA (Association of European Automobile Manufacturers)

Carbon dioxide (CO_2) is considered the main greenhouse gas after water vapor and is partly responsible for global warming. Therefore, CO_2 emissions must be reduced (Fig.1.5).

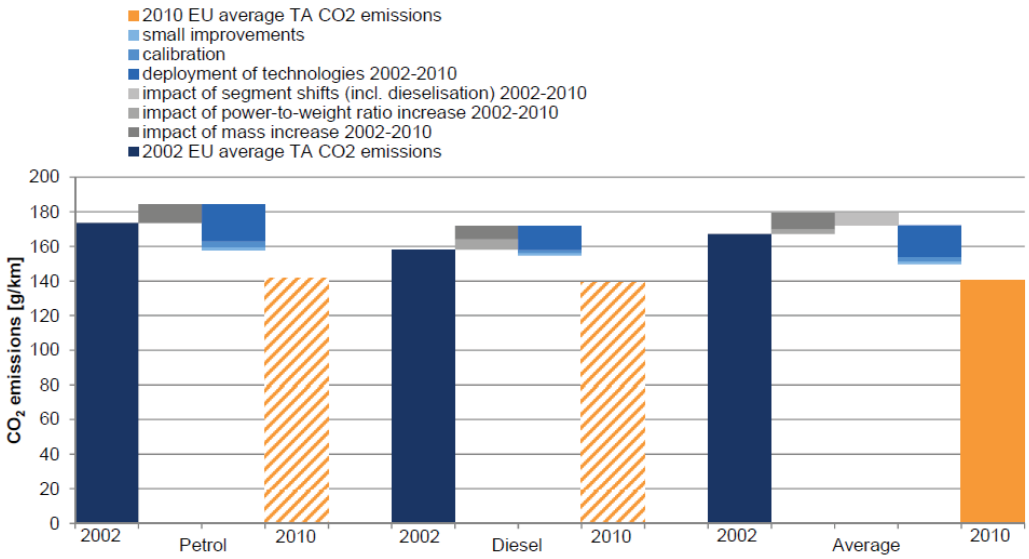

Fig.1.5 Estimation of the net CO_2 reduction resulting from technology deployment in passenger cars between 2002 and 2010

Overall, the major attention paid to the problem of reducing emissions is beginning to pay on CO_2 emissions. Thus, initiatives and objectives that have been established by the European institutions and governments [Xiong and Cai, 2006, Yildiz, et al., 2010] contribute to reduce the quantity of CO_2 produced by the combustion of gasoline and diesel automobile engines. The average slope of decline of emitted CO_2 is approximately 30g/km between 2002 and 2010 due to the use of different technologies. Knowing that approximately 2.28kg of CO_2 is produced per liter of burned gasoline and 2.6kg per liter of burned gasoil, the only way to reduce CO_2 emissions is to minimize the fuel consumption. This thesis proposes a strategy to improve engine efficiency and therefore to optimize fuel economy. Nowadays, the problem posed to researchers is to find the most favorable compromise, ecologically speaking, between drivability, performance and pollutant emissions. In order to get a good compromise, the engine torque has to be regulated precisely [Heywood, 1988].To achieve this goal the quantity of gas entering the cylinders has to be estimated and controlled [Johnson, 2001].

1.5 Engine system

Fig.1.6 shows the theoretical representation of the Clapeyron diagram from Beau de Rochas cycle which corresponds to the operation of a 4-stroke engine [Guzzella and Onder, 2009, Colin, et al., 2007].

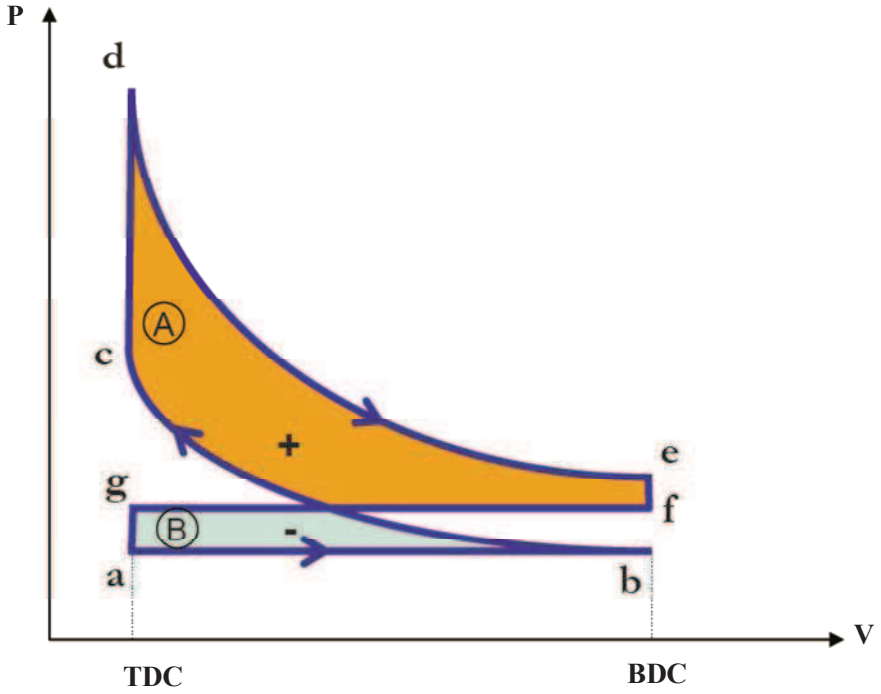

Fig.1.6 Clapeyron Diagram for Beau de Rochas cycle

This cycle operates on two revolutions (720° of crank angle) and has 4 phases [Heywood, 1988] which are detailed in the following and on Fig.1.7:

Intake Stroke

The piston descends from **a** to **b**, i.e. from the top dead center (TDC) to the bottom dead center (BDC), corresponding to the opening of the intake valve and the exhaust valve closing at the same time (**g**). Due to the increase in the volume of the cylinder a depression is created. This depression facilitates filling up the cylinder with air-fuel mixture (gasoline engines) or air and EGR (diesel engines).

Compression Stroke

Around **b** (BDC), intake valve is closing. The piston travels from **b** (BDC) to **c** (TDC) so that pressure and temperature rises and the volume decreases during this stroke. At the end of compression a spark plug ignites the air-fuel mixture (Gasoline engine) or a quantity of fuel is vaporized into the cylinder (Diesel engine). At this moment, the combustion is initiated (**c**).

Power Stroke

Combustion occurs and lasts for a very short time where the piston near the TDC. This combustion can be seen as constant volume combustion (**d**). Combustion changes the composition of the gas mixture to that of exhaust products and increases the temperature and pressure in the cylinder to a very high peak value pushing the piston away from TDC. This is the stroke which produces the torque output of

the engine cycle. As the piston travels from **d** (TDC) to **e** (BDC), cylinder volume is increased, causing pressure and temperature to drop.

Exhaust Stroke

The exhaust valve is opened just before the BDC (**e** to **f**). As the temperature and the pressure are still higher than the atmospheric pressure, the burned gases are pushed out of the cylinder towards the exhaust valve. The exhaust process lasts from the opening of the exhaust valve (**f**) until the closing of the one near the TDC (**g**). This exhaust stroke pushes most of burned gas out of the cylinder into the exhaust system, but some of the exhaust gases are left due to the dead volume. Just before the exhaust valve is closed completely, the intake valve restarts to open. The intake stroke will begin at this moment.

On Fig.1.7, the orange area corresponds to the positive work, while the blue area corresponds to the negative work (due to the pumping loses).

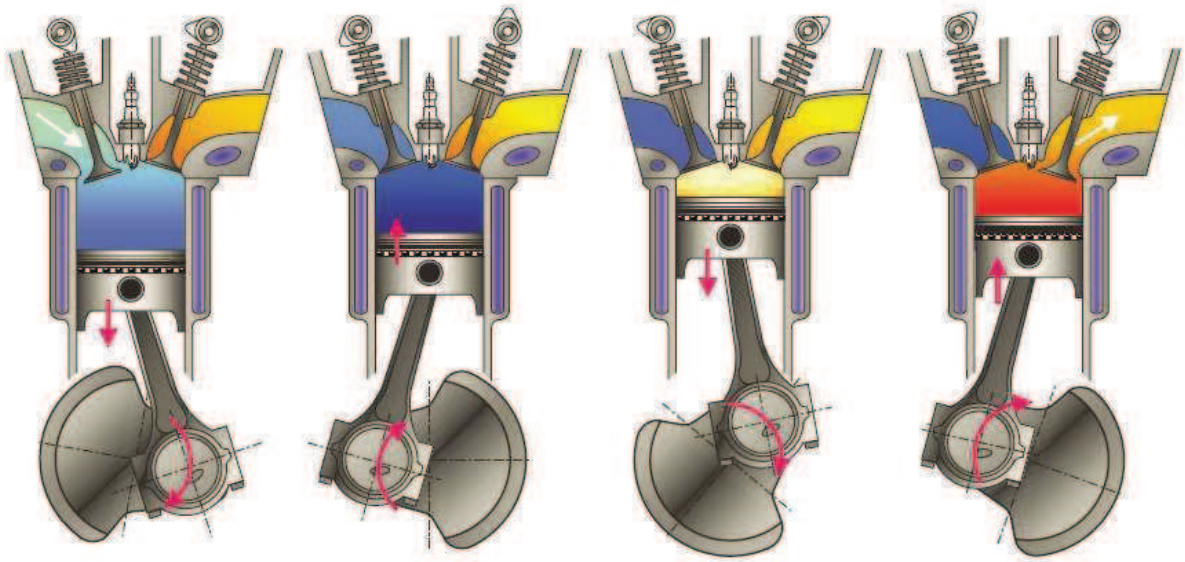

Fig.1.7 Four strokes for a gasoline engine

As we noticed, Diesel engines also have 4 strokes processes. The main difference between Compression-Ignition (CI) and SI are between compression stroke and power stroke. The ignition way is different. In diesel engine, there is very little fuel compressed in the compression stroke: only the air in the cylinder which is compressed to a very high pressure. At one moment, the injected fuel is mixed with the compressed hot air in the cylinder, the combustion starts instantaneously, it thus does not need a spark.

1.6 Gas mixing in the cylinder

In order to describe the relation between the fuel and the air in the cylinder, the equivalence ratio of the combustion ϕ and the relative air/fuel ratio λ are defined by:

$$\phi = \frac{\frac{m_{fuel}}{m_{air}}}{\left(\frac{m_{fuel}}{m_{air}}\right)_{stoechiometry}} \quad (1.5)$$

$$SCP = \left(\frac{m_{air}}{m_{fuel}}\right)_{stoechiometry} \quad (1.6)$$

$$\lambda = \phi^{-1} = \left(\frac{m_{air}}{m_{fuel}}\right) SCP^{-1} \quad (1.7)$$

where SCP is the stoichiometric coefficient parameter, which is function of the composition of fuel, AFR the Air to Fuel Ratio, FAR the Fuel to Air Ratio.

If ϕ is bigger than 1, then the gas mixture is called rich, i.e. insufficient oxygen is present to oxidize fully the fuel C_xH_y into exhaust products such as CO_2, H_2O, carbon monoxide CO, Hydrogen. If ϕ is smaller than 1, it is called lean, i.e. with excess of air. To sum up, the combustion process has three types:

- Fuel-lean mixtures: $\phi < 1, \lambda > 1$
- Stoichiometric mixtures: $\phi = 1, \lambda = 1$
- Fuel-rich mixtures: $\phi > 1, \lambda < 1$

The stoichiometric ratio ϕ has a very important impact on the pollutant emissions gas in gasoline engines, this relation is depicted in Fig.1.8.

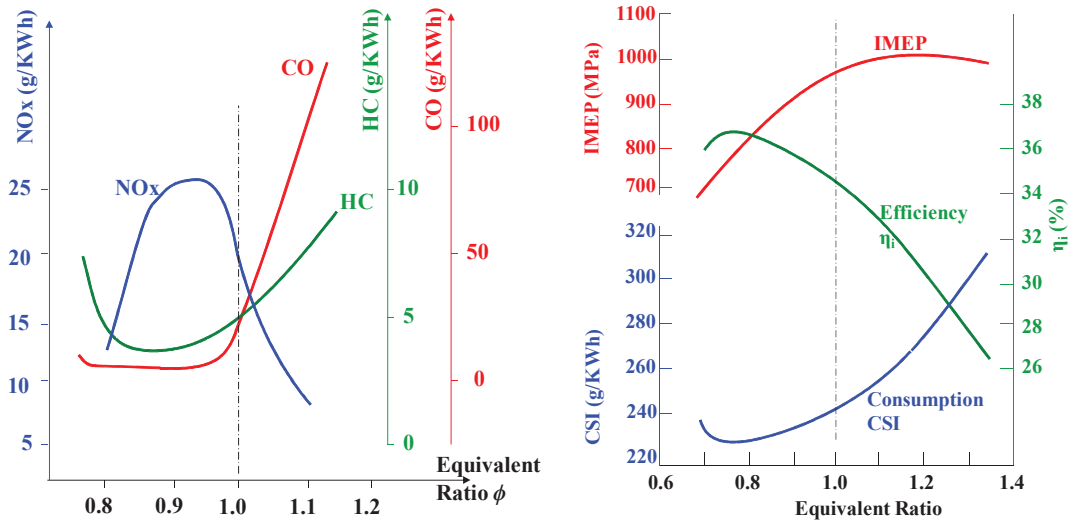

Fig.1.8 Behavior of CO, HC, NOx, CSI, η_i and IMEP versus equivalence ratio ϕ

From these two figures in Fig.1.8, we see that CO and HC have a different trend than NOx; IMEP (indicated mean effective pressure: average cylinder pressure over engine cycle), CSI and η_i do not change in the same way in the function of equivalent ratio:

- if $\phi < 0.85$, HC reduces by degrees, if $\phi \geq 0.85$, HC progressively increases,
- if $\phi \leq 0.77$, CO reduces by a small degrees, if $0.77 < \phi < 0.98$, CO almost keeps constant, if $\phi \geq 0.98$ increases dramatically,

- if $\phi < 0.96$, NOx increases continuously until the maximum value; if $\phi \geq 0.96$, NOx begins to decrease,
- if $\phi < 0.75$, CSI reduces by some small degrees, if $\phi \geq 0.75$, CSI progressively increases, i.e., $\phi = 0.75$ is the equivalent ratio, corresponding to the minimum consumption
- if $\phi < 0.75$, η_i increases by a small degrees until to the maximum value 37% ($\phi = 0.75$), if $\phi \geq 0.75$, η_i progressively begins to decrease,
- if $\phi<1.2$, IMEP progressively increases, if $\phi \geq 1.2$, IMEP progressively increases reduces by a small degrees.

Therefore, in order to find an optimal value, i.e. a compromise among CO, HC and NOx, equivalence ratio ϕ is often set to unit for a gasoline engine. Even with ϕ equals to 1, the pollutant emissions still cannot meet the emissions standards, so that after treatment technologies need to be used. Since year 1981, because the two-way catalytic converter was not able to reduce NOx emissions, the three-way catalytic converter (TWC) is used which is then detailed.

1.7 Pollutant emission post treatment technology

TWC's efficiencies depend on several parameters: temperature, gas flow and equivalence ratio. High efficiency is obtained where the engine operates around the stoichiometric, e.g. AFR between 14.6 and 14.8 for gasoline engine and this range is a little different for auto gas, natural gas and ethanol fuels, which requires experimental data while using those fuels. For conventional gasoline vehicles, a closed-loop control is realized with one or more oxygen sensors.

As we said, TWC system works effective within a narrow range of air-fuel ratios near stoichiometry for gasoline engines. Hence, to get high efficiency of the TWC, the equivalence ratio ϕ must oscillate in this stoichiometric band, i.e. the exhaust gas oscillates between rich and lean condition. It is very important to note that if this band is exceeded or does not reach the minimum level of air/fuel ratios, conversion efficiency falls very dramatically. Consequently, there are two cases if this right situation is not satisfied:

- If *AFR*<14.6 there is less oxygen and the reduction of NOx is not well supported.
- If *AFR*>14.8 the excess fuel consumes all oxygen, in this case, no exhaust oxygen can be used for the process of the catalyst, only stored oxygen is available for this process.

These trends can be found in Fig.1. 9. Note that for gasoline, *AFR* is around 14.7 (14.7g of air for 1g of fuel). This phenomenon [Andersson, 2005] is shown and adapted in Fig.1. 9. Facing to this problem, closed-loop control systems are needed that can deal with this conflict for the effective reduction of

NOx and HC oxidation. They can prevent the full oxidization of NOx reduction catalyst to occur, but replenish the oxygen storage material to avoid the fail of oxidation catalyst.

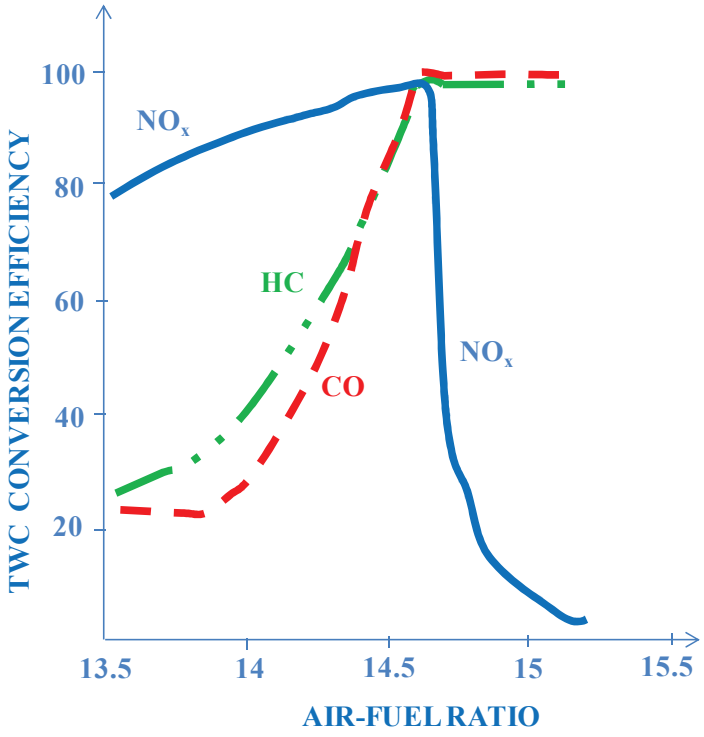

Fig.1. 9 TWC efficiency versus air/fuel ratio

1.8 Air path

Considering the internal combustion engine control, air path and fuel path are the most important. They determine the process of combustion. Air path is the path where gases trace from the intake to the exhaust pipes, so that the air is charging into the cylinders. It includes the turbocharger (turbine and compressor), throttles, exhaust gas recirculation. In the airpath management, multivariable control system needs to be used to control these actuators. It manages the air and the residual gases (mass, pressure and temperature) in the cylinder, which permits the fuel to produce the indicated torque of engine. The airpath is illustrated in Fig.1.10 for gasoline engine and Fig.1.11 for diesel engine. Nowadays, the airpath of advanced engine is equipped with turbocharger, pipes, intercooler, intake throttle, intake and exhaust manifolds, intake and exhaust valves and Exhaust Gas Recirculation.

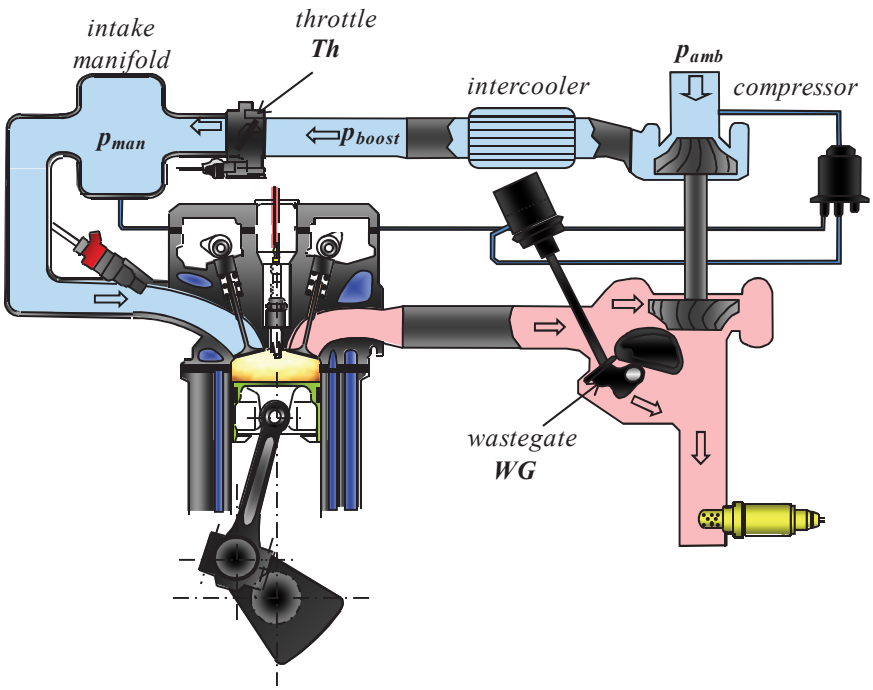

Fig.1.10 Classical air path of a gasoline engine with indirect injection

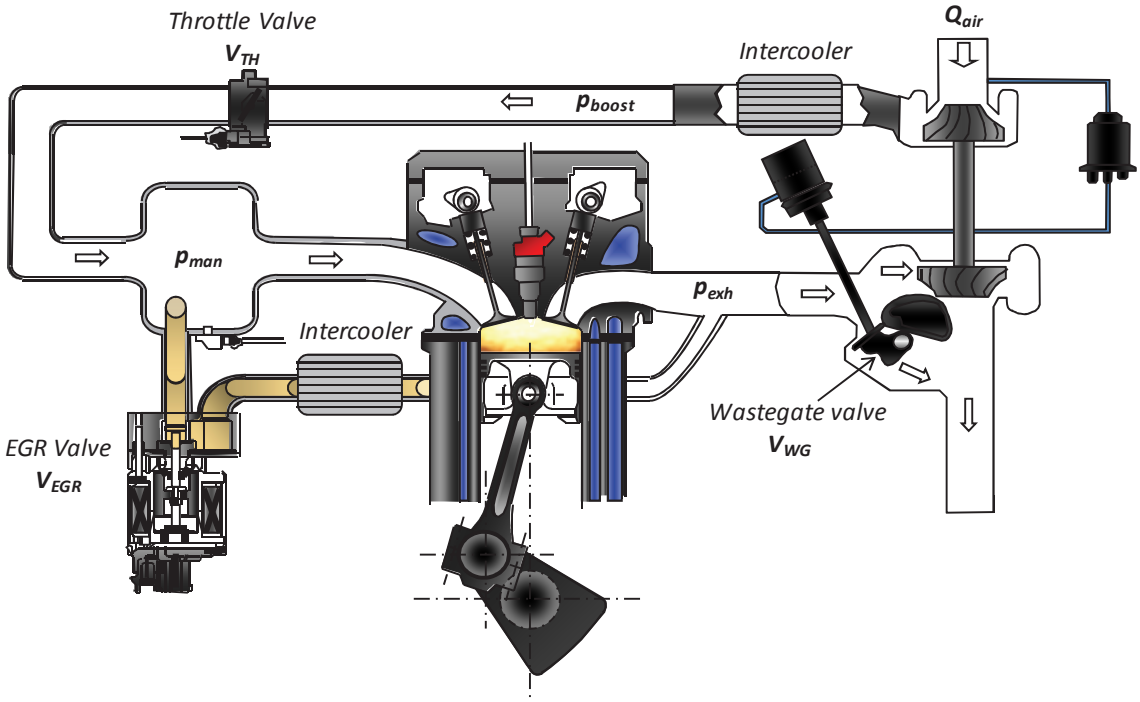

Fig.1.11 Classical air path of a diesel engine with direct injection

1.8.1 Turbocharger

Turbocharger, which is employed to recover the energy that is lost in the exhaust gases, is made with two components: turbine and compressor. The recovered energy by the turbine is used to drive the compressor through a shaft, and consequently, more air is forced into the inlet manifold (the principle can be found in Annex 5). On turbocharged engines, the turbine is mounted as close as possible to the cylinder exhaust ports so that the turbine can obtain high temperature (and so high energy)

1.8.2 Intercooler

The intercooler is used to cool down the air pressurized by compressor or the recirculated gases, so that the density of the entering fresh air or the recycled gases is (or are) increased. Hence, the power of the engine is improved.

1.8.3 Throttle

The throttle is a device that restricts the flow and thus permits to control the manifold pressure and so the in-cylinder mass. Hence, for a gasoline engine the torque is regulated by the throttle (throttle is opened depending on the need of engine power). Generally, the throttle is installed after the intercooler and before the intake manifold. A few years ago, it was directly connected to the gas pedal or the accelerator via mechanical linkage, and pressing the gas pedal allowed more air to enter the intake manifold. The throttle is shown in Fig.1.12. Nowadays the throttle is controlled by a DC motor.

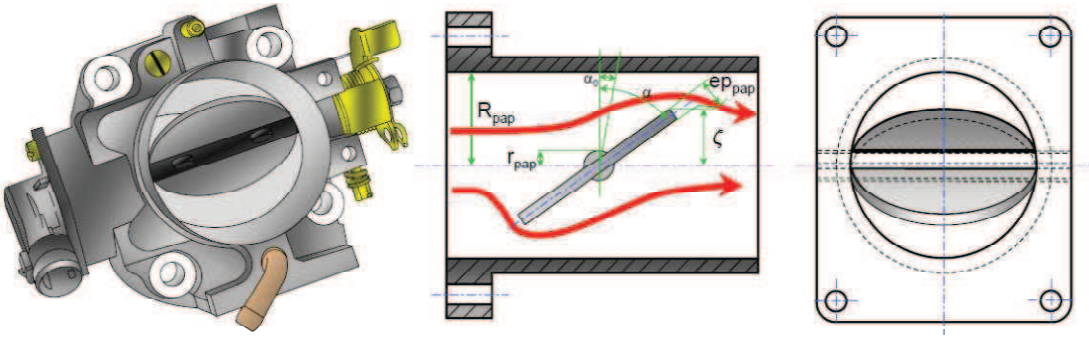

Fig.1.12 Throttle

The actuated throttle scaled control variable u_{th} is the opening percentage from 0% to 100%, which is a function of throttle's opening angle α with an aperture α_0. It is constrained by the saturation that is shown in Fig.1.12. A simple relation is defined as

$$\alpha = u_{th}\left(\frac{\pi}{2} - \alpha_0\right) + \alpha_0 \qquad \textbf{(1.8)}$$

and the opening area is given by

$$A_{th} = u_{th}\frac{\pi d_{th}^2}{4}\left(1 - \frac{cos\alpha}{cos\alpha_0}\right) \qquad \textbf{(1.9)}$$

where d_{th} is the throttle diameter [Pulkrabek, 2004, Wei and del Re, 2007, Alfieri, 2009].

The nonlinearity of area can be seen in Fig.1.13.

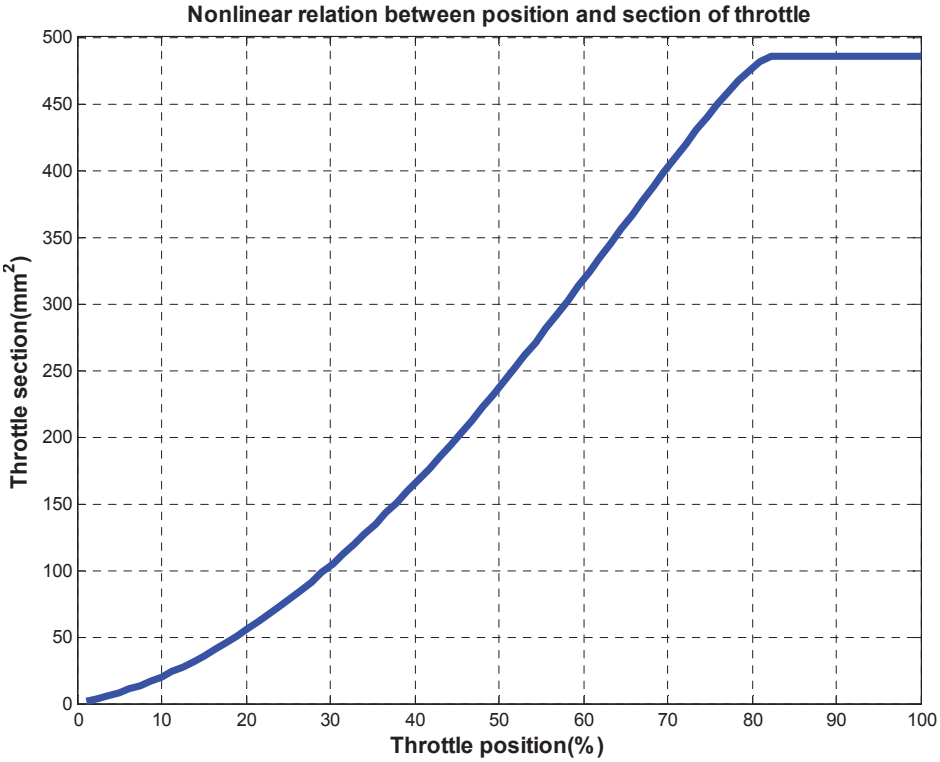

Fig.1.13 Throttle openness expressed by percentage and area

From this figure, the throttle area is found nonlinear with its position. A mass flow through this restriction area can be calculated as following. Considering the flow does not lose its energy while it is accelerating, all the thermal energy conserved in the flow can be converted into kinetic energy. Moreover, it is also converted into thermal energy after going through a narrow hole, without the occurrence of pressure recuperation. In addition, no temperature varies before and after the throttle.

If the fluid that goes through the valve is assumed compressible, Barré S^{t} Venant theory and equations can be used to describe this valve equation:

$$\dot{m}_{th}(t) = c_d . A_{th} . \frac{p_{boost}}{\sqrt{R.T_{boost}}} c_m \qquad \textbf{(1.10)}$$

$$C_m = \begin{cases} (\Pi)^{1/\gamma} \sqrt{\frac{2\gamma}{\gamma-1}\left[1-(\Pi)^{\frac{\gamma-1}{\gamma}}\right]} & if\ \Pi \leq p_{cr} \\ \sqrt{\gamma}\left(\frac{2}{\gamma+1}\right)^{\frac{\gamma+1}{2(\gamma-1)}} & if\ \Pi > p_{cr} \end{cases} \qquad \textbf{(1.11)}$$

$$\Pi = \frac{p_{boost}}{p_{man}} \qquad \textbf{(1.12)}$$

$$\gamma = \frac{c_p}{c_v} \qquad \textbf{(1.13)}$$

$$p_{cr} = \left(\frac{2}{\gamma+1}\right)^{\frac{\gamma}{\gamma-1}} \begin{cases} sonic\ for\ \Pi > p_{cr} \\ subsonic\ for\ \Pi \leq p_{cr} \end{cases} \quad \textbf{(1.14)}$$

where γ is the coefficient parameter of specific heat, c_p, c_v specific heat at constant pressure/volume, T_{boost} the temperature from upstream of throttle, c_d the discharge coefficient, c_m the mass flow parameter, Π the ratio of downstream pressure and upstream pressure, p_{cr} the critical pressure ratio, R gases property.

The surfacic air mass flow is given on example in Fig.1.14.

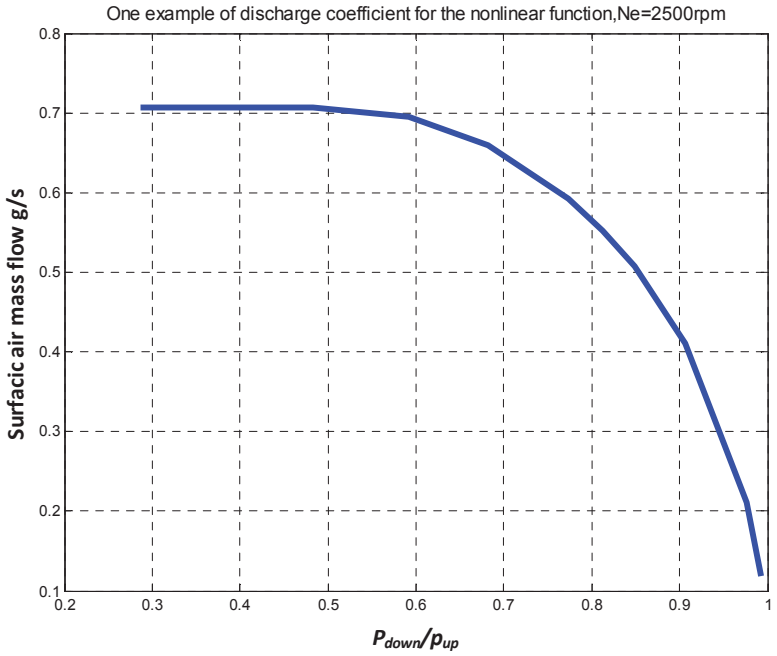

Fig.1.14 Barré de S^t Venant equation

From this figure, surfacic air mass flow (kg/s/m²) is nonlinear with the ratio of downstream pressure and upstream pressure.

1.8.4 Manifolds

The air charging is important because it influences the engine torque. Unfortunately, the air mass flow of the cylinder cannot be measured directly. In order to control this important variable, it has to be equivalently represented. It is hence often represented by the intake manifold pressure. The manifolds of gasoline and diesel engines are shown in Fig.1.15 and Fig.1.16. This is detailed below.

The pressure of the manifold

The structure of the manifold of a gasoline engine in the engine system is shown in Fig.1.15.

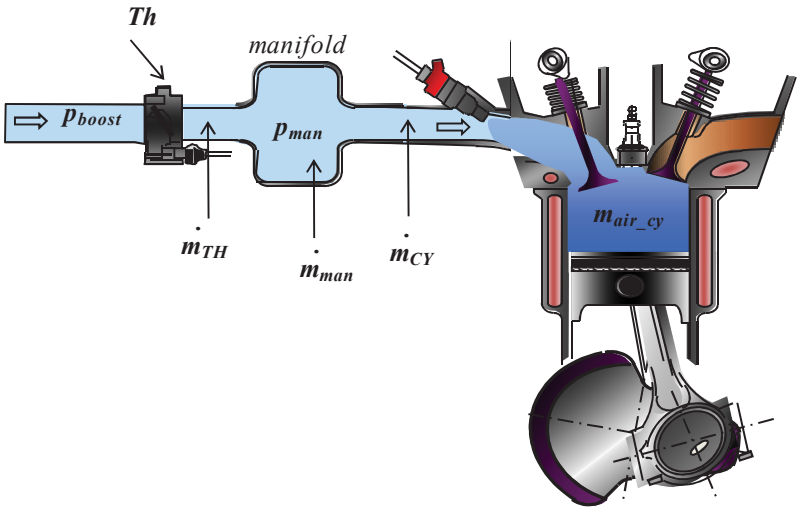

Fig.1.15 The structure of a gasoline engine intake manifold and cylinder

The manifold of a diesel engine is shown in Fig.1.16:

The calculation of the pressure assumes ideal gases and a constant manifold volume. Hence, this static pressure in the cylinder is chosen by its average value and calculated by the equation of Mayer ($r=c_p-c_v$). This pressure is obtained by

$$p = \frac{\sum_i m_i \bar{r} T}{V} \qquad \textbf{(1.15)}$$

where T and m_i are the temperature and mixing air-fuel in the intake manifold port, r the ideal gas, V the volume of manifold.

However, this equation is not related to the mass airflow in the cylinder, another equation is used to connect the mass airflow, engine speed and manifold pressure, it is given by

$$p_{man} = f\left(m_{air\_cy}, N_e, \dots\right) \qquad \textbf{(1.16)}$$

where m_{air_cy} is the air mass in the engine cylinder, assuming that there is no recycled exhaust gas, the temperature T is constant, $\bar{r}$ the constant ideal gas, V the constant volume of manifold in this model.

The estimation of the manifold pressure is provided with:

$$\frac{dp_{man}}{dt} = \frac{rT_{man}\frac{dm_{man}}{dt}}{V_{man}} \quad \textbf{(1.17)}$$

$$m_{air\_cy} = \int_0^{t_{TDC}} \dot{m}_{CY} dt \quad \textbf{(1.18)}$$

$$t_{TDC} = \frac{t_{cycle}}{n_c} = \frac{2 \cdot 60}{N_e n_c} \quad \textbf{(1.19)}$$

where $\dot{m}_{TH}$ is the downstream mass airflow of the throttle $\dot{m}_{CY}$ is the downstream mass airflow of the intake manifold. That is to say $(\dot{m}_{TH} - \dot{m}_{CY}M)$ is the airflow inside of the intake manifold. t_{TDC} is the period of one strike,

$$m_{air\_cy} = \dot{m}_{CY}.t_{TDC} = \dot{m}_{CY}\frac{2 \cdot 60}{N_e n_c} \quad \textbf{(1.20)}$$

where m_{air_cy} is assumed constant. The air mass flow downstream of the intake manifold is $\dot{m}_{man}$, and the mass airflow downstream of the throttle is $\dot{m}_{TH}$. Then, combine the equations (1.15) to (1.20) then the relation of p_{man} and m_{air_cy} given,

$$\frac{dp_{man}}{dt} = \frac{rT_{man}\left(\dot{m}_{TH} - \frac{m_{air\_cy} \cdot N_e n_c}{120}\right)}{V_{man}} = \frac{rT_{man}\left(\dot{m}_{TH} - \frac{m_{air\_cy}}{120}\right)}{V_{man}} \quad \textbf{(1.21)}$$

With this equation, m_{air_cy} can be controlled indirectly by p_{man}, *which is* then controlled by V_{TH}.

The structure of the manifold in a diesel engine in the engine system is shown in Fig.1.16.

.

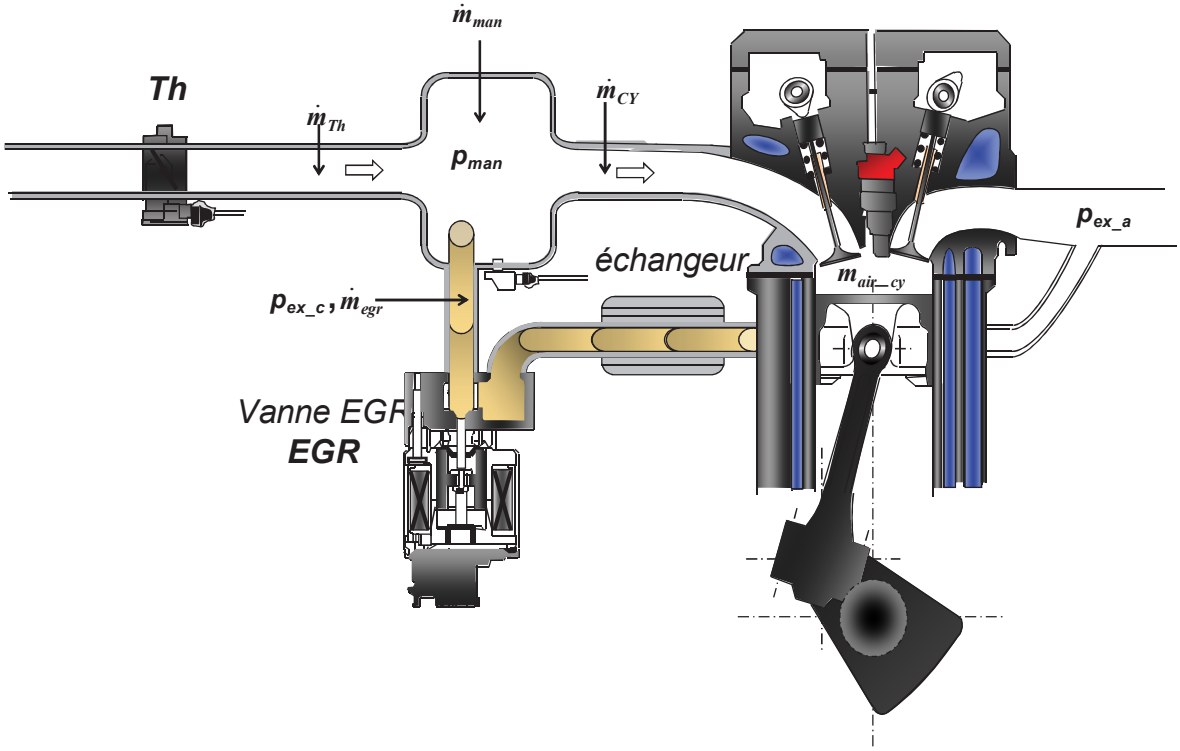

Fig.1.16 The structure of a diesel engine intake manifold and cylinder

The estimation of manifold pressure is provided with

$$\frac{dp_{man}}{dt} = \frac{rT_{man}\left(\dot{m}_{TH} - \frac{m_{air\_cy} \cdot N_e \cdot n_C}{120}\right)}{V_{man}} + \frac{rm_{man}\frac{dT_{man}}{dt}}{V_{man}} \qquad (1.22)$$

where m_{man} is the mass of the flow in the manifolds. With this equation, m_{air_cy} can be controlled indirectly by p_{man}, although it is more complex than in gasoline engine. This function shows the nonlinearity among p_{man}, m_{air_cy} and T_{man}.

While combining previous equations, p_{man} has a nonlinearity relationship with throttle position, which is the control variable that we need to control. In Fig.1.17, the completely static nonlinearity of manifold pressure is shown in function of the throttle opening.

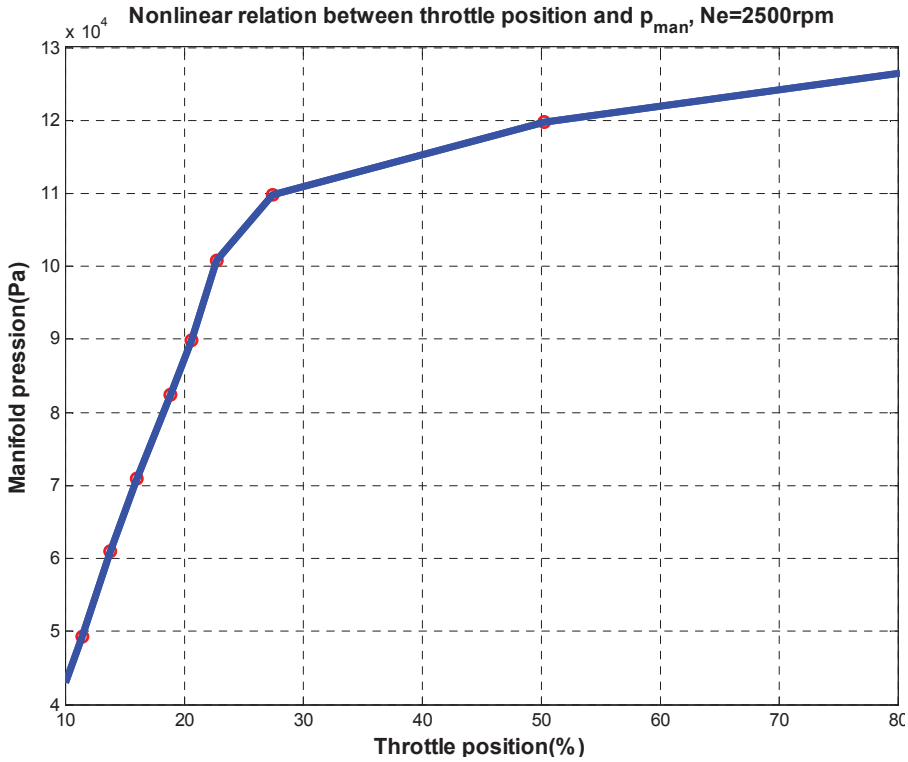

Fig.1.17 Intake manifold pressure versus throttle opening

Especially, in the figure of throttle position and manifold pressure in Fig.1.17 this nonlinear phenomenon is more evident. This nonlinear problem is treated by a normalization and linearization which is discussed in chapter 2.

1.8.5 Waste-gate

Waste-gate is a device that permits to get a predetermined level of boost or to prevent over boosting. It is used to prevent the very high cylinder pressure. Consequently, the speed of the turbocharger is regulated via waste-gate by bypassing some of the exhaust gases. Effectively, only parts of the exhaust gases are employed to drive the turbine to generate additional power, the rest of the exhaust gases are

directly exhausted to the downstream of turbine. Hence, Waste-gate is used to drive the turbine, hence the compressor, so that the engine can protect itself.

Waste-gate valves usually are classified into four types: manual, pneumatic, electric and hydraulic; or they can be separated in two sorts: internal and external waste-gates. Generally, Waste-gate acts on the boost pressure via a controlled diaphragm with a spring-loaded valve. A turbine with a waste-gate is a way to avoid damaging the engine. Hence, a waste-gate leakage is a common way to control the boost pressure. When boost pressure reaches a specified point, the waste-gate is opened to bypass the exhaust gases The waste-gate actuator is controlled by air pressure supplied by a hose, tapped into boost pressure reaches at the compressor discharge outlet. One example of real waste-gate valve is given in Fig.1.18

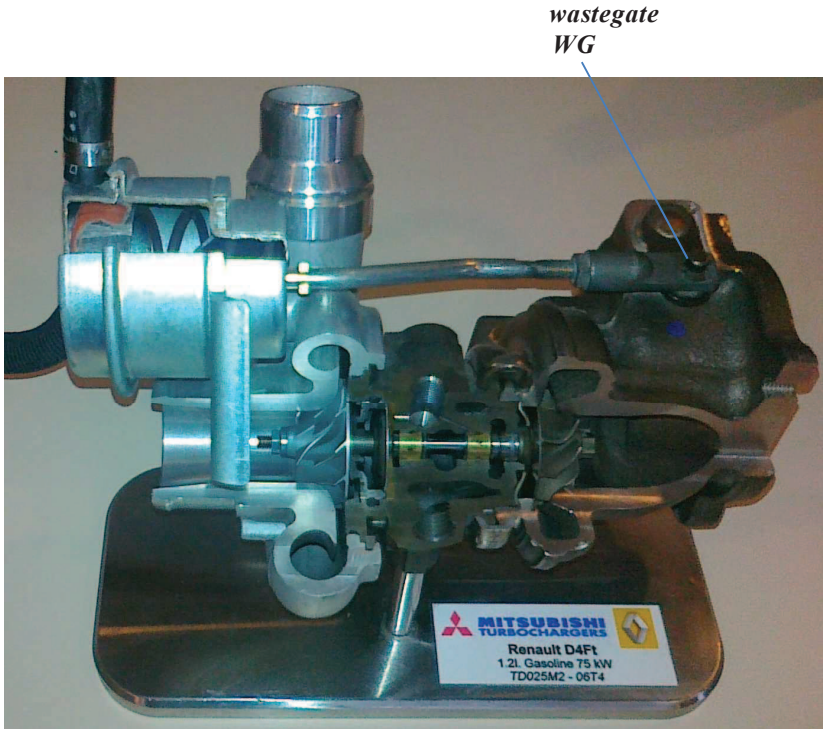

Fig.1.18 Waste-gate in Turbo system

For the description of the flow through the waste-gate, the isentropic compressible mass flows are used. They are modeled also by Barré St Venant theory and equations (see case 2 of §1.8.3 Throttle), which are reformed as below, and a simple scheme of waste-gate and turbocharger is shown in Fig.1. 19,

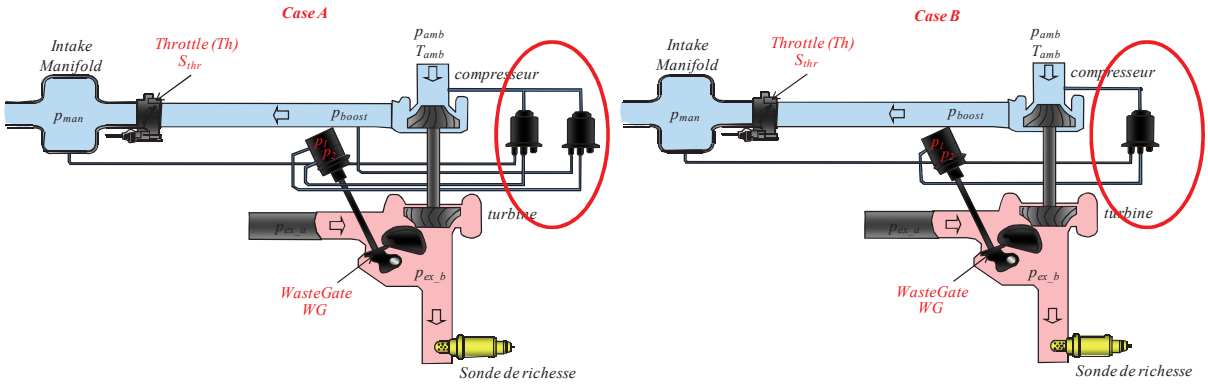

Fig.1. 19 Two cases of the scheme of waste-gate and turbocharger of gasoline engine, p_1 and p_2 are two pressures that are used to control the action of waste-gate

Case 1:

Waste-gate is regulated by p_1 and p_2, *i.e.*, p_{amb}, p_{man} and p_{boost}

$$p_1 = f(p_{amb}, p_{boost}),\ while\ p_{amb} \le p_1 \le p_{boost} \quad (1.23)$$

$$p_2 = f(p_{amb}, p_{man}),\ while\ p_{man} \le p_1 \le p_{amb} \quad (1.24)$$

p_1 and p_2 are controlled by some electrical valves.

If p_1=p_2, no reaction, i.e., waste-gate keeps its previous statue.

If p_1<p_2, waste-gate is going to be closed.

If p_1>p_2, waste-gate is going to be opened.

Case 2:

Same principal, but the waste-gate is only regulated by p_1 ($p_2 = p_{amb}$), *i.e.*, p_{amb} and p_{boost}

$$p_2 = f(p_{amb}, p_{man}) \quad (1.25)$$

Model of waste-gate flow are given below,

$$\dot{m}_{wg}(t) = c_d . c_m . A_{wg} . \frac{p_{ex\_a}}{\sqrt{R.T_{ex\_a}}} \quad (1.26)$$

$$\Pi_{wg} = \frac{p_{ex\_a}}{p_{ex\_b}} \quad (1.27)$$

c_d is the same which are refereed to (1.10) and (1.14).

Because the waste-gate flow is not measured, it is not possible to validate it directly with the experiment. The solution is to estimate it with the other variables, such as exhaust pressure or the speed of turbo.

This waste-gate mass flow is commonly given by look-up tables as shown in Fig.1.20.

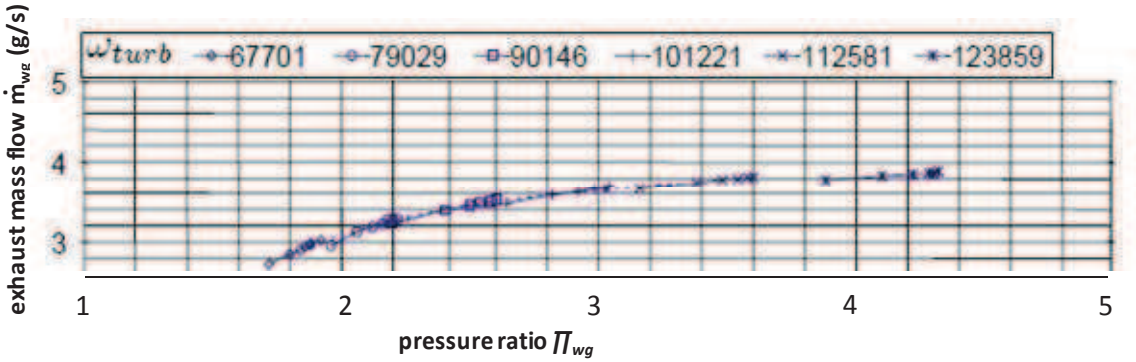

Fig.1.20 Example of air mass flow through compressor

From Fig.1.20, the pressure ratio is found exhaust mass flow is nonlinearity in function of exhaust pressure.

The waste-gate of our gasoline engine is a pneumatic waste-gate (case 1), which movement depends on the pressure of the manifold. To sum up, the waste-gate permits to achieve a pointed dynamical boost pressure.

1.8.6 EGR mass flow

Assuming the exhaust gas recycled via an EGR valve is in ideal case, i.e. no reverse flow when the pressure of the exhaust manifold is smaller than the pressure of the intake manifold, and we assume that no pressure drop occurs over the EGR cooler, for the reason of simplification of modeling. Thus, this model only introduces the EGR mass flow in the case of assumption above in the range of identified operating points. The figure of $\dot{m}_{egr}$ is shown in Fig.1.21, and the following equations are presented to describe the EGR mass flow rate and mass flow.

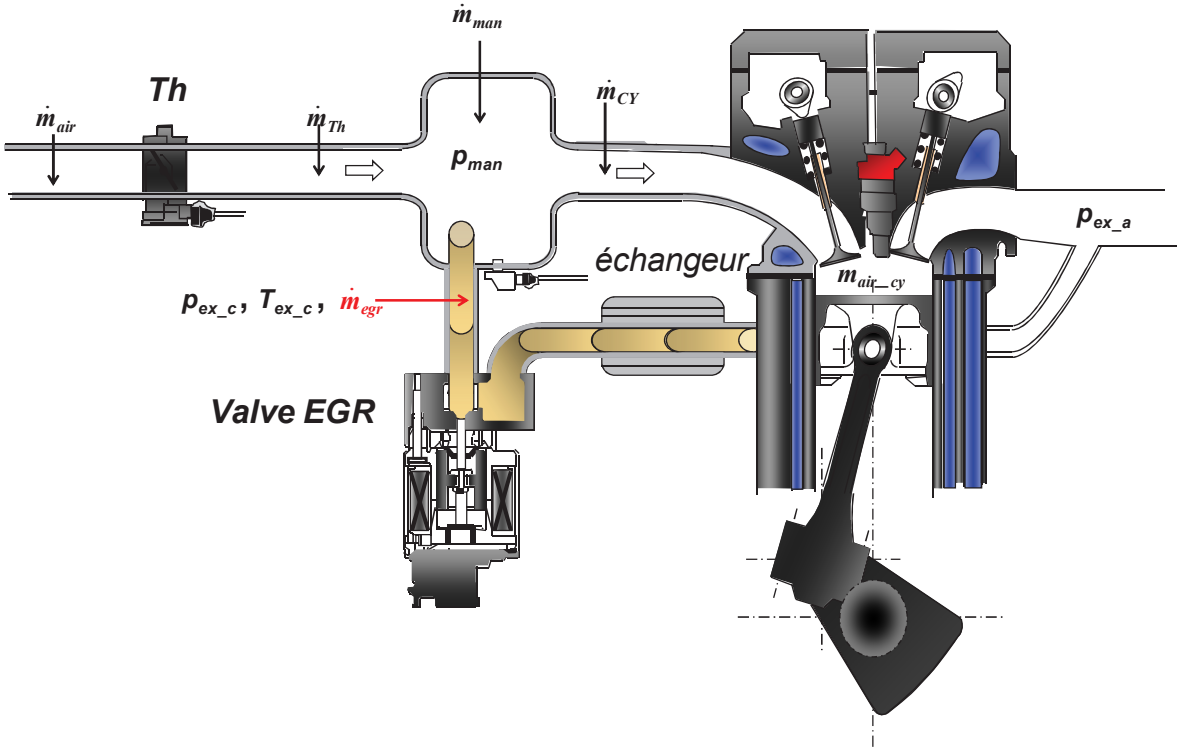

Fig.1.21 EGR mass flow in diesel engine

The EGR mass flow rate is defined

$$\eta_{egr} = \frac{\dot{m}_{egr}}{\dot{m}_{man}} = \frac{\dot{m}_{egr}}{\dot{m}_{egr}+\dot{m}_{Th}} = \frac{\dot{m}_{egr}}{\dot{m}_{egr}+\dot{m}_{air}} \quad \textbf{(1.28)}$$

where $\dot{m}_{man}$ is intake manifold mixing gas flow, $\dot{m}_{Th}$ the air mass flow before the intake throttle, $\dot{m}_{air}$ the air mass flow in the intake manifold.

$$\dot{m}_{egr}(t) = c_d . c_m . A_{egr} . \frac{p_{ex\_a}}{\sqrt{R.T_{ex\_a}}} \quad \textbf{(1.29)}$$

$$\Pi_{egr} = \frac{p_{ex\_a}}{p_{ex\_c}} \quad \textbf{(1.30)}$$

However, because the limitation of high temperature of EGR gas, $\dot{m}_{egr}$ is not proposed to measure, $\dot{m}_{air}$ or $\dot{m}_{Th}$ is thus proposed to meausre and control. Hence, $\dot{m}_{egr}$ is calculated by

$$\dot{m}_{egr} = \dot{m}_{man} \cdot \eta_{egr} = (\dot{m}_{egr} + \dot{m}_{Th})\eta_{egr} = (\dot{m}_{egr} + \dot{m}_{air})\eta_{egr} \quad \textbf{(1.31)}$$

$$\dot{m}_{egr} = \frac{\eta_{egr}}{1-\eta_{egr}} \cdot \dot{m}_{Th} = \frac{\eta_{egr}}{1-\eta_{egr}} \cdot \dot{m}_{air} \quad \textbf{(1.32)}$$

Combining (1.28) and (1.32), hence the relation of EGR valve is replaced via $\dot{m}_{air}$ and given by

$$\dot{m}_{air} = \frac{\eta_{egr}}{1-\eta_{egr}} \cdot \dot{m}_{egr} = \frac{\eta_{egr}}{1-\eta_{egr}} \cdot c_d . c_m . A_{egr} . \frac{p_{ex\_a}}{\sqrt{R.T_{ex\_a}}} \quad \textbf{(1.33)}$$

1.9 Torque and work

1.9.1 Torque modeling

In an engine, the torque is the force that combustion generates to force the piston to rotate on the crankshaft, which is a good indicator of an engine's ability to power the vehicle. Its unit is N.m or lbf.ft. The engine torque T_e is a nonlinear function of many variables, such as engine speed ω_e, ignition advance angle IA (the angle between the point of ignition and the point of TDC), in-cylinder air and fuel masses, EGR rate, etc. Hence, it can be expressed as follows. If the amount of mixture in the cylinder is changed, the engine torque is also changed.

$$T_e = f(IA, m_{air\_cy}, m_{fuel\_cy}, \omega_e, \dots) \quad \textbf{(1.34)}$$

$$m_{fuel\_cy} = m_{air\_cy} \cdot \lambda \cdot SCP \quad \textbf{(1.35)}$$

General for an optimized engine combustion, λ is 1, SCP is 14.6 for a gasoline engine, and larger than 14.6 depended on the performance of fuel for a diesel engine.

In order to predict the engine torque, several methods can be concluded:

- Detailed thermodynamic simulations
- Grid the space of all possible operating conditions, afterwards measurement and computation in each direction
- Physical equations modeling and computation

In gasoline engine, the torque is regulated via the air mass flow in the cylinder. This air mass flow has a relationship with intake manifold pressure p_{man} and boost pressure p_{boost}, which can be defined as below,

$$T = f(\dot{m}_{O2_{cylinder}}, \dot{m}_{fuel_{cylinder}}, \dot{m}_{neutral_{cylinder}}, IA, \dots) \quad \textbf{(1.36)}$$

Because $\lambda = 1$ is needed for the

$$T = f(\dot{m}_{air_{cylinder}}, , \dot{m}_{neutral_{cylinder}}, IA, \dots) \quad \textbf{(1.37)}$$

$$\gamma = \frac{c_p}{c_v} \quad \textbf{(1.38)}$$

$$\dot{m}_{air_{cylinder}} = f(p_{man}, \dots) \quad \textbf{(1.39)}$$

$$p_{man} = f(p_{boost}, A_{Th}, \dots) \quad \textbf{(1.40)}$$

From equations (1.35) to (1.40) p_{boost} and p_{man} can be used to control the amount of air mass flow inside of the cylinder, i.e., the engine torque if the other parameters are kept as constant. In gasoline engine, because the torque is regulated indirectly by the intake manifold pressure $p_{man,}$ which depends on the area of openness of the intake throttle (*TH*) given in §1.8.3. The manifold pressure p_{man} depends on boost pressure p_{boost}, which is controlled by the waste-gate WG. Hence, *TH* and *WG* are employed as the control actuators of gasoline engine in this thesis. The torque is produced via the combustion in the cylinder, and it is not regulated only by the air mass flow, it is controlled by fuel mass flow.

As ϕ<1 in the diesel engine (lean combustion), the air mass flow also needs to be controlled precisely. Moreover, the air mass flow and the EGR gas in the cylinder cannot be measured so that equivalent variables are needed. For this reason, the intake manifold pressure (p_{man}) and air mass flow (Q_{air}) can be considered as the measured variables. In the diesel engine, the torque depends at first order on the fuel mass flow in the cylinder (refer to the §1.9). In order to control the torque precisely in the diesel engine, an EGR valve (*EGR*) and *WG* are often utilized, *Th* is not employed often in diesel engines, because of the pumping loss. In this thesis, with and without *Th* are discussed. *Th* can be used to avoid the wrong backflow problem of EGR. Indeed, for diesel engine, the intake throttle can be used in order to reduce NOx with EGR mass flow. In this case, the EGR mass flow cannot be cycled into the intake manifold in two situations:

- if p_{ex}<p_{man}, the air and fuel mixture flows enter directly from intake manifold to the exhaust manifold;
- if p_{ex}= p_{man}, there is no EGR mass flow transformation.

Hence, one of solutions is employing *TH* to reduce p_{man}until p_{ex}> p_{man}, consequently, the EGR mass flow can be recycled all the time.

WG is employed in diesel engine system that shares the same principle of gasoline engine system.

Regarding the compromise among the fuel economy, pollutant exhaust emissions and performance, the combustion in the cylinder has to be controlled precisely. That is to say the amount of oxide and the fuel have to be controlled precisely. Because the amount of oxide accounts a constant percentage of air, the air is thus considered as the parameter to replace the oxide in the cylinder. Furthermore, because of the ideal combustion, the fuel and air has to be mixed at some certain ratio according to engine's characteristics. Lots of researches have dealt with the air mass control, fuel mass control or the relation of air mass and fuel mass. Because this dissertation is interested in the air path of ICE control, the fuel

mass control of fuel path is not detailed here. Due to the different ignition of gasoline engine and diesel engine, these two ICEs are detailed below.

The gasoline engine requires an equivalent ratio ϕ being fixed as 1, i.e. ϕ=1. The ratio of mass air/fuel (AFR) has been studied, and it is now a mature technology. Furthermore, fuel consumption can be reduced without increasing the power of the engine by turbocharging a naturally aspirated engine and downsizing the engine. Diesel engine requires ϕ less than 1, i.e. ϕ<1. The natural aspirated diesel engines also are well mastered. In order to realize this aim, the air charging control is one of the most important variables that must be controlled precisely.

In airpath loop, the compressor drives much more fresh air into the intake manifold. The energy recovered by the turbocharger is transformed into the manifold pressure to fill air in the cylinder. This filling air is used to decide the engine torque. This process is shown in Fig.1.15. Hence, the engine torque's requirement is function of air mass flow in the cylinder and the advance angle of ignition (refer to Fig.1. 6), of which determines the efficiency of the combustion, i.e. the consumption of SI engine (Fig.1.8). In addition, for the sake of practice, the parameters of mass air filling flow and the mass air flow inside of cylinder cannot be measured, an estimated of variable is therefore needed for their replacements. The chosen torques and engine speeds are shown in Fig.1. 22.

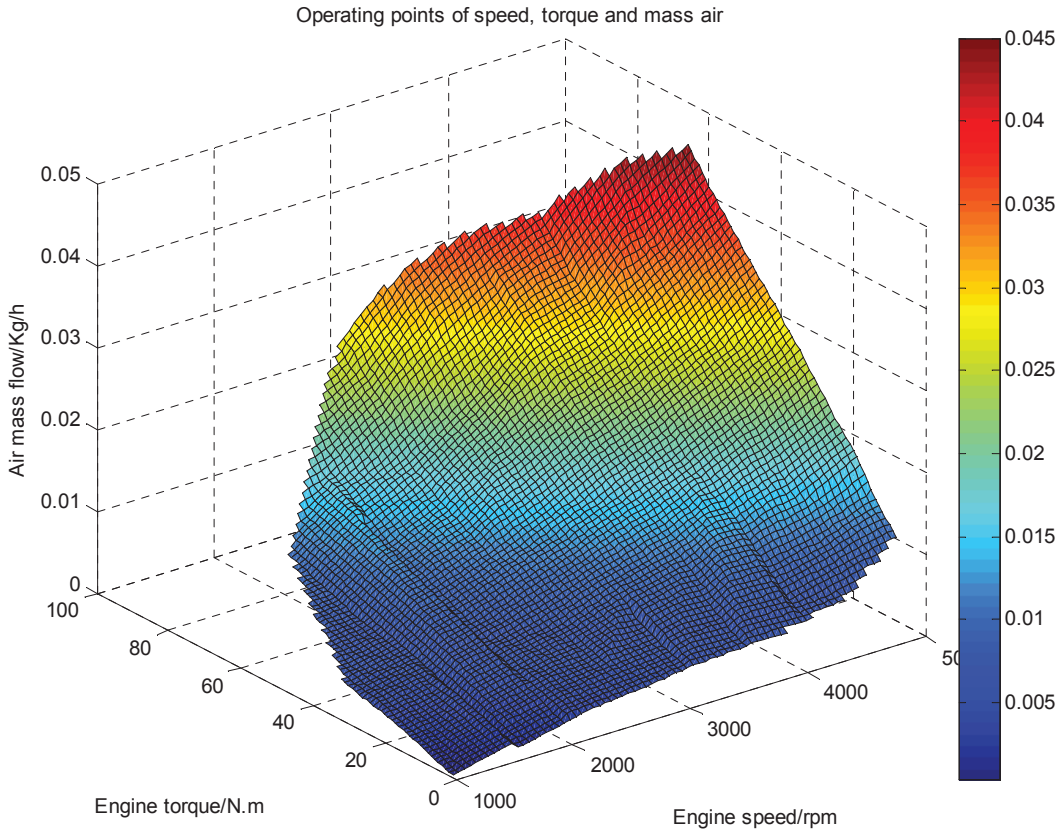

Fig.1. 22 Relation map of engine speed, airflow mass and torque in a smart gasoline engine

This figure shows a conventional torque in the function of speed and airflow mass, here the maximum torque is appears at 83N.m where engine speed is 2500rpm and airflow mass 0.1g/s.

1.9.2 Engine power

It is the power delivered by the engine and absorbed by the dynamometer, which is the rate at which work is done. Because it is the usable power delivered by the engine to the load, hence, brake power or "brake" is used also as power. It is defined as the product of torque and angular speed.

$$P = \omega_e T \qquad (1.41)$$

where ω_e is the engine speed (rad/s), T is the engine torque (Nm).

Engine torque and power are important variables that are a function of engine speed. They are taken to indicate the ability of engine's performance. For a natural aspirated engine, the maximum power and torque are fixed, but if they are turbocharged or supercharged, these maximum values are increased due to the additional power derived. The following figure is shows an example of engine power and torque in a turbocharged SI engine. Normally, the maximum engine power and torque do not arise at the same operating point.

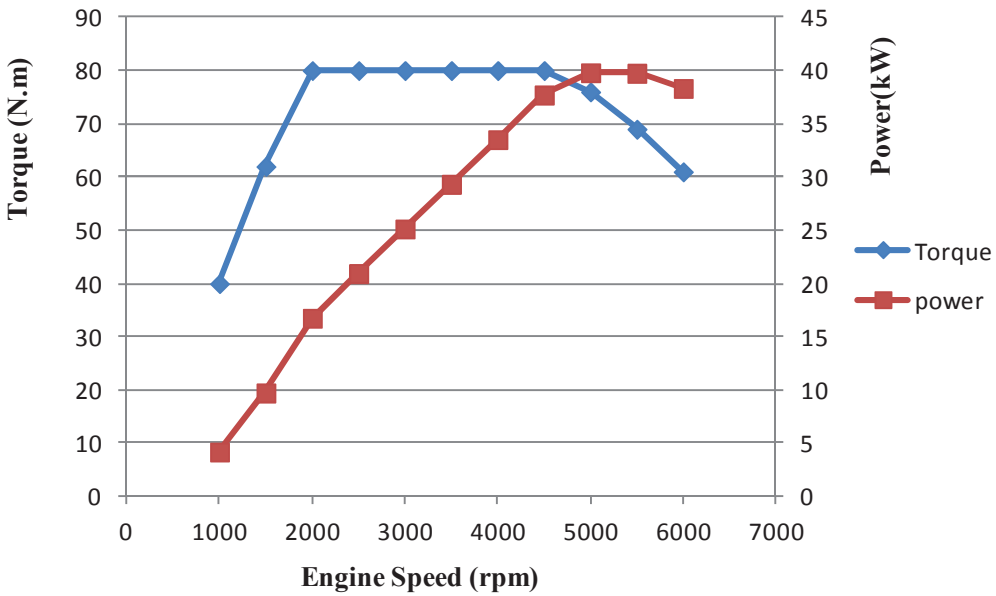

Fig.1.23 Engine power and torque curves

1.10 Engine Control System

The Engine Control System includes Air path control and fuel path control. Because of the introduction of electric and electronic components in advanced engines, the engine control system is more complex and powerful than ever before, so that the drivability and comfort of passenger cars can

be improved. Because of the stringent pollutant emissions standards, the requisite of fuel economy and the performance of the future vehicles, engineers and researchers have brought many actuators into engine control system. For example, a turbocharger was introduced to improve the fuel economy and performance. Furthermore, a waste-gate valve, a variable geometry turbochargers (VGT) or a variable nozzle turbochargers (VNT) is employed to take care of some problems that turbocharger cause. For example, an electrical throttle is introduced to improve the precision of air charging in the cylinder of a gasoline engine. And it is also introduced in diesel engines to improve the recycling of exhaust gases. For example, EGR valve is introduced to reduce the temperature of the combustion, i.e. reduction of NOx. Consequently, the degree of freedom of engine control system has been increased. The system thus needs some more powerful control, which takes all of these actuators into account, to meet the requirements of the control objectives.

Due to these requirements of advanced engines, i.e. pollutant emissions reduction, fuel economy and engine performance, this thesis introduces one unified robust control methodology. It is used to realize the whole process of engine control system while considering the pollutant emissions, fuel economy and engine performances. Because it is unified, it is thus applied both in gasoline engine and diesel engine with different actuators.

Because the general introduction provides the broad presentation of engine controls, the basic gasoline engine and diesel engine control scheme are introduced as follows.

1.10.1 Gasoline engine control

The basic control-oriented scheme of gasoline engine control is given in Fig.1.24.

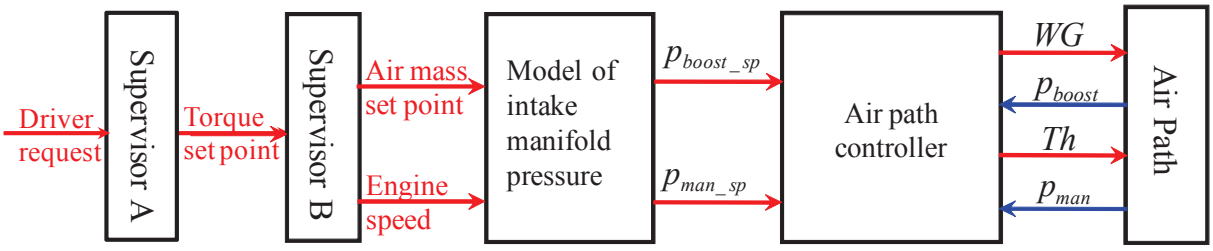

Fig.1.24 Scheme of gasoline engine control

As shown in this diagram, this gasoline engine air path control system is a two inputs two outputs MIMO control systems. In this scheme, engine torque is the control objective that has to be controlled precisely. First, the request of driver is translated into torque set point. With this torque set point, the air mass flow and engine speed in the cylinder are in function of torque set point. It is regulated by p_{man_sp} manifold pressure and p_{boost_sp} boost pressure set point. Then two parts of control variables: controlled variables p_{man} and p_{boost} that are regulated by WG and TH. Hence, the air path control includes boost pressure control and intake manifold pressure control.

1.10.2 Diesel engine control

The basic control-oriented scheme of diesel engine control is given in Fig.1.25.

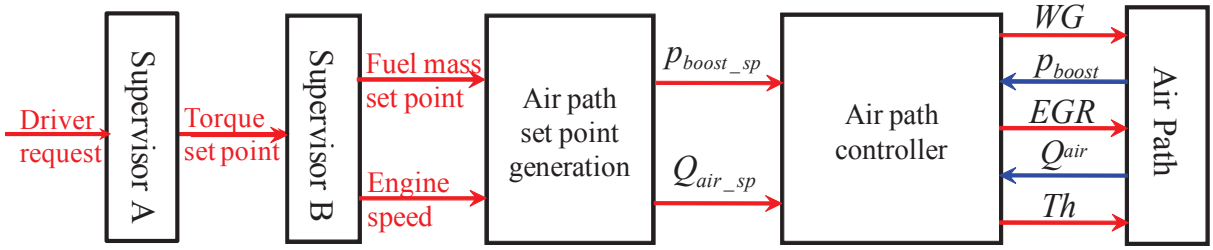

Fig.1.25 Scheme of diesel engine control with Waste-gate (*WG*) turbocharger

As shown in this diagram, this diesel engine air path control system is a three inputs two outputs MIMO control systems. In this scheme, the torque is the control objective that equivalently needs to be controlled precisely because it is related directly with compromised performance, pollutant emissions and fuel consumption.

First the driver request is expressed by the torque set point with a supervisor A, which is linked by the pedal and the ECU lookup table. Then, torque set point is transformed into two different set points: fuel mass set point and engine speed via another supervisor B. With these two types of set points, boost pressure p_{boost_sp} and Q_{air_sp} are used to give the references to the MIMO air path controller. This air path is operated by the actuators WG and Exhaust Gases Recycled (EGR). It is very important to note that an intake *Th* can be used to assure the recycling of the exhaust gases, because the phenomenon of backflow between intake manifolds and exhaust manifolds. In this case, the system can be modified as a three inputs two outputs the MIMO system.

1.11 Assumptions and limitations

Advanced engine systems are complicated systems, which contain uncertainty, nonlinearity, saturation, coupling, etc., and which call for the assumptions and limitations of engine systems. Engine systems work or operate in various engine speeds, torques, etc., which cause systems to be uncertainty systems. Because of the physical properties of various different actuators, the output of system contains much nonlinearity. Moreover, because of the physical limitation of actuators, some actuators maximum or minimum values are limited to the available area via their saturation area.

1.12 Conclusions

The performance of internal combustion engines is limited by the quantity of gas that the air path can bring into the cylinder. Turbochargers can increase this amount and it is for this reason that they are now commonly used, sometimes in combination with other components (waste-gate for example). If a

system is a multi-variable system, and if it contains several inputs and several outputs, this kind of system is Multi-input-multi-output system. This kind of system has coupling, and it comes from the different loops.

This chapter introduces the general presentation of internal combustion engine vehicles' opportunity, which shows the ICE still determines the vehicles marketing. However, challenges also exist, because more stringent and higher requirements are in pollutant emissions, fuel consumption and performance. Due to the different physical characteristics of different engines, these challenges should be treated differently. The motivation of this thesis is to employ the turbocharged engines to realize these requirements both in gasoline and diesel engine. It is chosen to reduce the pollutant emission while keeping the same engine's performance. Moreover, because of the vital importance of air path control in internal combustion engines, it is consequently taken as the control strategy of this thesis. Furthermore, due to the different physical control scheme of gasoline engine and diesel engine, they are explained more in control principle. Later, some assumptions and limitations are presented.

Chapter 2 presents the unified control methodology, chapter 3 employs and applies this methodology into a gasoline engine simulator, and chapter 4 applies it on a diesel engine simulator, next then on a diesel engine test bed. With the validation of gasoline and diesel engine systems, this methodology can be proved to be a unified robust control methodology in internal combustion engines.

These systems have the disadvantage of slowing the dynamics of filling-up the cylinder. The associated control strategies must fully exploit all dynamics of this complex system to ensure the power demand of the driver. This thesis proposed a unified simple control strategy to solve the problem of control systems for turbocharged engines. This unified control methodology is presented in chapter 2 and was applied to a turbocharged gasoline engine (Chapter 3) and a turbocharged diesel engine with exhaust gas recirculation (Chapter 4). The approach proposed is to simplify the design of multivariable control strategies for classical turbocharged engines. Experimental results are provided to demonstrate the relevance of the approach.

CHAPTER 2 Sequential robust control design methodology

Contents

2.1 Résumé

Ce chapitre propose une méthodologie unifiée de commande robuste qui peut être utilisée pour réguler les systèmes multivariables carrés et non-carrés. Après avoir montré la structure générale de la méthodologie, nous avons détaillé chacune des étapes de cette dernière. Après avoir conçu un modèle de validation basse fréquence 0D, un modèle boîte noire fréquentiel est conçue sur la base de résultats de l'excitation temporelle du système à contrôler et de la normalisation des données. Ce modèle fréquentiel est par la suite utilisé pour procéder à l'analyse approfondie des propriétés structurelles des systèmes MIMO non linéaires. La décomposition en valeurs singulières permet de connaître les directions prépondérantes de notre système multivariable et le degré de complexité qui est nécessaire pour contrôler les différentes boucles du système. Le « condition number » aide à comprendre le degré de sensibilité de notre système vis-à-vis des incertitudes non structurées. Cet outil montre aussi que l'étape de normalisation est un moyen de réduire les valeurs du « condition number » et donc de réduire la sensibilité à l'entrée des incertitudes non structurées. Les outils RGA et bande de Gershgorin permettent de trouver la forme du régulateur pouvant être utilisé pour contrôler le système et, par conséquent, la stratégie de contrôle à mettre en place. Avec cette information, une méthode de conception de commande peut être proposée. Finalement et en raison de sa simplicité, la méthodologie de placement de pôles est présentée et utilisée pour synthétiser des régulateur PIDA. La partie accélération est ajoutée au régulateur PID classique pour former des PIDA et permettre d'appliquer la méthodologie de placement de pôle sur des systèmes ayant un ordre inférieur ou égal à 3. L'autre avantage notable de ce type de régulateur simple concerne la facilité d'implémentation sur les systèmes réels. Par la suite, la stabilité robuste des systèmes SISO et MIMO est présentée.

2.2 Introduction

In Automatic control, many systems have several inputs and several outputs. This type of systems are much difficult to analyze and control because one input does not affect only one output, which is named coupling phenomenon [Guzzella, 2007]. The control theory for Single-Input Single-Output system is well developed contrary to those of Multi-Input Multi-Output systems. Hence, it is quite interesting to apply this theory to control MIMO plants. In the literature, a method called *sequential multi-SISO* is developed to control MIMO system with small coupling.

Due to physical characteristic of the plant, uncertainty is one of its important features, no matter SISO or MIMO systems. If this characteristic is not considered during the control design process, the accuracy or/and stability of the controlled system cannot be proved or maintained for all the operating point or uncertainty issue (if we consider one operating point).

Considering engine control, an operating point is defined in torque and speed. Uncertainties come for example from actuators and sensors nonlinearities. The driver demand is translated into torque demand at a given engine speed. This torque demand and engine speeds are inputs of a subsystem that converts them into air and fuel mass in cylinder set-points. Those quantities are converted into pressure set points. The nonlinearity of the actuator induces that one operating point can be obtained with many actuator set points. In addition, to satisfy all new control laws on pollutant emission and fuel consumption the engine systems comes to have several control variables (Exhaust gas recirculation, Throttle valve and waste gate actuator). Due to the definition below this system is a MIMO nonlinear and uncertain system. Coupling phenomenon and nonlinearity can bring some accuracy and instability problems. For reasons of system's robustness against uncertainty and coupling, a robust control design is necessary to ensure performance (accuracy and stability) in all conditions and operating points.

Furthermore, complexity of control engine system increases proportionally with control variables and/or objectives to satisfy. Due to the different type of combustion process and number of actuators and sensors used between spark ignition (SI) and compression ignition (CI) engine, many control process and control methods might be used. However, the control objectives what the engineer wants to satisfy do not differ whenever the engine (SI or CI). Indeed, those objectives are minimization of fuel consumption and pollutant emissions. Considering that and reason of robustness and cost, it will be interesting to develop a unified sequential robust control methodology that can be used in SI and CI engines. This methodology is detailed into this chapter and includes five parts: Input/output definition (A), System modeling (B), System Analysis (C), Control Synthesis (D) and Validation (E). The entire design process is summarized in Fig.2.1.

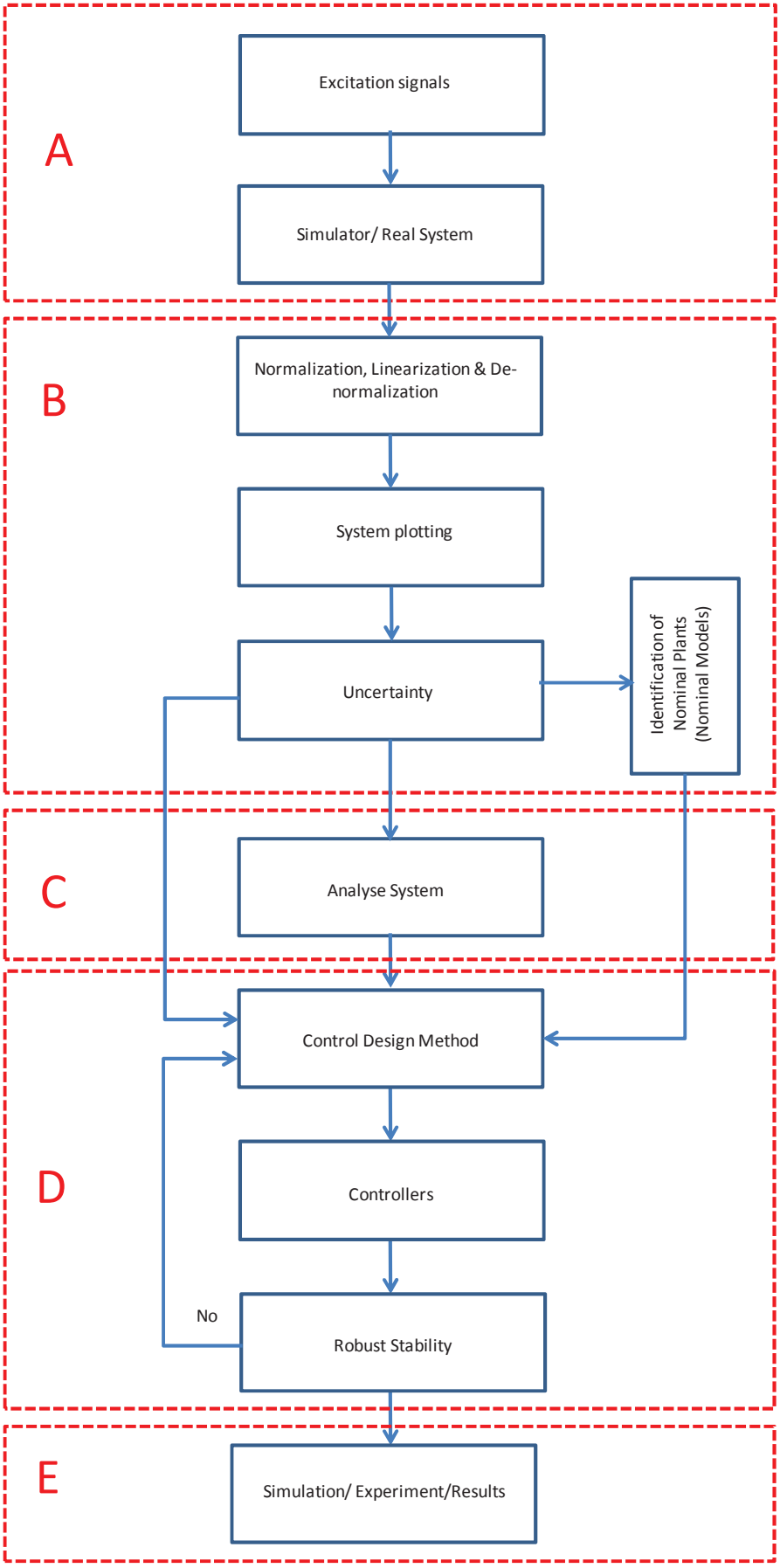

Fig.2.1 Flow chart of the Sequential Robust Control Design Methodology

2.3 System modeling

Our objective is to control a system which can meet a desired performance under some constraints. A classical engineer control approach to developed new control strategies for engine vehicles is an iterative process containing:

Understanding of the system based on a complete physical representation of the system,

Proposition of a control strategy based on a reduced model with simplified equation,

Validation of the strategy on the simulator relying on a much more detailed physics,

Experimental validation.

Hence, for step 1 to 3 some sort of model of system needs to be created to simplified the engineer work. These models are usually mathematic equations and this type of control strategies is called Model-based control design. Three kind of model can be discussed:

Non-thermodynamic model: Usually named *black-box model*, it is not based on physical equations but just on experimental data and leads to an input-output model.

Semi-physical model: It is the modeling method that based on physical principles and experiments to identify all parameters of the plants. This kind of model is named *gray-box model*.

Thermodynamic model: Based only on physical and mathematic equation, no experiments are needed. Generally used to find a model for nonlinear system they are usually called *white-box model*.

The type of model used will depend on a time share that we can loose to create this model and secondly on the degree of precision that is desired. Steps 1 to 3 can be done with different kind of model. Steps 1 and 3 require a physical model or semi-physical because they are steps where simulation results must be as close as possible to the real system. Consequently, to this step we need to create a gray-box model. To step 2, it does not require to have a physical model but just an input-output model with faithful behavior of the system. Generally speaking, engineer in charge of developing a new strategy to control an engine makes these three stages of design with the same gray-box model. That will contribute to great loss of time because it generates many round-trip between stages of modeling, design and validation. Indeed, a behavior previously neglected during stages of design and modeling stages may be blocking during the validation step. In this case the process must be repeated from the beginning. Applied to engine control and more precisely to Air-path control the problem is more complicated because the system is highly non-linear and composed with a large number of complex sub-systems. To reduce the design time of control laws we propose to develop two models:

The first one is a validation and understanding oriented model. It will be a gray-box model based on physics equation whose parameters are calibrated and estimated using data from the test-bench.

The second one is a control oriented model. It will be an input-output model or black-box model obtained by exciting the real system with particular signals. This model will be easy to obtain.

2.3.1 Gray-box model oriented understanding and validation

As mentioned above, the first stage of the proposed methodology is to create a gray-box model of our system. This model will be used to understand the real system and validate control strategy before try it on the real system. The type of model, its structure, its architecture and its complexity depends on the objectives and constraints to satisfy. Generally speaking, for the sake of engine control design validation (simulation and experiment), the engine control model can be classified into two types: high-frequency model and low-frequency model. They are described with more details in [Colin, 2006]:

High-frequency Model: It is the model which simulates the variables in the engine cycle. It is a precise but complicated calculation model, which is able to deal with these variables that cannot be measured easily or non measured variable, for example, the in-cylinder pressure.

Low-frequency Model: This is a mean value engine model (MVEM) used often for the validation of air-path control design of an engine system. This model is usually calibrated using data from test bench.

If we consider the dimension of the model, engine control model can be classified by zero-dimension (0D), one-dimension (1D) or three-dimension (3D) models. Summarized in [Heywood, 1988, Colin, 2006] these engine control models are also detailed as following:

0D model: It is the model which does not consider the spatial space. It takes simple flow models in cylinder, and has been extensively being used due to their models, i.e., short calculation time and less storage in computer. It has been successful to modeling the air/fuel ratio, EGR rates, fuel compositions and other operating parameters in internal combustion engine[Mo, 2008]. It cannot predict the emissions and completeness of combustion precisely, because it cannot easily capture the all/piston quenching effects. Furthermore, the mixing process cannot be captured during its induction [Shah, 2009].

1D model: It considers the acoustic and the gas inertia along one direction. It thus brings a better accuracy. The overall dynamic characteristics of intake and exhaust flows can useful be studied with 1D unsteady fluid model. Consequently, it can improve the accuracy of engine control model because of additional model parameters.

3D model: It is overall complicated physical model that takes three-dimensional for gases' propagation for modeling combustion. Evidently, it provides the best accuracy of modeling and

simulation. However, it increases the computation time and storage space. Hence, it is not too practical in engine control modeling [Shah, 2009]

In our case, a gray-box model is used to validate our control law. We want to build a control law for the air-path of diesel and gasoline engine therefore spatial dimensions are not interesting for us and we just need to have a very high precision on the amount and proportions of air that filled-up the cylinder and passed through the exhaust valve. Consequently we choose a gray-box 0D low frequency model that we will build in parallel of the black-box model (oriented control design). First time-savings is in this stage since choosing two models (one oriented design of the control law and the other oriented validation) allows combining and optimizing time needed for design.

2.3.2 Black-box model oriented control system: frequency identification

In parallel to this step we will also design an input-output model of the real system. To do that and obtained their original information (dynamic and static properties) we used particular signals for exciting all actuators and we captured all sensor signals. To a multivariable the process will be made sequentially. After exciting the first input with a particular signal (multi-sin, PRBS or SBPA) and the other input with a constant value provided by look-up table we collect all the output of the system. This work will be re-applied for each input of the system (Fig.2.2 and Fig.2.3). Section A details excitation signals used. Section B show some linearization and normalization process which will be useful to compare with input and output variables for different operating points and to design a linear controller for a nonlinear system. According to the previous step, a set of input-output frequency response can be obtained and a linear nominal model can be computed (section C).

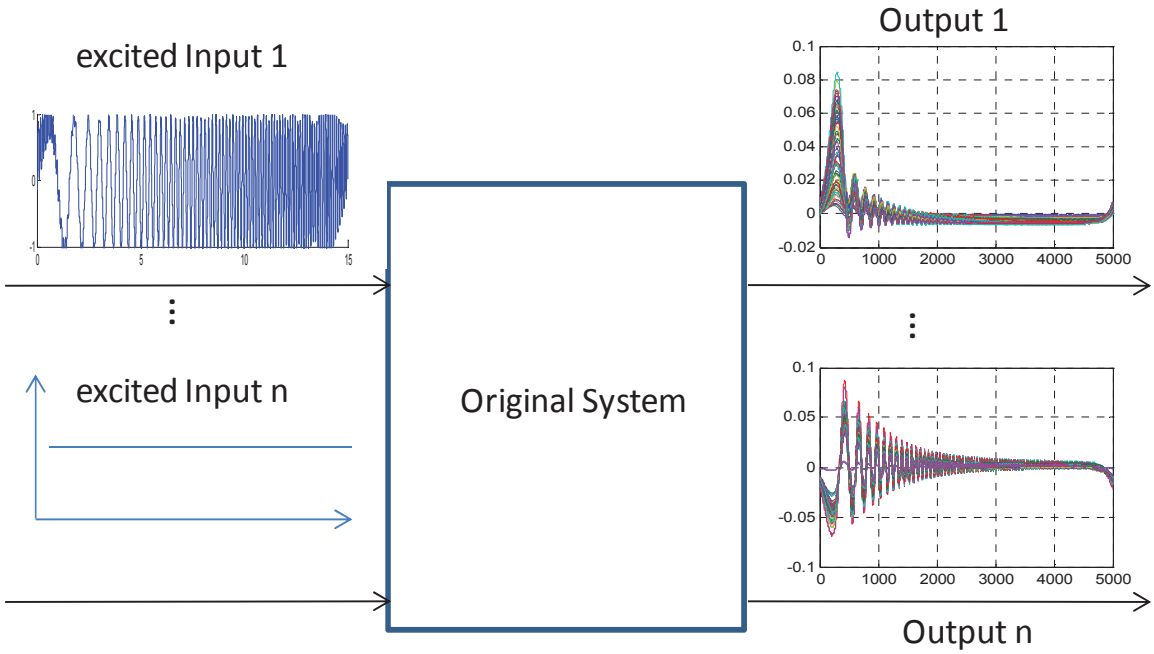

Fig.2.2 Excited signal of the first input to excite the system, get n excited outputs

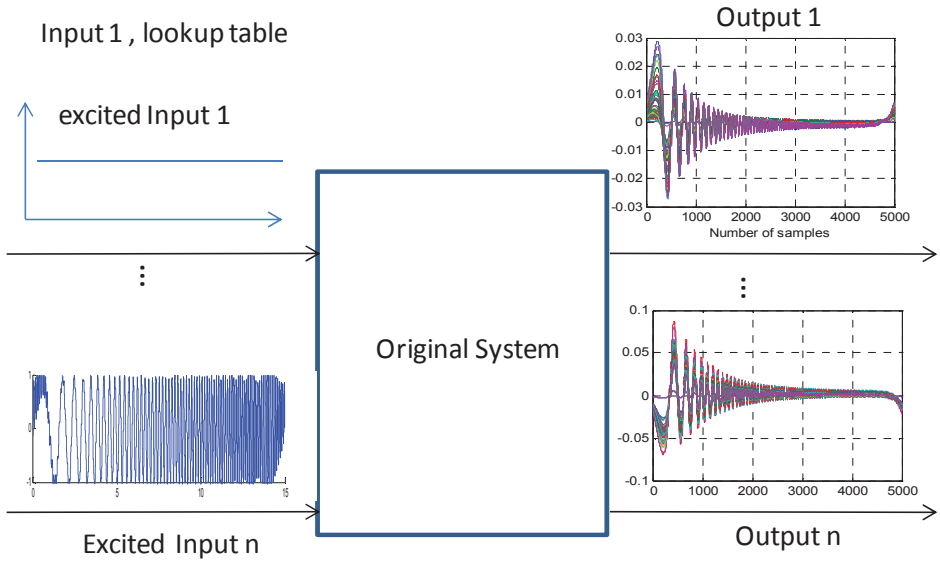

Fig.2.3 Excited signal of the nth input to excite the system, get n excited outputs

a. Signal Excitation

The systems respond to different sorts of input excitations in different ways. Observation of nonlinearity, characterizing or quantifying problem of the system lead to some excitations which are better to others. To derive the dynamic and static information of the system, the excited signals should be chosen between frequency modulated sinusoid (Chirp), pseudo-random binary sequence (PRBS) signals, and sum of sinusoids at different frequencies signal (Multi-sine). Those signals are presented in this section and a temporal representation is shown Fig.2.4.

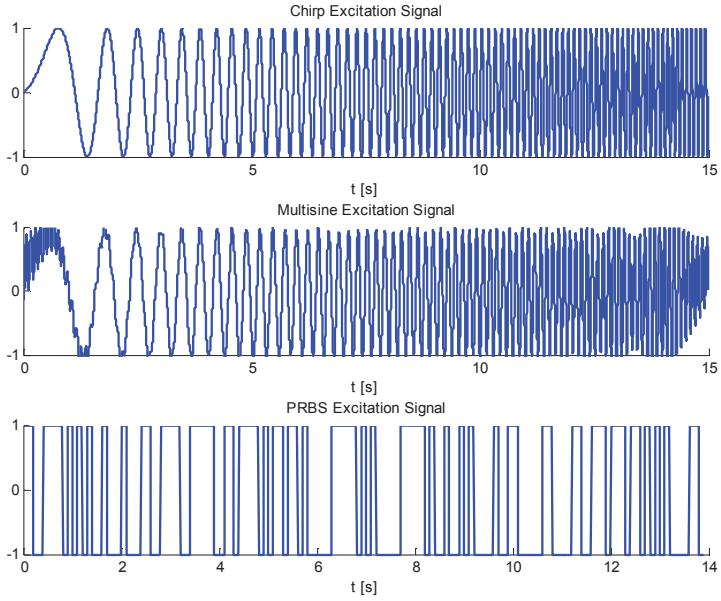

Fig.2.4 Temporal representation of three available signal excitations

Chirp Signals

This form of excitation is sinusoid signal with varying frequency. It can be effective in detecting nonlinearity and combines the frequency range. Chirp excitation can be linear or nonlinear. The nonlinear chirp signal can be designed to have a specific input power spectrum, within which can vary at given frequency range. This simplest form of chirp has a linear sweep characteristic so the signal takes the form

$$f(t) = F\sin\left(\alpha t + \beta t^2\right) \qquad \textbf{(2.1)}$$

where α and β are chosen as proper start (minimum frequency) and end (maximum frequency) frequencies. At any given time, the instantaneous frequency of the signal is

$$\omega(t) = \frac{d}{dt}\left(\alpha t + \beta t^2\right) = \alpha + 2\beta t \qquad \textbf{(2.2)}$$

PRBS Signal

PRBS is one of binary sequence signal which is frequently used for the characterization of high-speed digital I/O interfaces. Because it is one form of noise, a discrete binary signal that switches between -1 and 1, and has ideal spectral properties. It can be easily generated in the laboratory. The actuating signals are of the ON-OFF type and where both the spectrum and the amplitude probability distribution of the test signal are important. Due to its simple hardware implementation, PRBS are used frequently in test and measurement equipment. PRBS codes are known as Maximum length Sequence codes or m-sequences.

Multi-sine Signal

It is a superimposing of a finite number of sinusoids which covers the frequency band from the minimum frequency to maximum frequency. A multi-sine signal is the sum of harmonically related sine waves

$$u(t) = u_0 + \sum_{k=1}^{F} A\cos(2\pi f_k t + \theta_k) \quad \textbf{(2.3)}$$

where $u(t)$ is the excitation signal, u_0 the average value, A the amplitude, F the total number of cosines, k the natural number and $f_k = l_k f_0, l_k \in \mathbb{N}$ the exciting frequencies, f_0 the sampling frequency, and θ_k the variable phase:

$$\theta_k = -k(k-1)\pi / F \quad \textbf{(2.4)}$$

The maximum signal time is determined as $T = 5f_{min}^{-1}$. To avoid leakage effects, only sine waves are received that are periodic with T, wherefore f_{min} and f_{max} might be slightly modified. The deviation between the frequencies in use is $\Delta f = 1/T$. The signal amplitude is not normalized but can be easily scaled utilizing the linear character of the signal.

The exciting signal frequencies f_k are chosen from f_{min} Hz to f_{max} Hz, depending on the system's effective response frequency range, f_0 is set by the Shannon theorem, the amplitude A and the average u_0 are chosen as a function of the system's constraints, such as saturation requirements and noise level [Colin, et al., 2011].

b. Data treatment

Afterwards, linearization and normalization is employed to treat those data and obtained from the original nonlinear system only temporal data with small variation around a constant nominal point (obtained from system's operating points). For all operating point these variables will be much easier to compare. Nevertheless, it is vital that the normalization does not change the fundamental systems characteristics such as stability and input-outputs behaviors [Guzzella, 2007].

Normalization

A nonlinear system is a system which can be defined by a set of nonlinear equations, which may be algebraic, functional, ordinary differential, partial differential, integral or a combination of these. It is one system that cannot satisfy the superposition principle; its output is not directly proportional to the input [Drazin, 1992]. Consider that our nonlinear system is governed by a ordinary differential equations (ODE):

$$\begin{cases} \dfrac{d}{dt} z(t) = f\big(z(t), v(t)\big) \\ w(t) = g(z(t), v(t)) \end{cases} \qquad \textbf{(2.5)}$$

where *z(t)* is state variable, *t* is time variable, *v(t)* and *w(t)* are the input and output variables, respectively.

Generally to time-varying systems, all states variables *z(t)* of the system vary around a nominal constant point z_0 and all inputs *v(t)* and outputs *w(t)* vary around nominal constant $v_0 \neq 0$ and $w_0 \neq 0$. Those constants are associated to the nominal point z_0.

The normalization consists of replacing *z(t), v(t)* and *w(t)* through the transformations :

$$\begin{cases} z(t) = z_0 \cdot x(t) \\ v(t) = v_0 \cdot u(t) \\ w(t) = w_0 \cdot y(t) \end{cases} \qquad \textbf{(2.6)}$$

where z_0 is the nominal point, v_0 and w_0 are the nominal constant input and output, respectively and *x(t)* are the states, *u(t)* the input and *y(t)* the outputs.

Due to this treatment, the new variables *x(t), u(t)* and *y(t)* will have no physical units and will be closed to zero. The derivative of normalized level variable will be:

$$\begin{cases} \dfrac{d}{dt} z(t) = z_0 \cdot \dfrac{d}{dt} x(t) \\ \dfrac{d}{dt} v(t) = v_0 \cdot \dfrac{d}{dt} u(t) \\ \dfrac{d}{dt} w(t) = w_0 \cdot \dfrac{d}{dt} y(t) \end{cases} \qquad \textbf{(2.7)}$$

Because systems that we want to control are always nonlinear and measurement noises [García-Nieto, et al., 2008] choosing one way to simplify data collected from the system to found the black – box model will be very proper and useful. The following normalized system can be then considered and the normalization process is illustrated in Fig.2.5:

$$\begin{cases} \dfrac{d}{dt} x(t) = f_0\big(x(t), u(t)\big) \\ y(t) = g_0(x(t), u(t)) \end{cases} \qquad \textbf{(2.8)}$$

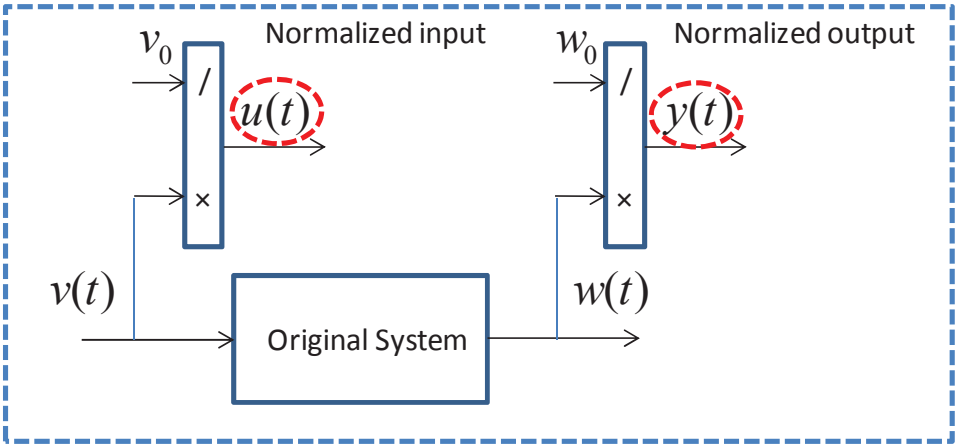

Fig.2.5 The normalized input *u(t)* and output *y(t)* of system

Linearization

It refers to finding the linear approximation to a function at a given point. In the study of dynamical systems, linearization is a method for assessing the local stability of an equilibrium point (x_0, u_0) of a system described by a set of nonlinear differential equations or discrete dynamical systems[Milnor, 2000]. If this equilibrium point has been used to normalize the vector $z(t)$ and the scalar $v(t)$, then the elements of the vector x_0 and scalar u_0 are either 1 or 0. If only small deviations from the normalized equilibrium points are analyzed, the following new variables can be used

$$\begin{cases} x(t) = x_0 + \delta x(t) with \left|\delta x(t)\right| << 1 \\ u(t) = u_0 + \delta u(t) with \left|\delta u(t)\right| << 1 \\ y(t) = y_0 + \delta y(t) with \left|\delta y(t)\right| << 1 \end{cases} \quad \textbf{(2.9)}$$

Due to the usefulness of normalization, it is important to mention that the normalization make the variables of linearization easily defined for small differences. Using Taylor series, the equation (2.9) can be expanded as follows,

$$\frac{d}{dt}\delta x(t) = \left.\frac{\partial f_0}{\partial x}\right|_{x=x_0,u=u_0} \cdot \delta x(t) + \left.\frac{\partial f_0}{\partial u}\right|_{x=x_0,u=u_0} \cdot \delta u(t) + \varphi(2) \quad \textbf{(2.10)}$$

The last term $\varphi(2)$ represents the influence of all higher-than-linear terms.

$$\lim_{\|x\|+\|u\|\to 0} \frac{\|\varphi(2)\|}{\|x\| + \|u\|} = 0 \quad \textbf{(2.11)}$$

This term can be neglected when the equation of (2.9) is met. [Guzzella, 2007]. The linearization is illustrated in Fig.2.6.

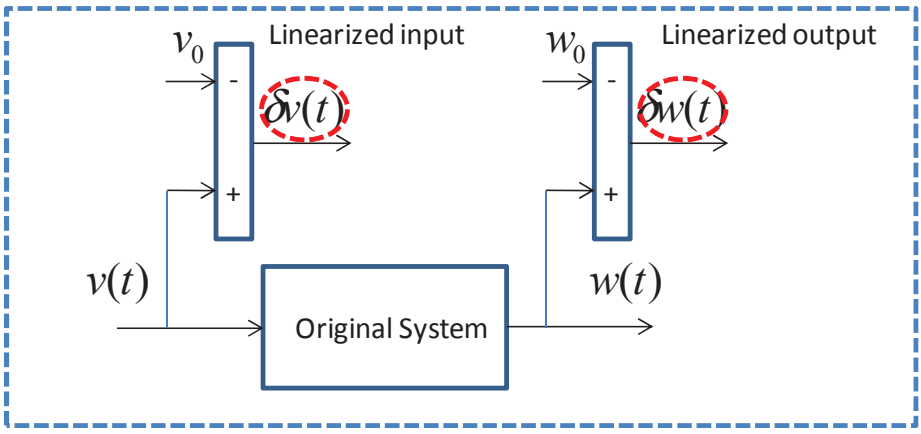

Fig.2.6 The normalized input *u(t)* and output *y(t)* of system

Describing a real dynamic system using a normalized and linearized mathematical model is convenient for analysis and synthesis of appropriate control systems. However, the controller obtained with this normalized and linearized system cannot be directly applied to the real system. Therefore, normalization and de-normalization blocks have to be added on a classical closed – loop control scheme.

De-normalization

The de-normalization is seen in equations (2.12)

$$\begin{cases} x_i(t) = 1 + \dfrac{z_i(t)}{z_{i,0}} \\ u(t) = 1 + \dfrac{v(t)}{v_0} \\ y(t) = 1 + \dfrac{w_j(t)}{w_{j,0}} \end{cases} \qquad \textbf{(2.12)}$$

$$\begin{cases} \dfrac{d}{dt}x_i(t) = \dfrac{d}{dt}z_i(t)/z_{i,0} \\ \dfrac{d}{dt}u(t) = \dfrac{d}{dt}v(t)/v_0 \\ \dfrac{d}{dt}y(t) = \dfrac{d}{dt}w(t)/w_0 \end{cases} \qquad \textbf{(2.13)}$$

Finally, the scheme of normalization, linearization, de-normalization is shown in Fig.2.7 where $x_0(t)$, $u_0(t)$ and $y_0(t)$are chosen as 1.

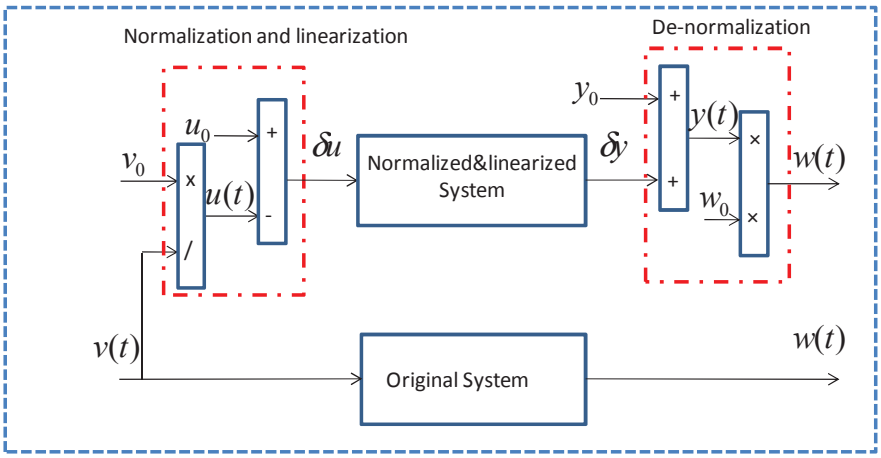

Fig.2.7 Scheme of the normalized and linearized system

Normalization and linearization of the input is given by equation (2.14), de-normalization of the output is given by equation (2.15),

$$\delta u(t) = u_0 - \frac{v_0}{v(t)} \qquad \textbf{(2.14)}$$

$$w(t) = w_0\left(y_0 + \delta y(t)\right) \qquad \textbf{(2.15)}$$

c. Frequency response and nominal frequency identification

In order to describe the system in the frequency domain, a fast Fourier transform is performed on the temporal and normalized data. To obtain the final frequency input-output model of the system cross-correlation, autocorrelation energy and power spectral density functions must be used. All those functions are presented here.

Cross-correlation

It is used to give an idea about the power of diversity of signals, and it is associated with energy and power signals [Shmaliy, 2006]. It is defined as:

$$\Phi_{xy}(\theta) = \int_{-\infty}^{\infty} x(t)y^*(t-\theta)dt \qquad \textbf{(2.16)}$$

where Φ is cross-correlation, x and y are two different shift signals, θ is phase, t is time.

Autocorrelation

It is the cross-correlation of a signal with itself, which is used to find signals with repeating patterns or/and signal influenced by noise, or identify the missing fundamental frequency in a signal simplified by its harmonic frequencies [Wikipedia, 2012]. It is defined by[Salivahanan and Vallavaraj, 2000],

$$R_{xx}(\theta) = \int_{-\infty}^{\infty} x(t)x^*(t-\theta)dt \qquad (2.17)$$

Energy (Power) Spectral Density

It is used to give the power carried by the signal which is defined as following,

$$\mathrm{E}\{R_{xx}(\theta))\} = \int_{-\infty}^{\infty} R_{xx}(\theta)e^{-j\omega\theta}d\theta = X(j\omega)X^*(j\omega) = |X(j\omega)|^2 \qquad (2.18)$$

The phenomenon of aliasing

It occurs if the sampling frequency is less than two times the frequency maximum of the real system. This sampling frequency is called under sampling. It means the signal has a corresponding attenuation of amplitude in the frequency domain, which is calculated by energy spectral density[Marques, 2010]. However, this is not a good signal to be chosen as an excited signal. The following Fig.2.8gives one example about Chirp, PRBS and Multi-sine excited signals' energy spectral density.

Application: how to choose the best signal while considering noise?

In order to validate the process of finding the frequency response of temporal signal we applied this process on the three different signal presented in section A. Using equation (2.16) to (2.18) the energy spectral densities of PRBS, multi-sine and chirp signals are computed in the desired frequencies [0.1Hz 10Hz]. As a result we can see Fig.2.8 that multi-sine signal generates less numerical noise than the other excited signals, thus it is an ideal signal excitation for system's modeling and identification.

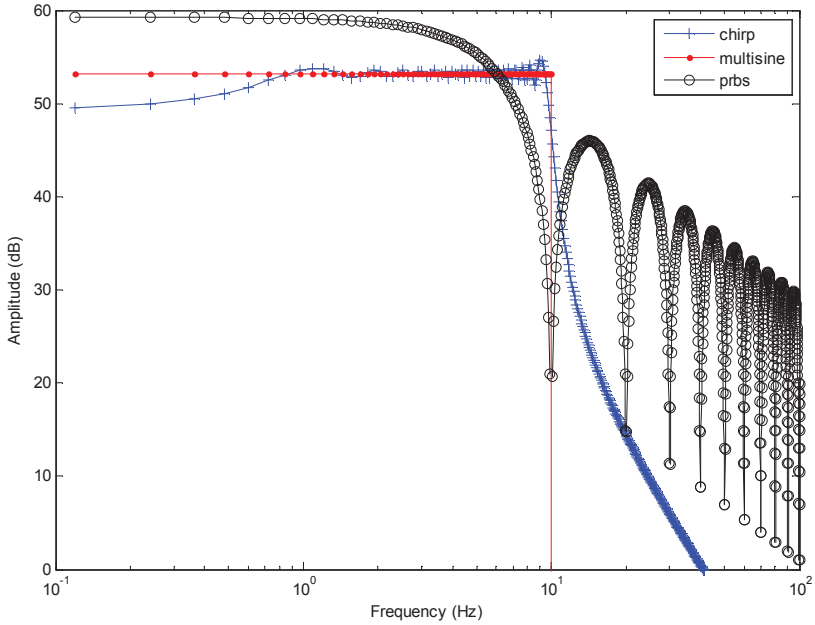

Fig.2.8 Responses of three signal excitations

After that the nominal process is chosen using the following equation:

$$G_{nom}(j\omega) = \frac{\overline{G(j\omega)} + \underline{G(j\omega)}}{2}, \forall \omega \qquad \textbf{(2.19)}$$

where $G_{nom}(j\omega)$ is the nominal process, $\overline{G(j\omega)}$ is the maximum of gain for all process at a given frequency, and $\underline{G(j\omega)}$ is the minimum of gain for all process at a given frequency. Simple linear models are finally obtained by minimizing the loss function with the sum of square errors(2.20), which is available in the system identification toolbox of Matlab®. There should be one model that can represent the nominal diagonal process of $G_{nom}(j\omega)$ well.

$$e(i) = y(i) - \hat{y}(i) \qquad \textbf{(2.20)}$$

where e is computed as the difference between the measured process output $y(i)$ and the model output $\hat{y}(i)$ for a given number N of training data samples i=1,..., N (N is called training data set). It is shown in Fig.2.9.

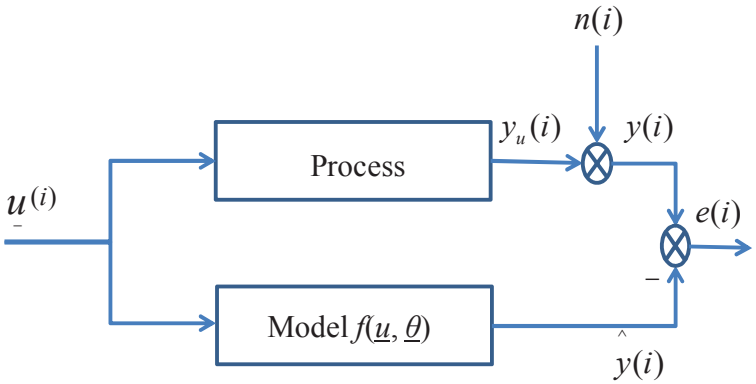

Fig.2.9 Process and model identification

2.4 MIMO system analysis

In order to analyze the coupling and uncertainty of the system, one systematic analysis methodology is proposed using Condition Numbers (CN), Relative Gain Array (RGA), Gershgorin Bands (GB) and Column Diagonal Dominant Degree (CD^3) tools.

2.4.1 Singular Values (SV)

Singular values are used to obtain reliable information about the plant principal gains of the system and indicate the largest and smallest gains for any input direction [Skogestad and Postlethwaite, 2005]. It is also one way to study the effect of input uncertainty.

Definition 1: Singular values are the square roots of the largest eigenvalues of the system:

$$\sigma_i(G(j\omega)) = \sqrt{\lambda_i(G(j\omega)^* G(j\omega))} = \sqrt{\lambda_i(G(j\omega)G(j\omega))^*} \quad \textbf{(2.21)}$$

λ_i is the eigenvalue of *G(jω)* G(jω)** and *G(jω)G(jω)*, G(jω)**is the transposed and conjugate matrix of *G(jω)**, σ_i is the i^{th} singular value of the system. *SV* can be computed using several methods like eigenvalue (2.22), singular value decomposition (2.23)or norm method.

a. Singular value Decomposition (SVD) method

The singular value decomposition method applied on a $m \times m$ real or complex matrix G is a factorization of the form:

$$G(j\omega) = U(j\omega)\Sigma(j\omega)V^T(j\omega) \quad \textbf{(2.22)}$$

where *U(jω)* is a $m \times m$ real or complex unitary matrix, *Σ(jω)* is an $m \times m$ diagonal matrix with nonnegative real numbers and *V*(jω)* (the conjugate transpose of *V*(*jω*)) is a $m \times m$ real or complex unitary matrix. The diagonal entries σ_i of *Σ(jω)* are known as the singular values of G [Wall M. E., et al., 2003].

$$\sum(j\omega) = diag(\sigma_1(j\omega), \sigma_2(j\omega), \ldots, \sigma_{\min}(j\omega)) \quad \textbf{(2.23)}$$

with

$$\sigma_1(j\omega) \geq \sigma_2(j\omega) \geq \ldots \sigma_{\min}(j\omega) \quad \textbf{(2.24)}$$

b. Norm method

$$\sigma_k(G(j\omega)) = \left\| G(j\omega)v_k(j\omega) \right\|_2 = \frac{\left\| G(j\omega)v_k(j\omega) \right\|_2}{\left\| v_k(j\omega) \right\|_2} \quad \textbf{(2.25)}$$

Where $v_k(j\omega)$ is the k^{th} columns of *V(jω)* named the input principal directions. This array has the special property that their gains are precisely the corresponding singular values. Consequently, the output response corresponding to the k^{th} columns of *U(jω)* equals to $G(j\omega)v_k(j\omega)$in fact will be equal to $\sigma_k(j\omega)$ times the k^{th} column of $U(j\omega)$. The columns of $U(j\omega)$ are commonly named the output principal directions and the $\sigma_k(j\omega)$the principal gains [Skogestad and Postlethwaite, 2005].

c. Maximum and minimum singular values.

They can be shown that the largest gain for any input direction is equal to the maximum singular value:

$$\bar{\sigma} = \sigma_1(G) = \max_{v \neq 0} \frac{\|Gv\|_2}{\|v\|_2} = \max_{\|v\|_2 = 1} \|Gv\|_2 \qquad (2.26)$$

And the smallest gain for any input direction (excluding the "wasted" inputs in the null space of G for cases with more inputs than outputs) is equal to the minimum singular value

$$\underline{\sigma} = \sigma_m(G) = \min_{v \neq 0} \frac{\|Gv\|_2}{\|v\|_2} = \min_{\|v\|_2 = 1} \|Gv\|_2 \qquad (2.27)$$

Thus, for any vector *d*, we have

$$\underline{\sigma}(G) \leq \frac{\|Gv\|_2}{\|v\|_2} \leq \bar{\sigma}(G) \qquad (2.28)$$

Defining $u_1 = \bar{u}, v_1 = \bar{v}, u_k = \underline{u}$ *and* $v_k = \underline{v}$, then it follows that

$$G\bar{v} = \bar{\sigma}\bar{v}\,,\; G\underline{v} = \underline{\sigma}\underline{v} \qquad (2.29)$$

The vector $\bar{v}$ corresponds to the input direction with largest amplification, and $\bar{u}$ is the corresponding output direction in which the inputs are most effective. The directions involving $\bar{v}$ and $\bar{u}$ are sometimes referred to as the "strongest", "high-gain" or "most important" directions (Fig.2.11). The next most important directions are associated with v_2 and u_2, and so on until the "least important", "weak" or "low-gain" directions which are associated with $\underline{v}$ and $\underline{u}$[Skogestad and Postlethwaite, 2005].

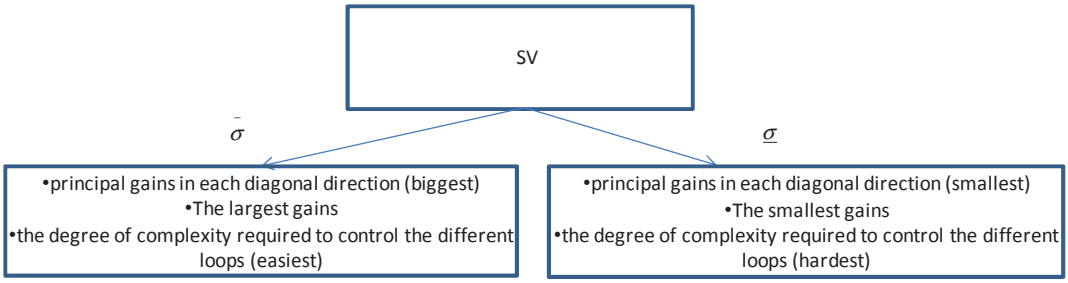

Fig.2.10 Scheme of SV

2.4.2 Condition Number (CN)

Condition number is a way to quantify the degree of directionality, and it is rigorously related to system error sensitivity and robustness, but it is scale dependent[Grosdidier, et al., 1985]. A large condition number indicates sensitivity to unstructured uncertainty. It is a measure of the sensitivity of the solution to system perturbations. Hence, it is a possible measure of the difficulty of controlling the system.

Definition 2: the condition number $\gamma(G)$ is defined by

$$\gamma(G) = \overline{\sigma}(G) / \underline{\sigma}(G) \qquad \textbf{(2.30)}$$

If γ is large (normally larger than 10), we say that it is **ill-conditioned**; and if γ is smaller (near 1), we say it is **well-conditioned**.

The CN depends strongly on the scaling of the inputs and outputs. To be more specific, if $D_I(s)$ and $D_O(s)$ are two diagonal scaling matrices, then the CN of the matrices $G(s)$ and $D_I(s).G(s).D_O(s)$ may be arbitrarily different. In general, the matrix $G(s)$ should be scaled on physical grounds, for example, the system can be divided each input and output by its largest expected or desired value.

The CN has been used as an input-output controllability measure, in particular it has been postulated that a large CN indicates sensitivity to input unstructured uncertainty and may indicate control problems:

- A large CN may be caused by the smallest value of SV, which is generally undesirable,
- A large CN may mean that the plant has a large minimized CN, or equivalently, it has large RGA elements which indicate fundamental control problems,
- A large CN does imply that the system's control performance is sensitive to "unstructured" (full block) input uncertainty (e.g. with an inverse-based controller).

A worst case analysis is particularly useful for ill-conditioned systems in the cross-over frequency range. This is due to the fact that such systems may provide large difference between nominal and robust performance.

Because of the dependence of CN, the best scaling matrix can be used to optimize the system, which lead to optimal condition number (OCN) tool. OCN is scale independent; it is used to find the minimum condition number over all possible scales by adding two diagonal scaling matrixes. This tool eliminates the scaling step necessary if we use the condition number tool only.

Definition 3 (Optimal Condition Number)

$$\gamma^*(G) = \min_{D_O, D_I} \gamma(D_O G D_I) \qquad \textbf{(2.31)}$$

where D_O and D_I are diagonal scaling matrices.

The OCN can also be computed by

$$\gamma^*(G) = \left\|\Lambda\right\|_{i1} + \sqrt{\left\|\Lambda\right\|_{i1}^{\ 2} - 1} \qquad \textbf{(2.32)}$$

$|| \Lambda ||_{i1}$: Induced 1-norm (maximum column sum) of the RGA-matrix (see following section for the definition of RGA) of G [Skogestad and Postlethwaite, 2005]. Besides, it is important to note that if OCN is large that implies large elements in the RGA [Grosdidier, et al., 1985].

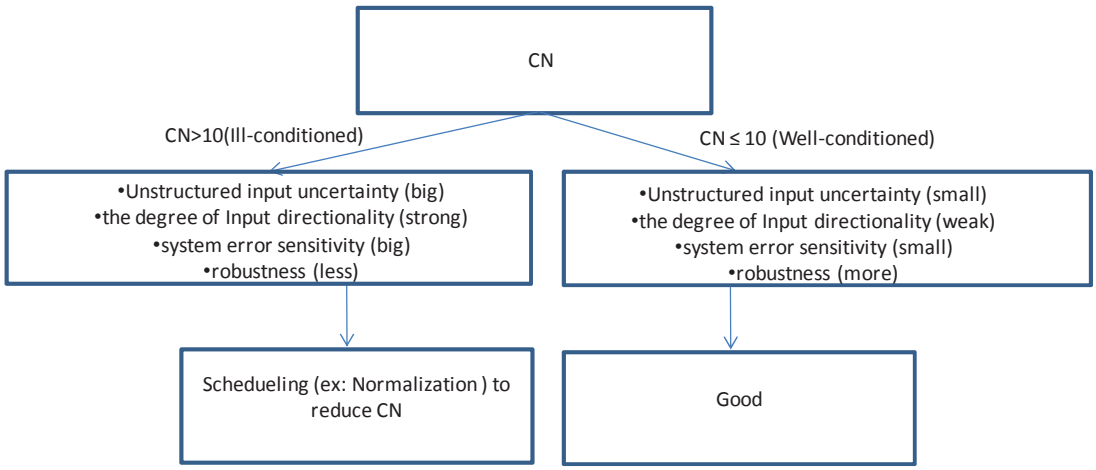

Fig.2.11 Scheme of CN

2.4.3 Relative Gain Array (RGA)

RGA is an indicator of sensitivity to uncertainty for a coupled system. It measures the degree of interaction or decoupling, in order to detect the potential difficulty of achieving robustness considering a diagonal multiplicative uncertainty at the plant input [Skogestad and Havre, 1996]. It provides a way of finding the desired pairing between controlled variables and manipulated variables [Skogestad and Postlethwaite, 2005]. The RGA, which is scale independent [Grosdidier, et al., 1985] is defined for a square system.

Definition 4: The relative gain array (RGA) of a nonsingular complex matrix G is a complex matrix, which is defined as [Skogestad and Postlethwaite, 2005]:

$$\Lambda(G(j\omega)) = G(j\omega) \times (G(j\omega)^{\dagger})^{T} \qquad \textbf{(2.33)}$$

where $G(j\omega)$ is a MIMO system at frequency ω, $\times$ represents element-by-element multiplication (Schur product) and $G(j\omega)^{\dagger}$ is the inverse of $G(j\omega)$ (pseudo-inverse for non-square matrix). The RGA matrix has number of interesting algebraic properties, of which the most important properties:

- it is independent of input and output scaling,
- its rows and columns sum to 1,
- the RGA is the identity matrix if G is upper or lower triangular,
- a relative change in an element of G equal to the negative inverse of its corresponding RGA element, $g_{ij} = g_{ij}(1 - 1/\lambda_{ij})$ yields singularity,
- plants with large RGA elements are always ill-conditioned, but the reverse may not hold,
- large RGA elements (larger than 10) at important frequencies for the control design indicates that the plant is fundamentally difficult to control due to strong interactions and sensitivity to uncertainty,

- diagonal input uncertainty is usually of more concern for plants with large RGA elements,
- if the sign of an RGA elements changes as we go from s=0 to s= ∞, then there is a RHP-zero in G or in some subsystem of G.

The usefulness of the RGA is summarized as two pairing rules:

Pairing 1: prefer pairings such that the rearranged system, with the selected pairings along the diagonal, has an RGA matrix close to identity at frequencies around the closed-loop bandwidth.

Pairing 2: avoid pairing on negative steady-state RGA elements as possible as one can.

Generally speaking, for a general square or non-square matrix which can be utilized the equations as follows,

$$\sum_{i=1}^{j} \lambda_{ij} = \left\| e_j^T V_r \right\|_2^2 < 1 \qquad \textbf{(2.34)}$$

$$\sum_{i=1}^{j} \lambda_{ij} = \left\| e_j^T W_r \right\|_2^2 < 1 \qquad \textbf{(2.35)}$$

Here V_r contains the r^{th} input singular vector for G, and e_j is an m x 1 basis vector for input r; e_i=[0 ...0 1 0 ... 0]^T where 1 appears in position j. W_r contains the first r output singular vectors for G, and e_i is an l x 1 basis vector for output wi; e_i =[0 ...0 1 0 ... 0]^T where 1 appears in position i.

From this it also follows that the rank of any matrix is equal to the sum of its RGA elements. Let the l *x* m matrix G has rank r; then

$$\sum_{i,j} \lambda_{ij}(G) = rank(G) = r \qquad \textbf{(2.36)}$$

The Non-square RGA matrix has two most important criteria to pair the inputs and outputs[Chang and Yu, 1990]:

- Input selection criteria: the input selection criterion is based on the sum of Λ columns. The i^{th} input is considered effective if the sum of the i^{th} column is large and vice versa. Therefore, the input that corresponds to the column with smallest sum can be eliminated. For m > n, NRGA is input scaling dependent,
- Output selection criteria: the output that corresponds to the row with smallest sum can be eliminated. For n > m, the NRGA is output scaling dependent.

The way to use this tools to determine if the controller must be centralized or decentralized is detailed in Fig 12.

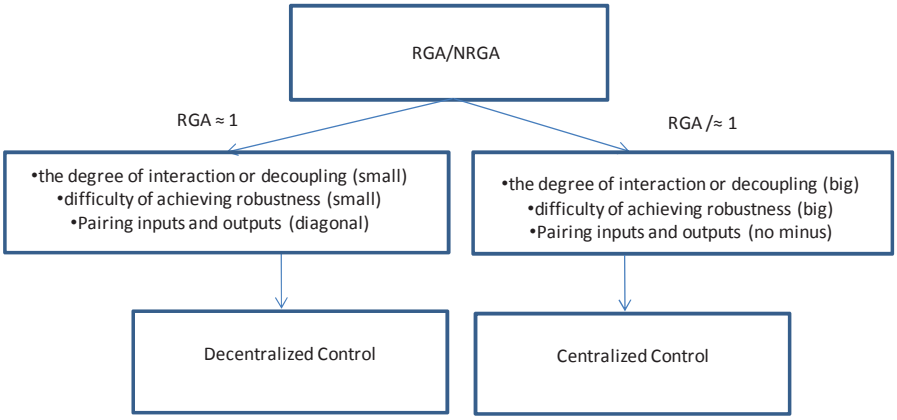

Fig.2.12 Scheme of RGA

2.4.4 Gershgorin Bands (GB)

For a MIMO system, the Gershgorin bands theory is a way to determine the coupling grade and the stability. If the Gershgorin bands are thin and exclude the critical point -1, the system G(s) is diagonally dominant and stable. It can then be considered as a decoupled system and so a decentralized controller will be sufficient [Garcia, et al., 2005].

Definition 6: In mathematics, a matrix is said to be diagonally dominant if for every row of the matrix, the magnitude of the diagonal entry in a row is larger than or equal to the sum of the magnitudes of all the other (non-diagonal) entries in that row. More precisely, the matrix G is diagonally dominant if

$$|g_{ii}| > \sum_{j \neq i} |g_{ij}| \qquad for\ all\ i \qquad (2.37)$$

Where g_{ij} denotes the entry in the i^{th} row and j^{th} column of G [Gene and F. Van., 1996].

Definition 7: Let G is a complex mxm matrix, with entries v_{ij}. For $i \in \{1,\ldots,n\}$, let $R_i = \sum_{i=1, i \neq j}^{m} |g_{i,j(s)}|$ be the sum of the absolute values of the entries in the i_{th} row. Let $D(g_{ii}, R_i)$ be the closed disc centered at g_{ii} with radius R_i. Such a disc is called a Gershgorin Disc[Gershgorin, 1931] .

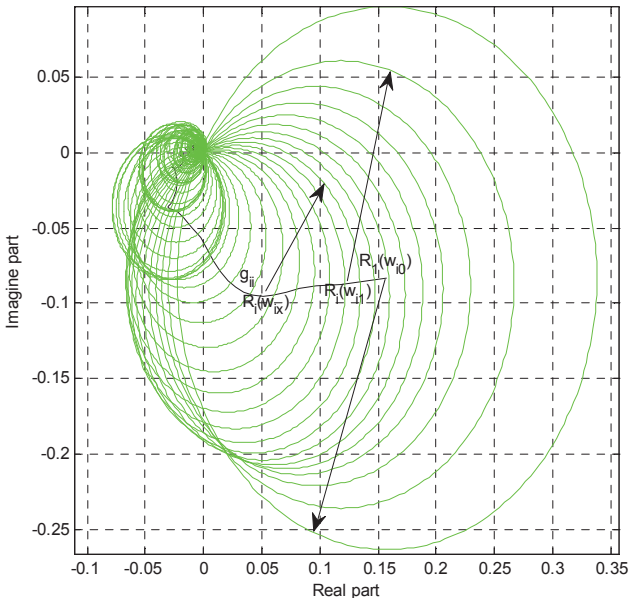

Fig.2.13 Nyquist plot of Gershgorin bands

Definition 8: On the Nyquist diagram of $g_{i,i}(s)$, on each point a circle with a radius of $min(\sum_{i=1,i\neq j}^{m}|g_{i,j(s)}|, \sum_{i=1,i\neq j}^{m}|g_{j,i(s)}|)$ is super imposed, which corresponds to the effect of the non-diagonal elements. The bands obtained in this way are called Gershgorin Bands [Skogestad and Postlethwaite, 2005].

Theorem 1: if the Gershgorin bands centered on the R_i exclude the origin (i.e. $G(s)$ is column diagonally dominant), the system is stable if and only if:

$$\sum_i n(g_{ii}) = -p_o \qquad \textbf{(2.38)}$$

where $g_{ii}$is the diagonal matrix, n is clockwise encirclements of g_{ii}, p_0 is the number of poles of the closed loop system in the right half plane.

Theorem 2: f the Gershgorin bands centered on the l_{ii} exclude the critical point -1 (i.e. $G(s)$ is diagonally dominant), the system is stable if and only if:

$$\sum_i n(l_{ii}) = -p_o \qquad \textbf{(2.39)}$$

where l_{ii} is diagonal closed-loop system's open loop gain.

Theorem 1 and Theorem 2 are only sufficient not necessary stability conditions due to be the nyquist chart analysis. If the bands overlap the critical point, conclusions about the stability or instability of the closed-loop system cannot be made, but we can conclude on the type of control system we can use (centralized, Decentralized or Multi-SISO) (Fig14).

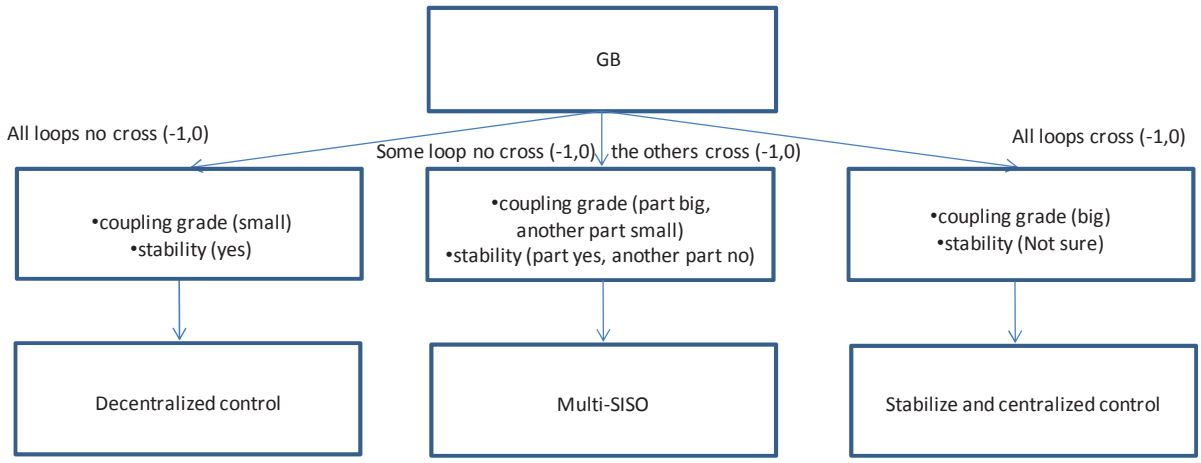

Fig.2.14 Scheme of GB

2.4.5 Column Diagonal Dominant Degree (CD^3)

CD^3 is a tool to analysis the system whether to use a simple Multi-SISO control method. To be more precise, if only considering the columns of the MIMO system, CD^3 can derive the conclusion that whether the system is applicable to use a simple Multi-SISO.

The worst-case size of the unstructured multiplicative uncertainty that needs to be taken into account to design a decentralized controller with the multi-SISO approach is given by the coupling degrees

$$\tau_{ci}(\omega_k) = \max\left\{ \sum_{\substack{1\le j\le N,\\ and j\neq i}} \frac{\left|G_{ji_n}(j\omega_k)\right|}{\left|G_{ii_n}(j\omega_k)\right|} \right\} for 1 \le i \le N \qquad \textbf{(2.40)}$$

at frequency ω_k, where τ_{ci} is the coupling degrees, G_{ii} is the diagonal plant, $G_{ji(i\neq j)}$ is the non-diagonal plant.

When within the desired closed-loop bandwidth all τ_{ci} are much smaller than 1, a decentralized controller can be designed with the multi-SISO approach (as the ellipsoids that model the unstructured uncertainty domain are small)[Colin and Chamaillard, 2011].

Finally, these tools functions can be collected as following (Fig 15). Thus, the control strategy is synthesized by this information, which is supported to understand system's coupling and uncertainty, and to choose the configuration of the control system.

,

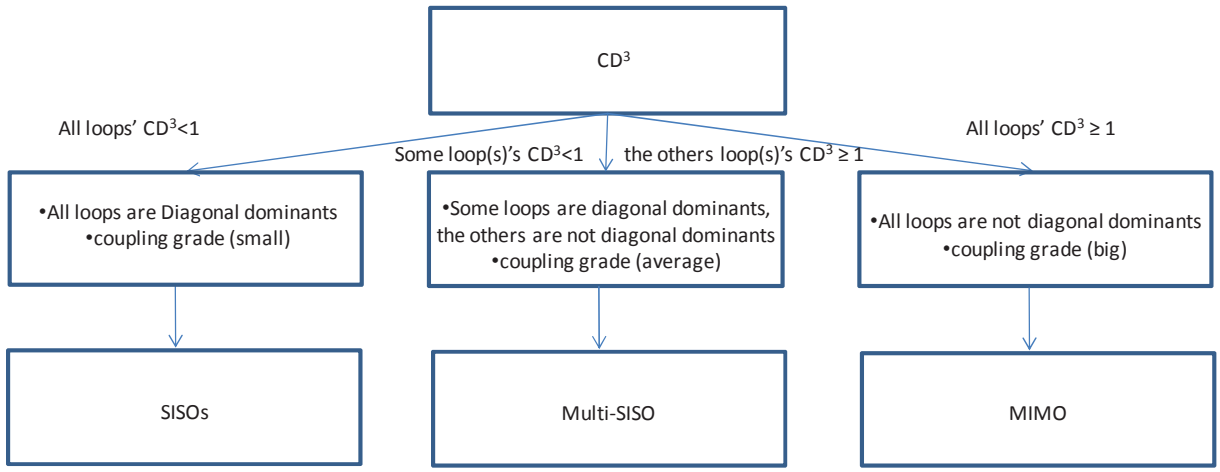

Fig.2.15 Scheme of CD³

2.5 Multi-SISO control system design

2.5.1 Specifications

The control design scheme depends on many factors such as reliability, complexity of the system and on whether the transfer function of the system is known or not. There are two methods to set the specifications in frequency domain and in time domain. In any case, the "best" possible controller C(s) has to be designed or selected and tuned, such that the desired performance specifications are met. A general control design scheme is presented in Fig.2.16.

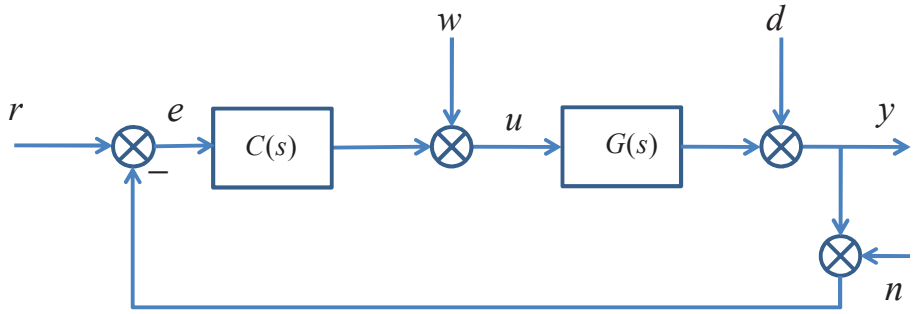

Fig.2.16 Standard feedback control system structure

where r is the reference signal, e is the error, w is the input system's disturbance, d is the system's output disturbance, n is the sensor noise, u is the input signal of the system.

The designed closed-loop system should at least fulfill these requirements:

1) the closed-loop system has to be stable,
2) disturbances $d(t)$ should have only a minimal influence on the controlled variable $y(t)$,
3) the controlled variable $y(t)$ must be able to track the reference signal $r(t)$ as fast and accurately as possible,
4) The closed-loop system should not be too sensitive to parameter changes of the plant.

To be able to access the performance of 2 and 3, in the ideal case, the relationship among errors, the process and the controller need to be quantified and these equations have to be satisfied:

$$G_D(j\omega) = \frac{Y(s)}{D(s)} = \frac{E(s)}{R(s) - D(s)} = \frac{1}{1 + G(s)C(s)} = 0 \qquad \textbf{(2.41)}$$

$$G_R(j\omega) = \frac{Y(s)}{R(s)} = \frac{Y(s)}{R(s) - N(s)} = 1 - G_D(j\omega) = \frac{G(s)C(s)}{1 + G(s)C(s)} = 1 \qquad \textbf{(2.42)}$$

where G_D is the disturbance rejection function, and G_R is the tracking transfer function that provides

d. Time domain Specifications

The proposed methodology is a model-based one, consequently to design the controller we must found a good nominal model to represent the system, either in the form of a differential equation or a transfer function $G_n(s)$. The nominal transfer function found at the end of the black-box modeling step will be used here. Generally speaking, the performance of feedback control systems includes two tasks: stead-state performance, which specifies accuracy when all the transients are decayed, and transient performance, which specifies the speed of response as discussed below.

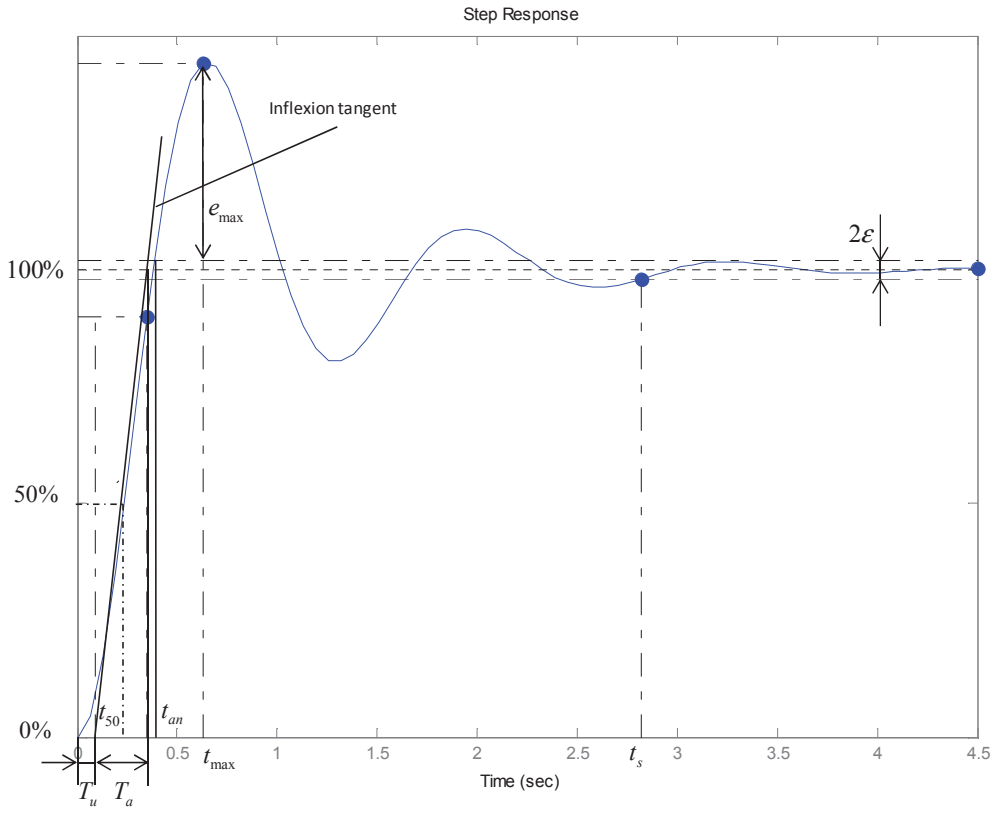

Fig.2.17 Response of step signal for tracking performance input main parameters of transient performance

The transient performance is usually defined for a step reference or step disturbance input response as shown in Fig.2.17. And these specifications are details below:

- σ% (Peak overshoot): It is defined as the maximum value of the response-time t_{max} in relation to its desired final value. It can be considered to be a measure of the relative stability of the system. It is given as below,

$$\sigma\% = \frac{y(t_{\max}) - y(t_n)}{y(t_n)} * 100\% \qquad \textbf{(2.43)}$$

  where t_{max} is the time of peak overshoot, t_n is the time of first reaching at the desired value, $y(t_{max})$ is the response value of the t_{max}, $y(t_n)$ is the response value of the t_n.
- e_{ss} (tracking steady-state error): It is defined as the equation (2.44) with the final-value theorem of the Laplace transform.

$$e_{ss} = \lim_{t\to\infty} e(t) = \lim_{s\to 0} \frac{sR(s)}{1+G(s)} \qquad \textbf{(2.44)}$$

- T_a (Rising time): It is defined as the time required for a response to go from 10% to 90% of its desired final value. Or as the time interval given be the intersection points of the inflexion tangent with the 0% and 100 % lines.
- T_u (Delay time): It is defined as the time required that the inflexion tangent line crosses the time axis.
- t_s (Setting time): It is defined as the time after which the response remains with a band of $\pm$ ε% about the desired final value, where ε is selected between 2% and 5%. It can be considered to be a measure of the relative stability of the system.
- t_{an} (Reaching time): It is defined as the maximum value of the response time t_{max} in relation to its desired final value. It can be considered to be a measure of the relative stability of the system.

e. Frequency Domain Specifications

Reasonable desired performances have been fixed as a function of the system dynamics and physical properties. The issue of specification is using the frequency-domain approach. Here, we present the upper bounds for the frequency responses of the complementary sensitivity function $T(j\omega)$ and the sensitivity function $S(j\omega)$. The following equation shows the relation between output, disturbance input and noise input.

$$Y(j\omega) = S(j\omega)\cdot D(j\omega) - T(j\omega)\cdot N(j\omega) \qquad \textbf{(2.45)}$$

The benefits of the proposed frequency-domain formulation are its precise arguments, the immediate interpretation in the frequency domain and the possibility to later integrate these

specifications in a systematic synthesis process. But the drawback of the frequency specification is that the specifications are directly formulated for the closed-loop system. Hence, to clarify what time-domain properties may be expected even if the specifications are met the relationship between time domain and frequency domain specifications will be detailed at the next paragraph. In additions, designing a proper controller *C(s)* is more difficult as working with closed-loop specifications renders this task. The specifications depend on the order of the system. The common designed equations are written in Table.2.1.

Table.2.1 Specification parameters for 1st, 2nd and 3rd order systems

System Order	Parameters	Representations
1st	T(s)	$\frac{\omega_n^{\,2}}{s^2+2\xi\omega_n s+\omega_n^{\,2}}$
	S(s)	$\frac{s^2+2\xi\omega_n s}{s^2+2\xi\omega_n s+\omega_n^{\,2}}$
2nd	T(s)	$\frac{\alpha\omega_n^{\,3}}{(s+\alpha\omega_n)(s^2+2\xi\omega_n s+\omega_n)}$
	S(s)	$\frac{s^3+(2\xi\omega_n+a\omega_n)s^2+(2a\xi\omega_n^{\,2}+\omega_n^{\,2})s^2+a\omega_n^{\,3}}{(s+\alpha\omega_n)(s^2+2\xi\omega_n s+\omega_n)}$
3rd	T(s)	$\frac{Rrq\bar{q}}{(s+R)(s+r)(s+q)(s+\bar{q})}$
	S(s)	$1-\frac{Rrq\bar{q}}{(s+R)(s+r)(s+q)(s+\bar{q})}$
		$R=\xi\omega_n,\ r=15\xi\omega_n,$
		$q=-2\xi\omega_n+\omega_n\sqrt{1-\xi^2}i,\ \bar{q}=-2\xi\omega_n-\omega_n\sqrt{1-\xi^2}i$

f. The relationship between time domain and frequency domain specifications

Generally speaking, the performance of feedback control systems includes two tasks: steady-state performance, which specifies accuracy when all the transients are decayed, and transient performance, which specifies the speed of response. In the time domain, steady-state error (e_{ss}) can be considered to be the accuracy of steady-state performance, peak overshoot (e_{max}) and setting time (t_s) can be considered to be the speed of response at transient's state. In the frequency domain, the resonant peak of complementary sensitivity function T corresponds to the steady-state performance, and the bandwidth ω_b of sensitivity function $S(j\omega)$ corresponds to

the transient performance. In addition, the degree of stability can be measured by the modulus margin ΔM in time domain, which is governed by the resonant of $S(j\omega)$ in the frequency domain. The relationship between time and frequency domain specifications are shown as following,

$$t_s \approx 3/\omega_b \quad \textbf{(2.46)}$$

$$t_s = \frac{-\ln 0.02 - \ln\sqrt{1-\xi^2}}{\xi\omega_n} \approx 3T_a \quad \textbf{(2.47)}$$

$$\xi = \sqrt{\frac{(\ln\sigma/\pi)^2}{1+(\ln\sigma/\pi)^2}} \quad \textbf{(2.48)}$$

$$\omega_n = \frac{\pi - \arccos\xi}{T_a\sqrt{1-\xi^2}} \quad \textbf{(2.49)}$$

$$G_s = -20\log_{10}|\Delta M| \quad \textbf{(2.50)}$$

where G_s is the resonant peak of $S(j\omega)$, ΔM is the modulus margin of the system in the nyquist chart.[Doré Landau, et al., 2011]. Furthermore, the system's response and performance really depend on one range of frequency ω_c, which is called the cutoff frequency, defined as the frequency at which the ratio of (output/input) has a magnitude of 0.707. It can be equally converted by the magnitude value given as below,

$$-20\log_{10}\left|\frac{Output}{Input}\right| = 3dB \quad \textbf{(2.51)}$$

If the sensitivity function is considered here, ω_c is described by an increase of 3dB from the start frequency [Stanley, 1998].

2.5.2 Proportional, Integral, Derivative and Acceleration control design

Linear system with order greater than 2 cannot be treated easily by the classical PID pole placement method. Due to the fact that PID cannot offer enough poles which the third orders systems need. Hence, finding controllers that can deal with this matter is very necessary. This paragraph presents a PIDA pole placement method which can deal with this issue. Considering the transfer function of the system $G(s)$ written:

$$G(s) = \frac{K_p}{\prod_{i=1}^{n} (1 + sT_i)^i} \quad \textbf{(2.52)}$$

where n is the order of the linear system. If the order of the system is less than two, a conventional pole placement design can be used [Mikleš and Fikar, 2007]. The corresponding PID controller can be written as:

$$C(s) = K\left(1 + \frac{1}{sT_i} + sT_d\right) \quad \textbf{(2.53)}$$

And the closed-loop transfer function will be written as:

$$T(s) = \frac{C(s)G(s)}{1 + C(s)G(s)} \quad \textbf{(2.54)}$$

Finally, the pole placement methodology consists on finding poles and zeros of the controllers by identification between the following equation and the desired dynamic of the closed-loop (57):

$$1 + C(s)G(s) = 0 \quad \textbf{(2.55)}$$

For example, to a first order system the transfer function generally used to model the closed-loop dynamic is a second order linear transfer function:

$$s^2 + 2\xi\omega_n s + \omega_n = 0 \quad \textbf{(2.56)}$$

where ω_n is the desired natural frequency, and ζ is the desired damping ratio.

For system with order greater than 2 PID pole placements cannot be used, classical PID is augmented with acceleration that mean one more zero, and consequently will be name PIDA. PIDA pole placement presented here has three zeros and four poles [Jung. S. and Dorf. R. C., 1996], because only the complex poles play the role of dominance, and the rest of two poles could be neglected, which are chosen 10 times left far from the dominant poles. Due to this one more zero, the third order system can choose these two dominant poles easily by eliminating the rest non-dominant poles. The PIDA control structure is defined in equation (2.57) without filter on velocity and acceleration and in equation (2.58) with filters. In real applications, the differentiator is often quite sensitive to high frequency and it is not easy to be adopted in practical implementations, for the convenience of application, most of the time, it is switched off. [Astrom and Hagglund, 2005]. Additionally, in PID control, due to the original controller being non-proper transfer function, which must be modified to be proper so that can be implemented in real industrial system. Here, the differentiator is operated by several derivative filters that are used to change the derivative part's action in PIDA control.

To sum up the PIDA offer one controller which can be achieved with the pole placement configuration and satisfy the performance of the third order system.

$$C(s) = K_P + \frac{K_I}{s} + K_D s + K_A s^2 \qquad \textbf{(2.57)}$$

$$C(s) = K_P + \frac{K_I}{s} + \frac{K_D s}{\tau_D s + 1} + \frac{K_A s^2}{(\tau_D s + 1)(\tau_A s + 1)} \qquad \textbf{(2.58)}$$

where $\tau_D(s) = \frac{K_D}{10}$ and $\tau_A(s) = \frac{K_A}{10}$.

Using definition of sensibility and complementary sensitivity function detailed in Table 1 and the pole placement method all parameters of the PI, PID and PIDA controller can be found. Table.2.2 sums up all those parameters as an expression of the desired closed-loop dynamics.

Table.2.2 PIDA control parameters for 1st, 2nd and 3rd order systems

Order	Parameters	Representations
1st	**K**	$K = \frac{2\xi\omega_n s - 1}{K_p}$
	T_i	$T_i = \frac{2\xi\omega_n s - 1}{\omega_n{}^2 T}$
2nd	**K**	$\frac{T_1 T_2 \omega_n{}^2 (1 + 2\alpha\zeta) - 1}{K_p}$
	T_i	$\frac{T_1 T_2 \omega_n{}^2 (1 + 2\alpha\zeta) - 1}{T_1 T_2 \alpha \omega_n{}^3}$
	T_d	$\frac{T_1 T_2 \omega_n (\alpha + 2\zeta) - T_1 - T_2}{T_1 T_2 \omega_n{}^2 (1 + 2\alpha\zeta) - 1}$
3rd	**K**	$\frac{Rq\bar{q} + R\bar{q}r + Rqr + q\bar{q}r - 1/T_1 T_2 T_3}{K_P}$
	K_i	$\frac{Rq\bar{q}r}{K_P}$
	K_d	$\frac{Rq + R\bar{q} + Rr + q\bar{q} + qr + \bar{q}r - (1/T_1 T_2 + 1/T_1 T_3 + 1/T_2 T_3)}{K_P}$
	K_a	$\frac{R + r + q + \bar{q} - (1/T_1 + 1/{}_1 T_2 + 1/T_3)}{K_P}$

where ω_n is the desired natural frequency, and ζ is the desired damping ratio, α is a turning parameter and fixed greater than *1*(for example, α=10). To facilitate synthesis of the pole placement, the classical coefficient α gives the necessary third order for *T*(s). ω_n and ζ have to be chosen with respect to the specifications. The desired poles are roots of (56). Note that, as is usual in pole placement, a simple filter is added to the controller to compensate the difference in zero terms between T(s) and desired closed-loop transfer function.

2.5.3 Sequential control design : Multi-SISO methodology

g. Methodology of Two-input Two-output system sequential control design

In a 2 x 2 system, if one loop of the system has a small interaction, another has a big interaction, which must be taken into account to design the controller, meanwhile, the small interaction loop's controller also should be considered; we called this control method Square Sequential Control design. In this case, an equivalent plant $G_{22}^{*}(s)$ must therefore be used [Colin, et al., 2011]. This equivalent plant is defined as a function of the first controller $C_1(s)$ on all plants:

$$G_{22}^{*}(s) = G_{22}(s) - \frac{G_{21}(s)C_{11}(s)G_{12}(s)}{1 + C_{11}(s)G_{11}(s)} \qquad \textbf{(2.59)}$$

With this equivalent equation, the controller design can use the same control design method as presented previously (Table.2.1 and 2.2).

h. Methodology of Three-input Two-output system sequential control design

In a 2 x 3 system, if only one loop (G_{1b}, G_{2b}) of the system has a big interaction, but the other loops (G_{1a}, G_{2a} and G_{1c}, G_{2c}) of the system have a small interaction. In this case, the loop (G_{1b}, G_{2b}) which has a big interaction must be taken into account the rest of the system to design this loop's controller, i.e., it needs to consider the rest loops and their controllers to design its controller. This control method is Non-square Sequential Control design. As a result, an equivalent plant $G_{ib}^{*}(s)$ must therefore be used, which is the extension of G_{22}^{*} in equation of (2.59). This equivalent plant is defined as a function of the first two controllers $C_{ia}(s)$ and $C_{ic}(s)$ on all plants:

$$G_{ib}^{*}(s) = G_{ib}(s) - \frac{G_{ia}(s)C_{ja}(s)G_{jb}(s) + G_{ic}(s)C_{jc}(s)G_{jb}(s)}{1 + C_{ja}(s)G_{ja}(s) + C_{jc}(s)G_{jc}(s)} \qquad \textbf{(2.60)}$$

where a, b and c are nature numbers 1, 2 and 3, i=1, j=2, or i=2, j=1.
With this equivalent equation, the controller design could be the same as presented above.

2.5.4 Windup and anti-windup

Due to the constraints and physical limitation of actuators some problems for the control system appears. Near upper or lower limits of actuators the integrator becomes unstable, its value starts to sum to infinity. This problem is called a windup problem. This phenomenon is interpreted as an inconsistency between the plant input and the states of the controller when the control signal saturates, any controller with relatively slow or unstable modes will experience windup problems if there are actuator constraints [Doyle, et al., 1987]. It can occur in loops where the process has saturations and the controller has integral action, because the nonlinear effect of plant input saturation that occurs with any real plant. When the process saturates the feedback loop is broken. If there is an error the integral may reach large values and the control signal may be saturated for a long time resulting in large overshoots and undesirable transients. There are lots of ways to counteract the windup. Tracking is a good way which is illustrated in the Fig.2.18, the system has an extra feedback path around the integrator [Astrom and Hagglund, 2005]. The signal e_s is the difference between the nominal controller output v and the saturated controller output u.

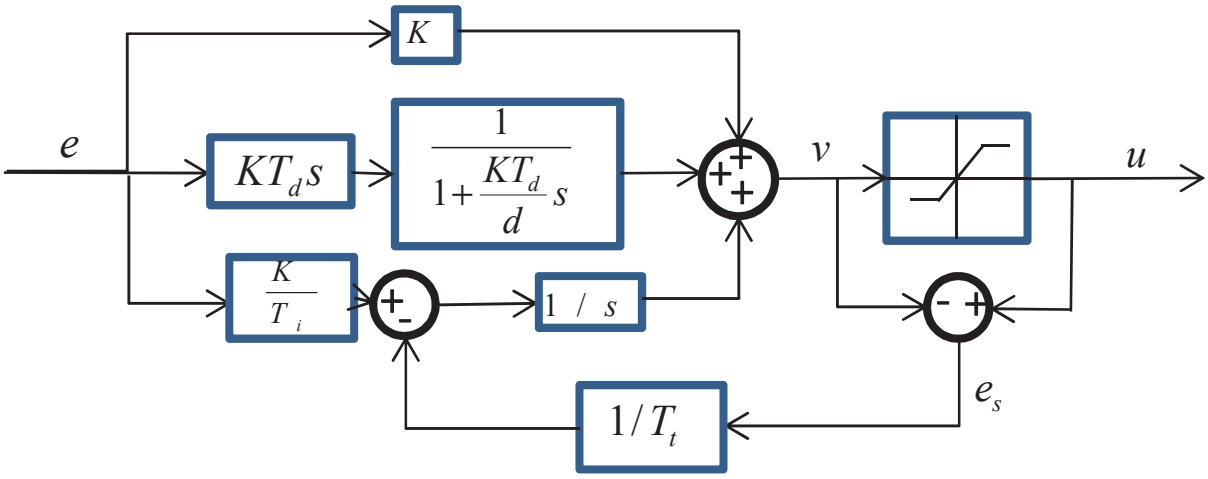

Fig.2.18 PID Anti-windup

Some simple rules have been suggested for the time constant T_t of anti-windup that was fixed at $T_t=T_i/2$ or $T_t=T_i$, $T_t=(T_i+T_d)/2$ or $T_t=\sqrt{TiTd}$, etc, where T_i is the time constant of the integral part, T_d is the time constant of derivative[Mikleš and Fikar, 2007].

2.6 Robust stability

2.6.1 Uncertainty modeling

The physical system always has quantitative errors and uncertainties, in order to represent this quantitative information, a largest possible model should be found. Such considerations are the vital issue for robust control feedback systems. When modeling dynamic systems, there are many types of uncertainties but only the three most used on control design for internal combustion engine will be presented here[Guzzella, 2007]: parametric uncertainty (structured

uncertainty), non-parametric uncertainty(unstructured uncertainty) and multiplicative uncertainty.

a. Parametric uncertainty

Many physical parameters sum up into few parameters such as time constants, gains, etc., are used in plants or control-oriented models. Usually, it is relatively easy to estimate the range of the physical parameters, either by analyzing the system design specifications, or by taking into consideration the expected boundaries for the nominal operating points. In addition, because these parameters are usually independent, the corresponding region in the physical parameter space is a simple "hyper prism".

However, when these physical parameters are mapped to the plants or control-oriented parameters, this independence is lost and very complex parameter regions can arise in the control-oriented parameter space. Just taking the extreme values of all plants and control-oriented parameters and treating them in the subsequent steps as independently are possible, but, in general, will produce very conservative results, and their usefulness in practice is rather limited because no well-developed control systems synthesis tools exist.

b. Non-parametric uncertainty

Since the object dealt with can be described using a transfer function, it is natural to use the same mathematical object to represent the uncertainty. Supposing the system is described by a nominal transfer function $N(s)$, and the corresponding uncertainty can be bounded using a transfer function $W_2(s)$ as well.

There are some assumptions: there is a linear and time-invariant model $N_t(s)$ which is not known but which exactly represents the system to be modeled. This "true" model is known to be included in a set S of models that is defined by a nominal model $N(s)$, an uncertainty bound $W_2(s)$ and an uncertainty generator Δ.

Both $N(s)$ and $W_2(s)$ are problem-specific transfer functions. They can be estimated using one of the approaches described as follows.

The variable Δ is a mathematical object that represents a well-defined set in the complex plane. As such, Δ has no physical interpretation but is a useful tool to form an good mathematical formulation. The used way to describe the uncertainty with these elements is to suppose that

$$N_t(s) \in S \qquad \textbf{(2.61)}$$

Where the set of transfer functions S is defined by

$$S = \left\{ G(s)(1 + \Delta W_2(s)) \middle| \|\Delta\| \le 1, \arg\{\Delta\} \in [-\pi, \pi] \right\} \quad \textbf{(2.62)}$$

To find suitable $W_2(s)$ for this system, the maximum distance $W_2(j\omega)^\dagger$ between the nominal plant N and all the G processes for each frequency must also be computed:

$$W_2(j\omega)^\dagger = \max\left(\frac{|N(j\omega) - G(j\omega)|}{|N(j\omega)|} \right) \forall \omega \quad \textbf{(2.63)}$$

$W_2(j\omega)^\dagger$ is point to point frequency description. The transfer function $W_2(s)$ for uncertainty bound modeling is also deduced as the best equivalent approximation of $W_2j\omega)^\dagger$, which can be high pass bands, low pass bands or all-pass bands in the following equations,

$$W_{21}(j\omega)^\dagger = \frac{A}{\frac{1}{\omega_1}s + 1} \quad \textbf{(2.64)}$$

$$W_{22}(j\omega)^\dagger = \frac{\frac{1}{\omega_2}s + 1}{\frac{1}{\omega_1}s + 1} \quad \textbf{(2.65)}$$

$$W_{23}(j\omega)^\dagger = \frac{\frac{1}{\omega_2}s + 1}{\frac{1}{\omega_1}s + 1} \cdot \frac{\frac{1}{\omega_3}s + 1}{\frac{1}{\omega_4}s + 1} \quad \textbf{(2.66)}$$

$W_{21}(j\omega)^\dagger$ is low pass bands, $W_{22}(j\omega)^\dagger$ is high pass bands, $W_{23}(j\omega)^\dagger$ is all pass bands, ω_1, ω_2, ω_3, ω_4 are the turning frequencies which used to shape these bands.

c. *Multiplicative uncertainties*

Multiplicative uncertainties [Manfred and Zafiriou, 2002] are concluded with multiplicative input and output uncertainties, which are quite common and important in our engine system. Hence, they are illustrated here by Fig.2.19 and Fig.2.20:

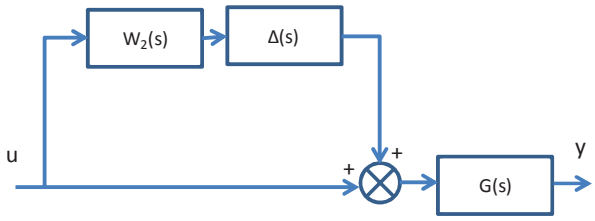

Fig.2.19 Multiplicative Input Uncertainty

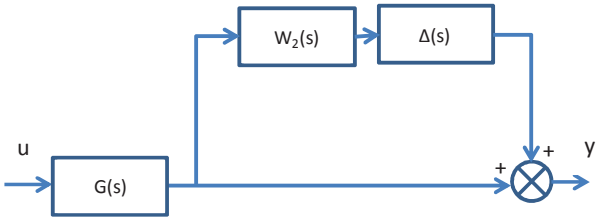

Fig.2.20 Multiplicative Output Uncertainty

2.6.2 SISO Robust Stability

The stability robustness can be checked with the Nyquist stability theorem, which includes the Nyquist plot and Bode diagram. There are nominal stability and robust stability theorems.

Theorem 3 [Guzzella, 2007]: Let n_+ be the number of poles with positive real part and n_0 the number of poles on the imaginary axis of the open-loop transfer function *L(s),* and let n_c be the number of encirclements of the point -1 by *L(jω)* counted positively in the counter-clockwise direction when ω is changed from $-\infty$ to $+\infty$. Then the closed-loop system *T(s)* is asymptotically stable iff $n_c = n_+ + n_0/2$,

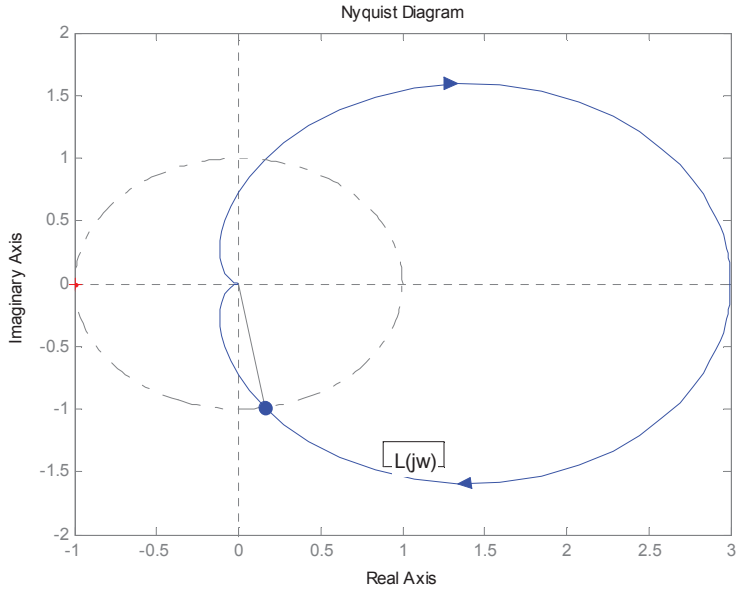

Fig.2.21 Nyquist stability theorem. in this diagram, $n_c=n_+=n_0=0$.

a. Modulus Margin(ΔM_M)

In a Nyquist plot, as the radius of the circle centered in critical point(-1,0) and tangent to the Nyquist plot of open-loop gain *L(s)*, i.e. the minimum distance between the critical point and *L(s)* is defined as stability Modulus Margin, which equals to the inverse absolute value of output sensitivity function linked to the uncertainties upon the plant model [Landau, et al., 2011], is defined as (2.67) and shown in

$$\left|\Delta M_M\right| = \left|1 + L(j\omega)\right| = \left|S(j\omega)\right|^{-1} \qquad \textbf{(2.67)}$$

where ΔM_M is to assure the robust stability of nominal system, if the modulus of S(s) is expressed in dB, one useful function is given

$$\left|S(s)\right|_{\max} dB = \Delta M_M{}^{-1} dB = -\Delta M dB \qquad \textbf{(2.68)}$$

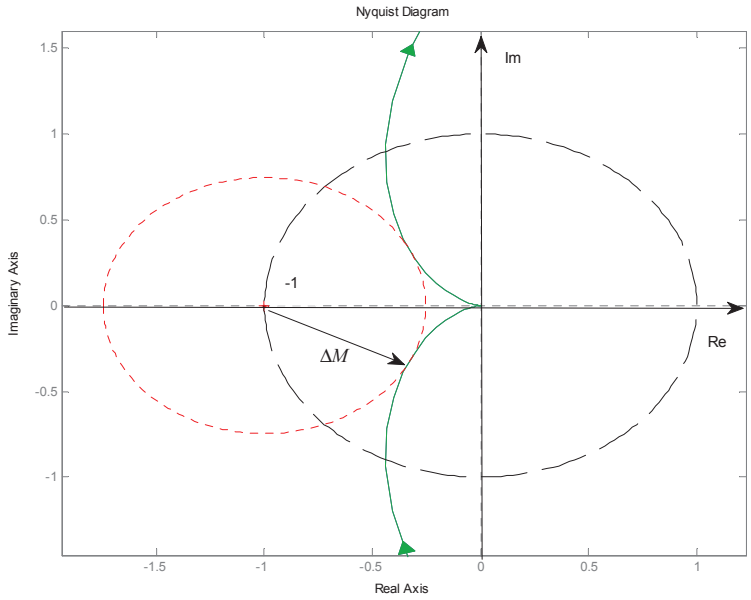

Fig.2.22 Modulus Margin in SISO system

It defines the maximum admissible value for the modulus of the output sensitivity function.

Theorem 4 (SISO's Robust Nyquist Stability Theorem)[Guzzella, 2007]**:**

The uncertain closed-loop system formed with a plant described by {*G(s), W₂(s)*} and a controller *C(s)* is asymptotically stable if the nominal closed-loop system is asymptotically stable and if the following inequality is satisfied

$$\left|W_2(j\omega) \cdot L(j\omega)\right| < \left|1 + L(j\omega)\right|, \quad \forall\, \omega \in [0, \infty] \qquad \textbf{(2.69)}$$

where $L(s)$ is the loop gain, and $L(s) = G(s) \cdot C(s)$. This theorem is shown as Fig 26,

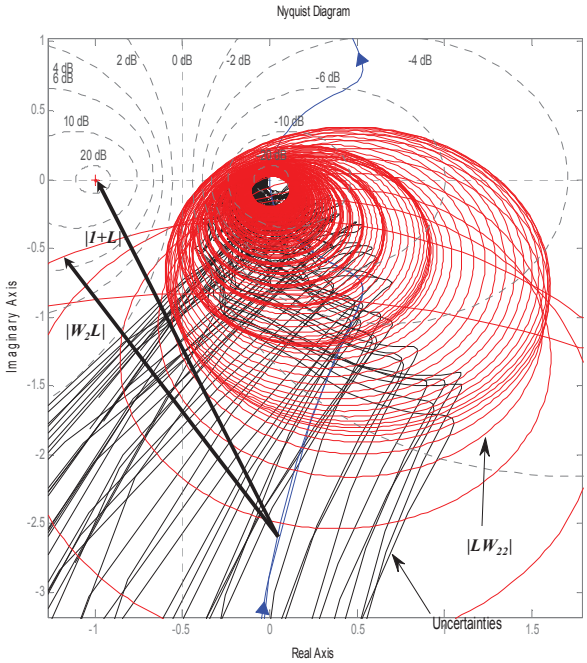

Fig.2.23 SISO Nyquist Robust Stability in Nyquist chart

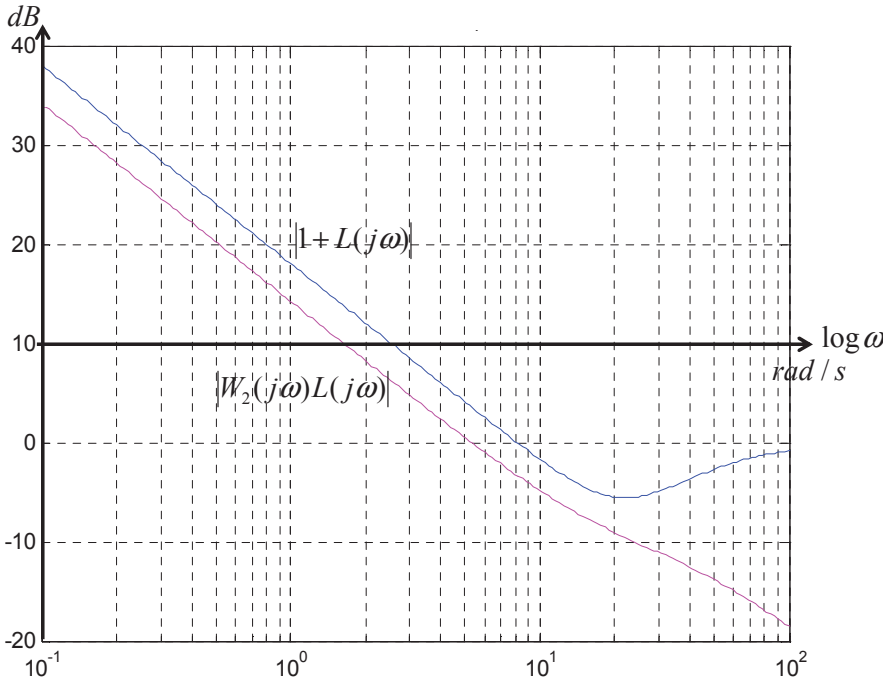

Fig.2.24 SISO Nyquist Robust Stability in Bode chart

However, this independent variable is only a scalar real quantity and in most cases, in particular those relevant in practice, plots with reasonable subsets of ω yield reliable results.

For a uncertainty system, its ΔM_M has two types of calculations:

- If the uncertainty is presented by its real Nyquist plants, ΔM_M is the minimum distance from the critical point to all uncertainties' plants.

- If the uncertainty is represented $W_2(s)$ by in equations from (2.61) to (2.69), ΔM_M is given

$$\Delta M_M = \left(\left|1 + L(j\omega)\right| - \left|L(j\omega) \cdot W_2(j\omega)\right|\right)_{\min} \quad \textbf{(2.70)}$$

2.6.3 MIMO robust stability

For the MIMO system, the stability can be classified by nominal stability and robust stability. When the uncertainty is described in 2.5.1, this sort of uncertainty occurs in different parts of the system which can be lumped into one single perturbation Π, which is defined as an unstructured uncertainty. This unstructured uncertainty can be described by a general M-Δ structure, where the uncertainty perturbation Δ satisfies $\overline{\sigma}(\Delta) \le 1$.

Theorem 5 (MIMO's Robust Stability Sufficient):

If the Gershgorin bands centered on the G_{ii} exclude the origin (i.e. $G(s)$ is column diagonally dominant), the system is stable if and only if:

$$\sum_i n(g_{ii}(j\omega)) = -p_0 \quad \textbf{(2.71)}$$

where g_{ii} is the diagonal matrix, n is clockwise encirclements of g_{ii}, p_0 is the number of poles of the closed loop system in the right half plane.

Theorem 6 (MIMO's Robust Stability Sufficient):

If the Gershgorin bands centered on the L_{ii} exclude the critical point -1 (i.e. G(s) is diagonally dominant), the system is stable if and only if:

$$\sum_i n(l_{ii}(j\omega)) = -p_0 \quad \textbf{(2.72)}$$

where l_{ii} is the diagonal closed-loop system's open loop gain.

Theorem 5 and 6 are only sufficient not necessary stability conditions due to being the nyquist array analysis. If the bands overlap the critical point, conclusions about the stability or instability of the closed-loop system cannot be made. Hence, the sufficient and necessary condition for MIMO's Robust Stability is given in below.

Theorem 7 (Sufficient and Necessary of MIMO's Robust Stability)

It is given by Rosen block, for a n inputs n outputs MIMO system, let C=diag{$C_{11},\ldots,C_{nn}$} be the matrix of the control gains, the inequality

$$\left|g_{ii}(s) + \frac{1}{c_{ii}}\right| > \sum_{j \ne i}\left|g_{ij}(s)\right|, \forall \mathrm{i} \quad \textbf{(2.73)}$$

is satisfied for the all Nyquist contour, the ith Gershgorin band of G(s) encircles the point $(1/k_i,0)$ N_i times anti-clockwise. We assume that there is no hidden unstable modes exist, the negative feedback system with $-G(s)*C$ return difference is stable if and only if [Corriou, 2004]

$$\sum_i N_i = P \qquad \textbf{(2.74)}$$

where P is unstable poles of $G(s)$.

It is necessary to give the robust stability modulus margin; there are three types of Modulus Margin. One is in terms of maximum sensitivity amplitude and Uncertainty bands $W_2(s)$, which is the minimum value of Module Margin distance (m_m) that is expressed in equation

$$\left|\Delta M_{\mathrm{M}}(j\omega)\right| = \left(\left|1 + l_{ii}(j\omega)\right| - \left|L(j\omega)W_2(j\omega)\right|\right)_{\min}, i \neq j \qquad \textbf{(2.75)}$$

where L is the nominal plant of uncertainty. This is one conservative way that not all the uncertainties and couplings will fill in all the uncertainty bands. One example of this modulus margin is given in Fig.2. 25

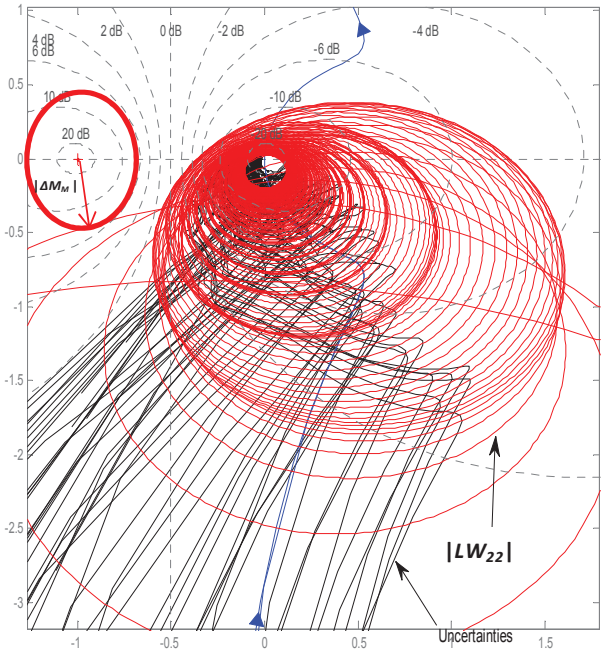

Fig.2.25 Modulus Margin $|\Delta M_M|$ of the first type

Another one is in terms of maximum sensitivity amplitude and Gershgorin bands, which is the minimum value of Module Margin distance (m_m) that is expressed in equation

$$\left|\Delta M_{\mathrm{M}}(j\omega)\right| = \left(\left|1 + l_{ii}(j\omega)\right| - \left|l_{ii}(j\omega)\sum_{i\neq j} l_{ji}(j\omega)\right|\right)_{\min}, i \neq j \qquad \textbf{(2.76)}$$

where this is one conservative way that all the uncertainties and coupling will fill all the uncertainty bands. This case if the coupling is not taken into the plants. One example of this modulus margin is given in Fig 30.

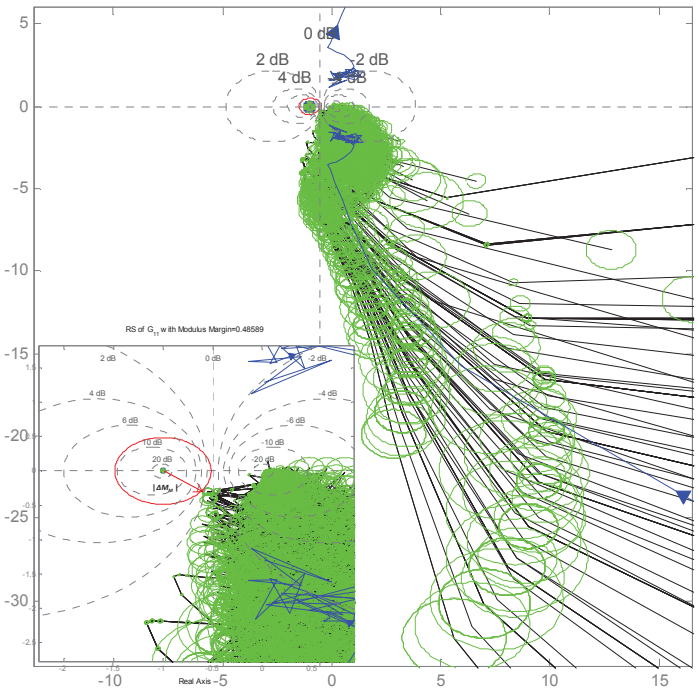

Fig.2.26 Modulus Margin $|\Delta M_M|$ of the second type

The last one is in terms of maximum sensitivity amplitude and real uncertainty plots, which is the

$$\left|\Delta M_{\mathrm{M}}(j\omega)\right| = \left(\left|1 + l_{ii}(j\omega)\right| - \left|l_{ii}(j\omega)\right|\right)_{\min}, i \neq j \qquad \textbf{(2.77)}$$

where this is not one conservative way that all the uncertainties and coupling will be considered in the Nyquist Chart directly without bands. This case is validated only if the coupling is taken into the new designed uncertainty plants in section 2.5.3. One example of this modulus margin is given inFig.2.27.

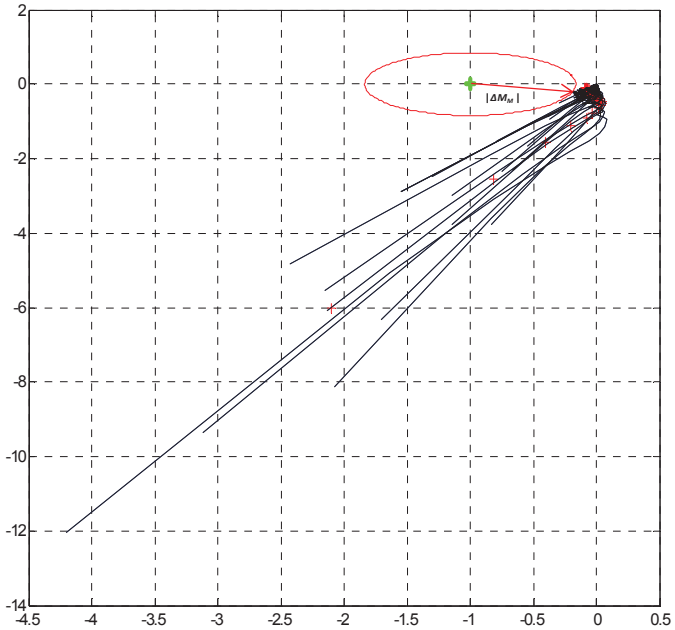

Fig.2.27 Modulus Margin $|\Delta M_M|$ of the third type

The stability analysis of the system with anti-reset windup and derivative filters needs to be carried out using the robust stability theorem, and its robust stability modulus margin distance arguments, and uncertainty in the plant model can be incorporated by increasing the closed loop gain.

2.7 Conclusions

This chapter proposes one unified robust control methodology which can be used to regulate square and non-square MIMO engine system. We have first proposed the frequency modeling, and then focused on an in-depth analysis of the structural properties of nonlinear MIMO systems. SV can describe the input direction and the degree of complexity that is required to control the different loops. CN assists in understanding the degree of unstructured input uncertainty and system error sensitivity. And it shows that the normalization step is one way to reduce the values of condition number, thereby reducing input unstructured uncertainty sensitivity. RGA and Gershgorin Bands analysis are used to find the system's control configuration; consequently, the control strategy is deduced. With this information, the system's uncertainty and coupling properties and a control design method can be derived. Furthermore, pole placement of PID and PIDA controllers are presented due to the practical usefulness, which are mainly chosen as our control strategy, because of different order systems which are smaller than 4^{th} order, they can give good performance which are able to meet the desired specifications. A further advantage is that a linear PI, PID and PIDA controllers are real time applicable and widely applied in industrial production. Afterwards, the robust stability in SISO and MIMO systems is presented to against the uncertainty and coupling, the robust stability modulus margin is expressed to depict the stability's ability.

Finally, this proposed method needs to be implemented in engine model (simulation) and real engine test bench (experiment) to verify the applicability of this robust methodology.

CHAPTER 3 Application: Airpath control of a gasoline engine

Contents

3.1 Résumé

Ce chapitre présente le contrôle du système « chaîne d'air d'un moteur essence ». Après une première partie liée à la compréhension du système à contrôler, la méthodologie présentée au chapitre précédent est appliquée au système considéré. L'objectif du contrôle proposé est de maîtriser la quantité d'air entrant dans le cylindre. Pour ce faire, les capteurs à notre disposition sont les mesures de pression dans le collecteur d'admission (p_{man}) et après le compresseur (p_{boost}). Les actionneurs disponibles sont le papillon d'admission et la vanne de décharge du turbocompresseur. La première étape de notre méthodologie consiste à modéliser notre système d'étude par deux modèles : le premier est un modèle boite grise basse fréquence utilisé pour comprendre le système et surtout pour valider notre loi de commande ; le deuxième est un modèle boîte noire permettant de concevoir notre régulateur et de valider sa robustesse. Il est prouvé dans ce chapitre que notre stratégie appliquée au contrôle de la chaîne d'air du moteur SMART (essence) permet bien d'obtenir un régulateur multi-SISO robuste aux incertitudes non-paramétriques du système. Les résultats montrent des performances satisfaisantes et respectant les spécifications faites lors de la conception du régulateur en termes de dépassement et de robustesse vis-à-vis des temps de montée.

3.2 Introduction

In the global automobile marketing, gasoline engine cars have dominated for ages due to its mature technology (Fig.3.1). Moreover, it easealy meets the European Emission Standards compared to diesel engine automobile.

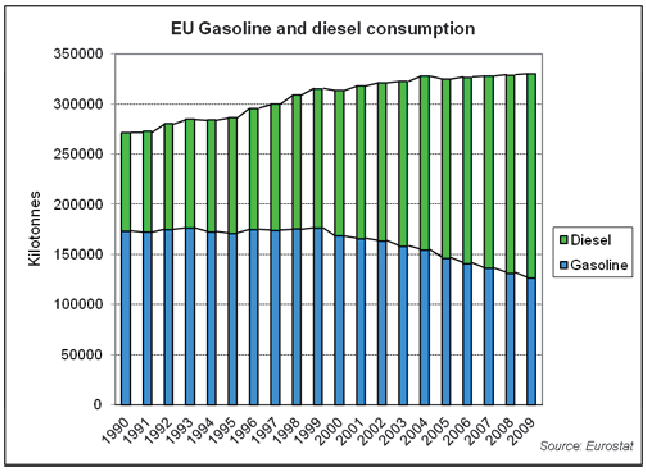

Fig.3.1 Fuel consumption from 1990 to 2009 (source: Eurostat)

Advanced gasoline engine control system is one of the most complex systems in control domain. Gasoline engine have a low thermal efficiency. Normally, the maximum thermal efficiency is about 35% which is used to power the automobile. More than half of the thermal power is lost, this loss include friction, noise, air turbulence, water and oil pumps and electrical generator. In other words ,

approximately 70% of fuel is burned for work which is not used for powering the car. Hence, this low thermal efficiency has to be improved to lower fuel consumption and pollutant emissions.

Thus, reducing the fuel-consumption and lowering pollutant emissions while keeping good performance has become one of most important task of automobile engineers and researchers.

The torque control of vehicle can be expressed by the hierarchy and module structure presented in Fig.3.2 [Colin, 2006].

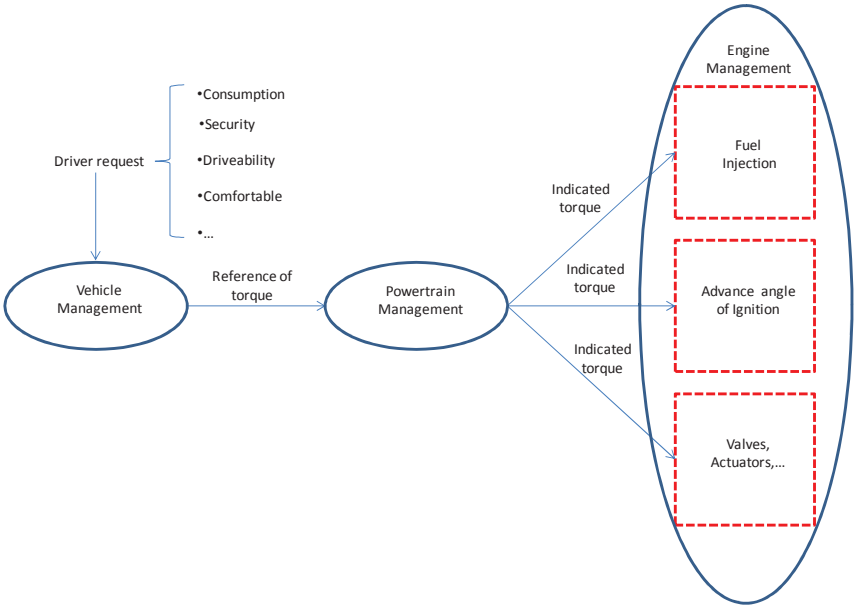

Fig.3.2 Hierarchy of the torque control structure

Vehicle Management: It must oversee all technical aspects of the vehicle in order to guarantee the execution of the design specification, technical feasibility and difficulties [Jürgens, 2000]. Its function is to manage vehicle's onboard operations and to implement commands from the mission manager. It includes the management of the vehicle's mission time line, such as stop, start, park, etc; and the creation of some proper operating modes, component configurations, and resources, such as gear, fuel, sensors, for each mission segment, monitoring the vehicle's health and security, and handling contingencies.

Powertrain Management: The powertrain refers to the group of components that generates power and delivers it to the road surface. It contains engine, transmission, driveshaft and any of the internal workings of the engine. All of its components are used to transform stored energy into kinetic energy for propulsion purposes, multiple power sources and non-wheel-based vehicles[Wikipedia, 2012]. This management generates an effective torque that the driver required, and transfers it to an indicated torque. It is the link between the Vehicle Management and Engine Management.

Engine Management: It is also named electronic engine control unit (ECU). It determines the mass of fuel to be injected by estimating the desired cylinder air charge. Moreover, it controls many electrical systems or subsystems in vehicles. All kinds of ECUs are assembled together into a vehicle's computer.[Wikipedia, 2012] It is the management that compromises the performance, consumption and pollution, which includes the airpath and fuel path.

3.3 Application description

In this part, we will apply the methodology which is presented in chapter 2 on a MCC Smart gasoline engine, which is equipped with a turbocharger and indirect injection. This engine has three cylinders and a maximum torque of 88N.m. Its main characteristics are given in Table 3.1.

Real Gasoline Engine's Characteristics	
Bore X Displace	63.5 x 63mm
Number of cylinders	3 (in line)
Maximum Work	40/55 at 5250 tr/min
Maximum torque	88N.m from 2500rpm to 4000rpm
Compression ratio	10
Turbo compressor	Fixed Geometric Garrett GT12
Distribution	2 valves per cylinder
Injection	Indirect multipoint
intake manifold pressure	From 0.3 to 1.8 bar

Table.3.1 Parameters of the Smart Engine

The considered system, shown on Fig. 6, can be described as follows. Fresh air is aspirated into the intake pipe in an ambient pressure, which is next compressed by a compressor. Afterwards, it is cooled down by the intercooler, with a pressure called boost pressure (p_{boost}). Fresh air entering into the cylinder is adjusted by the opening degree (measured by the surface of openness) of the throttle (TH) placed just before the intake manifold pressure (p_{man}). Later, this air is used to mix with fuel vapor, which enters the cylinders. This mixture is burned in the cylinder to produce the torque of the engine and exhaust gases. After exhausting burned gases through the exhaust pipe, gases are collected by the exhaust manifold. The exhaust flow is then split into two parts: the turbine and wastegate flows. For example, at low load, the turbine is totally bypassed (flow through the wastegate) and at high load, the turbine is controlled, so that the engine is in the limitation of security, which is realized by distributing only a part of exhaust gases with a wastegate valve (V_{WG}).

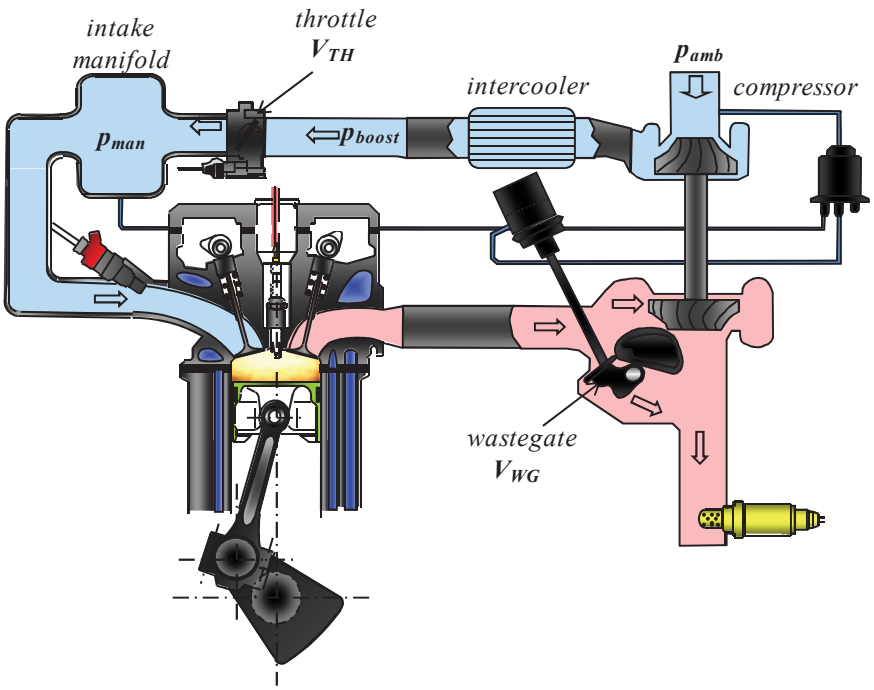

Fig.3.3 Classical air path of a gasoline engine with indirect injection

The goal is to control the airpath of a gasoline engine. Many articles and thesis [Abou, et al., 2002] demonstrate that the mass air flow entering into the cylinder is strongly related to the pressure in the intake manifold p_{man} and consequently to the position of the throttle. Moreover, high fuel consumption and damages to the turbine and the engine may occur if the exhaust gases which are used to drive the turbine increase too much. Compressor speed and consequently the boost pressure are thus increased too much without appropriate control of the wastegate valve. A wastegate is thus used to discharge the exhaust gases flow passing through the turbine and consequently decreasing the boost pressure. However, the exhaust pressure and turbine speed sensors are too expensive to be used in a vehicle. Therefore, the classical solution is the use of a boost pressure sensor. Besides, for reasons of the optimum of performance, consumption and emissions, the wastegate valve needs to be fixed regarding to engine speed and torque conditions [Hillier, 1996]. As mentioned before the objective is to control the indicated torque and more precisely the quantity of fresh air entering into the cylinder. Fig.3.4 shows in dotted blocks at the top all variables of the airpath. Intake throttle and wastegate valve are the inputs or manipulated variables. The manifold pressure and boost pressure are the outputs or the controlled variables. The fuelpath is not discussed in this dissertation, see [Guzzella and Onder, 2009, Heywood, 1988, Pulkrabek, 2004, Kiencke and Nielsen, 2000] for more details on this part. The airpath engine control scheme used is illustrated in Fig.3.5.

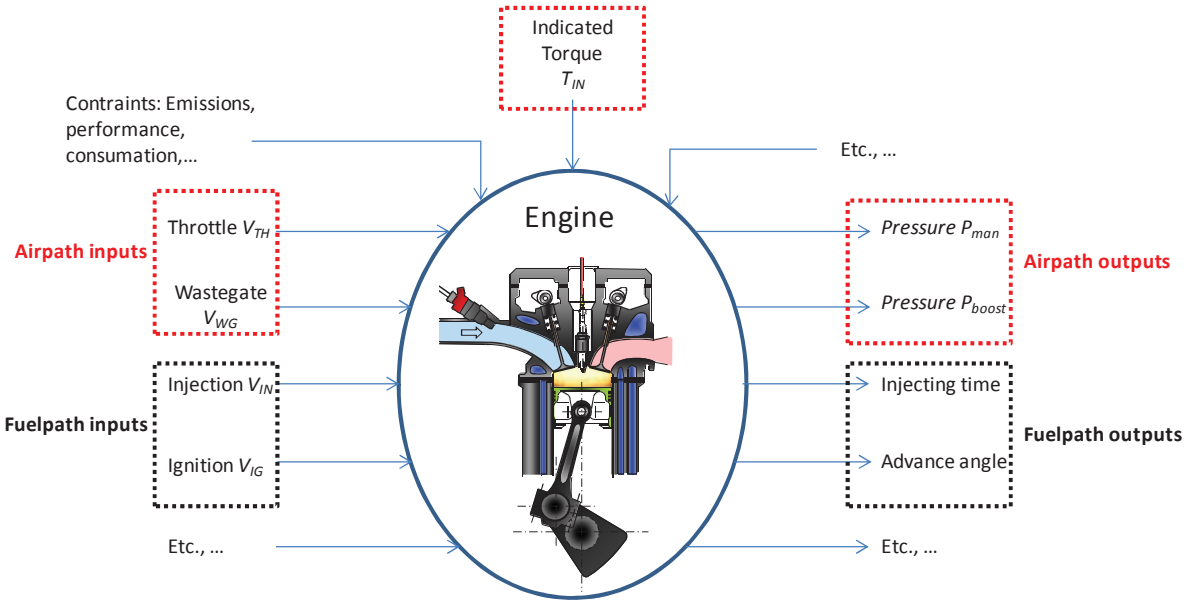

Fig.3.4 Engine's overall control system

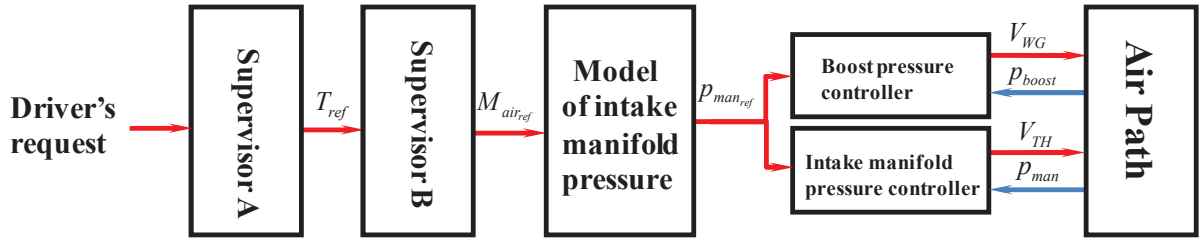

Fig.3.5 Global control scheme for the air path of a gasoline engine

This control scheme describes the airpath control process: the pedal position fixed by the driver is translated in a torque reference T_{ref} via a supervisor. Then this torque is mapped to $M_{air_{ref}}$ and then $p_{man_{ref}}$, regulated via controllers, which will be detailed in the following. These controllers are embedded in ECU and communicate with the engine system.

3.4 System modeling

3.4.1 Gray-box model of gasoline engine system

Due to the fact that engine is made up of many components, such as several nonlinear actuators, manifolds, receivers, cylinder; the airpath system is a complicated nonlinear and calibrated system. It is necessary to describe this complex system via some models, for the convenience of model-based control design. As we noticed in Chapter 2 two kinds of model will be built. The first built model is a precise model in agreement with the behavior of engine system. This model would be named "the ideal model". Nevertheless, a model of system always has error consequently the degree of accuracy must be defined in accordance to the degree of validation that the engineer needs before trying its new control strategy on the real system. Unfortunately, more precise model brings more computation time and increases complexity of the sub-models. In order to stay competitive, the period of validation has

to be reduced as low as possible. Consequently, the model accuracy and computation efficiency must be compromised together in order to find some optimized or acceptable solutions.

Because the control objective is to control the indicated engine torque, we need to know the precise air mass flow that fills-up each cylinder but we don't need to have information on the combustion process. Hence, 0D model is used to validate our control strategies before applying it on the real test-bench. The grey-box 0D model created to validate the control strategies was made with the software AMESim and the combustion part of the engine is described with a Mean Value Engine Model (MVEM). It is a control oriented model that neglects the discrete cycles of engine. In this model, the complete process in the cylinder and cycle by cycle's estimation are not described. The advantage is that it can be calculated in real time, so with a low computation time. A MVEM model computes mean variables, such as mean mass flow rate, mean enthalpy flow rate and indicated output torque from the inlet pressure, engine speed with lookup tables (e.g. volumetric efficiency or part of fuel energy that is lost in the exhaust gases).

The overall model was identified and calibrated with experimental data coming from the SMART engine. The other components of the model are described as follows.

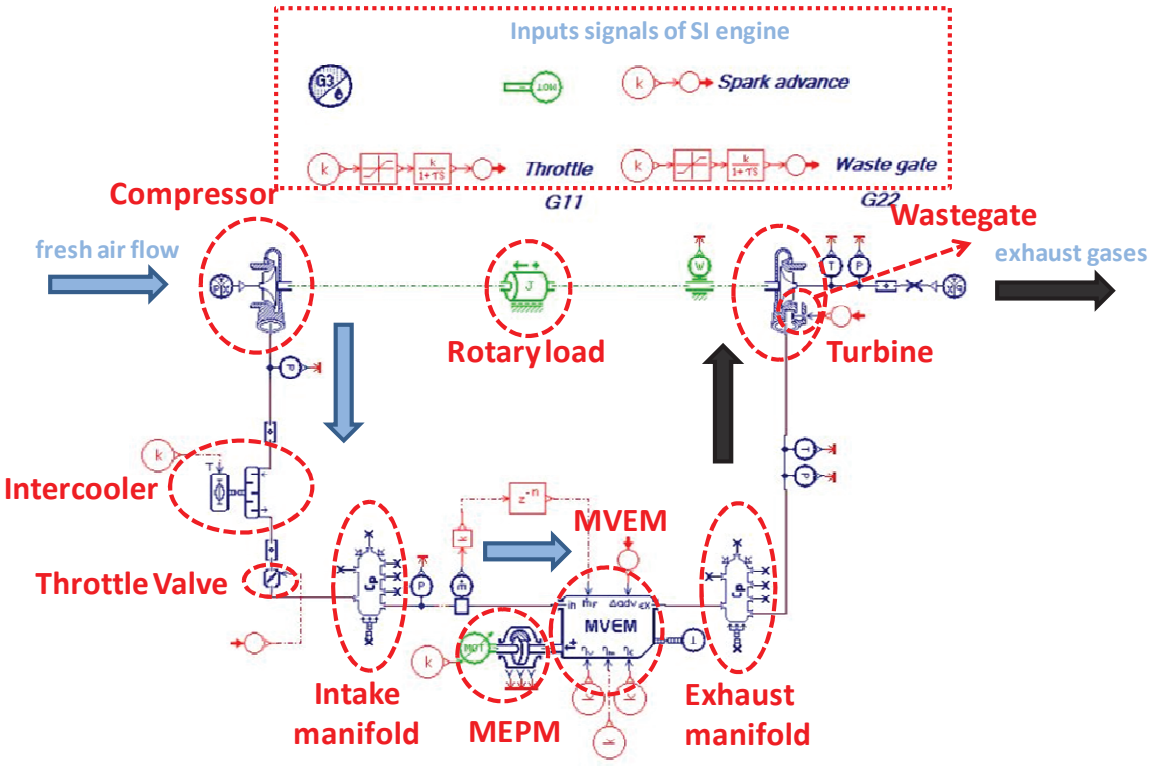

Fig.3.6 Air path model of a turbocharged gasoline engine

The used model is illustrated in Fig.3.6. The important components, such as turbocharger (Compressor and Turbine), intercooler, throttle valve, manifolds and wastegate are presented in Chapter 1. The inputs are throttle and wastegate valves. The outputs are intake manifold and boost pressures.

The interaction between the different models is illustrated in Fig.3.7. First, MCC Smart Engine Test Bench processes some experimental data for providing some lookup tables. These lookup tables are utilized in order to calibrate the complete MVEM 0D simulator. Second, the sequential robust control design methodology is applied to this simulator to validate performance of the control design. Finally, if the MCC Smart Engine Test Bench is available, the real experiment can be done for the final validation of control design. The application of robust control design methodology is detailed as following.

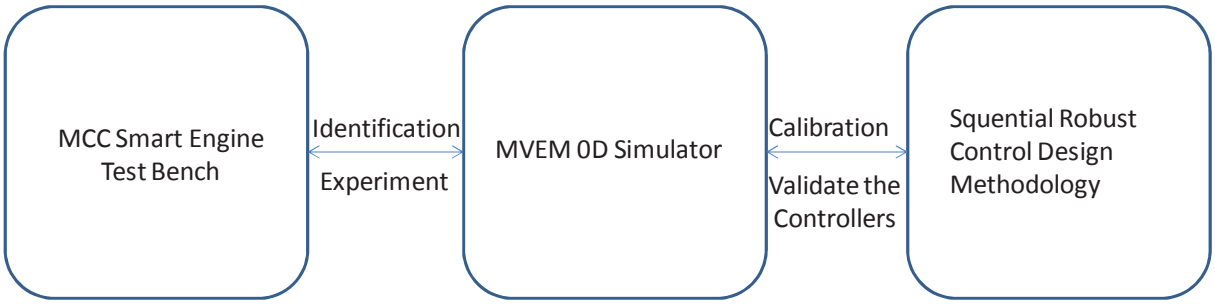

Fig.3.7 Interaction in different models for gasoline engine control

3.4.2 Black–box modeling

An operating point is usually defined in engine speed and torque. In order to consider many engine operating points, the system working area is gridded in 113 couple of engine speed and torque (Fig.3.8). Torque is from 0Nm to 83Nm, speed is from 700 rpm to 5000 rpm. To compute the identification, the superposition theorem is used: exciting the first input and capturing all the temporal outputs and restarting the process for the second output. The real system is usually controlled under a fuel consumption minimization choice with pumping losses minimization. In steady state, when the wastegate is regulated from 0% to 100% closeness, the throttle is full opened (100%); while the throttle is regulated from 0% to100% openness, the wastegate is also full opened (0%). Originally, 113 SISO operating points are available. Nevertheless to compute the analysis and apply our methodology MIMO operating points are needed. Here, operating points above 60Nm are used a second time considering that all actuators must be used at the same time.

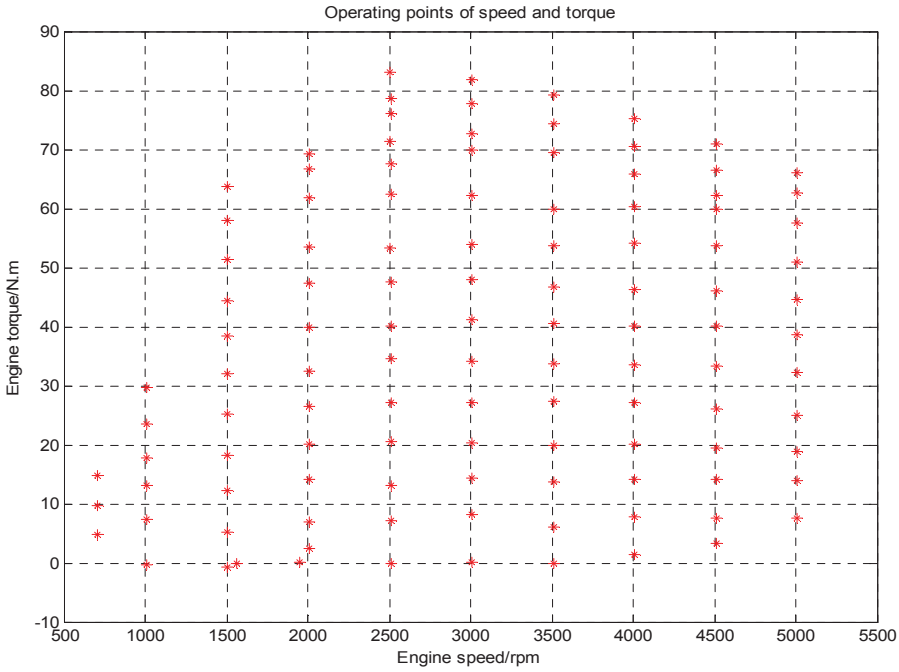

Fig.3.8 113 operating point

In this section, system identification is split into three parts. First, the excited input signals are chosen to obtain information on the system. Afterwards, this signal is applied to the real system and output signals are collected. Second, the input/output signals are normalized to facilitate the comparison of variables and linearized the system. Third, a Fourier Transform is used to compute the frequency data.

a. Excitation Signal

Compared with the spectra of chirp and pseudo-random binary sequence (PRBS) signals (chapter 2), the multi-sine signal generates less numerical noise than the other excited signals. Therefore, for both inputs V_{TH} and V_{WG}, a multi-sine signal was chosen.

$$u(t) = u_0(t) + \sum_{k=1}^{F} A\cos(2\pi f_k t + \theta_k) \qquad (3.1)$$

The exciting signal frequencies f_k are chosen from 0.2 Hz to 10 Hz according to the dynamic of p_{man} and p_{boost}, f_0 has to be larger than $2f_{max}$ according to Shannon's theorem, f_0 is set to be $1kHz$ in order to obtain much information. The amplitude A is chosen while considering intake throttle and wastegate valves' saturation requirements and noise levels [Colin, et al., 2011]. The average value of inputs is set by experimental data (Fig.3.9), which was processed in some conventional situation. Excitation signals and result signals are shown in Fig.3.10 and Fig.3.11.

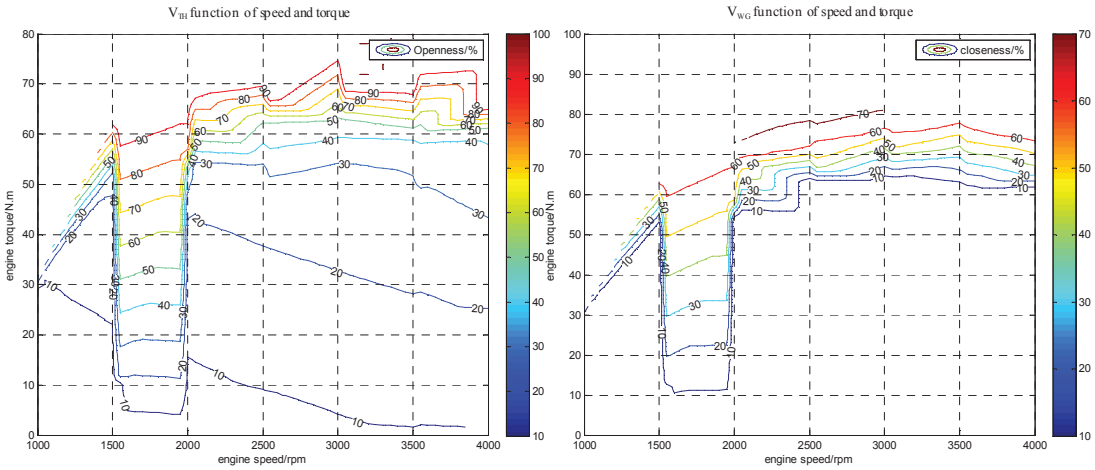

Fig.3.9 Average value of inputs given by experimental data

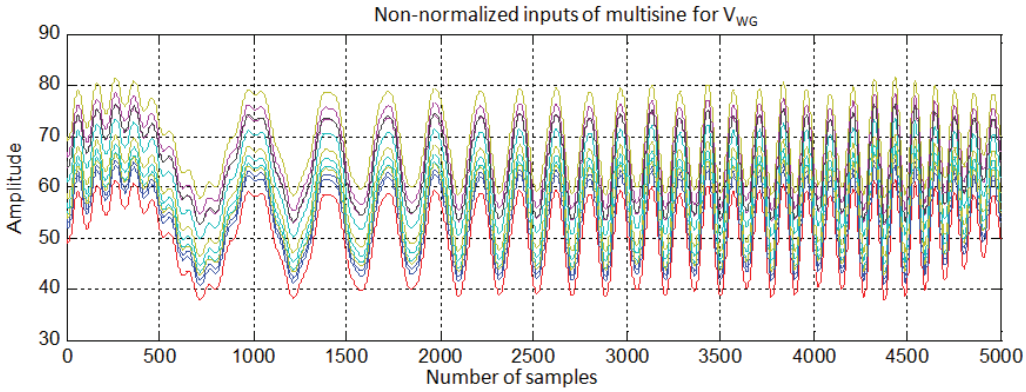

Fig.3.10 Input multi-sine excitation signal for wastegate

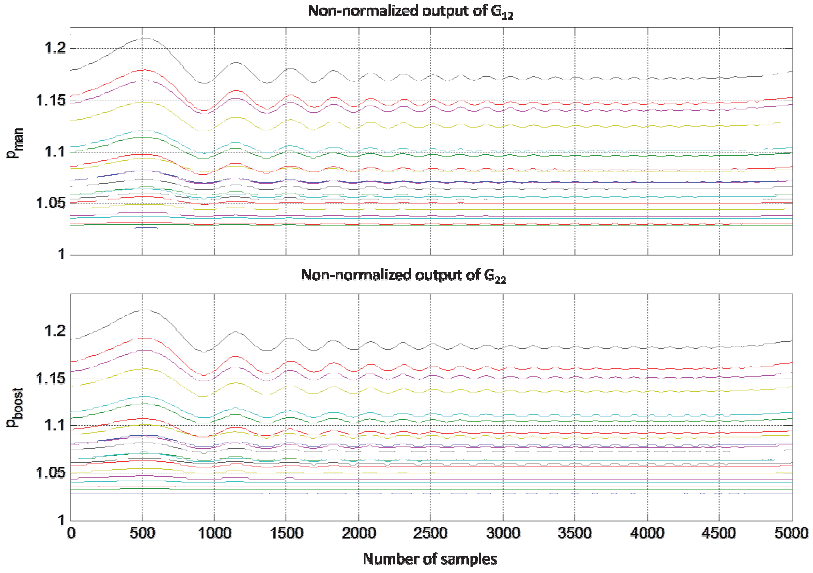

Fig.3.11 Example of output signals captured on p_{man} and p_{boost}

b. Data processing

As seen in chapter 2, the data can be treated around a small neighborhood and constant nominal point with the function of normalization and linearization, which are main prerequisites for system analysis and controller synthesis [Guzzella, 2007]. Hence, the input and output signals of this engine control system are normalized and linearized using the average constant value for input Fig.3.9 and output detailed inFig.3.12. The treated inputs and outputs thus obtained can be seen in Fig.3.13 and Fig.3.14

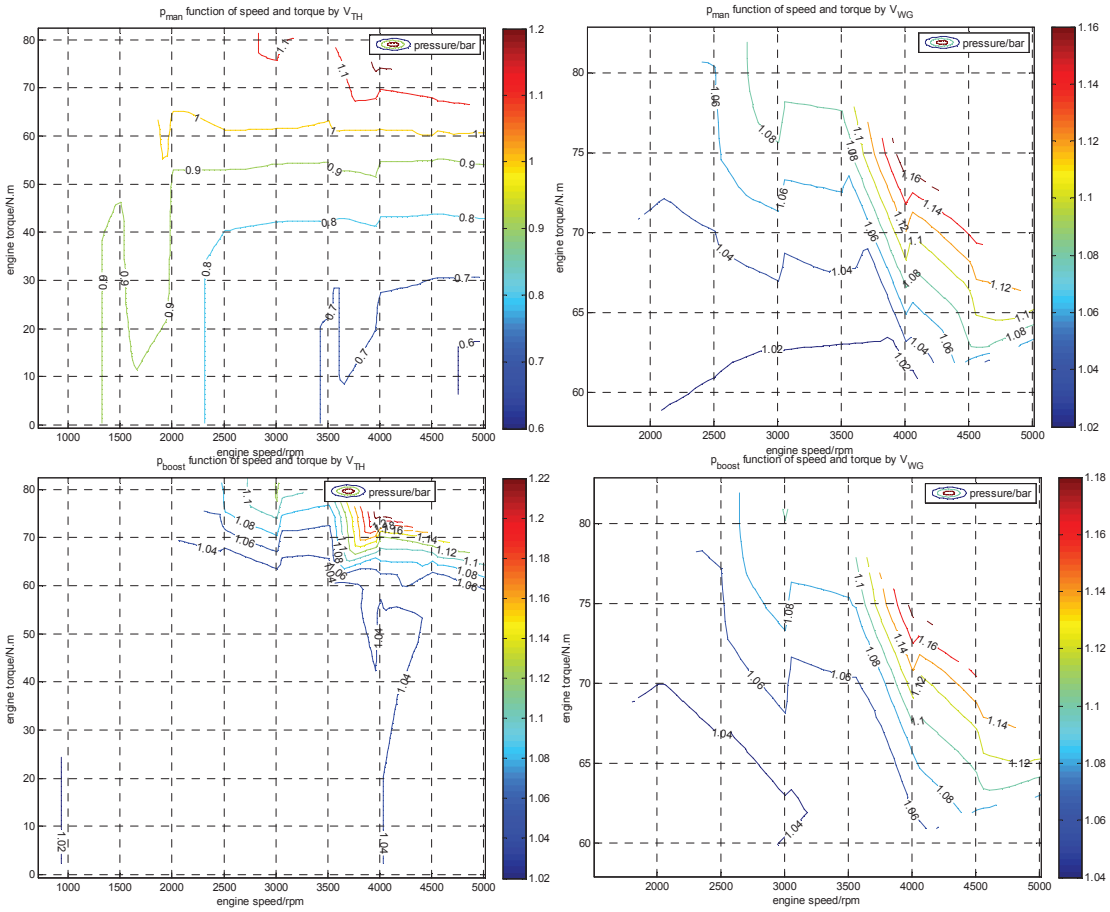

Fig.3.12 Nominal constant value of output used to normalize and linearize the data

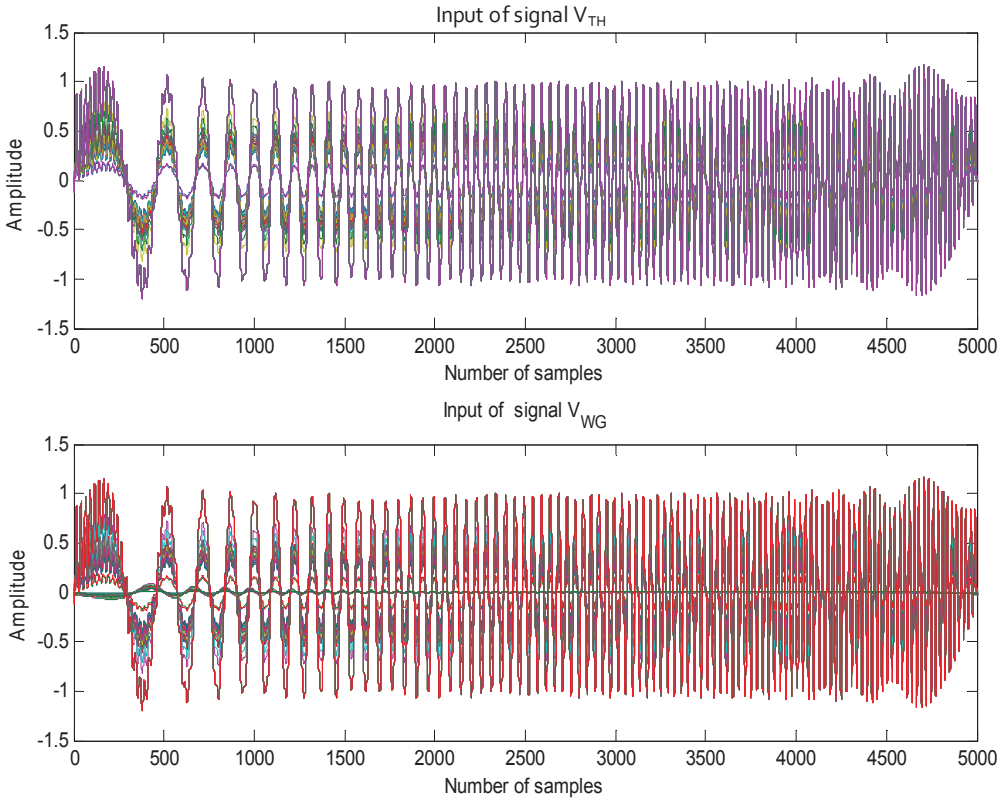

Fig.3.13 Two Normalized input signals V_{TH} and V_{WG} of Multi-sine signals

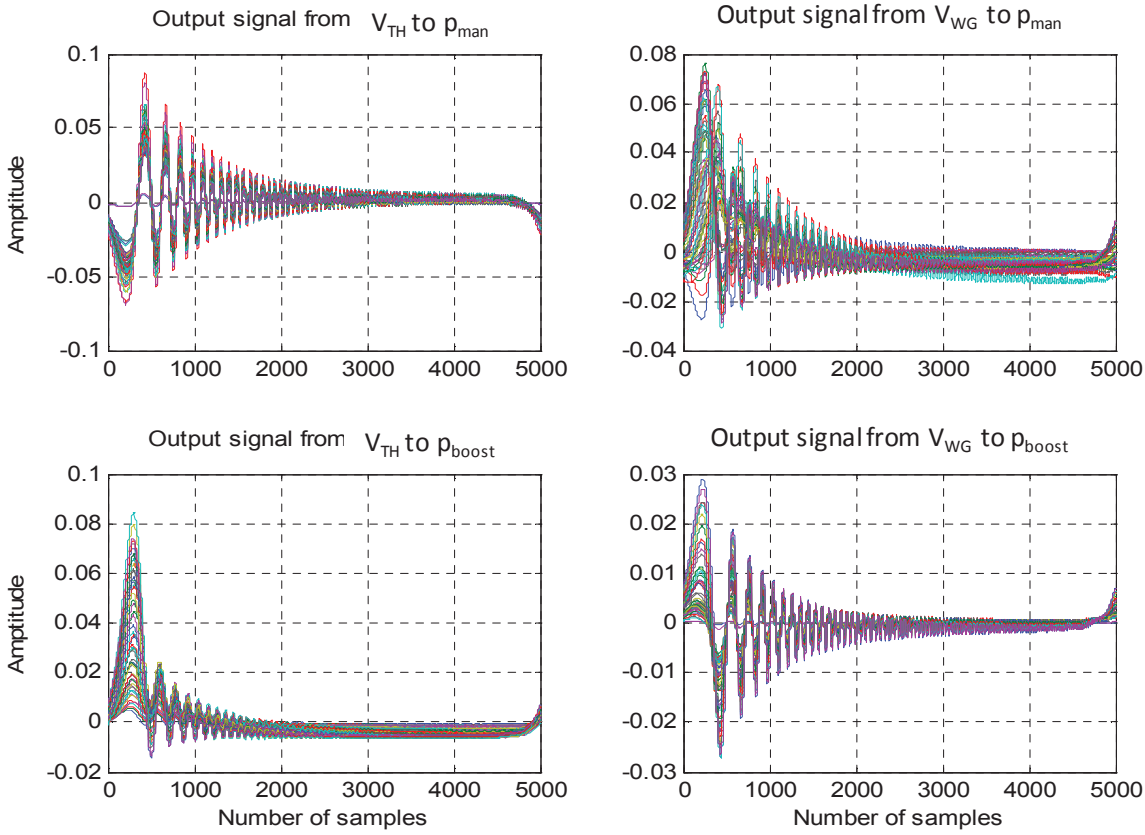

Fig.3.14 Four normalized output signals of p_{boost} and p_{man}

From these figures, we found that inputs and outputs have magnitudes ~~between~~ around -1 and 1. With the help of normalization and linearization, the system is treated for each operating points in order to linearize the system and compare these signals easily. Using Fast-Fourier transform, the frequency response of our normalized and linearized system for each operating points is created (Fig.3.15). This MIMO system is described by four subsystems G_{11}, G_{12}, G_{21} and G_{22} in Bode chart:

G_{11} is from V_{TH} (in % openness) to p_{man} (in bar),

G_{12} is from V_{WG} (in % closeness) to p_{man} (in bar),

G_{21} is from V_{TH} (in % openness) to p_{boost} (in bar),

G_{22} is from V_{WG} (in % closeness) to p_{boost} (in bar).

From this figure, the magnitudes of these subsystems could be seen. All of them almost have the same band of variation of gain of about 30 dB, there is thus 30dB of variation in this system. Moreover, G_{11} has a maximum gain of about 0 dB, G_{21} has a maximum magnitude of about -20dB, G_{12} and G_{22} almost have the same maximum magnitude of about -10dB.

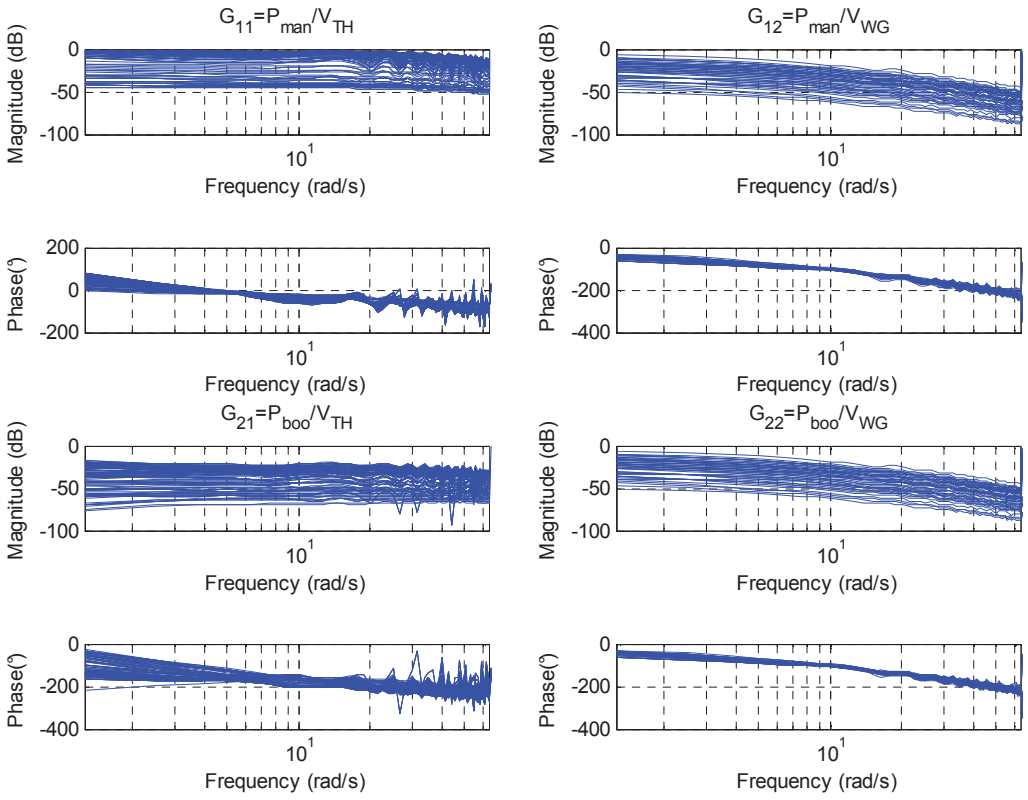

Fig.3.15 Bode diagrams of the normalized process

To prove and see the contribution of the normalization and linearization to the frequency representation of the system, Fig.3.16 compares the same couple of speed and torque with the frequency response for the non-normalized and normalized system.

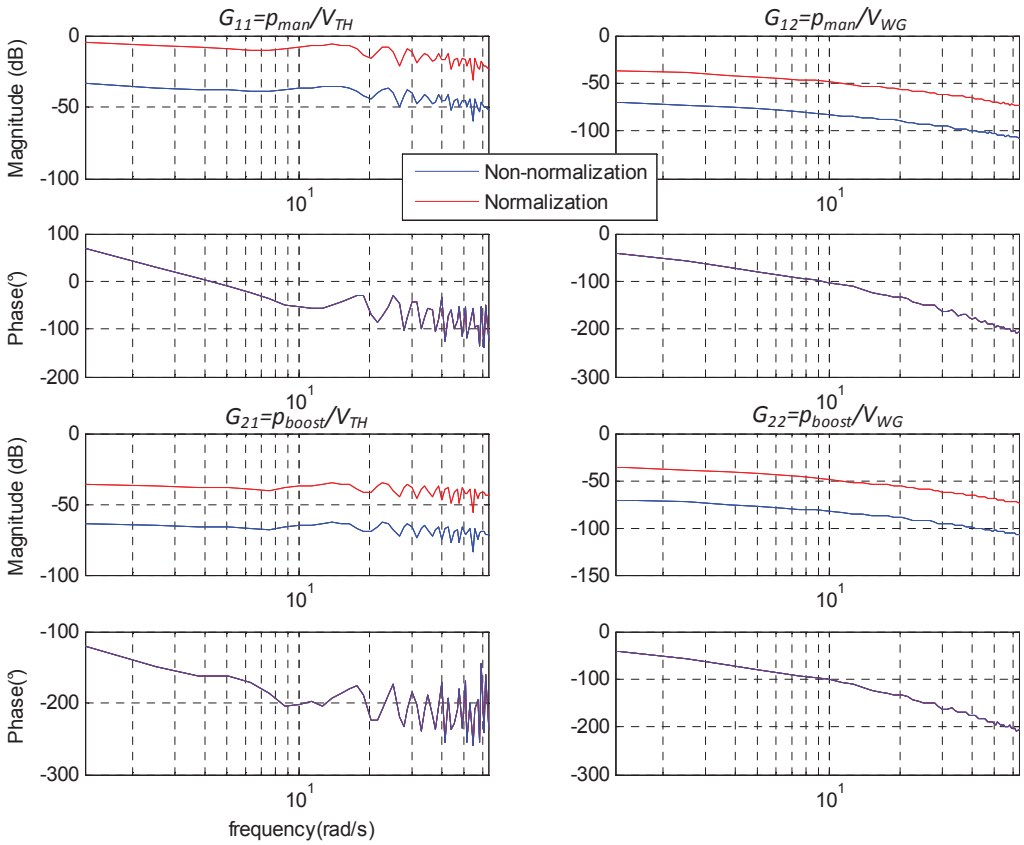

Fig.3.16 Comparison between non-normalized and normalized frequency at Ne=2000rpm, torque=53N.m

c. Nominal frequency identification

The proposed methodology uses the frequency domain for modeling, analyzing and designing a control system. It is a model-based control design methodology consequently a nominal mean-value model of the frequential representation of the 113 operating points must be found. The next step of the methodology consists in finding this nominal transfer function using system identification toolbox of Matlab® while minimizing the sum of square errors between the frequency response of the nominal transfer function and the mean-value frequency model for all operating points.

All frequency responses of the engine system will be considered as uncertain around a nominal process and will be described on a Bode diagrams (Fig.3.17). This uncertainty is multiplicative and non-parametric due to its actuators' dynamic description. Robustness of the design control will be proved if the control obtained with the nominal transfer function is validated for all operating point described by the frequency response.

Second or third order linear models can represent the nominal diagonal processes of $G(j\omega)_{nominal}$ well :

$$N_{ij}(s)=\begin{cases}\dfrac{0.46}{(0.028s+1)(0.02s+1)} & \text{if } i=1, j=1\\ \dfrac{0.51}{(0.72s+1)(0.02s+1)^2} & \text{if } i=1, j=2\\ \dfrac{-0.04}{0.03s+1} & \text{if } i=2, j=1\\ \dfrac{0.21}{(0.50s+1)(0.027s+1)^2} & \text{if } i=2, j=2\end{cases} \quad (3.2)$$

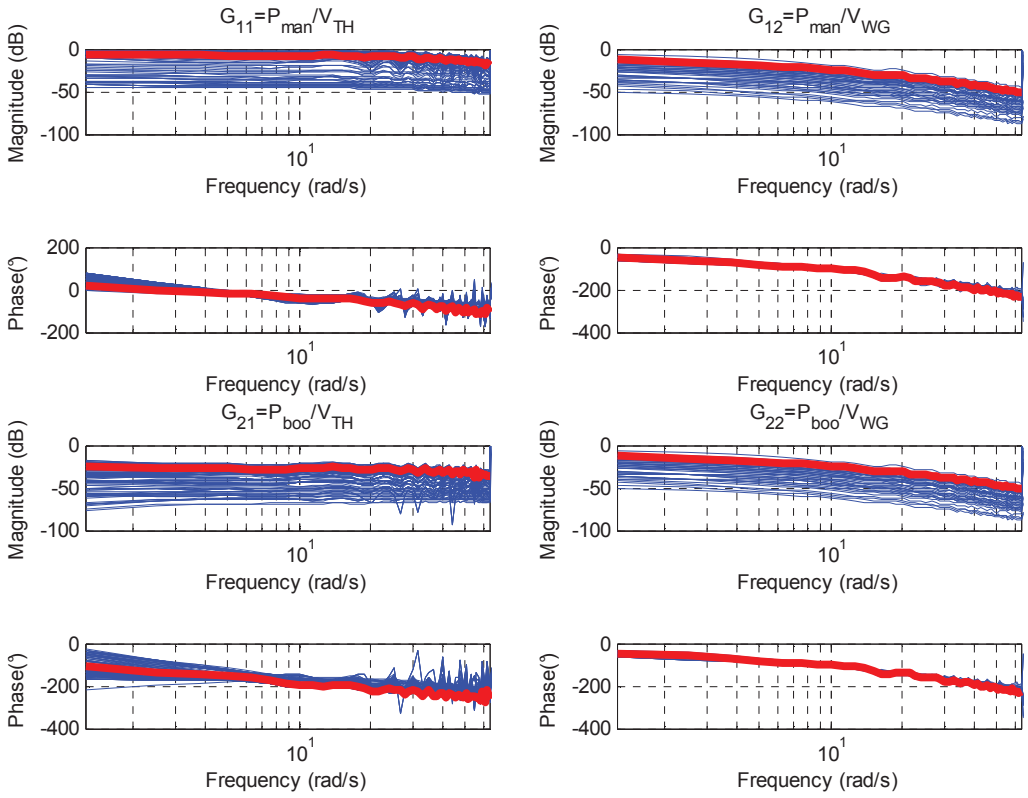

Fig.3.17 Nominal plants for Bode diagrams of normalized and linearized process with crossing and no-crossing operating points

3.5 System analysis

SVD, CN, RGA, GB and CD[3] are tools that can be employed to regard the degree interaction of each loops but to use them we need a MIMO frequential response. Consequently all these tools will be computed on the 26 MIMO operating points.

3.5.1 Singular value decomposition

Fig.3.18 shows that all of $\overline{\boldsymbol{\sigma}}$ and $\underline{\boldsymbol{\sigma}}$ are smaller than 1. The transformed input-output pair corresponding to $\overline{\boldsymbol{\sigma}}$ is the direction with the greatest gain on the plant; this loop is therefore easier to control. The transformed input-output pair corresponding to $\underline{\boldsymbol{\sigma}}$, in contrast, is the direction with the lowest gain on

the plant, making this loop more difficult to control. It is not possible, however, to assure which loop is easier to control and which loop is more difficult to control.

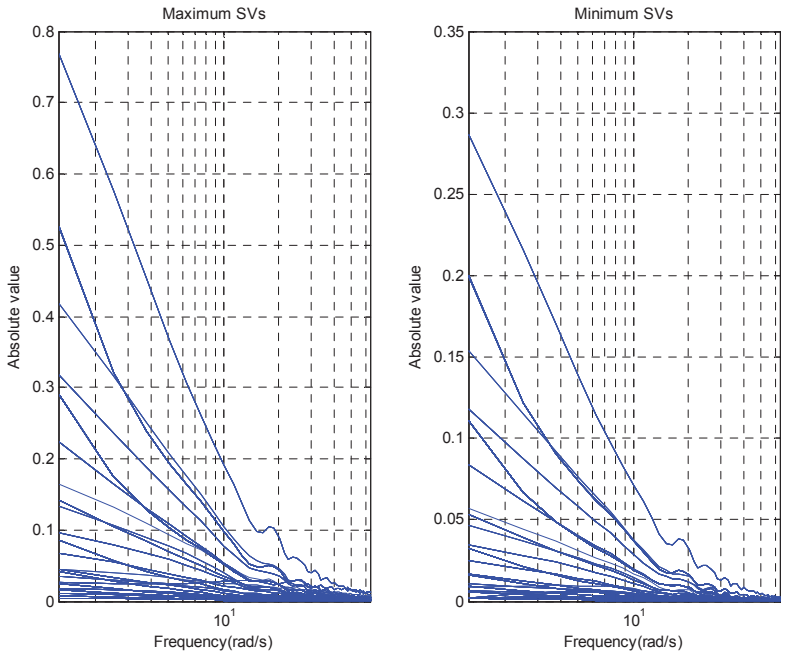

Fig.3.18 SVs of 2x2 crossing MIMO system for two loops

3.5.2 Condition number

Looking at the condition number, we found that the non-normalized CN is larger than the normalized CN. Hence, normalization is proved one way to decrease the CN, the sensitivity of input uncertainty is thus decreased. It is more important to note that normalized CN are smaller than 10 for frequency below 15 rad/s. Consequently, the input uncertainty cannot pose some control problems.

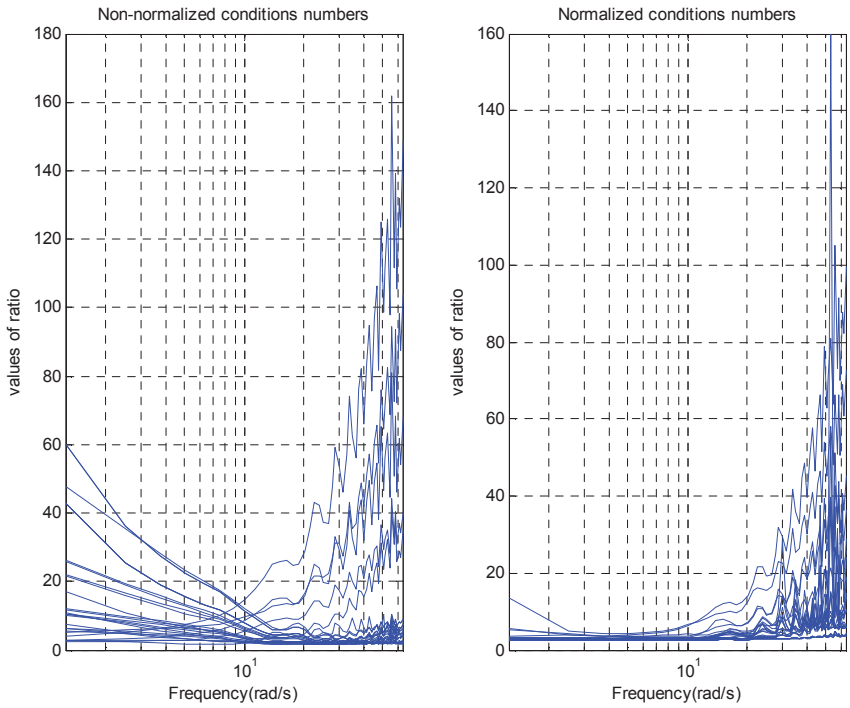

Fig.3.19 CN of 2x2 crossing MIMO system for two loops

3.5.3 Relative gain array

From Fig.3.20, all diagonal RGA elements almost approach the unit. No RGA elements are greater than 10; the non-diagonal RGA elements are almost near zero, hence, this figure tells us that the decentralized control can be employed, thus G_{11} and G_{22} should be chosen as the model-based plants to design the controller of the system considering all operating points.

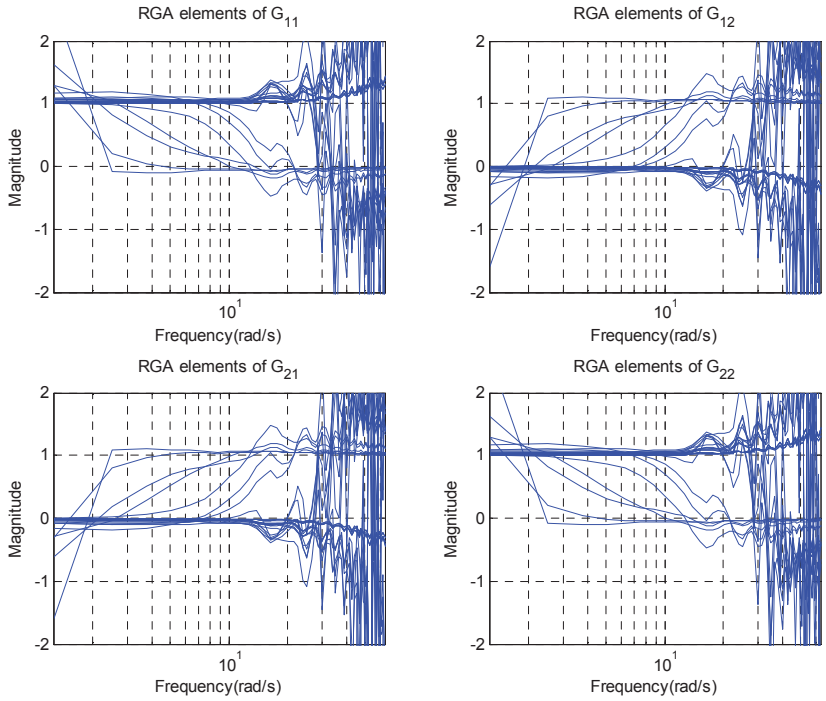

Fig.3.20 RGA of 2x2 crossing MIMO system for two loops

3.5.4 Gershgorin bands

From Fig.3.21 the GB of first loop and second loop have stable GB while considering the column Gershgorin circles, which are presented as the loop's coupling. Moreover, this coupling degree is quantified by the CD^3, which is shown as below.

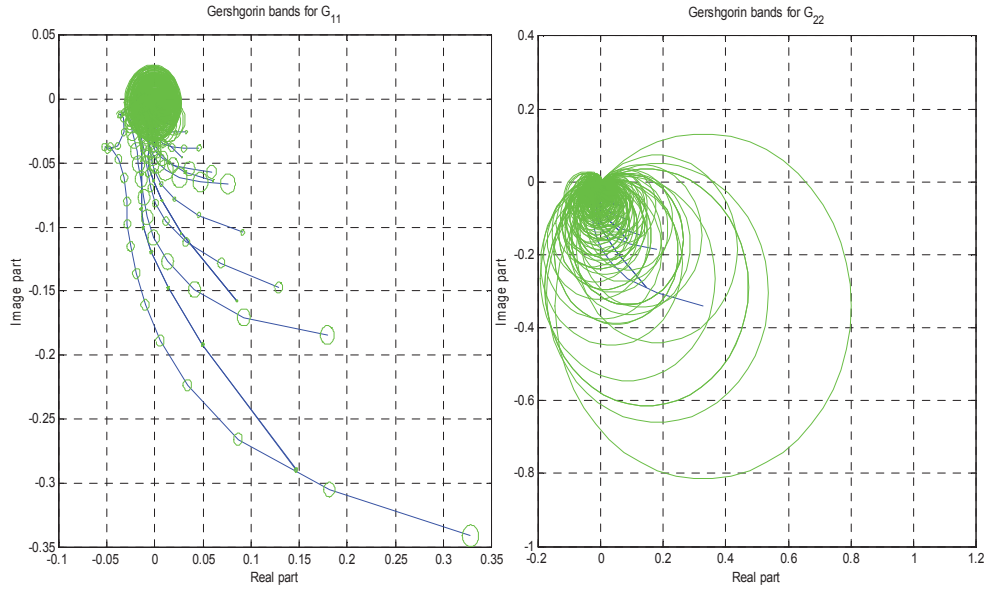

Fig.3.21 GB of open-loop 2x2 MIMO system for two loops

3.5.5 Column diagonal dominant degree

It is plotted in Fig.3.22, some of operating points of first loop has big coupling.

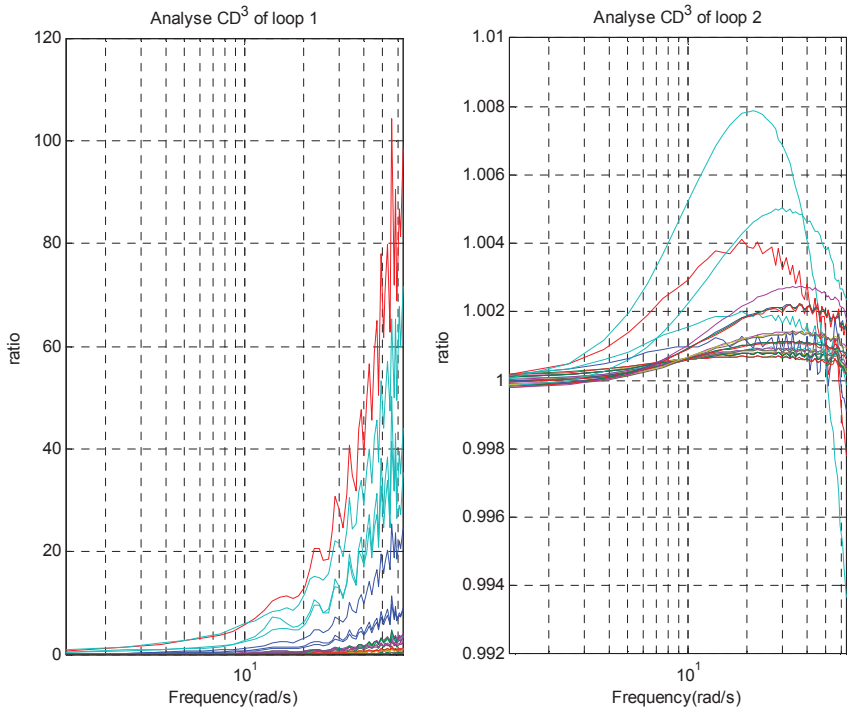

Fig.3.22 CD^3 of open-loop 2x2 MIMO system for two loops

The analysis of MIMO operating points shows that this system can use a decentralized control. It means the multi-SISO control method can be used. Furthermore, the no-crossing operating points (91 operating points for the first loop and 22 operating points for the second loop) should also be analyzed to understand the coupling insides of the loop. Hence, the GB and CD^3 are analyzed in these no-crossing operating points.

a. GB for SISO operating points

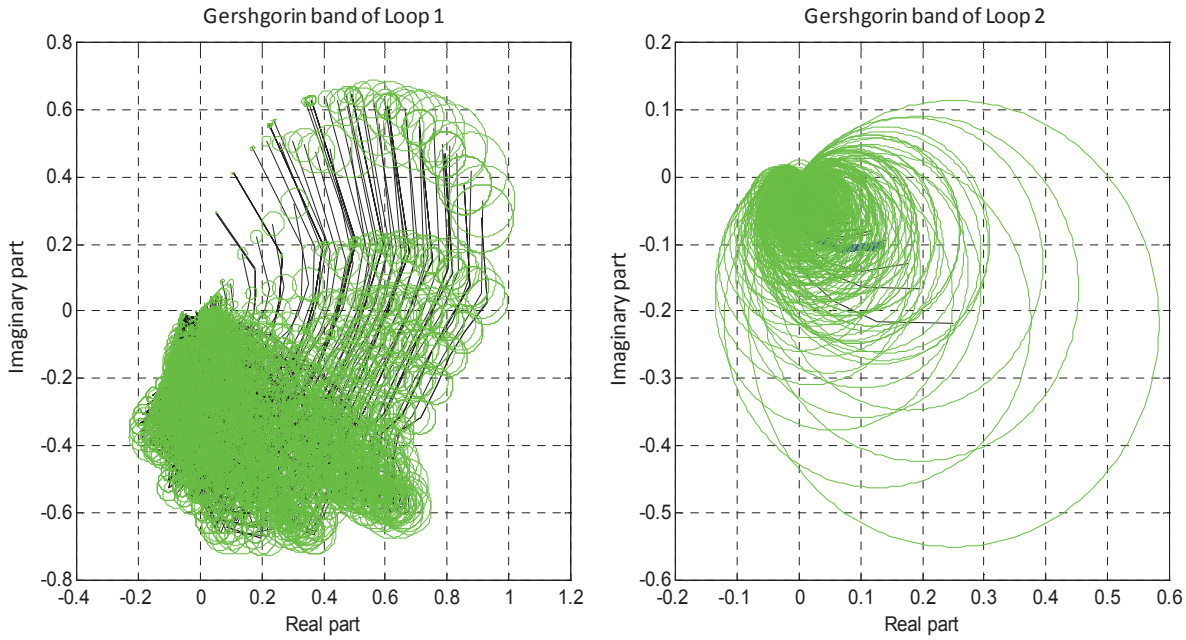

Fig.3.23 GB of open-loop 2x2 MIMO system for two loops (gasoline)

Regarding the GB, the first loop has quite small interaction, due to its small green cycles and no cross the critical point (-1,0), i.e. G_{21} disturbs G_{11} weakly, it is stable in closed-loop; but the second loop has a big interaction, i.e. G_{12} disturbs G_{22} greatly , there is even no green cycle encircling the critical point. It is also stable in closed-loop. But there are some big green cycles. This is discussed more in CD^3 as follows.

It permits to understand the degree of coupling of the system. These two loops' CD^3 of the system is plotted in Fig.3.24.

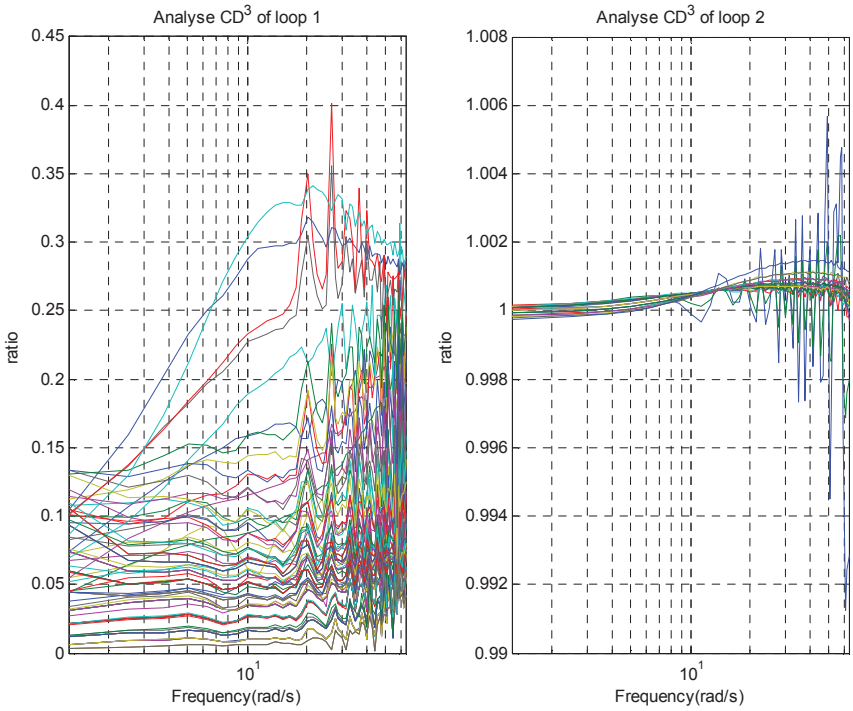

Fig.3.24 CD^3 of open-loop 1x2 MIMO system for two loops (gasoline)

Looking at Fig.3.24, none of both loops have small CD^3. The value of the first loop is near zero consequently to control this loop we can use a SISO control. The second loop value is near the unit, G_{12} dominates G_{22} and a SISO control should not be used for this loop.

3.5.6 Conclusion of MIMO system's analysis

According to the analysis of crossing MIMO operating points and no-crossing SISO operating points: Singular value decomposition and condition number tools show that this system has no problem of input uncertainty regarding the crossing operating points. Relative gain array tools proved a decentralized control strategy regarding the 26 crossing operating points. Gershgorin bands applied to no crossing operating points (91 and 22 points) show that the first loop has small interaction, i.e. G_{21} disturbs G_{11} weakly, but G_{12} disturbs G_{22} more than the first loop. The degree of coupling quantified by CD^3 confirms that first loop can use SISO control strategy; the second also can consider the SISO control strategy while considering a longer response of loop 2 in order to be robust and stable. Combining the crossing operating points and no-crossing operating points, the analysis demonstrates that a Multi-SISO control can be employed.

3.6 Robust control synthesis

Due to nominal plants of G_{11} are second order linear systems, the controller of the first loop can be designed by PID pole placement methods according to the Table 2.1 in chapter 2. The second loop uses an equivalent plant G_{22}*(s) which is function of the first loop's controller $C_1(s)$ and the nominal transfer functions:

$$G(s)_{22}^{*} = G_{22}(s) - \frac{G_{21}(s)C_{11}(s)G_{12}(s)}{1+C_{11}(s)G_{11}(s)} \quad (3.3)$$

Considering system dynamics and physical properties, reasonable desired performances have been fixed:

- the overshoots were set at 3% for both p_{man} and p_{boost},
- the response time were fixed to 0.3s and 1.5 for p_{man} and p_{boost} respectively,
- the bandwidths of the nominal function must be 2 and 13.2 rad/s, respectively.

And the performances of these two nominal loops are plotted in Fig.3.25

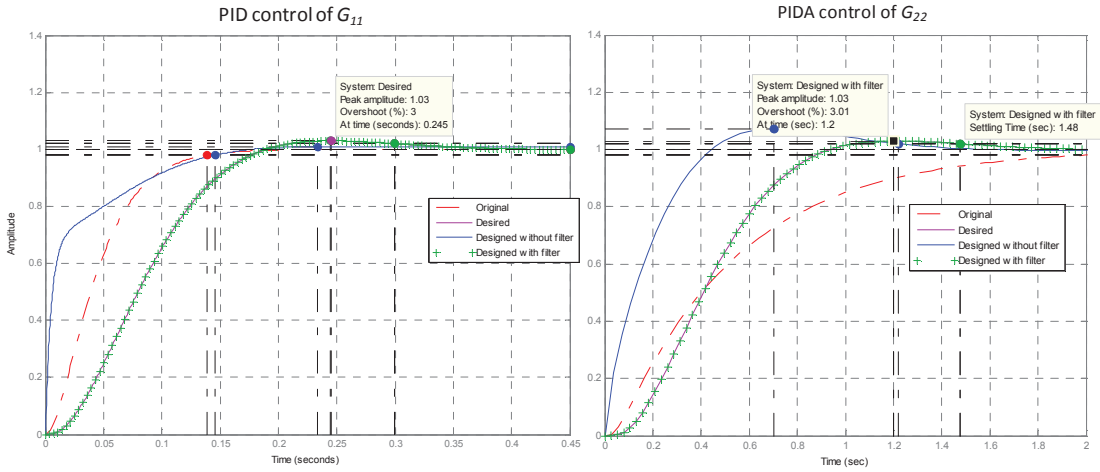

Fig.3.25 PID and PIDA pole placement design, original: the nominal model of subsystem G_{11} and G_{22}^{*}; desired: the designed system T_{11} and T_{22}created via the performance; designed without filter: $G_{11}*C_{11}$ and $G_{22}^{*}*C_{22}$; designed with filter: $F_{11}*G_{11}*C_{11}$,and $F_{22}*G_{22}^{*}*C_{22}$.

Because the second and third orders systems cannot realize the same performance without additional transfer function such as filters, their corresponding controllers and filters are on equations (4) and (5)

$$C_{ij}(s) = \begin{cases} 8.1 + \frac{153}{s} + \frac{0.2s}{\frac{0.2}{10s}+1} & if\ i = 1 \\ 6.9 + \frac{19.9}{s} + \frac{0.3s}{\frac{0.3}{10s}+1} + \frac{0.002s}{\left(\frac{0.3}{10s}+1\right)\left(\frac{0.002}{10s}+1\right)} & if\ i = 2 \end{cases} \quad (3.4)$$

$$F_{ij}(s) = \begin{cases} \frac{1}{0.001814s^2+0.05603s+1} & if\ i = 1 \\ \frac{1}{s^3+61.17s^2+935.3s+3035} & if\ i = 2 \end{cases} \quad (3.5)$$

When the controllers are fixed by the pole placements, their robustness need to be proved afterwards for all operating points, while considering the uncertainty and coupling of the system.

For the coupling, the 2x2 MIMO system's robust stability can be verified by GB in the form of Nyquist diagram. Two loops are separated in following figures. (see Fig.3.26 and Fig.3.27)

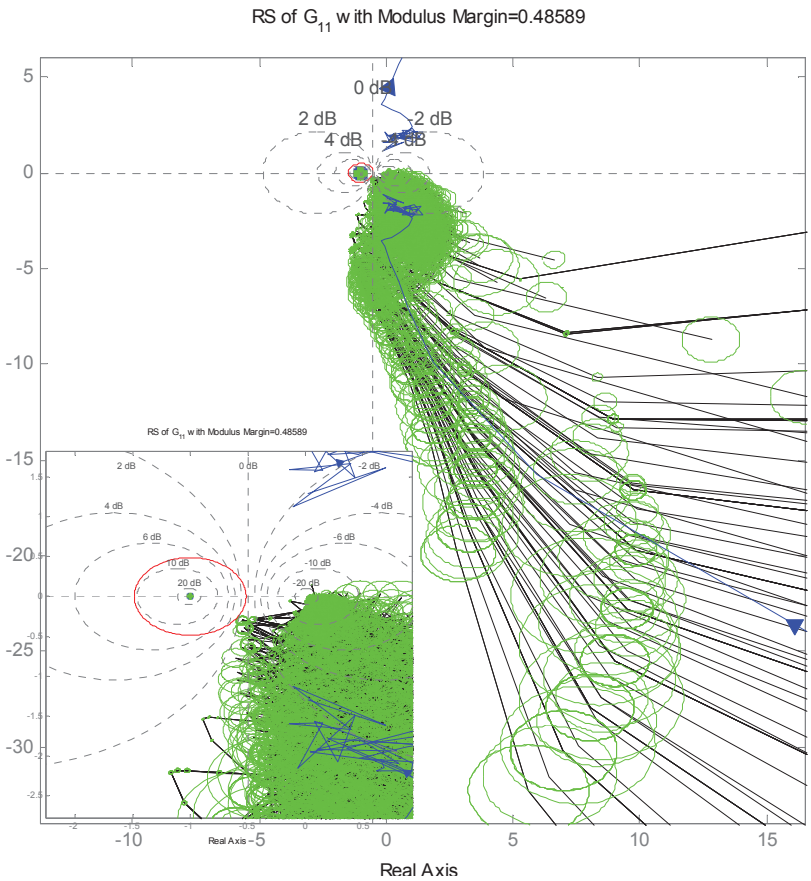

Fig.3.26 GB of closed-loop 2x2 MIMO system for loop 1 on 91 operating points (gasoline)

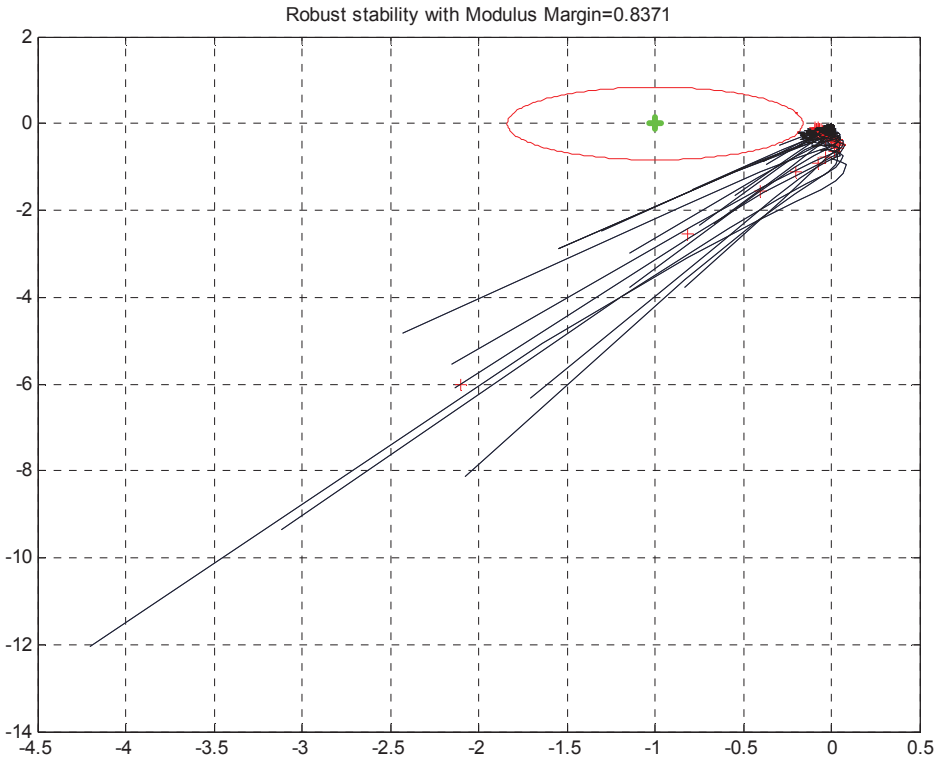

Fig.3.27 GB of closed-loop 2x2 MIMO system for loop 2 on 22 operating points (gasoline)

Fig.3.26 and Fig.3.27 show that both loops are stable and have enough modulus margins (loop1: 0.4859, loop2:0.8371) against the uncertainty and coupling. This system is thus robust stable.

3.7 Simulation results

The Robust multi-SISO control design was validated in all its operating points; the control test is a scenario of torque while the engine speed is set constant. It is depicted in Fig.3.28.

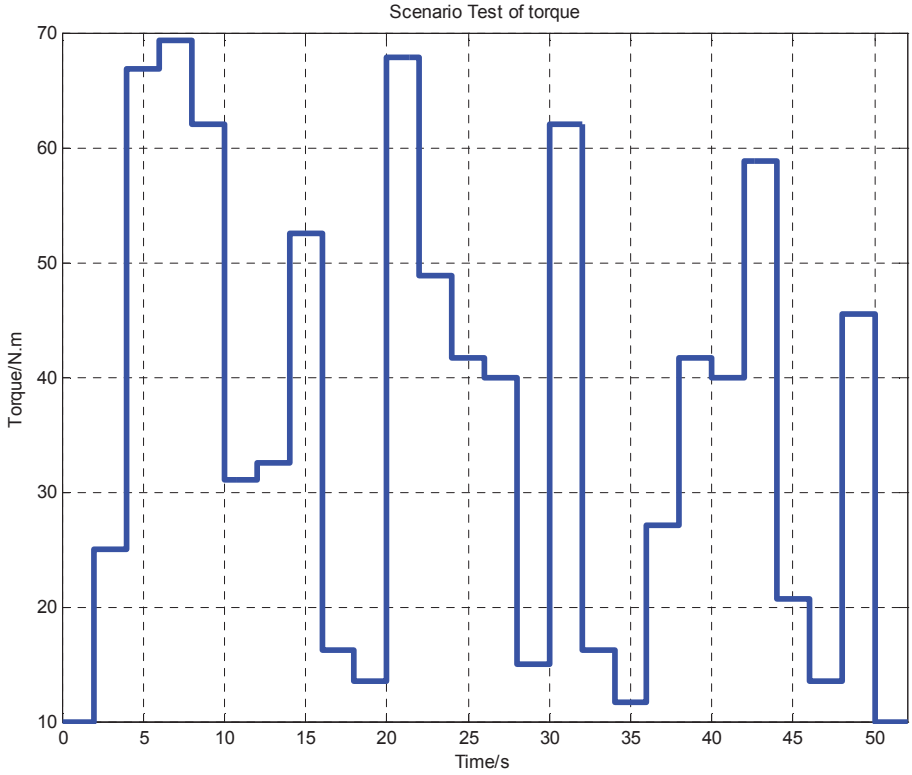

Fig.3.28 Test scenario for torque

This scenario was tested for different engine speeds, but only 2000rpm, 3000rpm and 4000rpm are shown here. The specifications are recalled here: for the loop of p_{boost}, its response time is 1.5s and its overshoot is 3%; for the loop of p_{man}, its response time is 0.3s and its overshoot is 3%. It shows the tracking of p_{man} and p_{boost} in Fig.3.29, Fig.3.30 and Fig.3.31 at engine speed 2000 rpm. Looking at the Fig.3.29, p_{man} and p_{boost} can track the reference very well, a classical anti-windup was used here. Two zooms are made in Fig.3.30 and Fig.3.31.

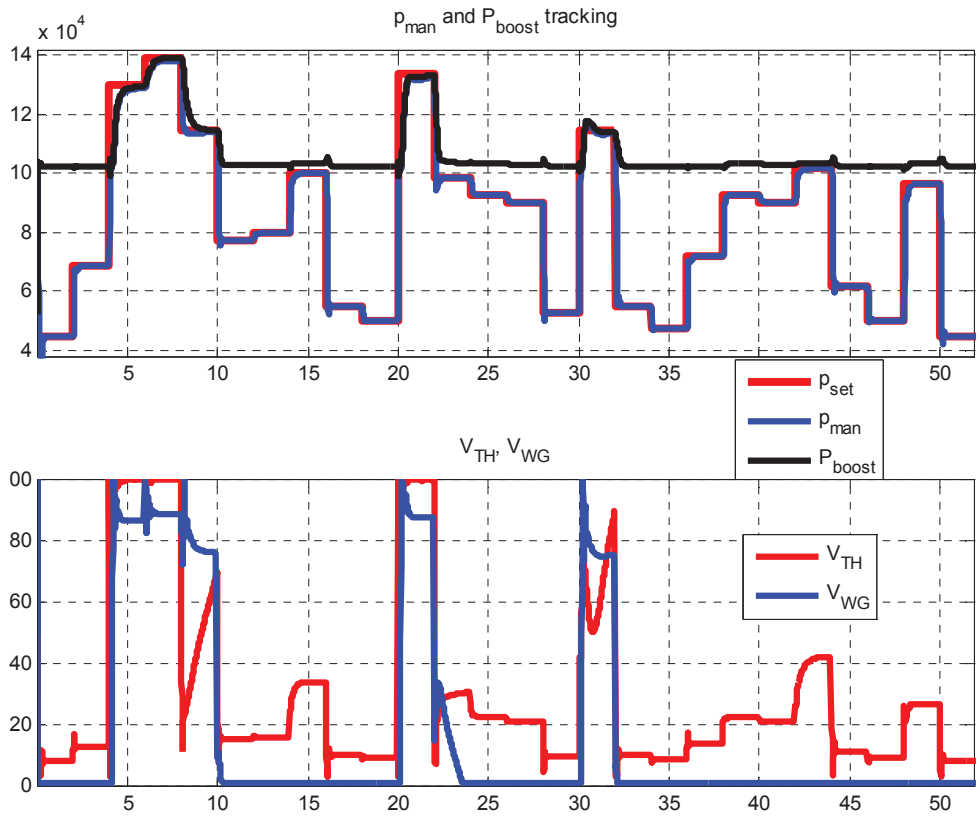

Fig.3.29 p_{man} and p_{boost} (top), V_{WG} and V_{EGR} (bottom) at 2000 rpm

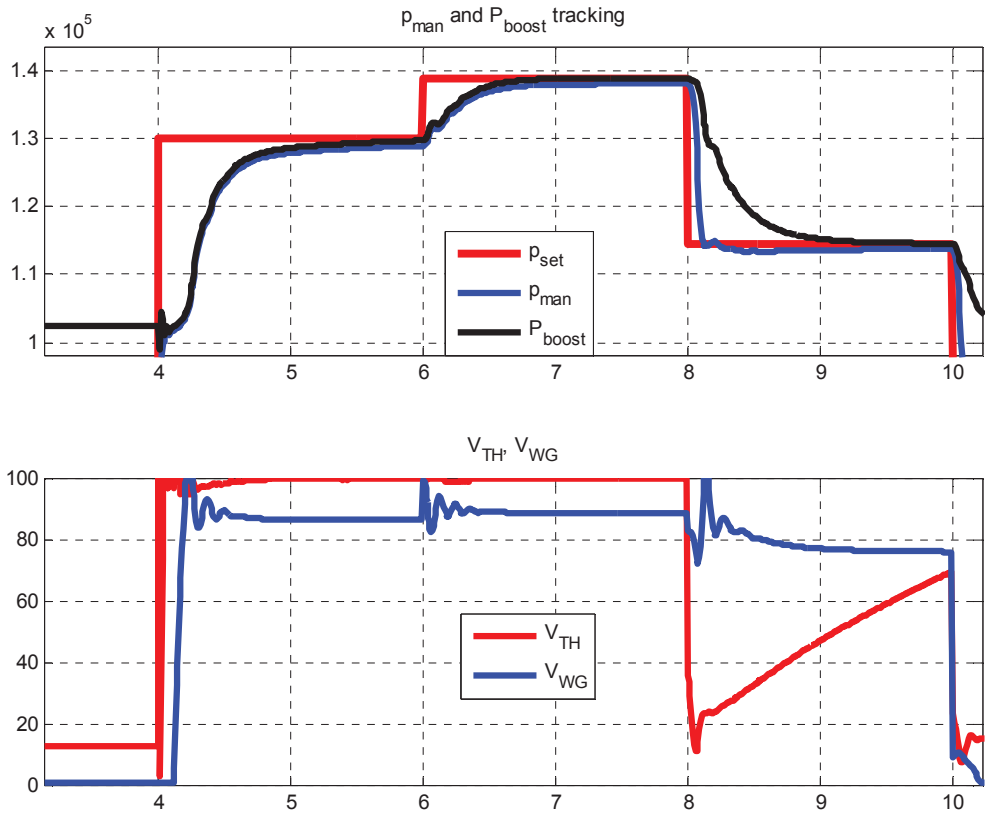

Fig.3.30 Zoom in the result from 3s to 11s, p_{man} and p_{boost} (top), V_{WG} and V_{EGR} (bottom) at 2000 rpm

Look at the details, below 4s, p_{man} can track the set pressure very well because it is smaller than the ambient pressure, but p_{boost} cannot be smaller than 1 bar. Hence, during this period, p_{man} is only controlled by V_{TH}, the performance of p_{man} depends on V_{TH}. Later, from 4s to 8s, the response of p_{man} and p_{boost} are quite the same because the throttle is almost full opened all the time, the pressure is increased, during this period, p_{man} and p_{boost} are controlled by the wastegate. Hence, the performance of p_{man} and p_{boost} depends on V_{WG}; From 8s to 10s, the torque is decreased, consequently, the set pressure is decreased also, the wastegate does not need to close for the lower torque demand, from this moment, p_{boost} and p_{man} respect the desired control design (response time: 0.3s for p_{man} and 1.5s for p_{boost}).

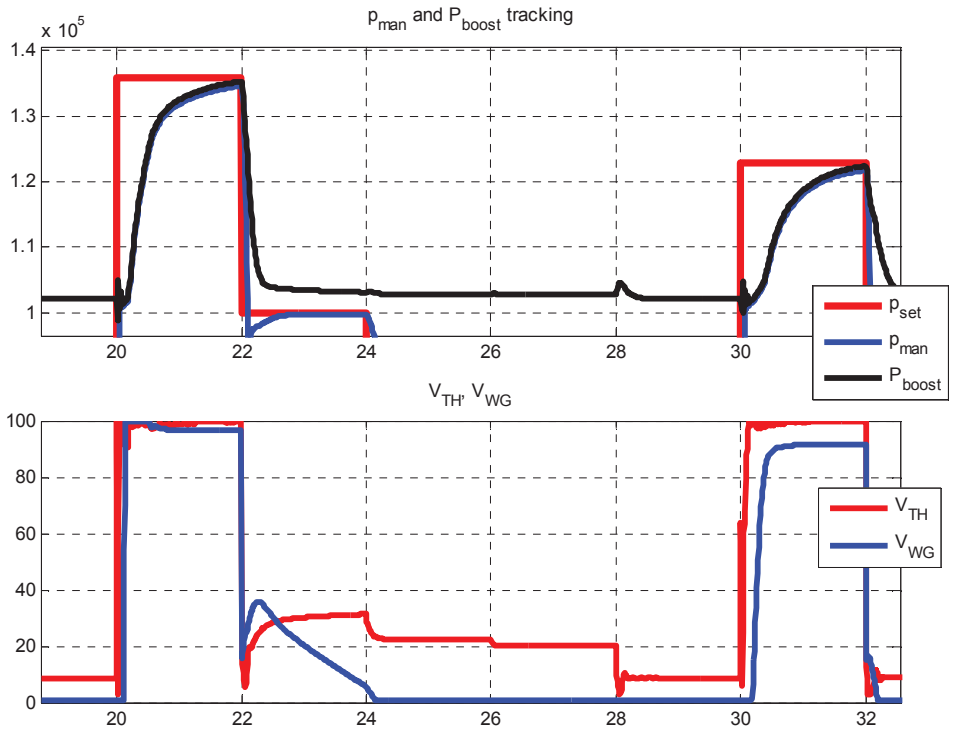

Fig.3.31 Zoom in the result from 19s to 32.5s, p_{man} and p_{boost} (top), V_{TH} and V_{WG} (bottom) at 2000 rpm

From Fig.3.31, we found that p_{man} and p_{boost} kept the same response time from 20s to 22s, 30s to 32s. The responses satisfy the performance of p_{boost}, because V_{TH} is saturated, V_{WG} is used to realize the responses of p_{man} and p_{boost},; From 22s to 30s, the set pressure is decreasing during this period, when it is lower than 1bar, p_{boost} stops to response but remains constant, except one moment at 28s, p_{boost} has a small oscillation because of V_{TH} has a small oscillation.

In Fig.3.32, the responses of p_{man} and p_{boost} are stable with several small oscillations. They occur at 8s, 20s and 30s, because at these moments the system is controlled only by V_{WG}, and in this case, the feedforward filter is not very fitted, but the performance can be reasonably realized with these small oscillations. The control system reacts reasonably quite well with overshoots at these moments.

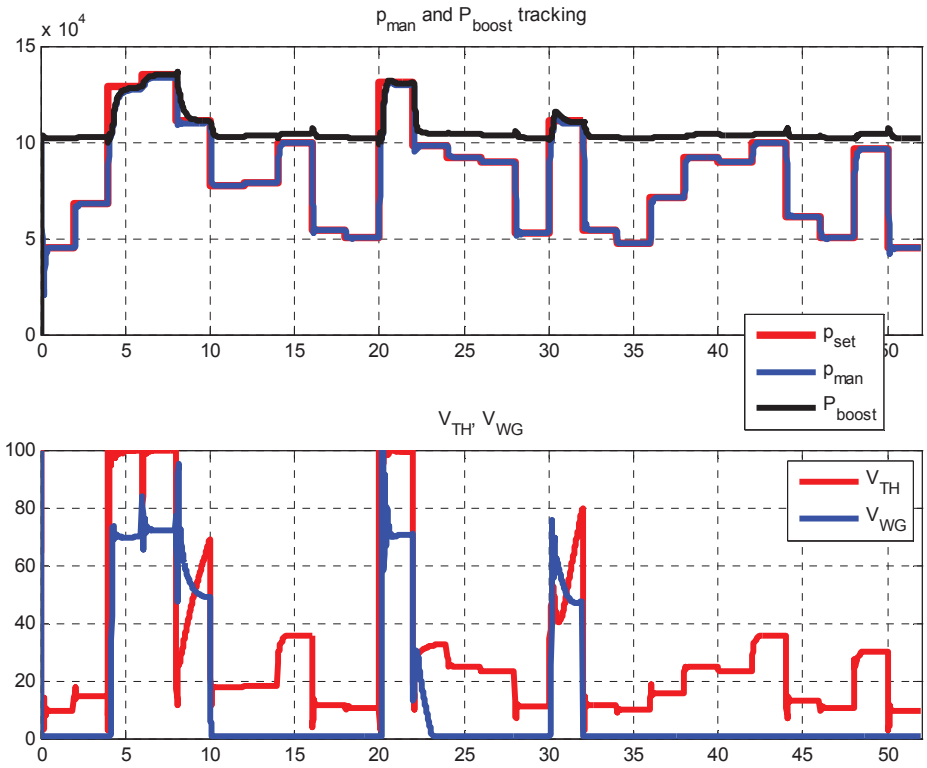

Fig.3.32 p_{man} and p_{boost} (top), V_{WG} and V_{EGR} (bottom) at 3000 rpm

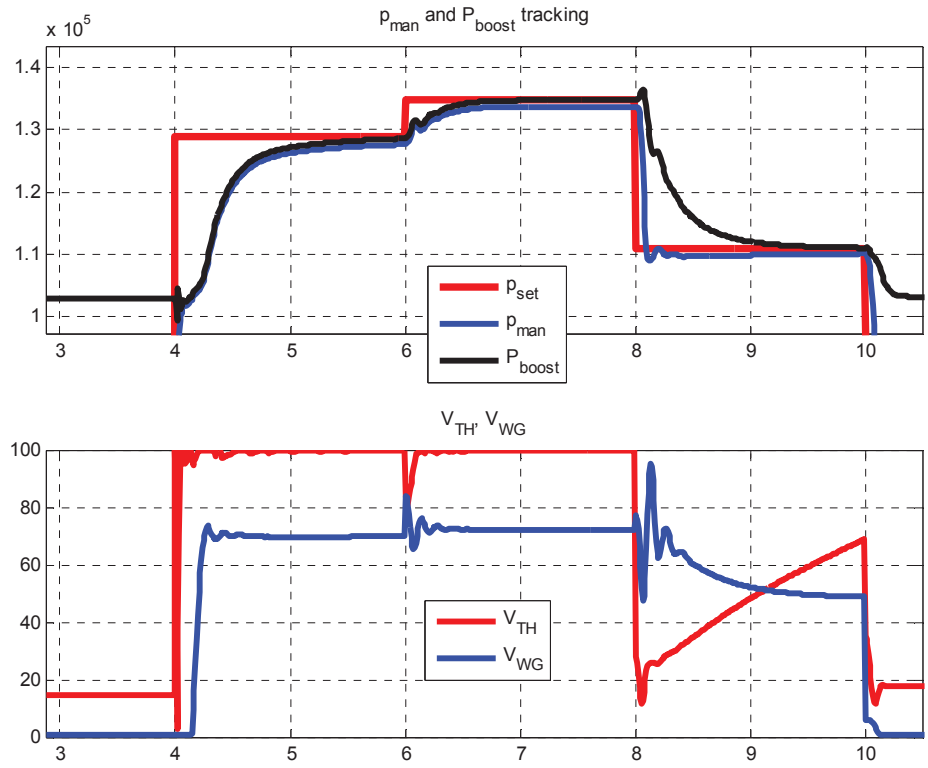

Fig.3.33 Zoom in the result from 3s to 9s, p_{man} and p_{boost} (top), V_{WG} and V_{EGR} (bottom) at 3000 rpm

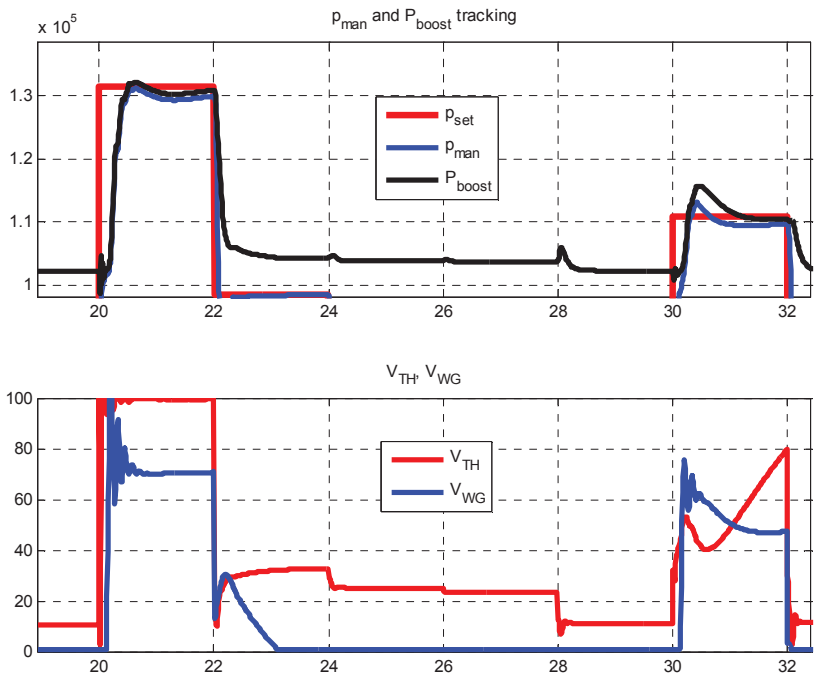

Fig.3.34 Zoom in the result from 19s to 32.5s, p_{man} and p_{boost} (top), V_{WG} and V_{EGR} (bottom) at 3000 rpm

Furthermore, looking at the other figures Fig.3.33 and Fig.3.34, the responses of p_{man} and p_{boost} (top), V_{TH} and V_{WG} (bottom) can follow the references, because Waste-gate and intake throttle react at the same time. Some oscillations appear on the Waste-gate actuators when p_{boost} should respond quickly than its specifications. In these cases, the controller of V_{WG} can provide a quick response time but with much more oscillations because of sensitivity of differentiators.

The responses of p_{man} and p_{boost} have good performances. In Fig.3.35 from 8s to 10s, 21s to 23s and 29s to 31s we clearly see a coupling behavior of our system, i.e., V_{TH} and V_{WG} react at the same time to realize the set constant torque. Hence, we found that if both actuators react at the same time, the system's performance will have some smaller problems (overshoot and oscillation)

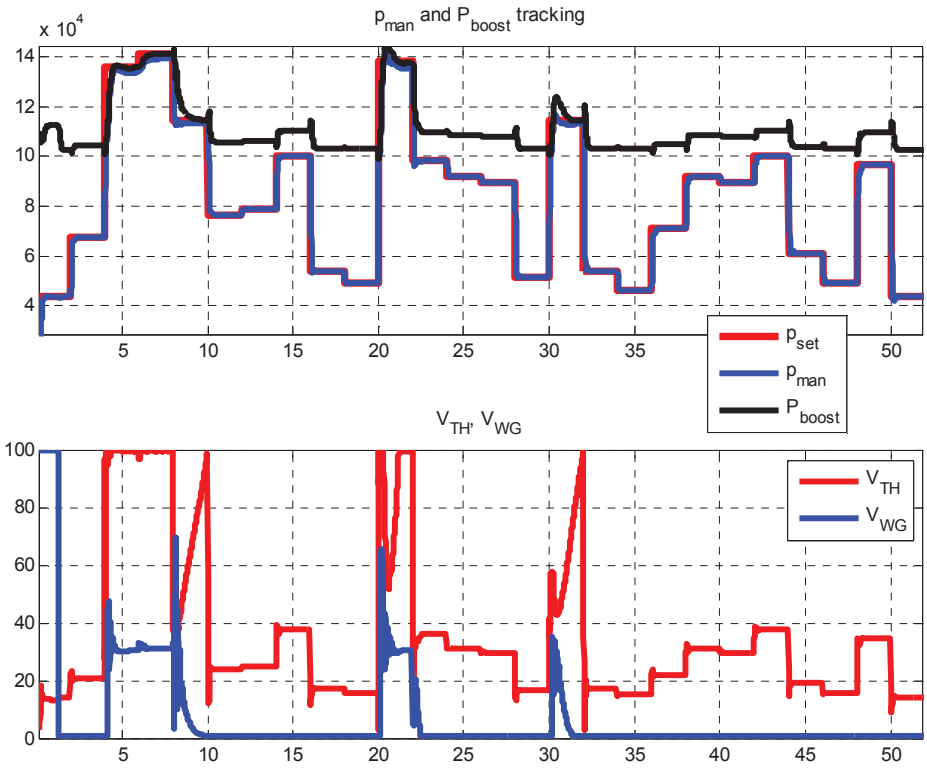

Fig.3.35 p_{man} and p_{boost} (top), V_{WG} and V_{EGR} (bottom) at 4000 rpm

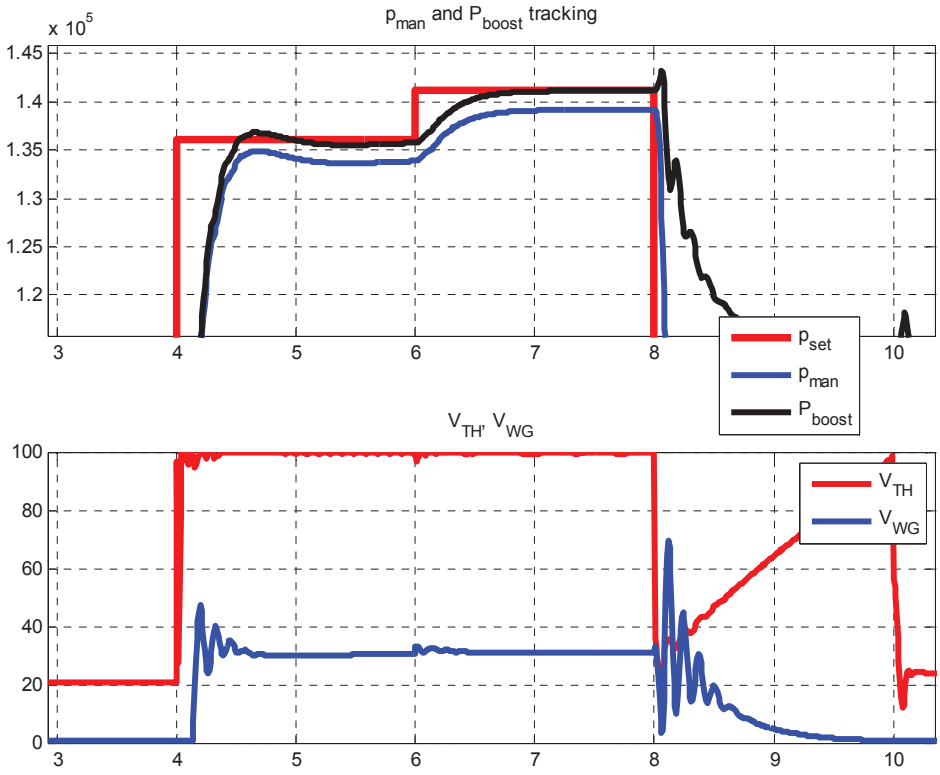

Fig.3.36 Zoom in the result from 3s to 10.5s, p_{man} and p_{boost} (top), V_{WG} and V_{EGR} (bottom) at 4000 rpm

From Fig.3.36, p_{man} has a little steady state even with a wide-open throttle and a boost pressure that follows the reference. It is due to throttle losses in the intake pipe. However, this problem could be solved by increasing the reference of p_{boost}.

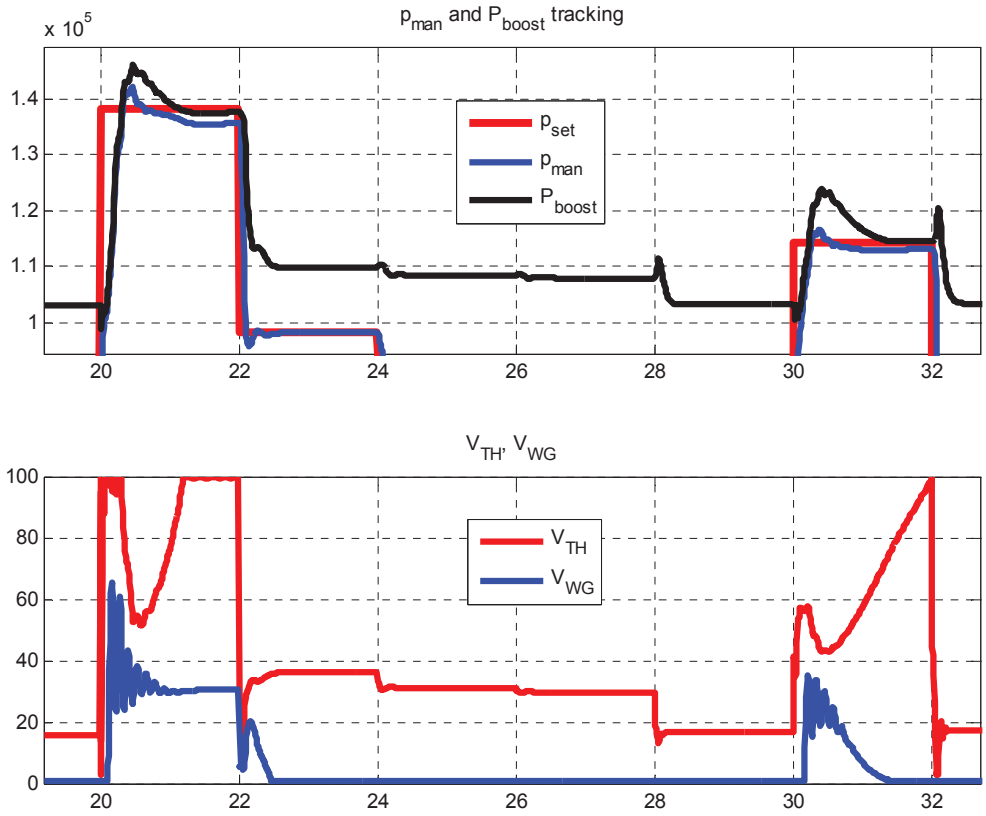

Fig.3.37 Zoom in the result from 19s to 32.5s, p_{man} and p_{boost} (top), V_{WG} and V_{EGR} (bottom) at 4000 rpm

Looking at Fig.3.35, this result shows a good performance through the overall time. The specification is almost achieved, although with a small overshoot at 20.5 s and 30.5 s, p_{man} andp_{boost} are tracked well with a little large overshoot, because of the same reason that both actuators react. In order to have much more details, this figure is plotted from 3s to 11s in Fig.3.36 and from the 18s to 33s in Fig.3.37. Except for these limitations of actuators, this control system can meet the desired performance that has been set before. Hence, this multi-SISO control strategy is validated on all operating points, which demonstrates the good performance and stability robustness.

3.8 Conclusions

This chapter has first presented the considered gasoline vehicle and especially its air path. Then the control objectives of this gasoline engine are given so that the in-cylinder air mass has to be regulated. However, as it cannot be measured directly, an intermediate and measurable variable, the intake manifold pressure p_{man}, is necessary to represent this in-cylinder air mass. The intake manifold pressure p_{man} model (refer to §1.8.4) is thus presented. Moreover, due to the link between intake manifold pressure and boost pressure p_{boost}, and to the protection of the turbine and engine at high

speed and torque, the boost pressure (refer to §1.8.5) is thus controlled. These two variables (p_{man} and p_{boost}) are controlled by two actuators: intake throttle and Waste-gate valve. The robust control design methodology is tested on a gasoline engine simulator, which is built in PRISME laboratory in Orleans, the modeling, identification, analysis, robust control design are thus done on this simulator. Finally, the validation of its design is also done on the same simulator. The obtained performance satisfies the specifications in terms of overshoot and disturbance robustness requirements, against the coupling and uncertainty. However, there are some oscillations because of sensitivity of anti-windup and differentiators. Therefore, this methodology is proven for this gasoline engine simulator.

CHAPTER 4 Application: Air path control of a diesel engine

Contents

4.1 Résumé

Ce chapitre présente le contrôle du système « chaîne d'air d'un moteur à allumage par compression ». La méthodologie proposée au chapitre 2 est d'abord appliquée à un système ayant 2 entrées (vanne de recirculation des gaz brûlés et vanne de décharge du turbo) et 2 sorties (débit d'air et pression dans le collecteur d'admission). L'objectif de cette première application, réalisée en simulation, est de maîtriser la quantité d'air entrant dans le cylindre et de maîtriser la consommation du moteur. Dans la deuxième partie de ce chapitre, la stratégie est cette fois appliquée à un système augmentée d'un actionneur (papillon d'admission). L'objectif, cette fois ci, est d'aller plus loin dans le compromis NOx et consommation, à l'aide d'un degré de liberté supplémentaire. La validité de ces deux applications est prouvée par un grand nombre d'essais sur simulateur mais aussi sur banc d'essai où les quantités de NOx sont abaissées durant les transitoires de couple et de régime.

4.2 Introduction

In order to comply with diesel engine emission standards, the fuel and air path must be accurately controlled. This chapter focuses especially on the air path of turbocharged diesel engines equipped with an EGR and a wastegate (to bypass the exhaust gas). Sometimes, when the most important requirement is NOx, the throttle can also be used [Guzzella and Amstutz, 1998, Van Nieuwstadt, et al., 1998] in order to increase EGR and thus decrease NOx.

A certain number of studies can be found, which taking EGRs and turbochargers into account on the air path of a diesel engine. In [Van Nieuwstadt, et al., 1998, Guzzella and Amstutz, 1998], VGT and EGR control strategy is employed to maintain a positive pressure drop over the EGR valve and obtains the desired efficient EGR rates. For example, H infinity control [Wei and del Re, 2007], LPV control without EGR [Lee and Sunwoo, 2012] was used to control the air path of a diesel engine. Another method, tested on the diesel engine, is inverse optimal control which gives a robust nonlinear control [Wahlström and Eriksson, 2008]. Ortner and del Re [Ortner and del Re, 2007] proposed the use of new set points of data-based models to design a Model-based predictive controller (MPC) for diesel engines. Internal Model Control (IMC) can also be used to control a diesel engine. IMC and feedforward methods are combined to obtain good control performance [Nitsche, et al., 2007]. In [Arnold, et al., 2009] fuzzy controller was proposed, without using a physical model. A nonlinear predictive control based on local networks for air management in diesel engines was discussed in [García-Nieto, et al., 2008]. In [Chauvin, et al., 2007] authors demonstrate the relevance of motion planning in the control of the air path with EGR.

Compared with these strategies, the idea is to develop a simple control design methodology to control the air mass flow and boost pressure using EGR and wastegate valve. Considering coupling and

uncertainty, this complex 2x2 MIMO system should be controlled with a nonlinear MIMO controller to achieve robustness and performance. The control strategy proposed in this chapter is a sequential PID pole placement which is simple to design, while the stability robustness is guaranteed against uncertainty and coupling. The advantage of this methodology is that coupling and uncertainty are considered for the last loop's processing. Before processing the control methodology, the properties of the MIMO system need to be analyzed. Consequently, a MIMO process coupling analysis and a Robust Sequential Multi-SISO control are employed. Above all, one methodology that is easy to follow and to execute is proposed, with a control using less computation time and more economical.

This chapter presents first the considered diesel engine's control issues. After the description of the diesel engine simulator, the control is designed and validated, and it is a two-input and two-output square MIMO system. Afterwards, this diesel engine system is extended to the real engine experiment. This MIMO system is extended to a three-input-two-output non-square MIMO system, and it is tested with a non-square controller as well as its square controller.

4.3 Application description

The methodology of chapter 2 has been applied first to the gasoline engine (chapter 3). To verify the generality, it is applied now to a diesel engine simulator and on a test bench (PSA DW10 ATED). The main characteristics of the engine are given in Table 4.1. This engine has four cylinders and a maximum torque of 250N.m.

Real Diesel Engine's Characteristics	
Bore X Stroke	85 X 88mm
Number of cylinders	4
Volume of cylinders	1996cm^3
Maximum power	80kW at 4000 tr/min
Maximum torque	250N.m
Compression ratio	18
Turbo compressor	Wastegate actuated
Injection	Common rail

Table.4.1. Parameters of the PSA DW10 engine

Control objectives are to optimize diesel engine performance, fuel economy and pollutant emissions. The air path of the considered diesel engine contains:

- a turbocharger: one of the best solutions for reducing fuel consumption, and equally for improving performance if the cylinder volume remains constant [Colin, et al., 2007],
- a wastegate: allows the reduction of the negative effects of turbocharger inertia (long torque time response), especially in low load condition,
- an EGR valve: proved to be a very efficient way of reducing NOx,
- an intake throttle: proved to be efficient in the reduction of NOx and / or fuel consumption when it is used in addition to EGR valve and / or wastegate.

In this chapter two ways of this strategy are proposed. Firstly a square multivariable controller is designed which will be tested in simulation. Secondly, a non-square multivariable controller is designed which will be tested on a real engine test bench. Both strategies try to reach a good compromise between fuel consumption and NOx emissions, but the non-square controllers manage to achieve a better one with the help of a third actuator (throttle) which allows a third degree of freedom.

The overall control system of this diesel engine is shown in Fig.4.1; the applied system is a turbocharged equipped and direct injection engine. The main aim of the diesel engine control is to regulate the indicated torque and more precisely the fuel mass entering into the cylinder. Fig.4.1 shows in red dotted blocks all variables of the air path and in black dotted blocks variables of the fuelpath. Te intake throttle (V_{TH}), wastegate valve (V_{WG}) and EGR valve (V_{EGR}) are the input or manipulated variables, air path and boost pressure and mass air flow are the controlled variables, of the air path. The air path engine control scheme usually used is illustrated in Fig.4.2.

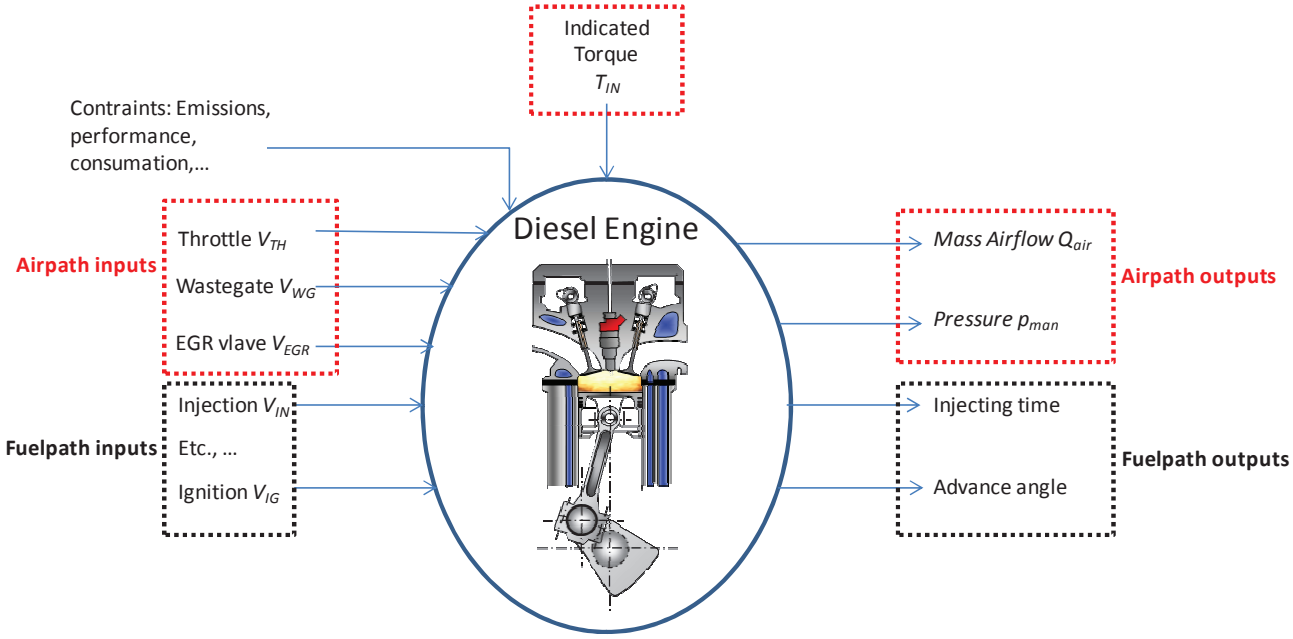

Fig.4.1 Diesel engine overall control system

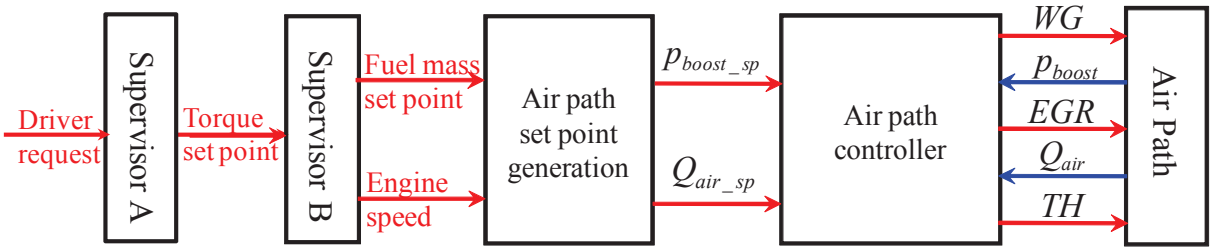

Fig.4.2 Global control scheme for the air path of a diesel engine

This system has three inputs and only two outputs. The first step is applied the strategy considering that the throttle is constantly fully-opened. The system becomes a 2x2 multivariable one. The objective of the designed controller is to lower fuel consumption and pollutant emissions. The second step will be to employ all the inputs (throttle, EGR valve, wastegate) to control the two outputs of the multivariable engine system. This time the controller will be used to better optimize ~~more~~ the pollutant emissions.

4.4 Validation on a diesel engine simulator

4.4.1 System modeling

Gray-box model of diesel engine system

A gray-box engine model, used to describe physical flows such as the intake or exhaust flow, needs short computation time and less computer storage. Therefore, for tuning the design process, a 0D model is generally used. In addition, this model is employed to validate the air path control design, which corresponds to a low-frequency model using a MVEM to describe the combustion part. The structure of this diesel engine air path is shown in Fig.4.3; this simulator is built in PRISME Lab, Orléans with real data collected. Compared with the gasoline engine simulator presented in chapter 3 an EGR valve, which is used in advanced engine control systems.

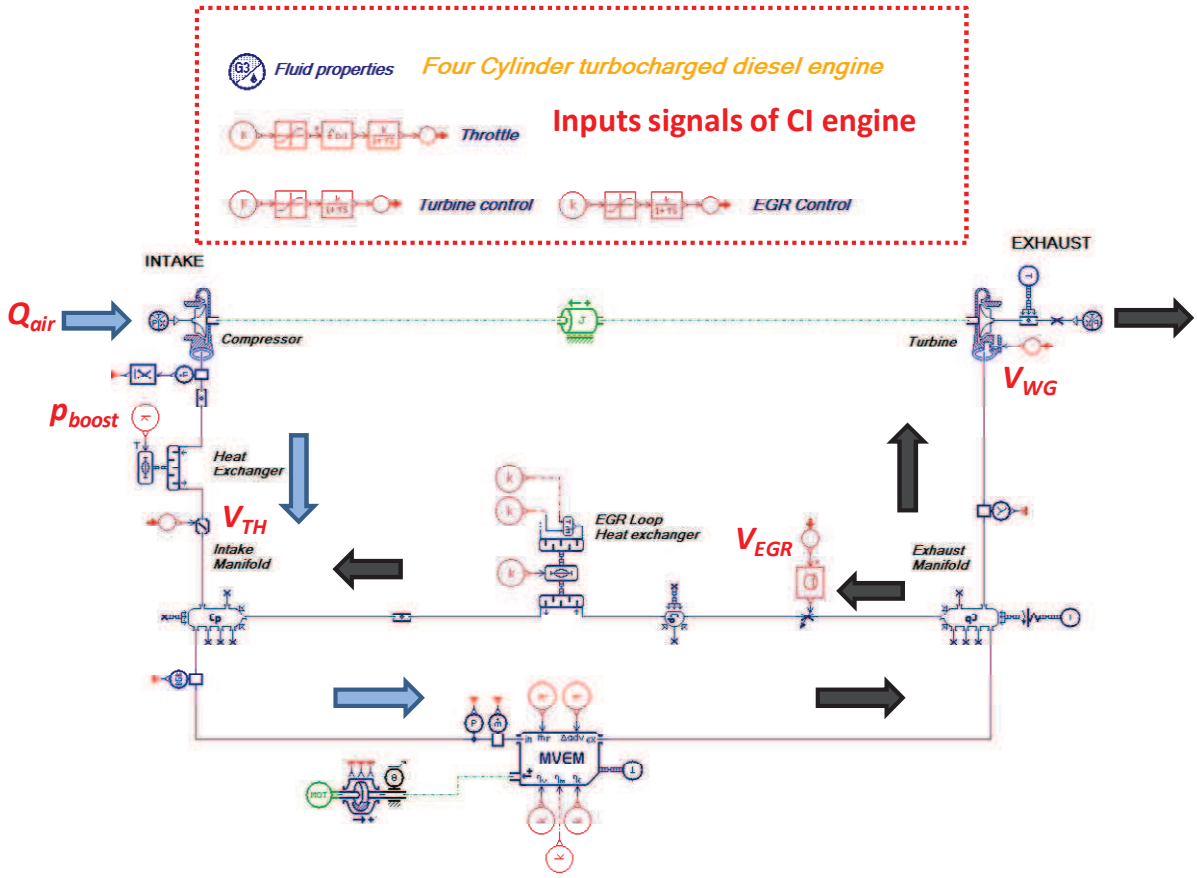

Fig.4.3 Air path of a turbocharged diesel engine

The EGR is employed to reduce the pollutant emissions (NOx). It recycles exhaust gases in the intake system to dilute the fresh air; consequently, the combustion temperature can be reduced, and results in less nitrogen oxides being produced. It is normally used in diesel engines to comply with the standards. The simulator mentioned here is based on the PSA DW10ATED diesel engine, which is a 2.0L turbocharged 4-cylinder diesel engine with direct injection. All the air path actuators are pneumatic (wastegate, EGR and throttle). The simulator model is a nonlinear model based on physical equations (e.g. thermodynamic principles for volumes, Barré de St Venant equations for restrictions…) and look-up tables (e.g. volumetric efficiency, turbocharger…). All the simulation results shown here were obtained using LMS/AMESim.

Black-box modeling

In order to consider numerous engine operating points the system working area is gridded to 54 couple of engine speed and torque (Fig.4.4). The torque is from 25Nm to 125Nm, speed is from 1000 to 4000 rpm. The corresponding values of the actuator for the 54 operating points are shown in Fig.4.5. These values are produced using real data from the engine test bench.

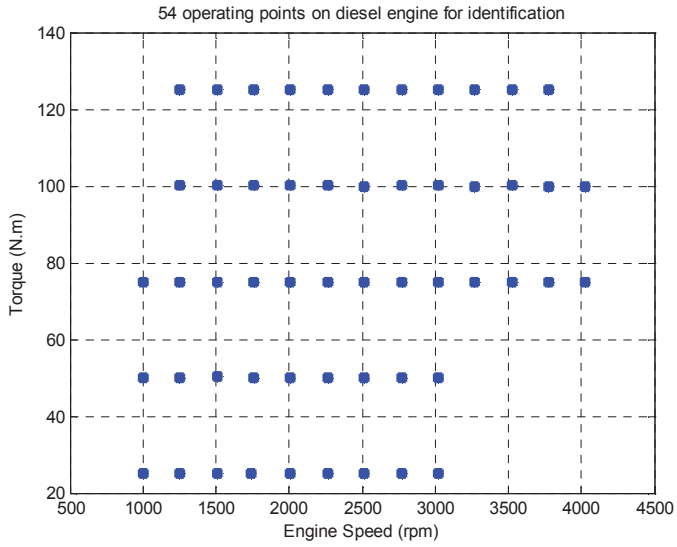

Fig.4.4 54 operating points

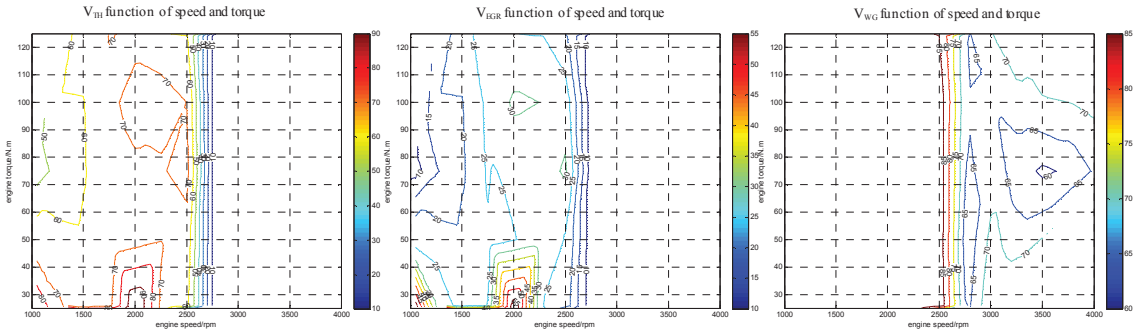

Fig.4.5 The 54 operating points spread over the engine working situations

In this section, the system identification is split into three parts. Firstly, the excited inputs signals are chosen to obtain the information in the system, afterwards, the output signals are collected while exciting the input. Secondly, the input/output signals are normalized to facilitate the comparison of variables and linearize the system. Thirdly, a Fourier Transform is used to calculate the frequency data.

a. Excitation Signal

Regarding the engine's physical characteristics, the parameters of multisine have been chosen and given in Table.4.2. The constraints of V_{EGR} are [0, 82], and V_{WG} [40, 80], respectively.

Actuator	Average	Magnitude	fmin , fmax	Saturated values	Ops
EGR	V_{EGR}	$V_{EGR}\pm 10\%$	0,2~40Hz	[0 82] %	1000 -4000rpm
WG	V_{WG}	$V_{WG}\pm 10\%$	0,2~40Hz	[40 80] %	25 -125Nm

Table.4.2. Configuration of input signals of multi-sine

These excited signals are shown in Fig.4.6 (Input) and Fig.4.7 (Output). The chosen method is to activate the output with sufficient movements of controlled variables, i.e., airflow mass and boost pressure, whose absolute amplitude should bigger than their noise amplitude. Hence, airflow mass should be larger than 0.3g/s and boost pressure 0.005bar. These conditions are accepted regarding the output of these absolute amplitudes of output signals.

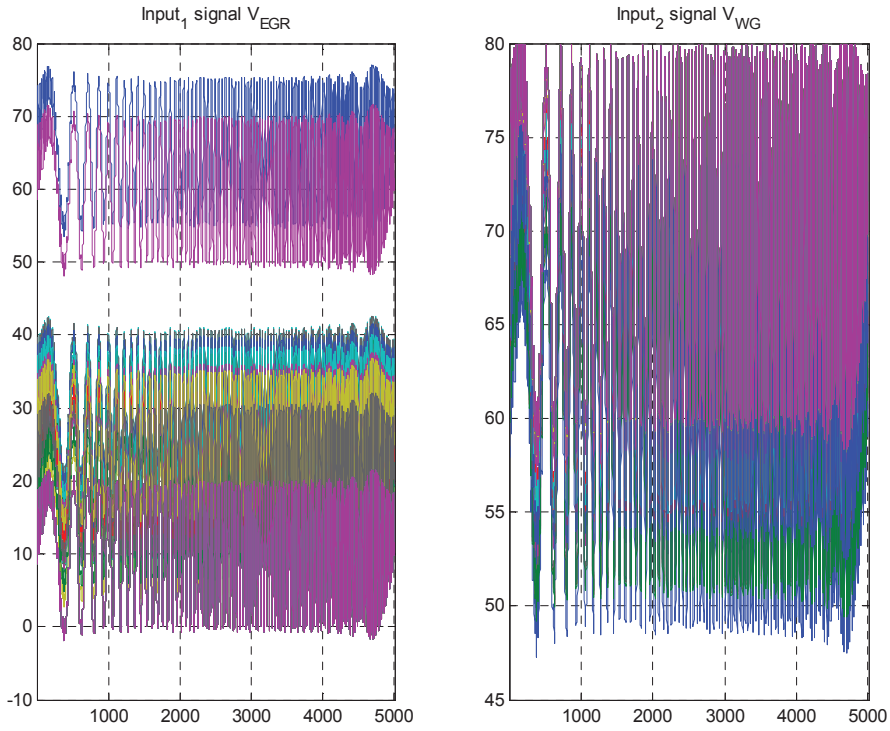

Fig.4.6 Excited inputs of V_{EGR} and V_{WG}

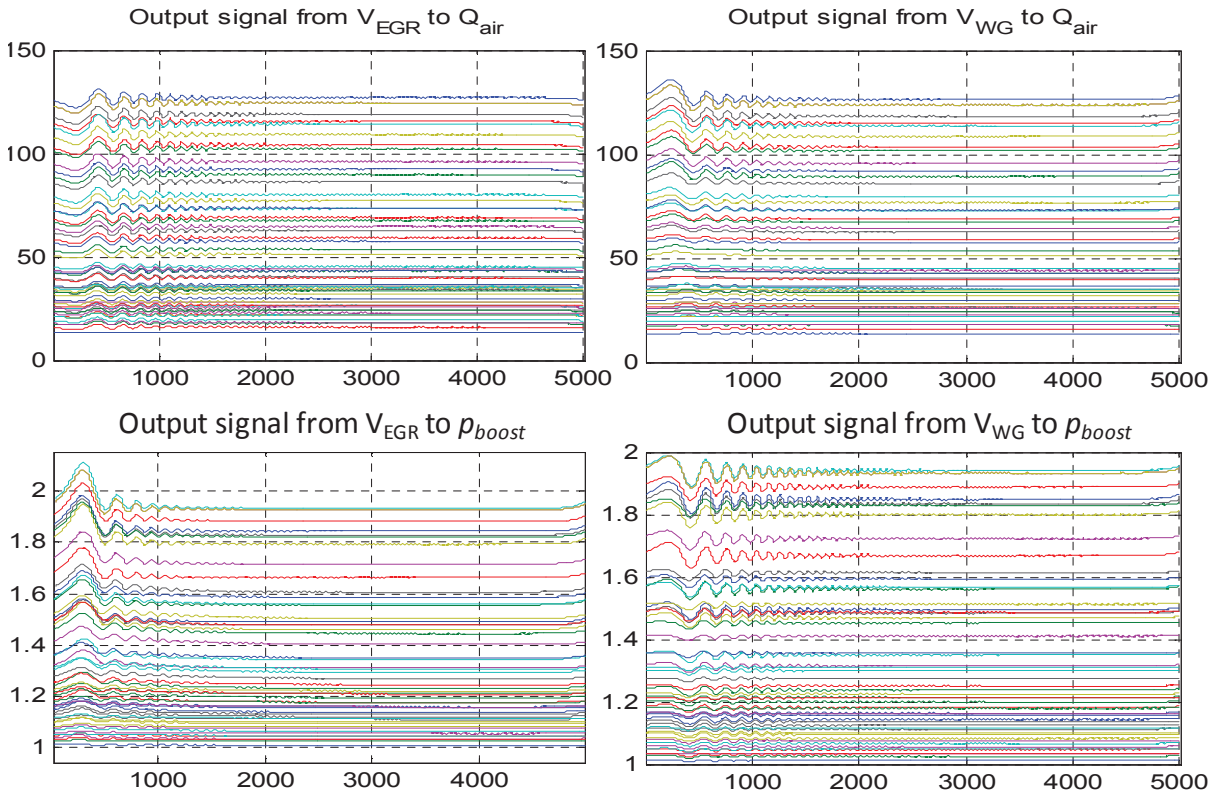

Fig.4.7 Excited outputs of air path loop

b. Data processing

From these exciting signals, the input and output signals have different units and average values. Therefore, it is difficult to compare the small difference among these signals. They are thus normalized for the analysis and synthesis of an appropriate control system (see Chapter 2). Processed input and output signals are then operated around 0. Normalized inputs and outputs are displayed in Fig.4.8 (inputs) and Fig.4.9 (outputs)

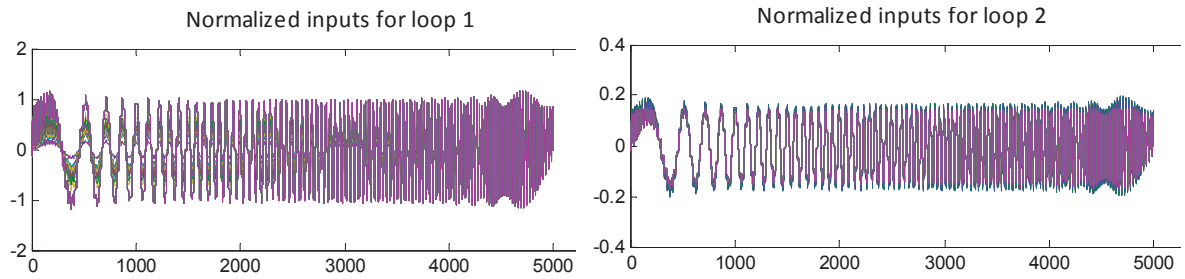

Fig.4.8 Normalized excited input signals

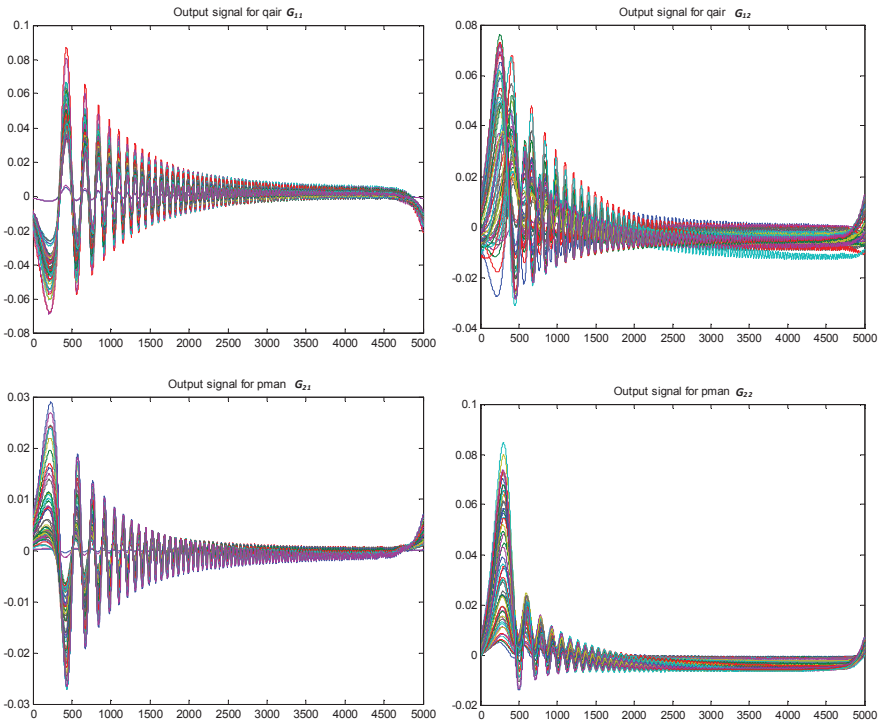

Fig.4.9 Normalized excited output signals

Fast Fourier Transform is used to calculate the bode diagrams of this uncertainty system, which is described as follows and shown in Fig.4.10,

- G_{11} is from V_{EGR} (as %) to Q_{air} (in g/s), static non linearity about 15dB.
- G_{12} is from V_{WG} (as %) to Q_{air} (in g/s), static non linearity about 30dB.
- G_{21} is from V_{EGR} (as %) to p_{boost} (in bars), static non linearity about 30dB.
- G_{22} is from V_{WG} (as %) to p_{boost} (in bars), static non linearity about 20dB.

c. Nominal frequency identification

Because this application is applied to a model-based control methodology, a model is needed to design the robust controller. Using an average of uncertainties and a Matlab identification toolbox, the nominal model is computed. It is presented by a frequential representation shown in Fig.4.10. From these nominal identification figures, four second orders linear transfer function can be employed to identify the nominal plants.

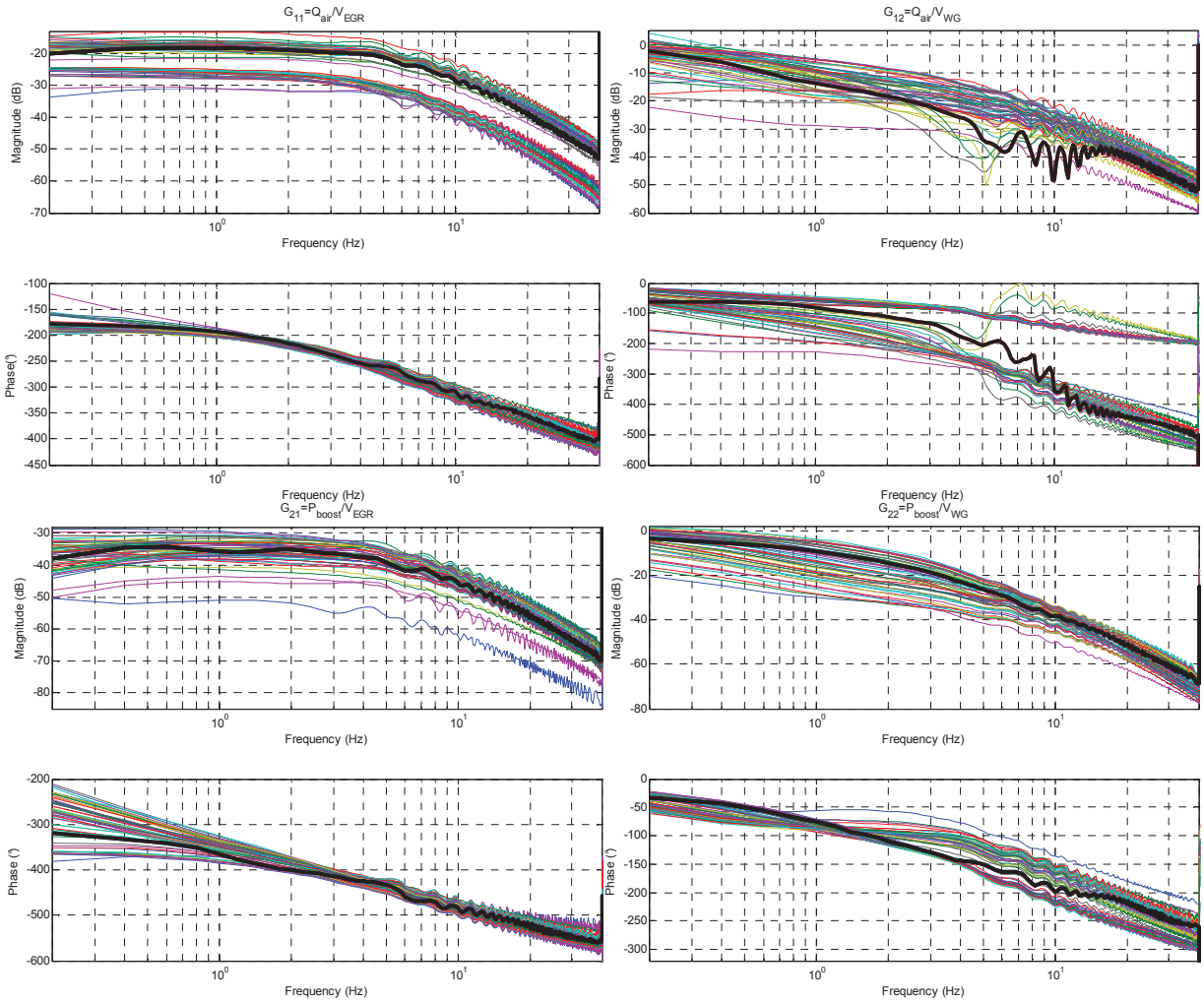

Fig.4.10 Bode diagrams of the process $G(j\omega)$ (54 operating points)and the nominal plant $G_{nom}(j\omega)$ (thick black solid curves)

From the bode diagram, nonlinearity can be observed, and all uncertainty of system is depicted. Afterward, the frequency responses of this system are collected for the preparation of MIMO system analyses. The nominal plants are identified and collected as

$$G_{nom_{ij}}(s) = \begin{cases} \dfrac{-0.13}{(0.027s+1)^2} & if\ i=1, j=1 \\ \dfrac{1.32}{(1.03s+1)(0.035s+1)} & if\ i=1, j=2 \\ \dfrac{0.018}{(0.025s+1)^2} & if\ i=2, j=1 \\ \dfrac{0.74}{(0.72s+1)(0.02s+1)} & if\ i=2, j=2 \end{cases} \quad (4.1)$$

4.4.2 System analysis

Coupling and uncertainties of the system will be studied using SV, CN, RGA, GB and CD^3 tools.

Singular Values analysis

Fig.4.11 shows that whatever the frequency, most $\overline{\sigma}$ are smaller than 1 and $\underline{\sigma}$ are smaller than 0.1. Consequently the system is ill-conditioned and easier to be controlled.

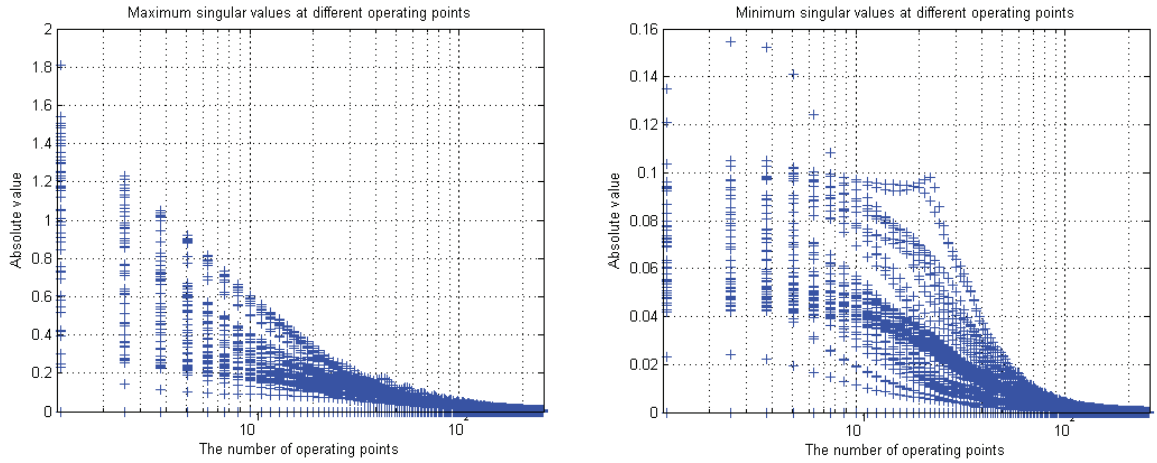

Fig.4.11 Maximum $\overline{\sigma}$ (left) and minimum $\underline{\sigma}$ (right) singular values at 54 operating points from 2 rad/s to 250 rad/s, system with normalization

Condition number analysis

From Fig.4.12, the CN for the normalized system is decreased compared with the non-normalized system, the maximum CN value is reduced from 3000 to less than 100. However, the normalized CN is still bigger than 10, which confirms that the plant is ill-conditioned. In both cases, the system is more sensitive at high frequencies but within acceptable limits. If we compare Fig.4.12 with Fig.4.13, the value of the condition number can be minimized with the optimal condition number (OCN). From Fig.4.13, before 60rad/sec most of the optimal condition number values are smaller than 10, implying that at these operating points and under this frequency, the system is not very sensitive to input unstructured uncertainty. Except for two operating points, the values of OCN are larger than 10, from 60 rad/s to higher frequencies, which means that the system is ill-conditioned. In this case, the system may be sensitive to uncertainty.

As the maximum OCN is about 13, the ill-conditioning can be considered acceptable especially if crossover frequencies of the closed-loop are lower than 10rad/s [Skogestad and Morari, 1987]. In this case, the maximum OCN values range from 1 to 3, which imply that the system is well-conditioned.

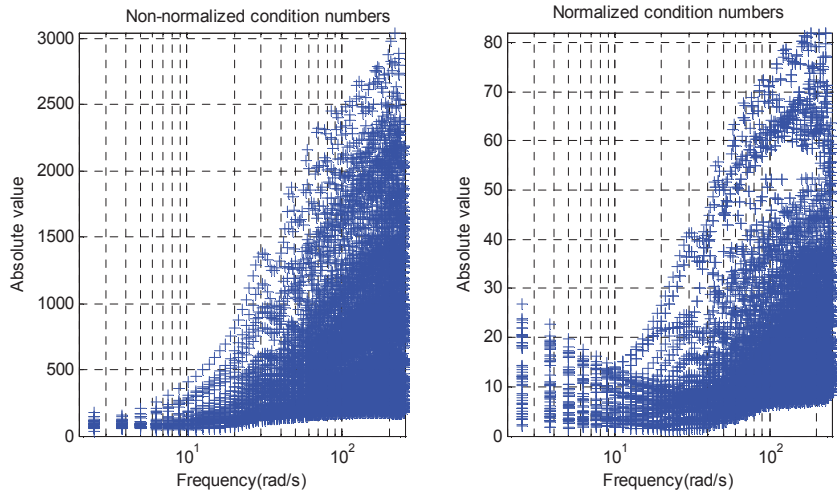

Fig.4.12 Without and with normalization of 2x2 MIMO system's CN

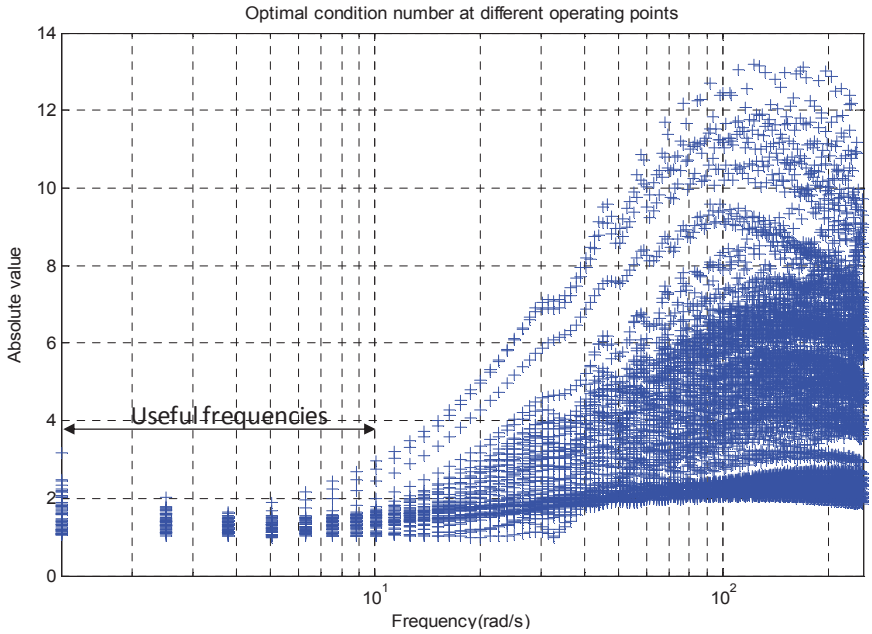

Fig.4.13 Optimal Condition numbers on 54 operating points from 2 rad/s to 250 rad/s.

Relative Gain Array analysis

Another way to find the degree of coupling and the pairing of inputs/outputs of a MIMO system is to use the Relative Gain Array (RGA).

For example, the RGA is computed at two frequencies (2 and 250 rad/s):

$$\Lambda(G(j2)) = \begin{bmatrix} 0.92 - 0.048\mathrm{i} & 0.078 + 0.048\mathrm{i} \\ 0.078 + 0.048\mathrm{i} & 0.92 - 0.048\mathrm{i} \end{bmatrix}$$

$$\Lambda(G(j250)) = \begin{bmatrix} 1.67 - 1.93\mathrm{i} & -0.67 + 1.93\mathrm{i} \\ -0.67 + 1.93\mathrm{i} & 1.67 - 1.93\mathrm{i} \end{bmatrix}.$$

From these two frequencies, their diagonal RGA-elements have positive real values and near unit elements; hence, if only these two points are considered, the diagonal elements can be processed to achieve the desired pairings of inputs and outputs. The RGA is shown from 2 rad/s to 250 rad/s in Fig.4.14.

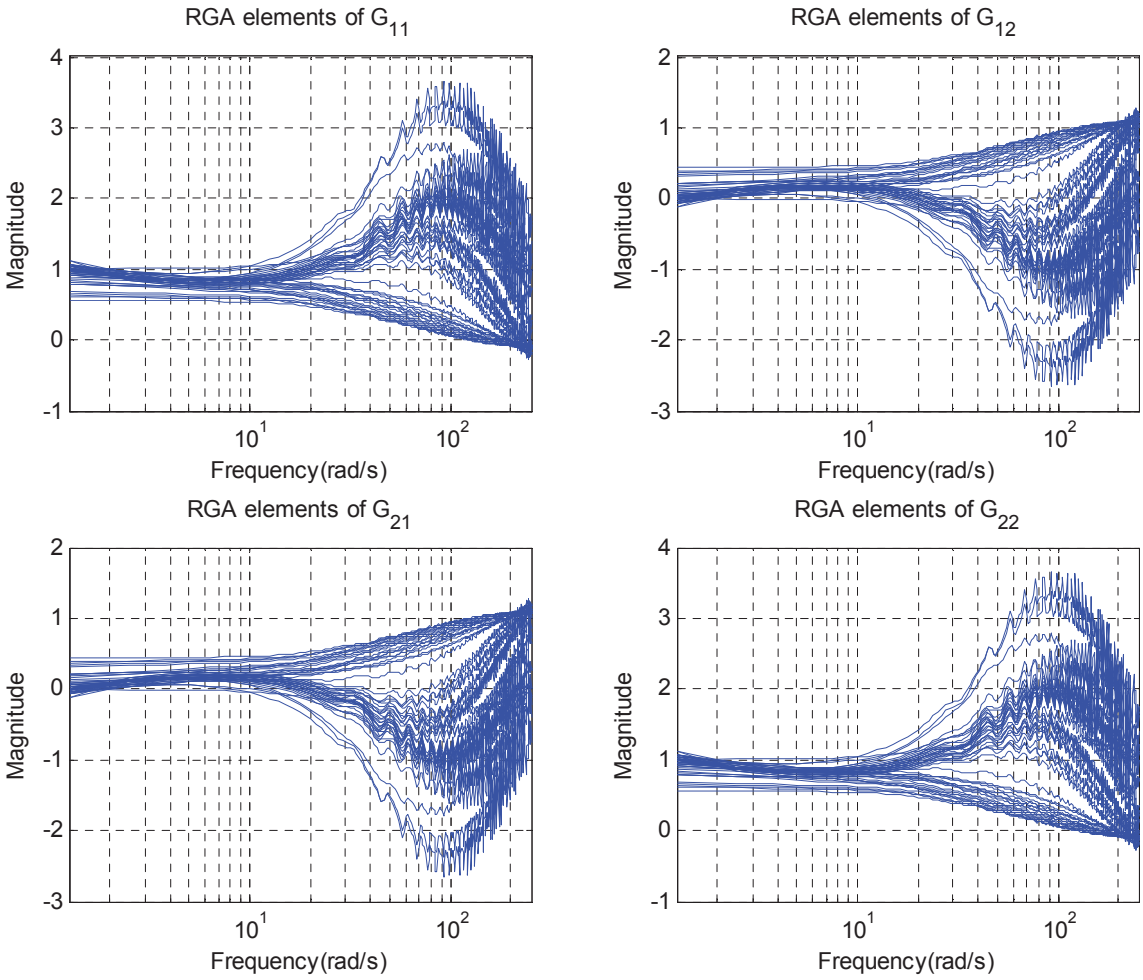

Fig.4.14 Real part of the RGA elements on 54 operating points (2rad/s to 250rad/s)

Fig.4.14 shows that all real parts of the RGA-elements are smaller than 4, i.e. they are not large RGA-elements. For frequencies below 15 rad/s the values of RGA for G_{11} and G_{22} are close to 1 and for G_{12} and G_{21} are close to zero. Moreover off-diagonal RGA-elements have negative values they should be avoided to pair these as inputs and outputs. Hence, G_{11} and G_{22} should be chosen as the main plants. Before 15 rad/s, RGA-elements are smaller than 1.2 (in fact close to unity matrix), which implies a major link from input to output on the diagonal. The manipulated variable V_{EGR} (resp. V_{WG}) therefore affects the output Q_{air} (resp. p_{boost}) more directly. Hence, two single-loop controllers can be used for this system.

Gershgorin bands analysis

The bands and diagonally dominant elements are plotted in Fig.4.15.

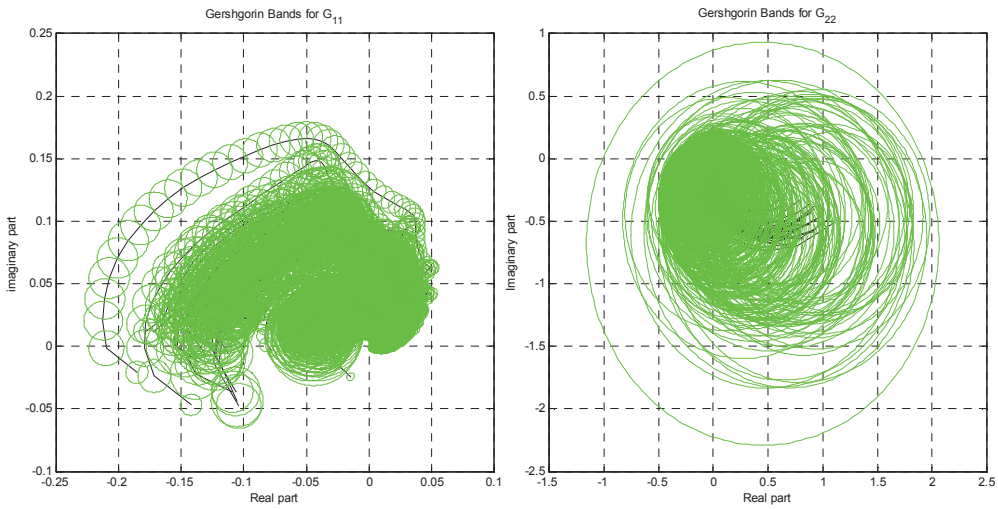

Fig.4.15 The Gershgorin Bands in 54 operating points (On the left: GB for loop 1; on the right: GB for loop 2; center curves are G_{11} and G_{22}, circles are the disturbances of G_{21} and G_{12})

From the left-hand graph of Fig.4.15, it can be seen that in loop 1, G_{11} has thin bands and excludes the critical point, and that the disturbance of loop 1 is small; this loop is therefore highly decoupled and stable.

The right-hand graph in Fig.4.15 shows that in loop 2, G_{22} has very thick bands and for one operating point includes the critical point. Therefore, loop 2 G_{22} is coupled with G_{12}, when considering a decentralized controller, coupling must be taken into account for the synthesis. However, it is important to mention that the stability conditions are only sufficient but not necessary, hence it cannot be concluded that this loop is unstable.

CD³ analysis

The CD³ analysis is used to measure the degree of coupling for different loops of the system. The CD³ analyses of the two loops are plotted in Fig.4.16.

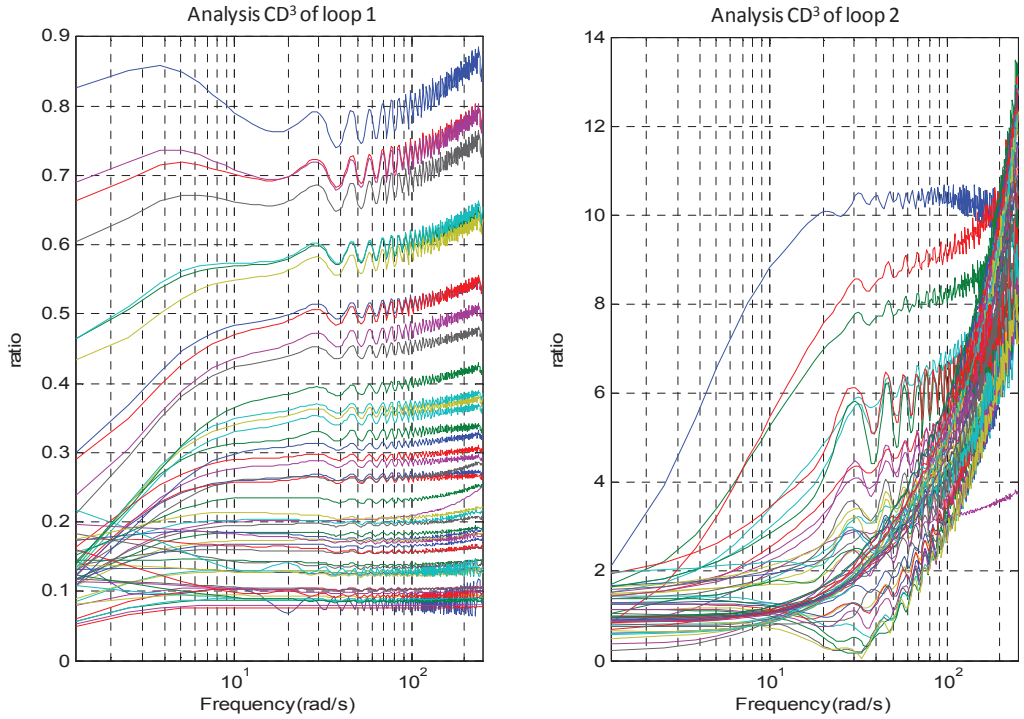

Fig.4.16 CD^3 of open-loop 2x2 MIMO system for two loops (diesel simulator)

The left of this figure, it has small CD^3, the maximum value of CD^3 is 0.88 for the first loop (EGR valve to Air mass flow) consequently coupling of G_{21} cannot bring big disturbance toward G_{11}. But the second loop has larger CD^3, the maximum value is more than 13.3 at high frequency and behind 4rad/s the CD^3 is lower than 3. Consequently in the second loop (wastegate to boost pressure) G_{12} dominates G_{22} because it has more gain than G_{22} and if we choose a lower frequency unit for the second loop, this overall system can use decentralized control. Moreover, the first loop can take SISO control design but the second loop cannot use a real SISO control design.

Conclusion of MIMO System's Analysis

Considering the MIMO analysis tool, the first loop has minor coupling, but the second loop has very significant coupling, as a result, the control will be a sequential Multi-SISO Robust control strategy. One loop uses SISO control design and the other uses the previous control design (sequential). Afterwards, this new system can be taken as two SISO loops. Before designing the controller, frequency identification tools are used to define the diagonal transfer function of the nominal process:

$$G_{nom_{ii}}(s) = \begin{cases} \dfrac{-0.13}{(0.027s+1)^2} & \text{if } i = 1 \\ \dfrac{0.74}{(0.72s+1)(0.02s+1)} & \text{if } i = 2 \end{cases} \qquad \textbf{(4.2)}$$

The PID pole placement can then be used. Hence, this global control scheme is shown in Fig.4.17. Air mass flow and boost pressure are two references which are controlled by actuators of EGR and wastegate. Finally, the nominal transfer function of the plant is chosen diagonally:

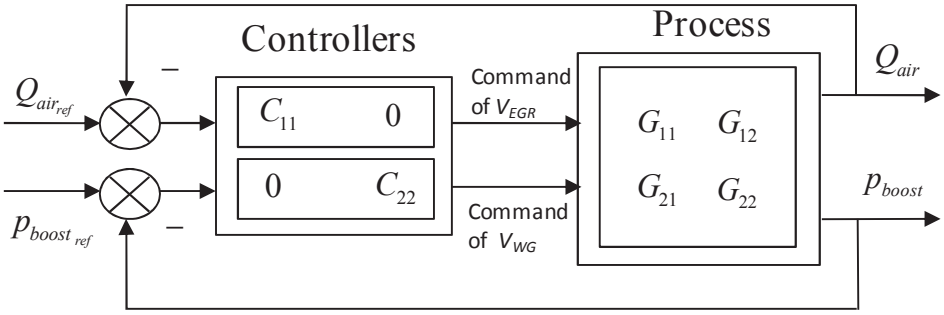

Fig.4.17 Global control scheme of diesel engine control

4.4.3 Robust control synthesis

Due to nominal plants of G_{11} are second order linear systems, the controller of the first loop can be designed by PID pole placement methods. The second loop use an equivalent plant G_{22}*(s) which is defined as a function of the first loop's controller $C_1(s)$ and all transfer function of the nominal plants. Considering system dynamics and physical properties, reasonable desired performances have been fixed:

- the overshoots were set at 3% for p_{boost} and 5% Q_{air},
- the response times were fixe to 0.3s and 1.5 for p_{boost} and Q_{air} respectively,
- the bandwidths of the nominal function must be respectively 2 and 10 rad/s.

The open loop system and controller are rewritten here:

$$G_{ii}(s) = \frac{K_p}{(T_1 s + 1)(T_2 + 1)} \quad \textbf{(4.3)}$$

$$G_{ii}(s) = \frac{K(T_i T_d s^2 + T_i s + 1)}{T_i s} \quad \textbf{(4.4)}$$

$$T(s) = \frac{C(s)G_{ii}(s)}{1 + C(s)G_{ii}(s)} \quad \textbf{(4.5)}$$

In order to find the controller, a desired third order system $T_{des}(s)$ is also rewritten here:

$$T_{des}(s) = \frac{\alpha\omega_n^3}{(s + \alpha\omega_n)(s^2 + 2\zeta\omega_n s + \omega_n^2)} \quad \textbf{(4.6)}$$

Control design for Loop 1

As demonstrated by the analysis, a SISO approach will be used for the first loop. Hence, the pole placement method is used directly on $G_{11}(s)$ to find the PID controller parameters for loop 1. Using the given specifications, the controller parameters are found to be K=-26.5726, T_i=-0.0564 and T_d=-0.0332.

Control design for Loop 2

G_{22} has coupling with G_{12} (G_{22} is not diagonally dominant); an equivalent plant G_{22}*(s) must therefore be used. In 2x2 MIMO system, if one loop is very slightly coupled, the other loop is coupled to a large extent, the greatly coupled loop can be represented by an equivalent plant G_{22}*(s) which is defined as a function of the first loop's controller $C_1(s)$ on all plants:

$$G_{22}^{*}(s) = G_{22}(s) - \frac{G_{21}(s)C_{11}(s)G_{12}(s)}{1 + C_{11}(s)G_{11}(s)} \quad \textbf{(4.7)}$$

The equivalent plant is found as depicted as:

$$G_{22}^{*}(s) = \frac{0.89}{(0.2s+1)(0.06s+1)} \quad \textbf{(4.8)}$$

Because these nominal plants are second order systems, their controllers can be designed by PID pole placement methods according to Table.2.1 in chapter 2.

$$C_{ii}(s) = \begin{cases} -26.5726 - \dfrac{0.0564}{s} - \dfrac{0.0332s}{\frac{0.0332}{10}s+1} & \text{if } i = 1 \\ 2.178 + \dfrac{0.2669}{s} + \dfrac{0.1451s}{\frac{0.1451}{10}s+1} & \text{if } i = 2 \end{cases} \quad \textbf{(4.9)}$$

When the controllers are set by pole placements for a nominal model, their robustness for all operating points needs to be proved afterwards.

4.4.4 MIMO system's uncertainty and coupling

To propose a robust approach for the controller, the uncertainties are first described. On parametric uncertainty, assuming that the system is described by a nominal transfer function N(s), then the associated uncertainty can be modeled using an uncertainty bound described by a transfer function $W(s)$ [Guzzella, 2011]. Here a multiplicative uncertainty description is used, where the set S is defined:

$$\boldsymbol{S = \{N(s)(1 + \Delta W(s)) \,|\, \|\Delta\| \leq 1, \arg\{\Delta\} \in [-\pi, \pi]\}} \quad \textbf{(4.10)}$$

where Δ is the uncertainty generator which has no physical meaning.

To find suitable $W(s)$ for this system, the maximum distance $W(j\omega)^{\dagger}$ between the nominal plant $N(j\omega)$ and all the processes $G(j\omega)$ for each frequency must also be computed:

$$\boldsymbol{W(j\omega)^{\dagger} = max\left(\frac{|N(j\omega) - G(j\omega)|}{|N(j\omega)|}\right) \forall \omega} \quad \textbf{(4.11)}$$

$W(j\omega)^{\dagger}$ is a point to point frequency description. The transfer function $W(j\omega)$ for uncertainty bound modeling is also deduced as being the best equivalent approximation of $W(j\omega)^{\dagger}$. Respectively for G_{11} and $G_{22}{}^{*}$, $W(j\omega)^{\dagger}$ are:

$$W_{11}(s) = \frac{0.02s+0.82}{0.015s+1} \quad \textbf{(4.12)}$$

$$W_{22}(s) = \frac{0.08s+1}{0.04s+1} \quad \textbf{(4.13)}$$

It can be noted that $W_{11}(s)$ (for plant G_{11} considering Gershgorin bands) and $W_{22}(s)$ are two high-pass filters (for plant $G_{22}{}^{*}$).

MIMO System's Coupling

Fig.4.18 shows the Gershgorin bands for loop 1 and uncertainty bounds $W(s)$ of loop 1 and loop 2. The coupling interaction of Loop 1 (Gershgorin bands) is covered by the overall uncertainty. Hence, for loop 1, all the uncertainties and disturbances are well described by the uncertainty bound $W_{11}(s)$. For loop 2, since $G_{22}{}^{*}$ takes into account the overall system with the first closed loop, $W_{22}(s)$ also describes uncertainty and disturbances well.

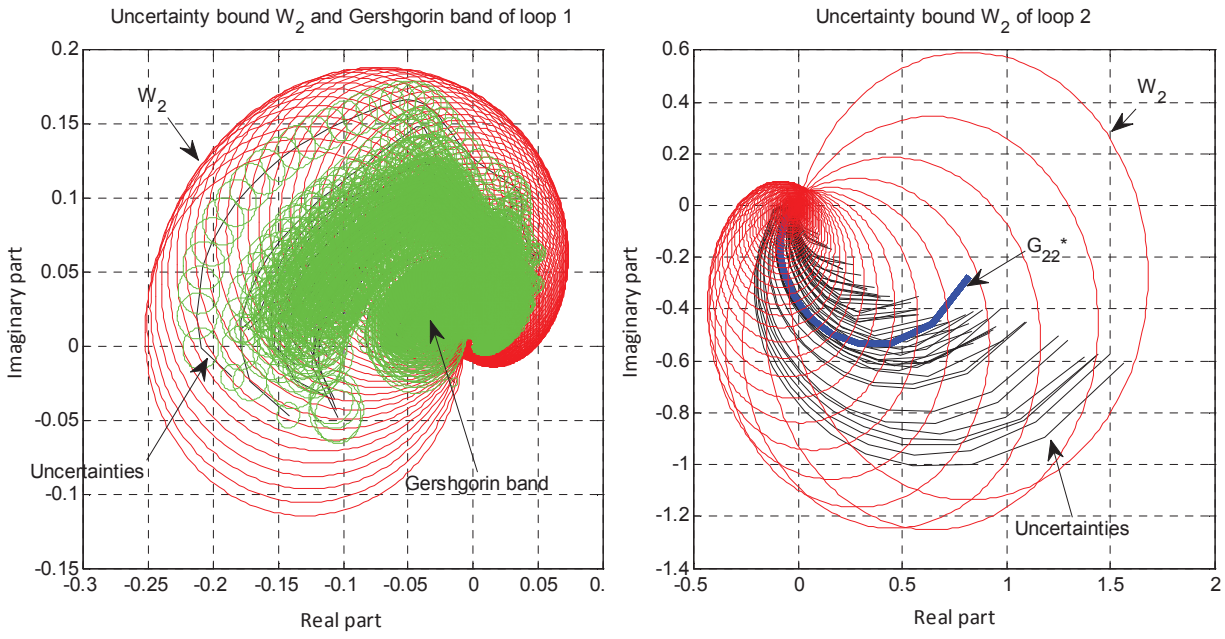

Fig.4.18 Gershgorin bands for loop 1 (left) and uncertainty bounds *W*(*s*) of loop 1 (left) and loop 2 (right)

Stability robustness validation

The stability robustness can be proved using the Nyquist stability theorem.

$$|\boldsymbol{L(s)} \cdot \boldsymbol{W(s)}| < |\mathbf{1} + \boldsymbol{L(s)}| \quad \textbf{(4.14)}$$

where $L(s)$ is the loop gain, and $L(s)= N(s)\cdot C(s)$. The bounds of two loops are plotted in Fig.4.19. It can be seen that in both cases the critical points are never encircled ($L_{11}W_{11}$, $L_{22}W_{22}$).

Hence, these two loops have stability robustness, in terms of both uncertainties and disturbances. Moreover, it is important to mention that the stability margins in terms of maximum sensitivity amplitude and the uncertainty bands and Gershgorin bands, which the minimum value of ($|1+L(j\omega)|$-$|L(j\omega)W(j\omega)|$) is 0.317 for the first loop and 0.4491 for the second loop.

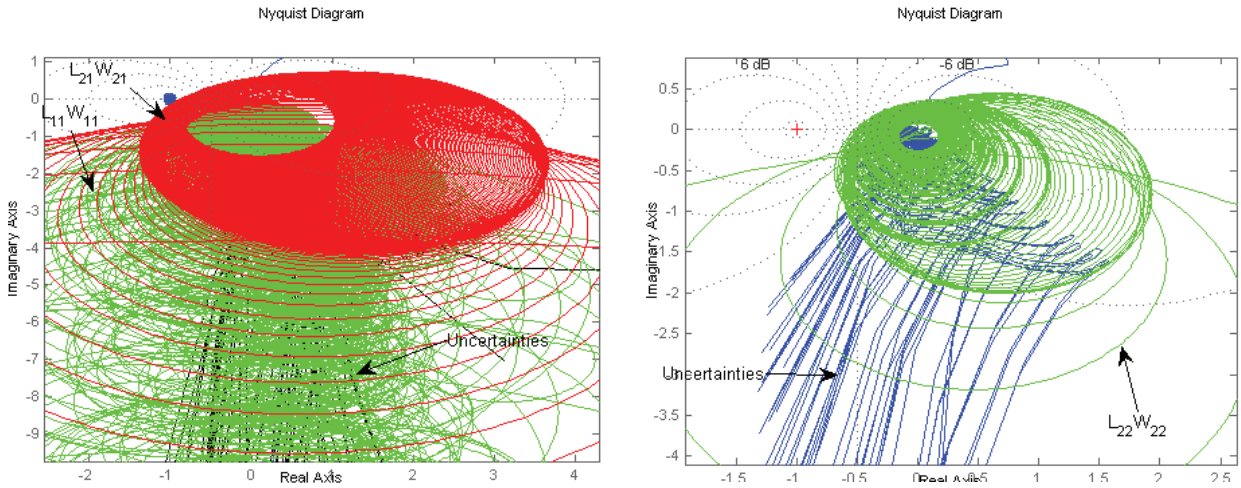

Fig.4.19 Nyquist stability proof for Loop 1 (left) and Loop 2(right). $L_{11}W_{11}$, $L_{22}W_{22}$ are loop gains of uncertainties, L_{21} is the Gershgorin disturbance bands of loop 1.

4.4.5 Simulation results

The Robust Sequential Multi-SISO control design has been validated for various test scenarios. To validate the controller the fuel mass was varied each 4 seconds during 30 seconds from 10 to 40 mg/cycle (Fig.4.20). It is thus the key point controlling the indicated torque which varies from 25Nm to 125Nm. The indicated torque set points are transferred to the boost pressure p_{boost} and mass airflow Q_{air}, to verify the performance of the control design.

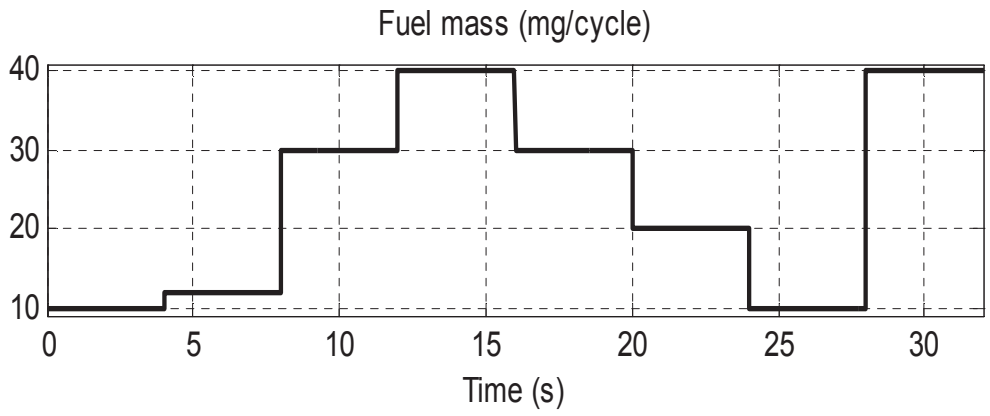

Fig.4.20 Test scenario for fuel mass flow in simulation

All the results presented here were obtained using the Multi-SISO controller designed before. Considering static saturations of the actuators (V_{EGR} and V_{WG}) in a real engine, a classical anti-reset windup was added [Mikles and Fikar, 2007]. The time constant T_t of anti-windup was fixed at T_t=T_i /2. The analysis of stability of the system with anti-reset windup can be carried out using small-gain arguments, and linear norm-bounded uncertainties in the plant model can be incorporated by increasing the block Δ shown above equation (4.10) with linear blocks.

The simulation is verified at a constant engine speed of 1500 rpm and 2500 rpm. The V_{EGR} limit goes from 0% to a maximum openness limit which depends on the engine speed, and the limit for V_{WG} goes from 40% to 80% of closeness limit. The static states ~~dynamic~~ of the actuators of EGR and WG valves are modeled by step signals. The controller has been validated on different transients as shown in Fig.4.21 and Fig.4.22, which show the control results for the two different engine speeds considered. Therefore, the good behavior and robustness of the control results for both loops (Q_{air} and p_{boost}) according to the specifications can be found. In these figures, the Q_{air} response can follow its set point, the beginning of response signals have some initial problems, which is caused by some improper initial values inside the simulator. The PID control is a little aggressive at 9s and 12s because of the sensitivity of the differentiator for the mass airflow at 2500rpm.

As expected, the closed loop system is stable without oscillation and steady state error. Concerning dynamic performance, it appears that the closed loop behavior is robust against the uncertainty and modeling errors, with regard to engine speed and torque variations. Due to the approach (only one controller synthesis for one nominal system) the dynamic behavior is not constant but nonetheless remains highly acceptable. It is worth noting that this is due to the normalization (and de-normalization) step, which creates an implicit feedforward and gain scheduling into the control scheme.

In addition, as it can be seen in Fig.4.22 (between 15s and 16s V_{EGR} saturates at 30%), the actuator saturation effects are well mastered thanks to the anti reset windup.

All in all, the results show that the control design meets our robustness control design requirements against coupling and uncertainty, thus validating the performance.

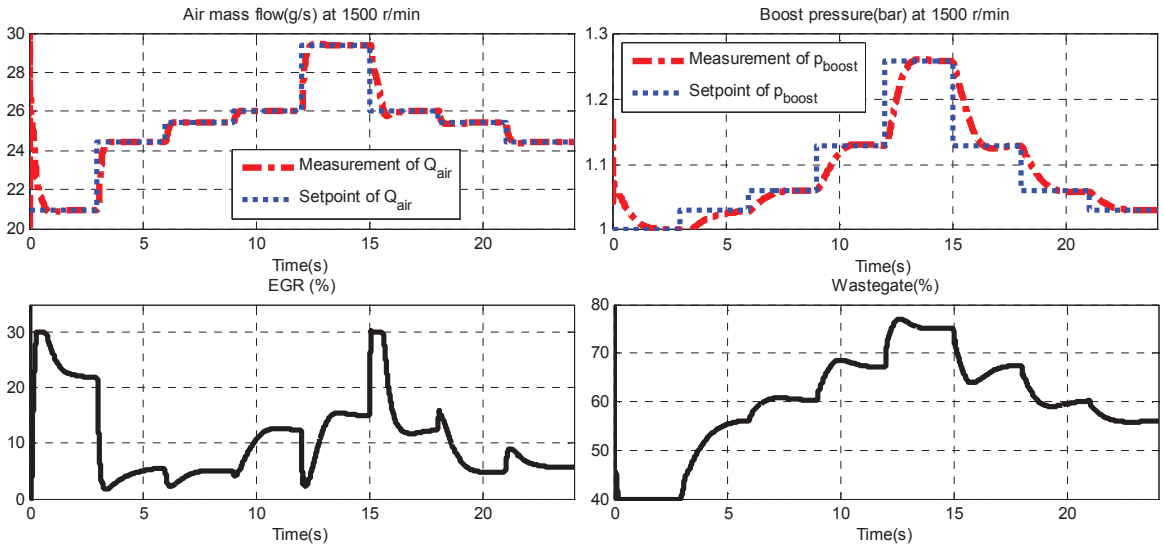

Fig.4.21 Q_{air} and V_{EGR} (left), p_{man} and V_{WG} (right) at 1500 rpm

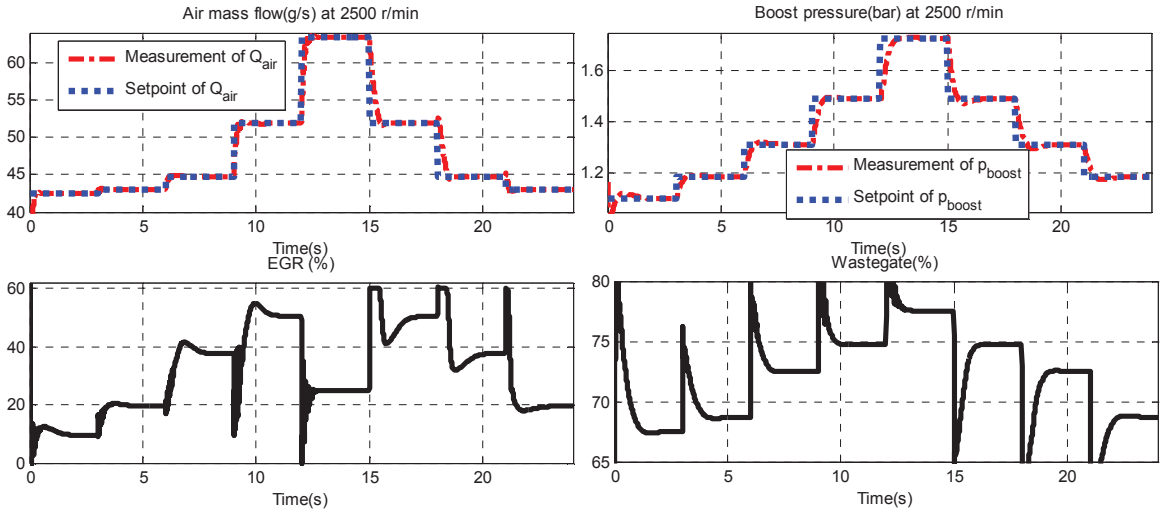

Fig.4.22 Q_{air} and V_{EGR} (left), p_{man} and V_{WG} (right) at 2500 rpm

4.5 Validation on a diesel engine test bench

4.5.1 System modeling

Compared with the gasoline engine control and diesel engine simulator, this diesel engine control is extended from a 2x2 square MIMO control system to a 2x3 non-square MIMO control system. The application of this unified robust control design methodology works well on the square MIMO diesel engine. Next step, the 2x3 non-square MIMO control system is verified via the experiment of diesel engine control, which is presented as follows (Fig.4.23).

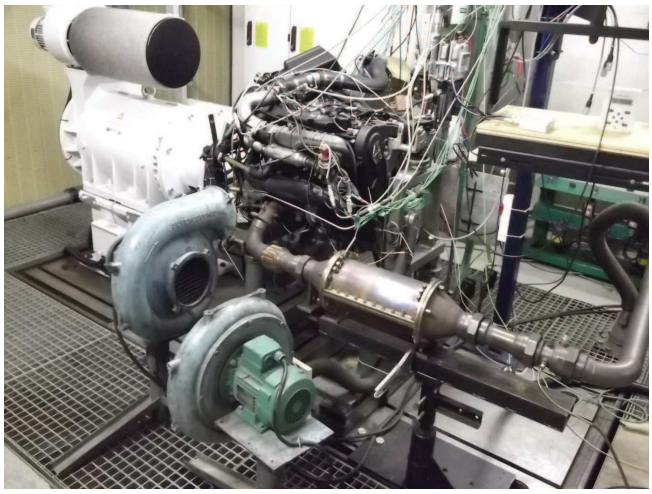

Fig.4.23 PSA DW 10 diesel engine test bench

The control objective of this application is to lower the NOx emissions the same output as in the simulation part Q_{air} and p_{boost} is needed to be controlled. The main difference is that the intake throttle is used as the third actuator. The process is therefore 2x3 MIMO systems i.e. V_{TH}, V_{EGR} and V_{WG} are taken as inputs; Q_{air} and p_{boost} are taken as outputs. As the intake throttle can help to control the air mass flow, i.e. the EGR mass flow indirectly, through the states of the intake and outlet receiver, it is good to maintain a pressure variation over the EGR valve [Guzzella and Amstutz, 1998]. Because of pumping losses, V_{TH} can be kept fully opened when it is as possible. The global principle is similar to the first part.

Black Box modeling

The operating points are chosen at 73 points while varying the speed from 1000rpm to 4000rpm and the torque from 15 N.m to 200 N.m (at 2250rpm) (Fig.4.24). The positions of three actuators for identification are shown in Fig.4.24.

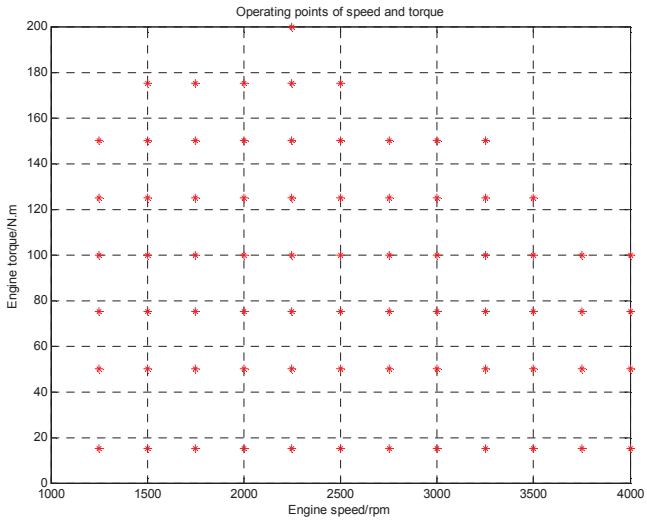

Fig.4.24 The positions of EGR, Wastegate and Throttle of 73 operating points

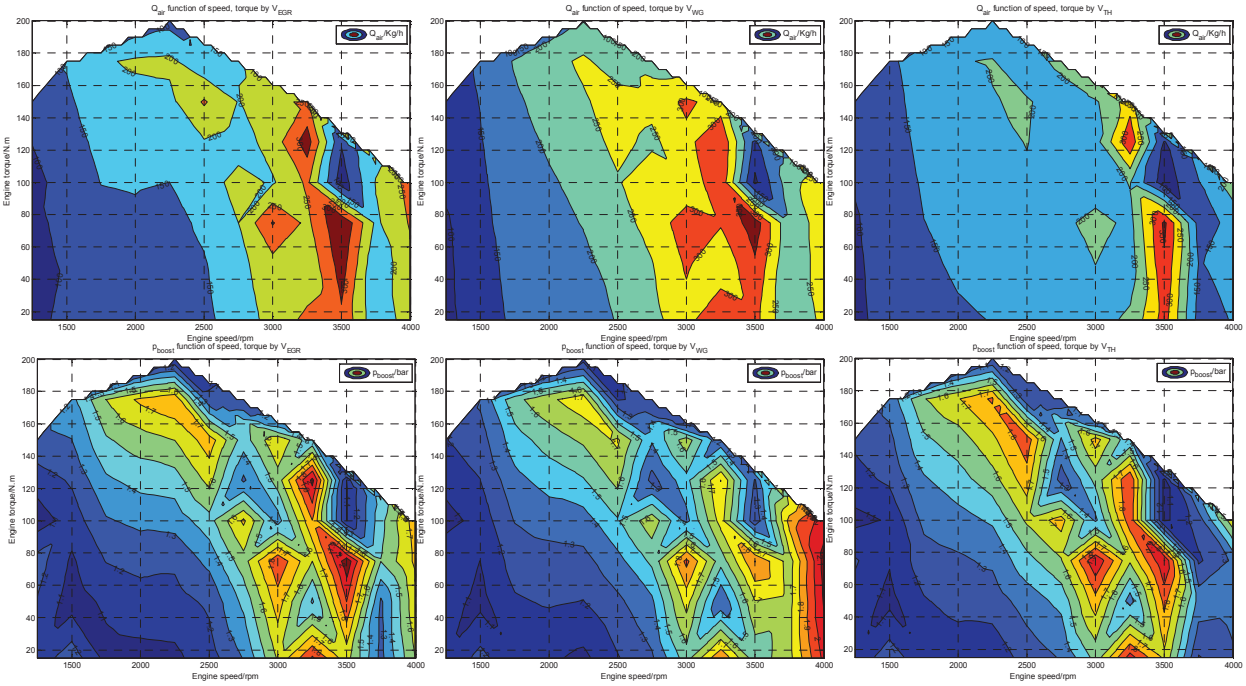

Fig.4.25 The mean values of Q_{air} and p_{boost} of 73 operating points

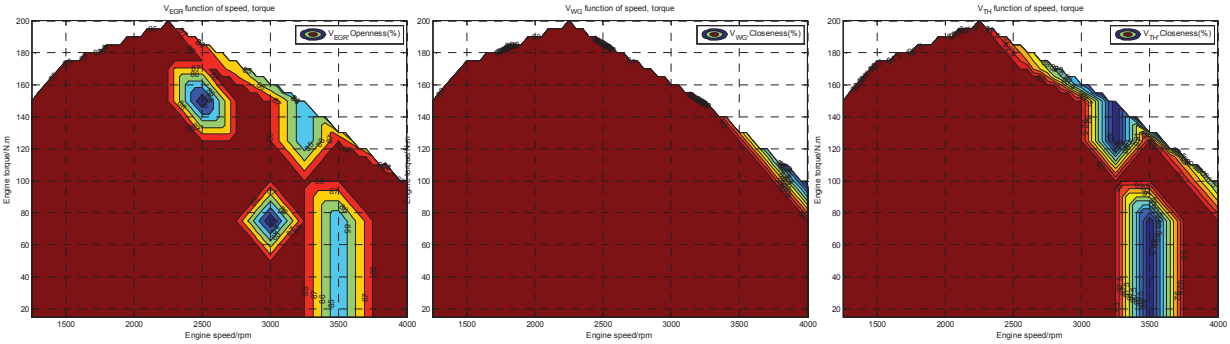

Fig.4.26 The positions of EGR, Wastegate and Throttle of 73 operating points

Due to the different calibration of actuators, the positions are chosen differently according to the response of control variables. Furthermore, the identification process needs a signal to excite this system; the system is identified in frequency domain when the data are collected via the Fourier Transform.

a. Excitation Signal

Regarding this diesel engine and actuators physical dynamic characteristics, their parameters of excitation signals are chosen as in Table 4.3

Actuator	Average	Magnitude	fmin,fmax	Non-saturation	Ops
EGR	84%	8~16%	0,1~3Hz	[80 96] %	1000-4000rpm
WG	80~90%	6~22%	0,1~1Hz	[72 95] %	15-200Nm
TH	84~88%	10~20%	0,1~3Hz	[78 98] %	

Table.4.3 Parameters of excitation signals of actuators

From this table, the average and magnitude values are set by their opening or closing position areas, fmin and fmax are set by step and sine signals, which depend on the actuator characteristics, Non-saturation derives the area of normal working without saturation, Ops gives the range of speed and torque. Then the excited signals and responses of this system are given in Fig.4.27, three inputs were employed to excite this system and collected the two output responses.

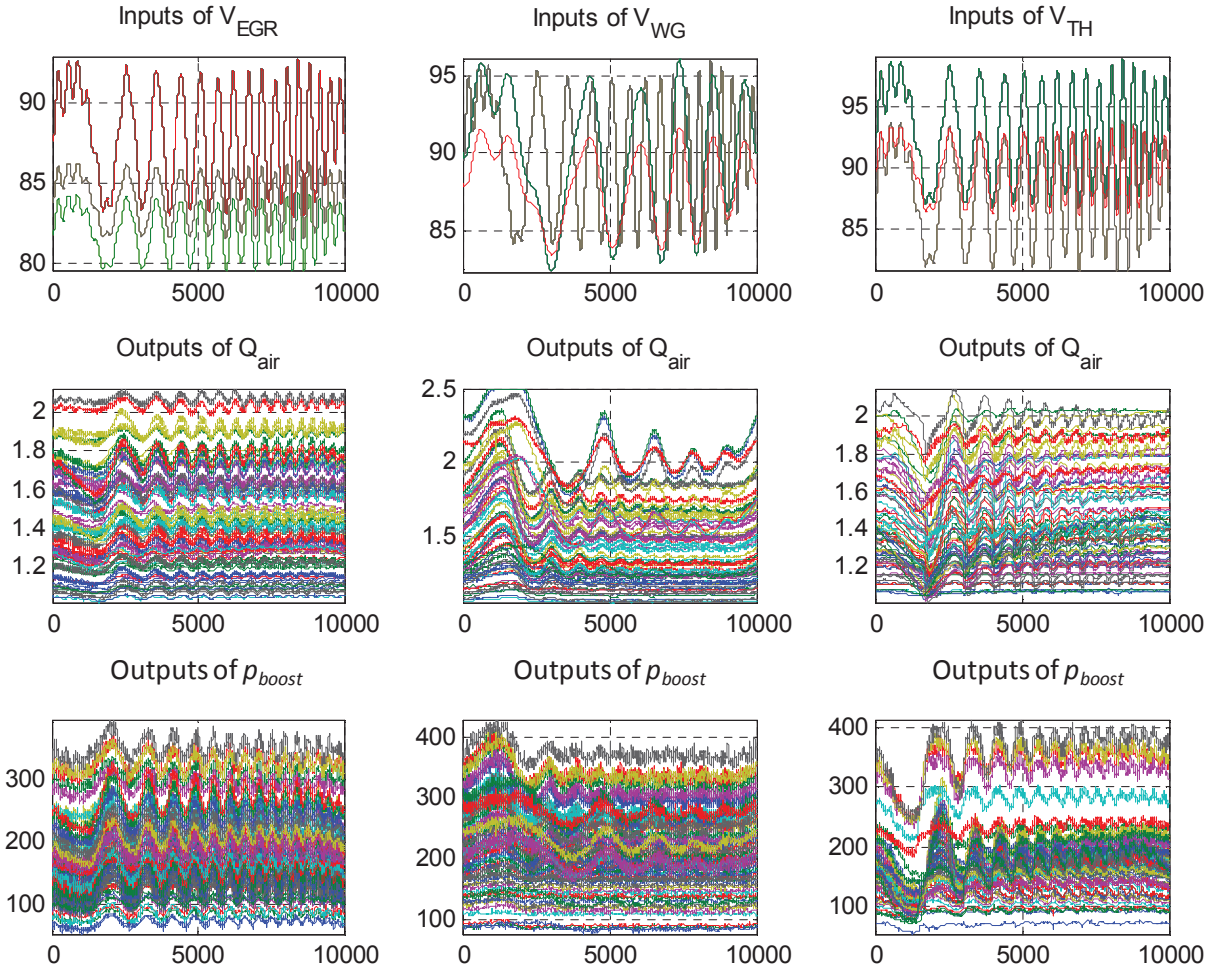

Fig.4.27 Signals identification of inputs and outputs

b. Data Processing

Input and output signals of this engine control system are normalized using the nominal constant value for input and output detailed in Fig.4.27. The process inputs and outputs obtained thus can be seen in Fig.4.28.

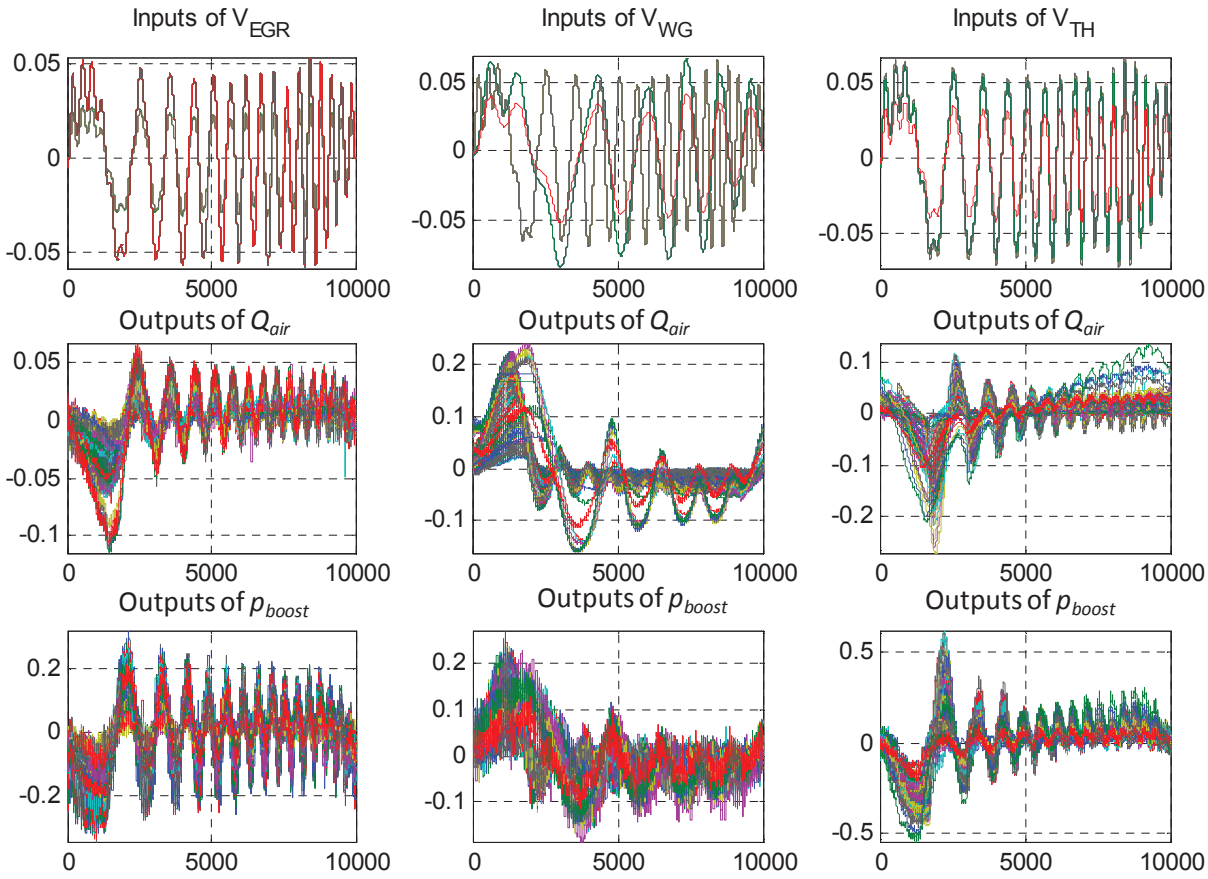

Fig.4.28 Normalized signals of inputs and outputs of identification

The process is transformed via Fourier Transform and described by a non- square system defined as follows:

- G_{11} is from V_{EGR} (in % openness) to Q_{air} (in g/s).
- G_{12} is from V_{WG} (in % closeness) to Q_{air} (in g/s).
- G_{13} is from V_{TH} (in % closeness) to Q_{air} (in g/s).
- G_{21} is from V_{EGR} (in % openness) to p_{boost} (in bar).
- G_{22} is from V_{WG} (in % closeness) to p_{boost} (in bar).
- G_{23} is from V_{TH} (in % closeness) to p_{boost} (in bar).

c. Nominal frequency identification

The nominal plants are presented in Fig.4.29 and collected in equations as follows. Second order models can represent the nominal diagonal processes of $G_{nom}(j\omega)$.

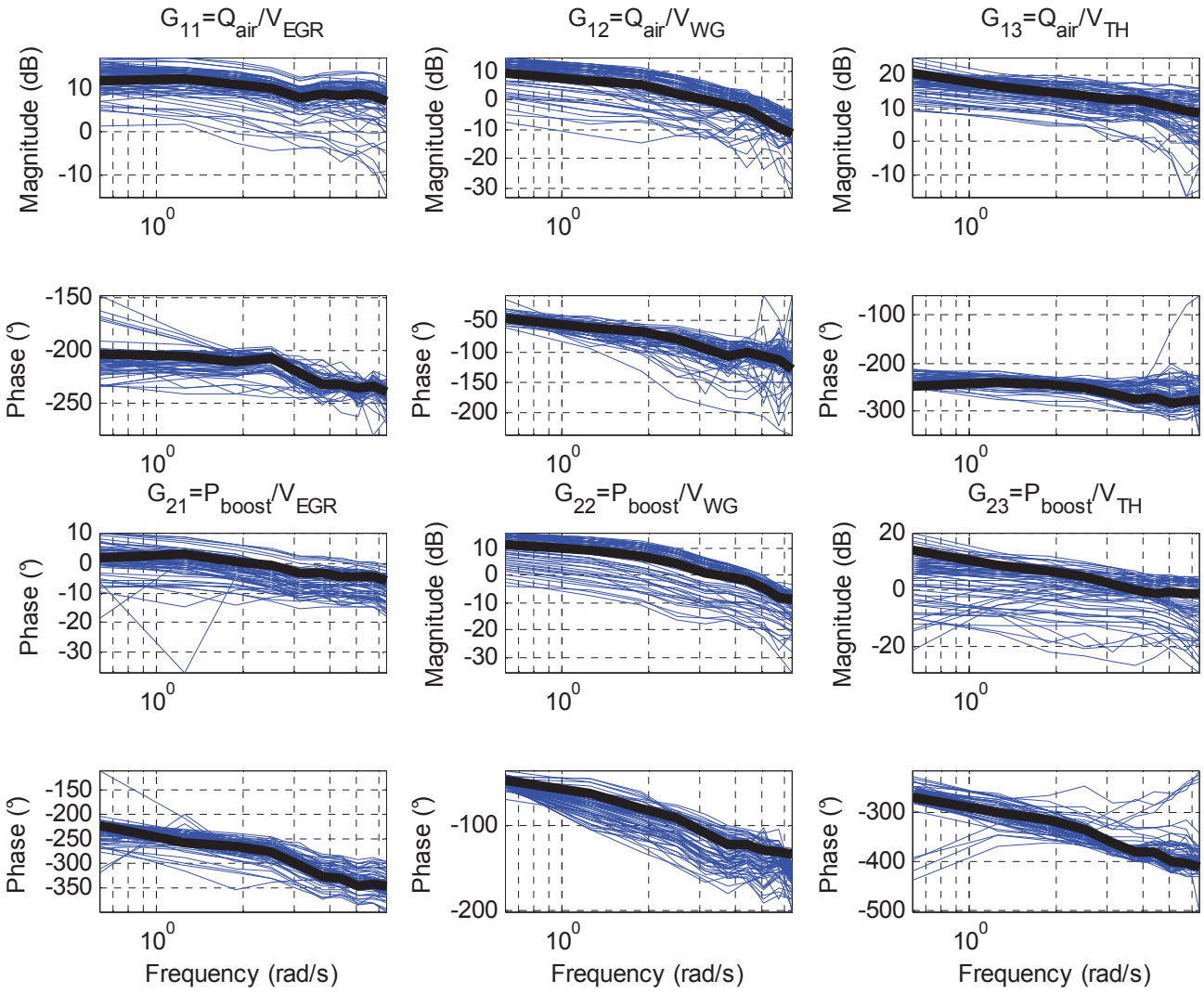

Fig.4.29 Nominal model and fitting plants of Non-square system

$$G_{ij}(s)=\begin{cases}\dfrac{-4.2}{(0.01s+1)(0.24s+1)} & \text{if } i=1,\ j=1\\ \dfrac{3.3}{(0.96s+1)(0.12s+1)} & \text{if } i=1,\ j=2\\ \dfrac{-21.4}{(2.2s+1)(0.05s+1)} & \text{if } i=1,\ j=3\\ \dfrac{-1.6}{(0.1s+1)^2(0.8s+1)} & \text{if } i=2,\ j=1\\ \dfrac{4.1}{(0.98s+1)(0.2s+1)} & \text{if } i=2,\ j=2\\ \dfrac{-19.3}{(0.03s+1)^2(5.3s+1)} & \text{if } i=2,\ j=3\end{cases} \qquad \textbf{(4.15)}$$

4.5.2 System analysis

Because the system is a complex system, coupling and uncertainty must be analyzed using CN, RGA, GB and CD^3 tools.

Condition Number (CN)

Fig.4.30 shows that the system is ill-conditioned. At least one loop has n input directionality.

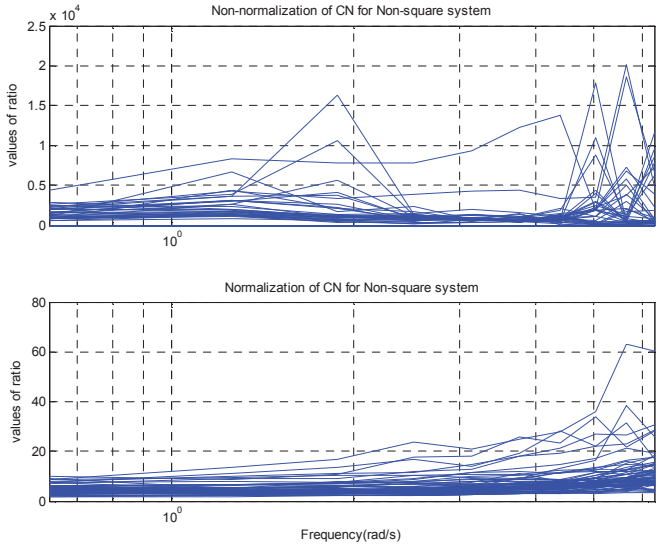

Fig.4.30 CN of diesel engine

Relative Gain Array (RGA)

Regarding Fig.4.31 elements G_{22} and G_{13} play an important role due to the sum of each column, while considering the closed-loop frequency bands of this system, which should take G_{22} and G_{13} as the defined controlled plants. However, the first loop shouldn't be neglected due to the importance of V_{EGR}, for the physical sense and therefore, G_{11} is taken as another defined controlled plant ,In addition, G_{21}, G_{12},G_{23} are quite smaller than G_{11}, G_{22} and G_{13}, respectively For these reasons, this system can use decentralized control.

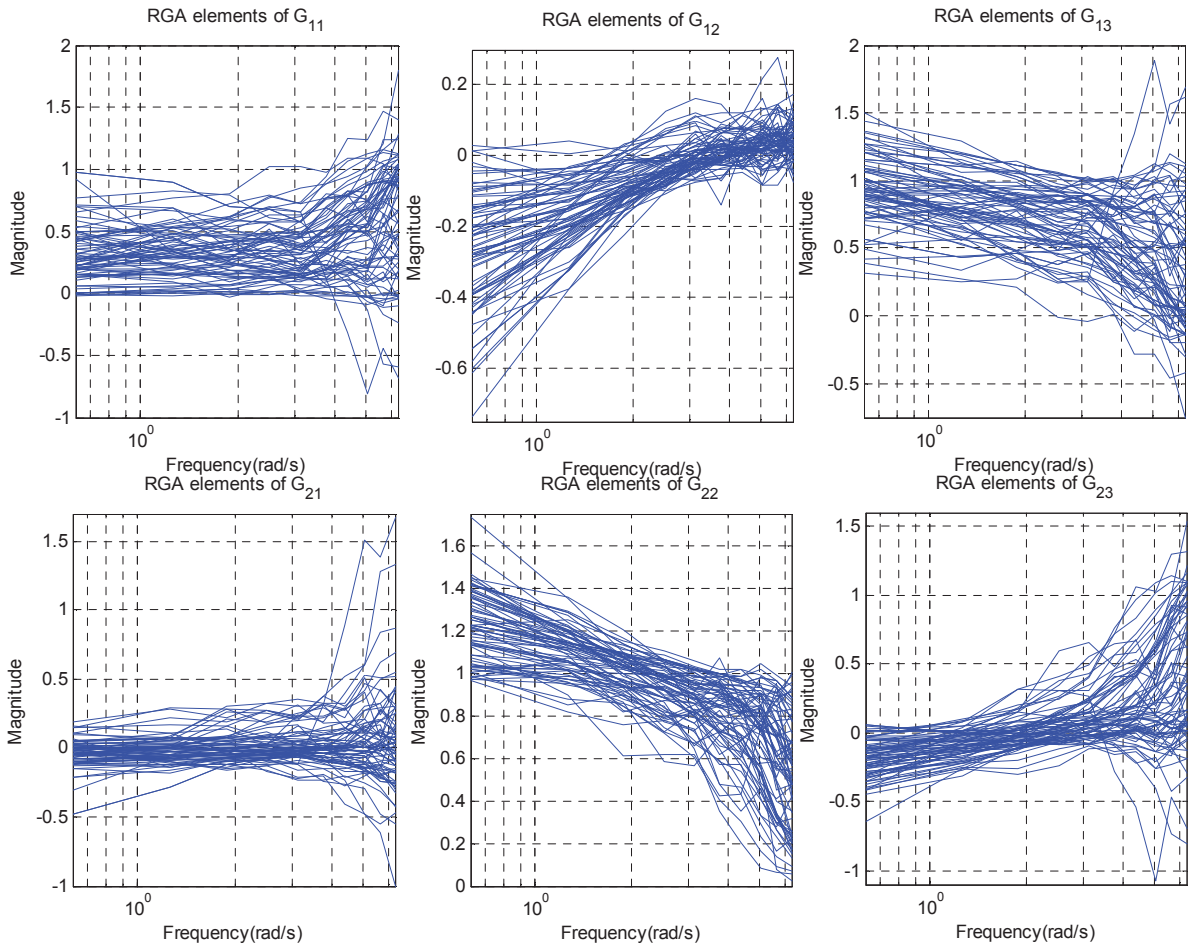

Fig.4.31 RGA of diesel engine

Gershgorin Bands (GB)

In Fig.4.32, the first loop and the third loop have small interactions, i.e. G_{21} slightly disturbs G_{11} and G_{32} disturbs G_{13} slightly. These loops are stable in closed-loops of unit inverse feedback; but the second loop has slightly large undesired interaction, i.e. G_{12} disturbs G_{22} a little more.

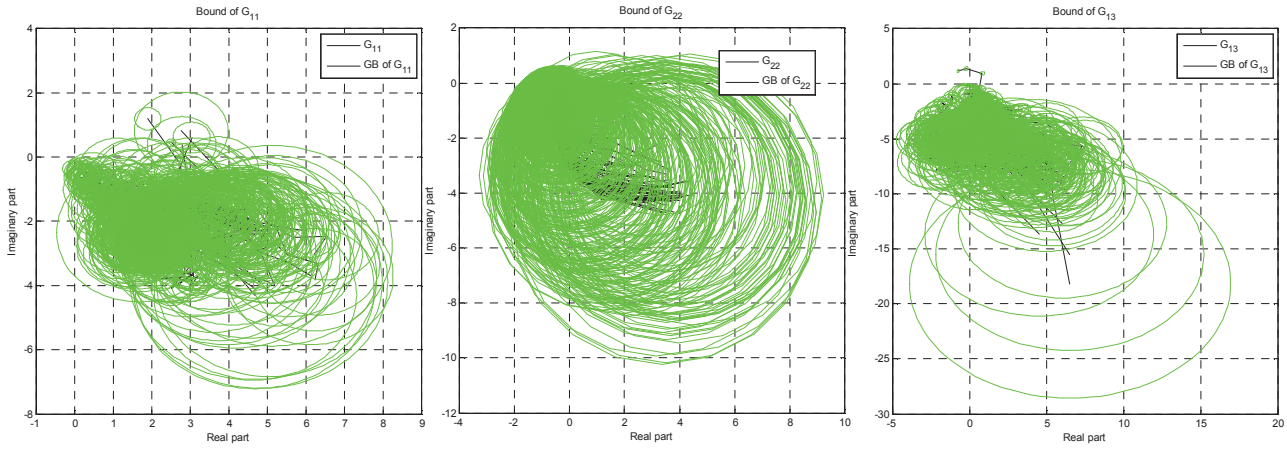

Fig.4.32 GB of diesel engine

Column Diagonal Dominant Degree (CD^3)

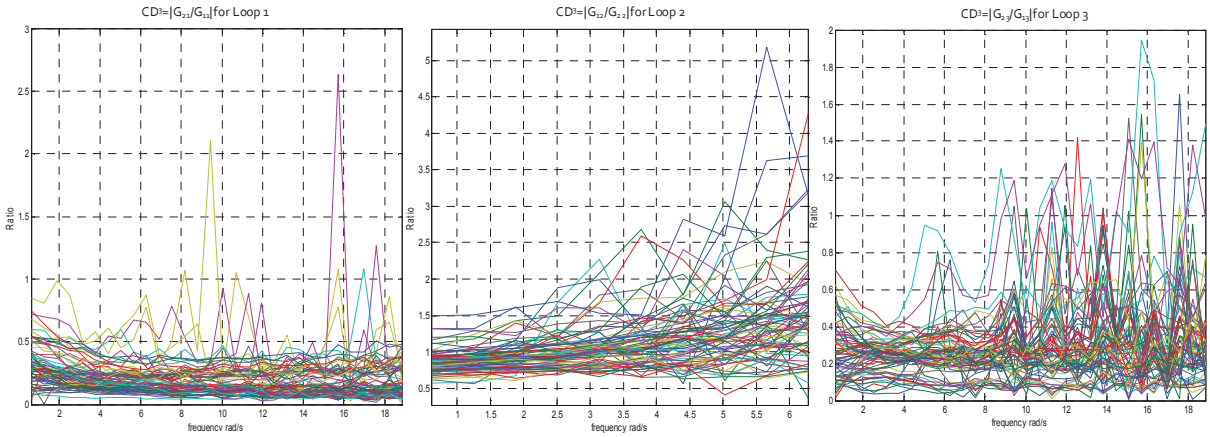

Fig.4.33 CD^3 of diesel engine

If just consider only the common frequency (0.1~1Hz) for these three loops, loop 1 (EGR to air mass flow) and loop 3 (intake throttle to air mass flow) are diagonal dominant, in other words, they can be treated as SISO loops with relatively/reasonable quite small coupling. The second loop (wastegate to boost pressure) is not diagonal dominant and coupling and uncertainties of this loop can be treated using an equivalent plant G_{22}* which is defined as a function of the other two loop controllers $C_1(s)$ and $C_2(s)$ and on all other transfer function of the plants.

Conclusion of Non-Square MIMO System's Analysis

Considering the MIMO analysis tool, the first and third loops have small coupling, but the second loop has noticeable coupling. In other words, the loop added when the intake throttle used is a loop that has no major coupling phenomenon and it can be controlled using a simple SISO controller. As before (simulation part) this system will be controlled using a sequential Multi-SISO Robust control strategy and frequency identification toolbox used to find the nominal transfer functions of the plant:

$$G_{ij}(s)=\begin{cases}\dfrac{-4.2}{(0.01s+1)(0.24s+1)} & \text{if } i=1,\ \text{if } j=1\\ \dfrac{3.9}{(0.96s+1)(0.1s+1)} & \text{if } i=2,\ \text{if } j=2\\ \dfrac{-21.4}{(2.2s+1)(0.05s+1)} & \text{if } i=1,\ \text{if } j=3\end{cases} \qquad \textbf{(4.16)}$$

The global control scheme is described in Fig.4.34. Air mass flow will be controlled by the EGR valve, the intake throttle and boost pressure by the wastegate.

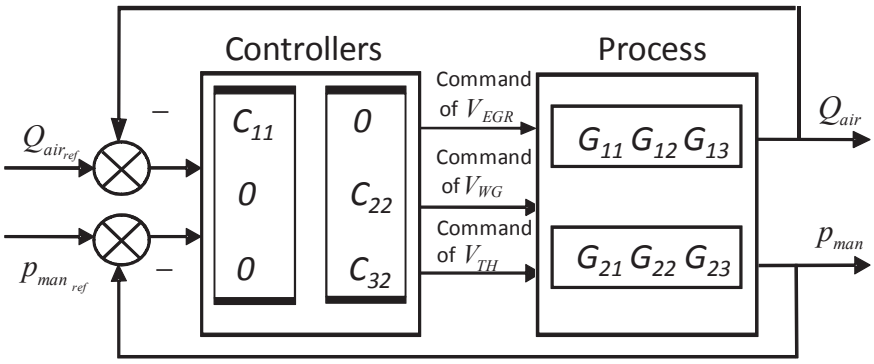

Fig.4.34 Global control scheme of diesel engine control

4.5.3 Robust control synthesis

Due to the diesel nominal plants are all second order linear models, controllers and filters can be designed by the PID pole placement methods. Take into account system dynamics and physical properties, reasonable desired performances have been fixed:

- the overshoots were set at 3% for Q_{air} (V_{EGR} with C_{11} and V_{TH} with C_{32}) and p_{boost} (V_{WG} with C_{22}),
- the response times were fixed at 2s and 2.5s for Q_{air} (V_{EGR} with C_{11} and V_{TH} with C_{32}), p_{boost}(V_{WG} with C_{22}) respectively,
- the bandwidths of the nominal function must be respectively 10rad/s, 12.5rad/s.

Additionally, the differentiators are very sensitive in real tests; some differentiators' filters have to be added. It is defined as follows,

$$C_f(s) = K_p\left(1+\frac{1}{T_i s}+\frac{T_d s}{1+\frac{T_d}{N}s+0.5\left(\frac{T_d}{N}s\right)^2}\right) \quad \textbf{(4.17)}$$

where N is a tuning parameter for fitting the differentiator filter.

The second loop has significant coupling, in this case interaction can be considered by an equivalent plant $G_{22}^*(s)$ defined as a function of the other two loops controllers $C_{11}(s)$ and $C_{32}(s)$ on all other transfer function of the plants:

$$G_{22}^*(s) = G_{22}(s) - \frac{G_{21}(s)C_{11}(s)G_{12}(s)+G_{13}(s)C_{32}(s)G_{12}(s)}{1+C_{11}(s)G_{11}(s)+C_{32}(s)G_{13}(s)} \quad \textbf{(4.18)}$$

The equivalent plant found for the system is:

$$G_{22}^*(s) = \frac{3.9}{(0.96s+1)(0.1s+1)} \quad \textbf{(4.19)}$$

Controllers and filters are depicted in the equations below:

$$C_{ij}(s)=\begin{cases} -0.088-\dfrac{0.59}{s}-\dfrac{0.03s}{\frac{0.03}{10}s+1} & \text{if } i=1, \text{if } j=1 \\ 1.9+\dfrac{3.2}{s}+\dfrac{0.39s}{\frac{0.39}{10}s+1} & \text{if } i=2, \text{if } j=2 \\ -0.66-\dfrac{1.3}{s}-\dfrac{0.069s}{\frac{0.069}{10}s+1} & \text{if } i=3, \text{if } j=2 \end{cases} \quad \textbf{(4.20)}$$

$$F_{ij}(s)=\begin{cases} \dfrac{1}{0.054s^2+0.15s+1} & \text{if } i=1, \text{if } j=1 \\ \dfrac{1}{0.12s^2+0.6s+1} & \text{if } i=2, \text{if } j=2 \\ \dfrac{1}{0.05s^2+0.5s+1} & \text{if } i=3, \text{if } j=2 \end{cases} \quad \textbf{(4.21)}$$

Performance and closed-loop stability against the uncertainty and coupling has to be validated for all operating points.

4.5.4 MIMO system's uncertainty and coupling

The 2x3 MIMO system robust stability can be verified by GBs in the form of a Nyquist diagram. Three loops are separated in each figure (Fig.4.35 ~ Fig.4.37)

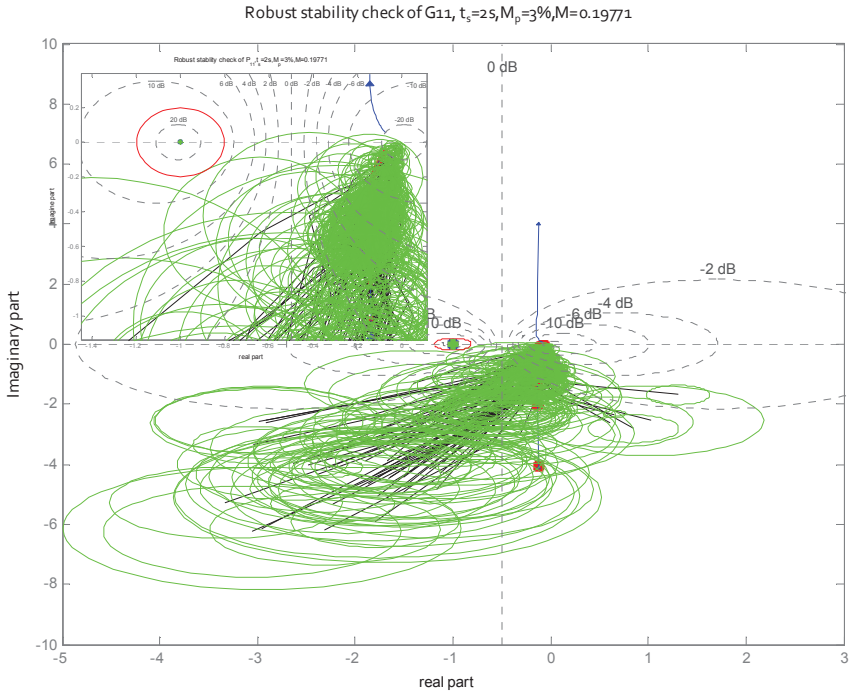

Fig.4.35 GB of closed-loop 2x3 MIMO system for loop 1 (diesel)

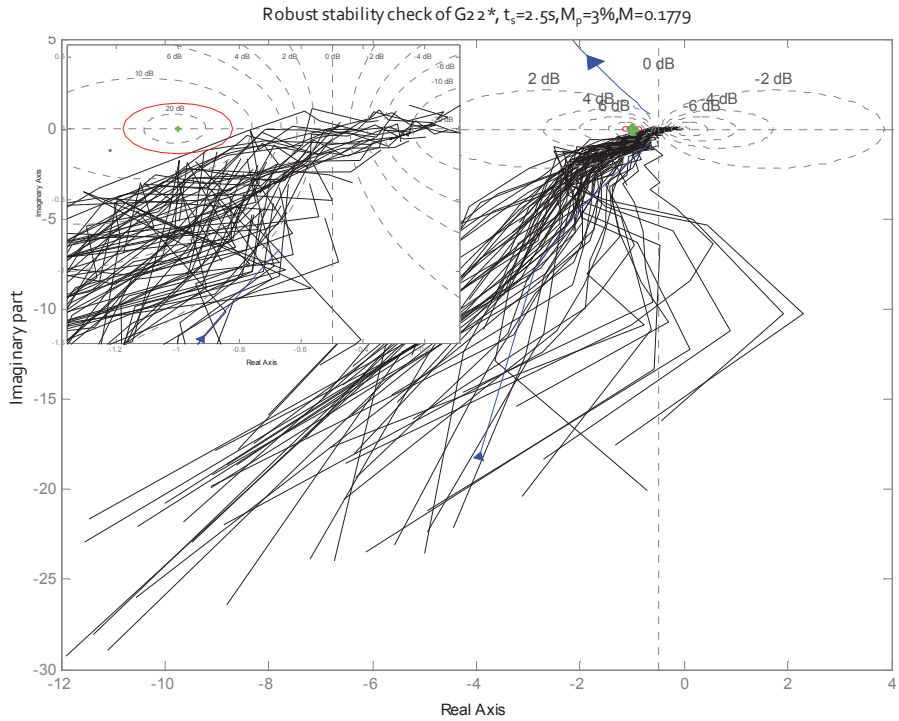

Fig.4.36 GB of closed-loop 2x3 MIMO system for loop 2 (diesel)

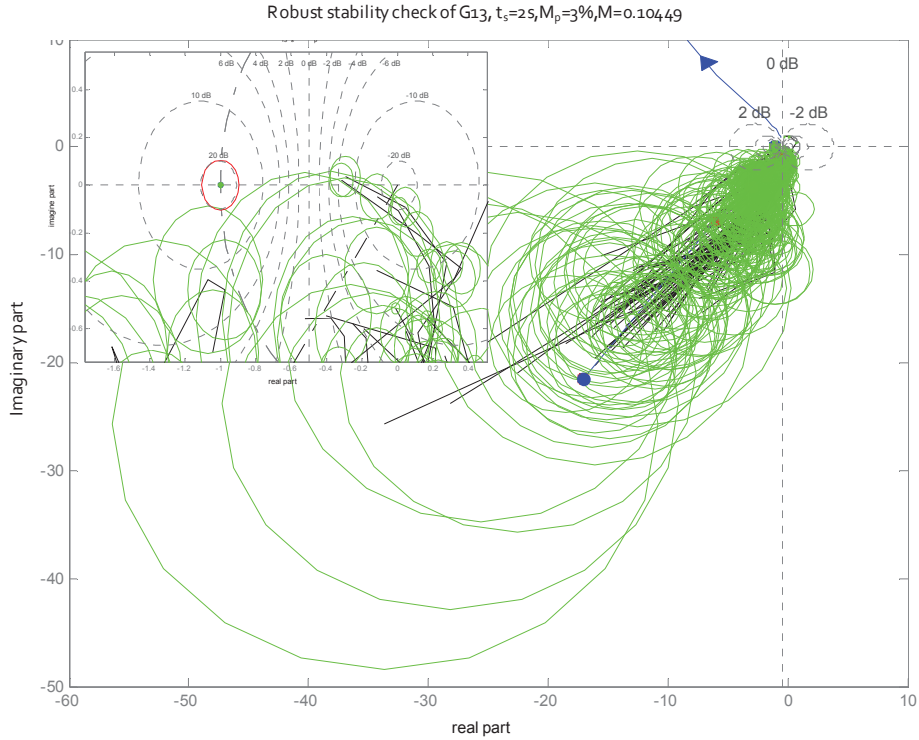

Fig.4.37 GB of closed-loop 2x3 MIMO system for loop 3

From these three loops' Gershgorin Bands and all plants' Nyquist graphs, all of them are stable and have a certain modulus margin (loop1:0.2, loop2:0.2, loop3:0.1) against the uncertainty and coupling.

4.5.5 Experimental results

Because the square controllers can be obtained from the non-square controllers, while the actuator V_{TH} is fully opened (77% saturated in this diesel engine test bench). Hence, this square is taken for comparative. Consequently, the square controllers are validated via Urban Driving Cycle (ECE-15), Extra-Urban Driving Cycle (EUDC), and Federal Test Procedure (FTP) 75 and Japan 10-15 Mode Cycle Emission Test Cycles.

a) ECE-15 Test Cycle

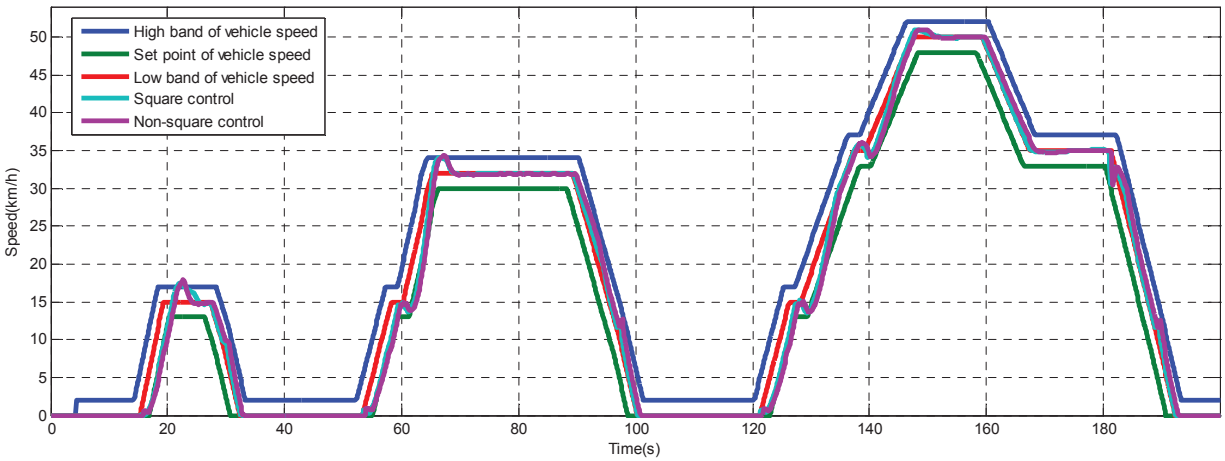

Fig.4.38 The vehicle speed response in ECE-15 Test Cycle: square and non-square control

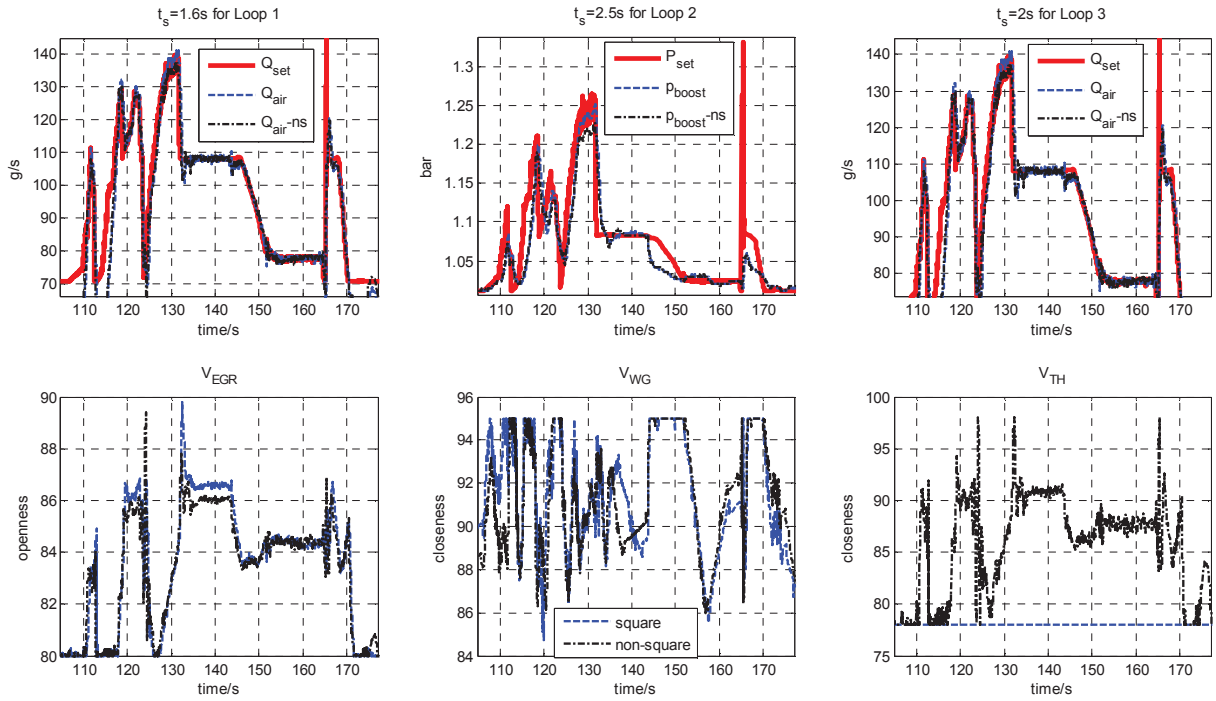

Fig.4.39 Q_{air} and p_{boost} performance and their actuators in ECE-15 Test Cycle: square and non-square control

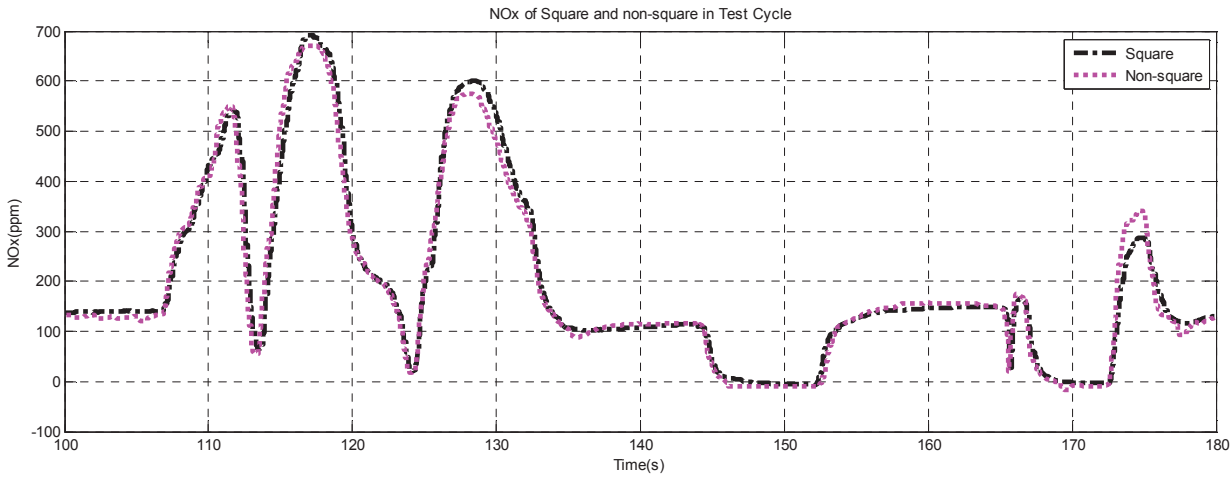

Fig.4.40 Emissions NOx in ECE-15 Test Cycle: square and non-square control

Looking at Fig.4.38, both the vehicle speed which are different by square controllers and non-square controllers can well follow the set point of vehicle speed, although the low speed at 15km/h that is overpass the high band because this engine speed is not well fitted by the feedforward reference. These two kinds of control strategies can keep following the vehicle speeds in this vehicle test.

From Fig.4.39 of ECE-15 cycle, globally the p_{boost} and Q_{air} can well follow the reference signals while speed and torque varying, except when Q_{air} is 70g/s, because the minimum air mass flow cannot reach this setpoint, due to the bad value of setpoint. Moreover, comparing to the systems that are regulated by square and non-square controllers, the system controlled by the square controllers have big overshoot, and the actuators V_{EGR} and V_{WG} react with more actions, i.e., bigger closeness and bigger closeness. Loop 1 worked well although a small problem of initial large value, because the engine's physical limitation, actuators V_{EGR} cannot react more between 100s and 110s for example.

The pollutant emissions NOx is reduced a little (about 2%) with the Non-square control, where comparing with its derived square control during from 100s to 180s of the test (the beginning is not comparable due to NOx sensor needs a long time to be well initialed.). This result is found in Fig.4.40. Hence, non-square control is a good way to decrease NOx with the function of intake throttle V_{TH}.

b) EUDC Test Cycle

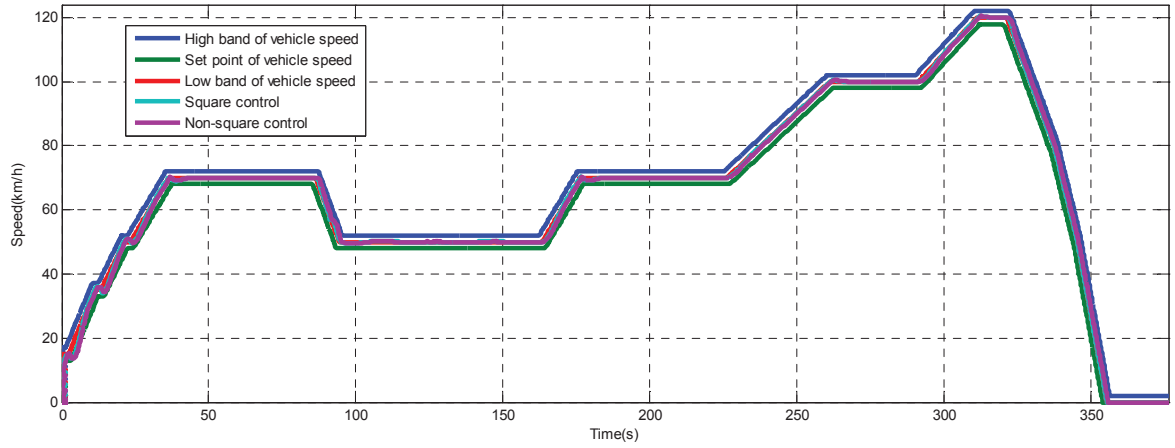

Fig.4.41 The vehicle speed response in EUDC Test Cycle: square and non-square control

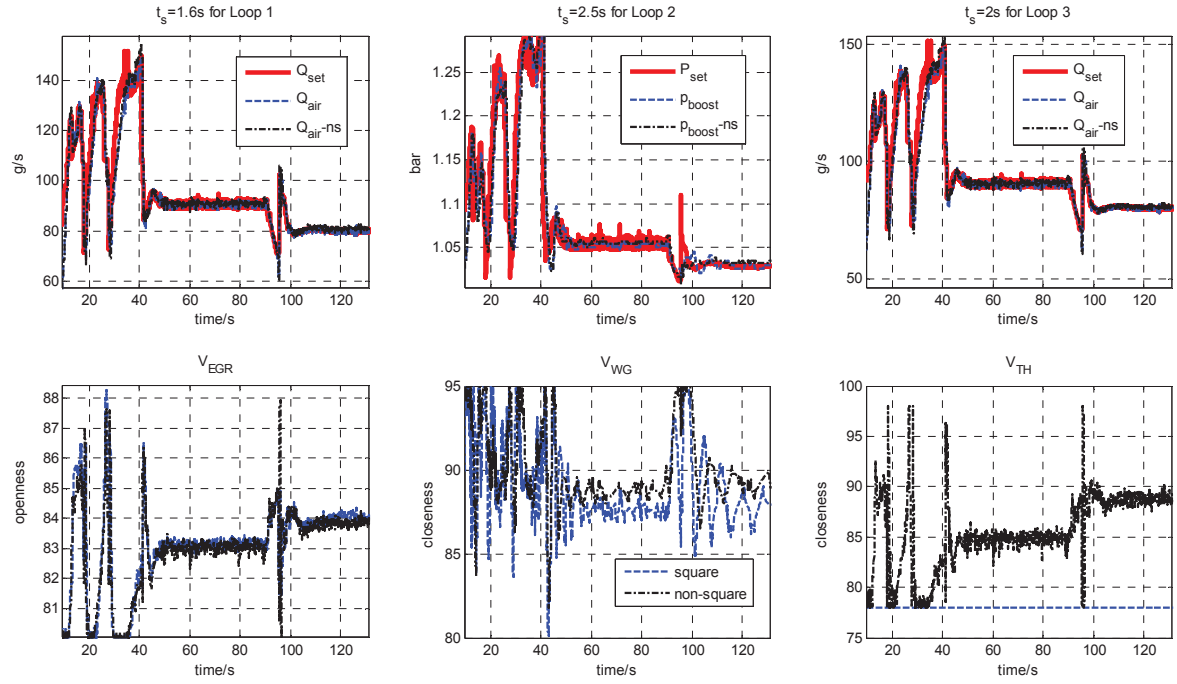

Fig.4.42 Q_{air} and p_{boost} performance and their actuators in EUDC Test Cycle: square and non-square control

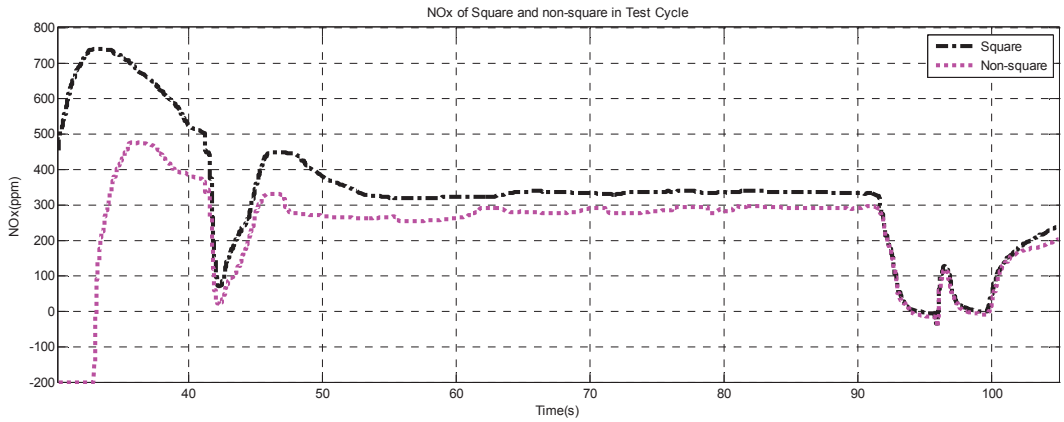

Fig.4.43 Emissions NOx in EUDC Test Cycle: square and non-square control

The vehicle speed response in Fig.4.41 shows a very good following performance in EUDC Test Cycle, small overshoot and quick response in total. Square control system and non-square control system do not have effective difference in this type of test.

From Fig.4.42 that present the EUDC part of the NEDC cycle, both of two loops can well follow the setpoint signals with different speed and torque variances. The problem is still the setpoint values which are caused by the physical limitation. This time, when comparing the square and non-square system, the square system has a little bigger oscillation with actuator V_{WG} of loop2, because the contribution of V_{TH} that is used to adjust the reaction of other actuators V_{EGR} and V_{WG}.

The amount of NOx is dramatically decreased in non-square control system than in square control system (Fig.4.43), the difference between them is more than 30% for the EUDC Test Cycle. Therefore, non-square control strategy is a more promising method to reduce NOx than square control in this cycle.

c) FTP Test Cycle

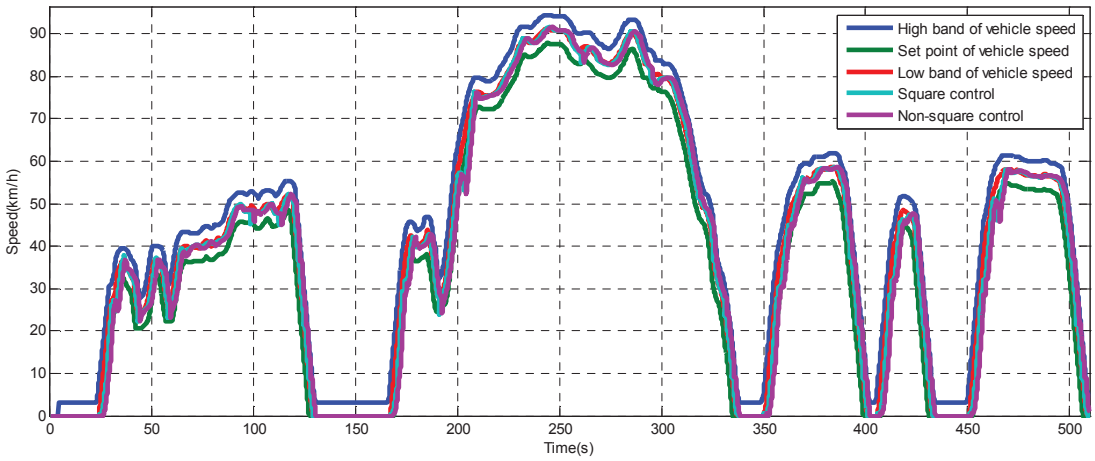

Fig.4.44 The vehicle speed response in FTP 75 Test Cycle: square and non-square control

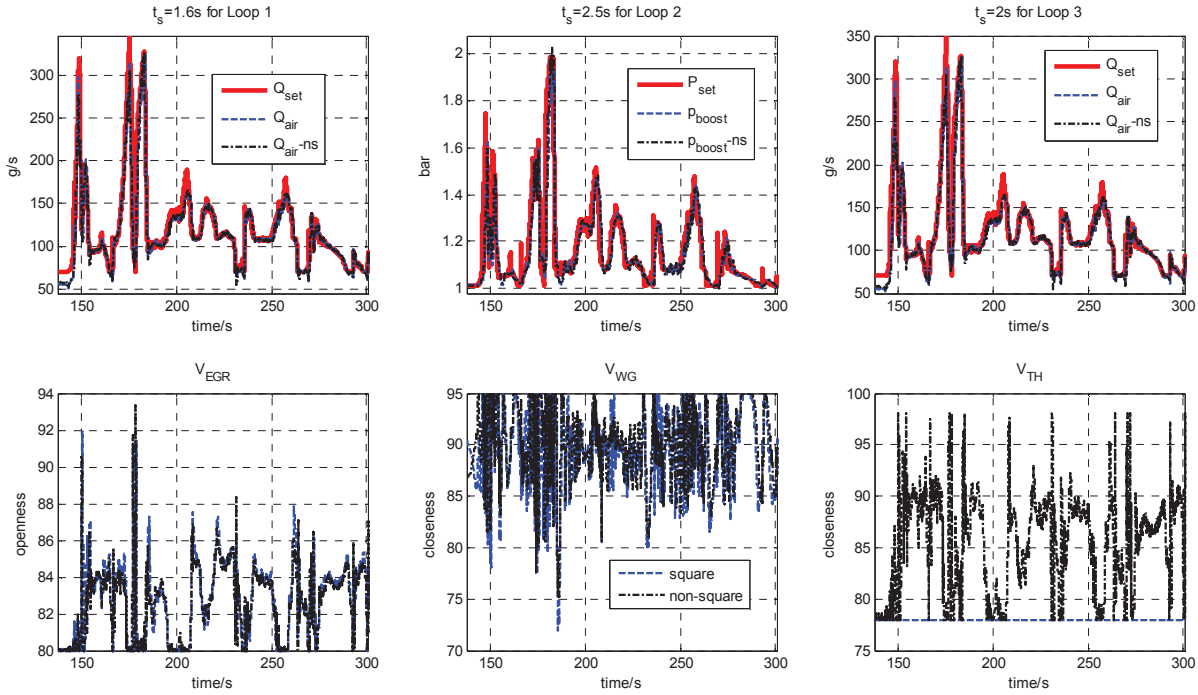

Fig.4.45 Q_{air} and p_{boost} performance and their actuators in FTP 75 Test Cycle: square and non-square control

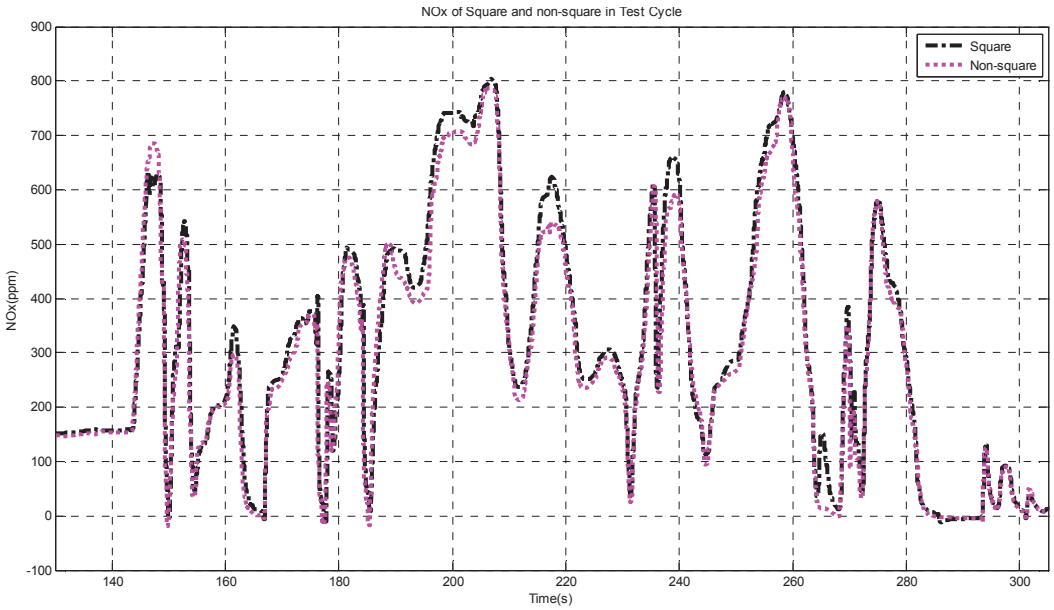

Fig.4.46 Emissions NOx in FTP 75 Test Cycle: square and non-square control

Fig.4.44 indicates the well tracking performance of designed controllers in this test cycle, although there is a small problem with the driver at 205s and 465s. Besides, in Fig.4.44 no big difference on tracking performance is found between the square and non-square control systems.

From Fig.4.45 of FTP cycle, both two output control variables Q_{air} and p_{boost} can very well follow the set points in this test cycle, the problem contains the initial values (Q_{air} cannot reach to 70g/s when it is

saturated) and low feedforward values. Moreover, the performances of square and non-square control systems also do not give big difference in this test cycle.

In Fig.4.46 the amount of NOx is also verified in square and non-square control system. Regarding to the amount of NOx, non-square control system reduces almost all this period, about 5% of NOx was reduced than square control system in this period of FTP test cycle.

d) Japan 10-15 Mode Test Cycle

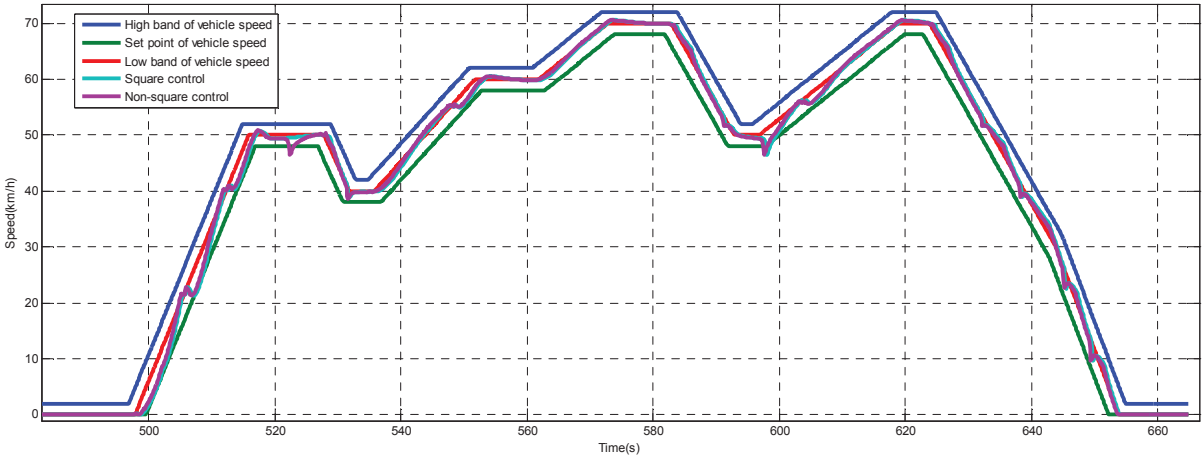

Fig.4.47 The vehicle speed response in Japan 10-15 Mode Test Cycle: square and non-square control

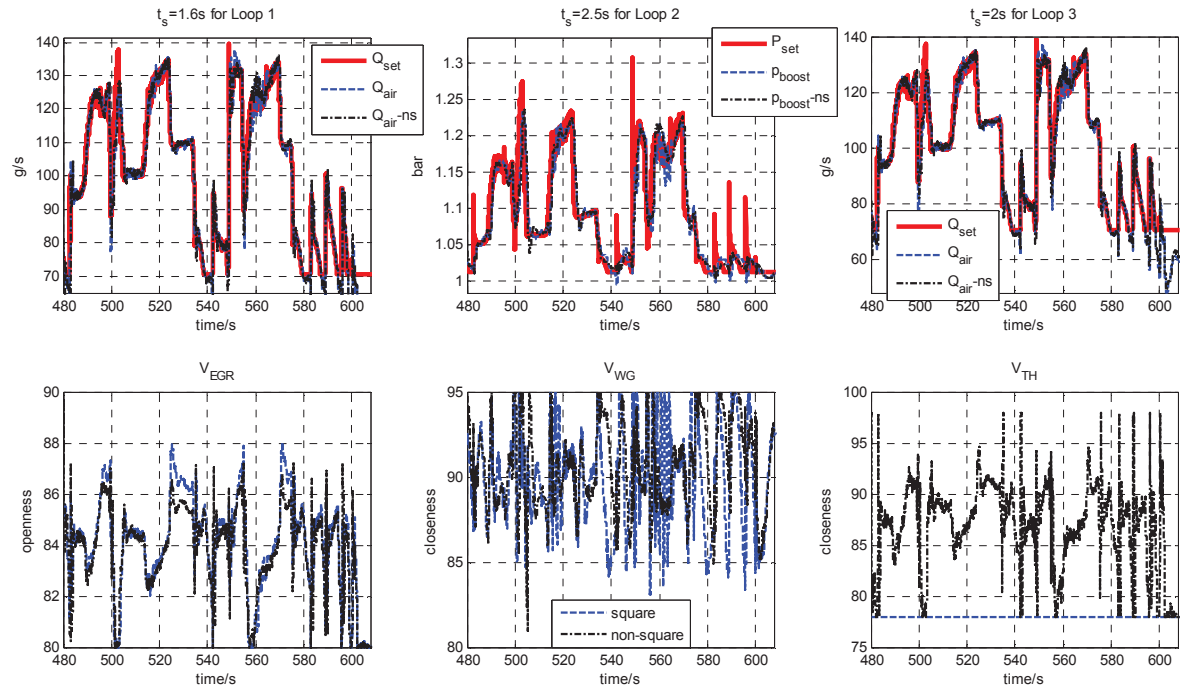

Fig.4.48 Q_{air} and p_{boost} performance and their actuators in Japan 10-15 Mode Test Cycle: square and non-square control

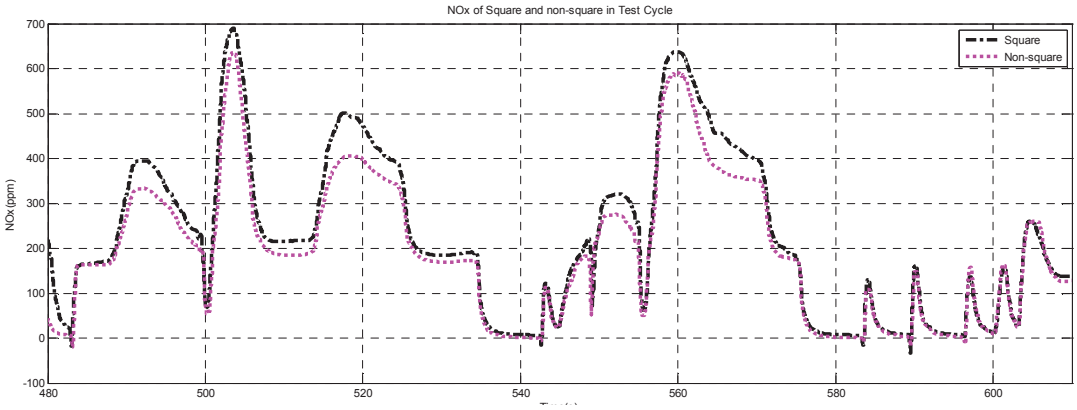

Fig.4.49 Emissions NOx in Japan 10-15 Mode Test Cycle: square and non-square control

From Fig.4.48 of Japan 10-15 Mode Cycle, good responses can be observed in this figure; same initial problems still exist (between 580s and 610s). The non-square control system keeps following the set points with fewer oscillations.

Moreover, the trend of reducing NOx (refer to Fig.4.49) is kept the same like in the other three Test Cycles, the reduction is up to 13.1% during this whole period of this figure. Considering to the NOx emissions, non-square control strategy is the better way to meet the emissions standards than square control strategy.

4.6 Conclusions

This chapter applies the methodology of chapter 2 in a diesel engine, which is first simulated on an OD low frequency model. This application is a 2X2 MIMO system; the control design was validated by changing torque at fixed speed, the simulated results have good responses. The control strategy was sequential robust multi-SISO approach, which was designed with PID controllers (for second order systems) or PIDA controllers (for third order systems). To verify this proposed approach on real engines, it was tested on air path of a turbocharged diesel engine, which was a 2x3 non-square MIMO system, one more actuator V_{TH} was added for the optimization of NOx emissions reduction. Hence, this 2X3 MIMO control system is compared with its derived 2X2 square MIMO system in this diesel engine via four vehicle test cycle: ECE-15, EUDC, FTP 75 and Japan 10-15 mode. The experimental results demonstrated good control performances of Q_{air} and p_{boost}, the non-square control strategy has better performance than its square control strategy. Above all, the pollutant emissions are dramatically reduced in the non-square control system. Hence, non-square is a promising strategy to reduce the exhaust emissions NOx.

Conclusions

A cause du temps demandé par le contrôle et la mise au point des moteurs à combustion interne, une méthodologie de commande robuste unifiée a été présentée dans cette thèse. Afin de relever les défis de mise au point des contrôles des moteurs essence et diesel, à savoir passer les normes d'émissions polluantes, minimisation la consommation de carburant et maintenir la performance, de nombreux actionneurs, tels que le turbocompresseur, le papillon d'admission et la vanne d'EGR sont utilisées. La particularité de la commande proposée est que, sous certaines conditions, les méthodes de commande monovariables peuvent être appliquées aux systèmes multivariables ; ce qui est facile et pratique pour les ingénieurs de mise au point.

Le premier chapitre a présenté les opportunités et les défis de véhicules à moteur à combustion interne de nos jours, où le moteur à combustion régit encore presque tous les véhicules sur le marché. Le point important de cette thèse est d'employer des moteurs turbocompressés afin de minimiser la consommation de carburant et satisfaire aux autres exigences gouvernementales (pollutions). Sous cet objectif, la commande de la chaîne d'air est le point le plus important à optimiser, il a donc été traité dans cette thèse.

Le deuxième chapitre a alors proposé une méthodologie unifiée de commande robuste qui peut être utilisée sur les systèmes multivariables carrés et non carrés. Un processus d'analyse du système MIMO est présenté. Tout d'abord, la décomposition en valeurs singulières permet de décrire les directions prépondérantes de notre système multivariable et le degré de complexité qui est nécessaire pour commander les différentes boucles. Le « condition number » aide alors à comprendre la sensibilité du système aux incertitudes non structurées. Il est alors montré qu'une étape de normalisation de la réponse fréquentielle du système peut être ajoutée afin de réduire la valeur de ce « condition number » et donc la sensibilité aux incertitudes non structurées. L'analyse dite RGA et des bandes de Gershgorin sont utilisées pour trouver la configuration de la stratégie de commande du système. Enfin, l'outil CD^3 permet de déterminer le degré de couplage de notre procédé. De cette analyse complète, la méthode de conception de la commande est déduite. Une stratégie de commande, basée sur le placement des pôles, est possible en raison de sa simplicité. La stabilité robuste est prouvée a posteriori prenant en compte les incertitudes et les couplages.

Le troisième chapitre a appliqué la méthodologie proposée pour la chaîne d'air d'un moteur essence turbocompressé. Puisque la masse d'air enfermée dans le cylindre ne peut être mesurée directement, une variable intermédiaire mesurée, la pression dans le collecteur d'admission est utilisée comme variable contrôlée. Les variables manipulées sont le papillon d'admission et la vanne de décharge du

turbocompresseur, la wastegate. Un simulateur, recalé sur des données réelles est alors utilisé. Tout d'abord, une identification est réalisée sur tous les points de fonctionnement. Plus précisément, un actionneur est excité pendant que l'autre est constant. La méthode de la commande est validée et donne des performances bonnes et raisonnables. Le couple du moteur est donc bien contrôlé par cette stratégie de la commande.

Le dernier chapitre a appliqué la méthodologie proposée pour la chaîne d'air d'un moteur diesel turbocompressé. D'abord, la stratégie de la commande est validée sur un simulateur recalé sur des données expérimentales. Les résultats des simulations montrent que le système de commande peut ainsi suivre les sorties (débit d'air et pression de suralimentation) tandis que le couple et la vitesse du moteur varient. Afin de contrôler plus précisément la recirculation des gaz d'échappement, un papillon d'admission est ajouté aux actionneurs utilisé par la stratégie de contrôle pour minimiser les émissions d'oxydes d'azote. Ainsi, un système multivariable non-carré est identifié sur le banc d'essai. Les résultats expérimentaux ont montré de bonnes performances de la commande sur le suivi de consigne. La commande multivariable non carrée développé permet de réduire les émissions d'oxydes d'azote d'un quart sur le cycle extra urbain européen et jusqu'à 30 % sur le cycle EUDC.

Dans l'ensemble, la méthodologie proposée de commande robuste est capable d'unifier la conception du contrôle de la chaîne d'air des moteurs essence et de moteurs diesel. Cette méthode pourrait également être étendue dans le cas de systèmes multivariables non carrés sur les moteurs essences et appliquée expérimentalement.

References

A. Stotsky and I. Kolmanovsky, "Application of input estimation techniques to charge estimation and control in automotive engines" Control Engineering Practice, vol. 10, p.1371-1383, 2002.

B. Abou, Y. Chamaillard, G. Corde, G. Gissinger, P. Higelin, N. Le Fort-Piat, and J. Malville, "Contrôle-commande de la voiture" Traité IC2. G. Gissinger and N. Le Fort-Piat, vol. 27, 2002.

C. Deng, G. Colin, Y. Chamaillard, and D. N. Gruel, "Sequential robust control design methodology application to the MIMO air path of a diesel engine" in IECON 2012-38th Annual Conference on IEEE Industrial Electronics Society vol., Montreal, Canada, p.2138-2143. 2012.

D. Garcia, A. Karimi, and R. Longchamp, "PID Controller design for multivariable systems using gershgorin bands" IFAC World Congress, vol. 16, 2005.

E. Alfieri, "Emissions-controlled diesel engine" Ph.D. Thesis, Eidgenössische Technische Hochschule ETH, Zürich, Place Published, 2009.

E. Eitelberg, "Macrodynamic feedback interaction between trade and production" International Journal of Robust and Nonlinear Control, vol. 17, p.203-224, 2007.

F. Vázquez and F. Morilla, "Tuning decentralized PID controllers for MIMO systems with decouplers" in Proceedings of the 15th IFAC World Congress vol., Barcelona, Spain. 2002.

G. Colin, Y. Chamaillard, G. Bloch, and G. Corde, "Neural control of fast nonlinear systems—application to a turbocharged SI engine With VCT" Neural Networks, IEEE Transactions on, vol. 18, p.1101-1114, 2007.

G. Colin, "Contrôle des systèmes rapides non linéaires-Application au moteur à allumage commandé turbocompressé à distribution variable" Ph.D. Thesis, Université d'Orléans, Place Published, 2006.

G. Colin, P. Lanusse, A. Louzimi, Y. Chamaillard, C. Deng, and D. N. Gruel, "Multi-SISO Robust Crone Design for the Air Path Control of a Diesel Engine" in IFAC World Congress 2011 vol., Milano, Italy. 2011.

G. Colin and Y. Chamaillard, "ENSAM Paris" in vol. 2011.

G. Zames, "Feedback and optimal sensitivity: Model reference transformations, multiplicative seminorms, and approximate inverses" Automatic Control, IEEE Transactions on, vol. 26, p.301-320, 1981.

H. P. Huang, J. C. Jeng, C. H. Chiang, and W. Pan, "A direct method for multi-loop PI/PID controller design" Journal of Process Control, vol. 13, p.769-786, 2003.

H. Procházka, I. D. Landau, 2003. "Pole placement with sensitivity function shaping using 2nd order digital notch filters", Automatica, 39(6), 1103-1107.

H. Gene and F. Van., "Matrix Computations" The Johns Hopkins University Press, vol. 1996.

I. Doré Landau, Lozano R., M. M'Saad, and A. Karimi, "Adaptive Control: Algorithms, Analysis and Applications" in vol.: Springer. 2011.

I. Horowitz, "Quantitative feedback theory" Control Theory and Applications, IEE Proceedings D, vol. 129, p.215-226, 1982.

I. Landau, D., , R. Lozano, M. M'Saad, and Karimi. A., "Adaptive Control: Algorithms, Analysis and Applications" Place Published: Springer, 2011.

J. B. Heywood, "Internal combustion engine fundamentals" vol. 1988.

J.F. Arnold, N. Langlois, and H. Chafouk. "Fuzzy controller of the air-path system of a diesel engine: Real time simulation", European Jornal of Operational Research vol 193, No 1, pp 282-288, February 2009

J. Chauvin, G. Corde, N. Petit, and P. Rouchon, "Motion planning for experimental airpath control of a diesel homogeneous charge-compression ignition engine" Control Engineering Practice, vol. 16, p.1081-1091, 2008.

J. Chauvin, A. Alberecht, G. Corde, and N. Petit "Modeling and control of a Diesel HCCI Engine", IFAC AAC, 2007.

J. Doyle and G. Stein, "Multivariable feedback design: Concepts for a classical/modern synthesis" Automatic Control, IEEE Transactions on, vol. 26, p.4-16, 1981.

J. C. Doyle, R. S. Smith, and D. F. Enns, "Control of plants with input saturation nonlinearities" in In proceedings of the 1987 American control conference vol., p.p.1034-1039. 1987.

J. Mikles and M. Fikar, "Process modelling, identification, and control" Place Published: Springer New York, 2007.

J. Marques, "Plate-forme d'aide à l'éco-conception de systèmes multiphysiques: démarche énergétique pour la validation et la réduction de modèles" Ph.D. Thesis, Université d'Orléans, Place Published, 2010.

J. Milnor, "Dynamics in one complex variable" in vol. 2000.

J. P. Corriou, "Process control: theory and applications" Place Published: Springer, 2004.

J. W. Chang and C. C. Yu, "The relative gain for non-square multivariable systems" Chemical engineering science, vol. 45, p.1309-1323, 1990.

J. Wahlstrom, L. Eriksson, 2008. "Robust Nonlinear EGR and VGT Control with Integral Action for Diesel Engines", Proceedings of the 17th World Congress, Seoul, Korea, p.2057-2062

K. J. Astrom and T. Hagglund, "Advanced PID Control" ISA- The Instrumentation, system, and Automation Society, vol. 2005.

L. Bakule, "Decentralized control: An overview" Annual Reviews in Control, vol. 32, p.87-98, 2008.

L. Guzzella and A. Amstutz, "Control of diesel engines" Control Systems, IEEE, vol. 18, p.53-71, 1998.

L. Guzzella and C. Onder, "Introduction to modeling and control of internal combustion engine systems" Place Published: Springer, 2009.

L. Guzzella, "Analysis and synthesis of Single-input Single-output control systems" Place Published: Verlag der Fachvereine Hochschulverlag AG an der ETH Zurich, 2007.

M. Manfred and E. Zafiriou, "Robust process control" Place Published, 2002.

M. Tham, "Multivariable control: An introduction to decoupling control" University of Newcastle upon Tyne, Newcastle upon Tyne, vol. 1999.

M. Van Nieuwstadt, P. Moraal, I. Kolmanovsky, A. Stefanopoulou, P. Wood, and M. Criddle, "Decentralized and multivariable designs for EGR-VGT control of a diesel engine" in Proc of the 2nd IFAC Workshop on Advances in Automotive Control vol. 1998.

M. Lee, M. Sunwoo, 2012. "Modelling and H∞ control of diesel engine boost pressure using a linear parameter varying technique", Journal of Automobile Engineering. vol. 226 no. 2 210-224

N. Bordet, "Modélisation 0D/1D de la combustion diesel: du mode conventionnel au mode homogène" Ph.D. Thesis, Université d'Orléans, Place Published, 2011.

N. Jain and A. G. Alleyne, "Comparison of SISO and MIMO control techniques for a diagonally dominant vapor compression system" in American Control Conference, 2009. ACC'09. vol., St. Louis MO-IL, USA: IEEE, p.1580-1585. 2009.

P. Andersson, "Air charge estimation in turbocharged spark ignition engines" Place Published: Department of Electrical Engineering, Linköping University, 2005.

P. G. Drazin, "Nonlinear systems" Place Published: Cambridge University Press, 1992.

P. Grosdidier, M. Morari, and B. R.holt, "Closed-loop properties from steady-state gain information" American Chemical Society, vol. p.p.221-235, 1985.

P. Ortner, L. del. Re, 2007. "Predictive control of a diesel engine air path", IEEE transactions on control systems technology, 15(3): 449-456.

Q. Xiong and W. J. Cai, "Effective transfer function method for decentralized control system design of multi-input multi-output processes" Journal of Process Control, vol. 16, p.773-784, 2006.

R. Nitsche, J. Hanschke, D. Schwarzmann, 2006. "Nonlinear internal model control of diesel air systems", E-COSM-Rencontres Scientifiques de l'IFP Proceeding, p.121-131.

S. A. Gershgorin, "Uber die abgrenzung der eigenwerte einer matrix" Известия Российской академии наук. Серия математическая, vol. p.749-754, 1931.

S. García-Nieto, M. Martínez, X. Blasco, and J. Sanchis, "Nonlinear predictive control based on local model networks for air management in diesel engines" Control Engineering Practice, vol. 16, p.1399-1413, 2008.

S. Jung. and Dorf. R. C., "Analytic PIDA controller design technique for a third order system." Decision and Control, Proceedings of the 35th IEEE. Vol. 3. IEEE, 1996.

S. Skogestad and M. Morari, "Implications of large RGA-elements on control performance" Industrial & engineering chemistry research, vol. 26, p.2323-2330, 1987.

S. Skogestad and K. Havre, "The use of RGA and condition number as robustness measures" Computers & chemical engineering, vol. 20, p.S1005-S1010, 1996.

S. Skogestad and I. Postlethwaite, "Multivariable feedback control: analysis and design" Place Published: Wiley, 2007.

S. Salivahanan and A. Vallavaraj, "Gnanapriya" Digital Signal Processing, McGraw-Hill/TMH, vol. 2000.

Stanley, "Modern Control System Theory and Design" Place Published, 1998.

S. S. Chughtai, A. Nobakhti, and H. Wang, "A systematic approach to the design of robust diagonal dominance based MIMO controllers" in Conference on Decision and Control, 2005 European Control Conference. CDC-ECC'05. 44th IEEE vol., Seville, Spain: IEEE, p.6875-6880. 2005.

T. V. Johnson, "Diesel emission control in review" SAE TRANSACTIONS, vol. 110, p.128-144, 2001.

X. Wei and L. del Re, "Gain scheduled H∞ control for air path systems of diesel engines using LPV techniques" IEEE transactions on control systems technology, vol. 15, p.406-415, 2007.

Y. Shen, W. J. Cai, and S. Li, "Multivariable Process Control: Decentralized, Decoupling, or Sparse" Industrial & Engineering Chemistry Research, vol. 49, p.761-771, 2009.

Y. Shen, W. J. Cai, and S. Li, "Normalized decoupling control for high-dimensional MIMO processes for application in room temperature control HVAC systems" Control Engineering Practice, vol. 18, p.652-664, 2010.

Y. Yildiz, A. M. Annaswamy, D. Yanakiev, and I. Kolmanovsky, "Spark ignition engine fuel-to-air ratio control: An adaptive control approach" Control Engineering Practice, vol. 18, p.1369-1378, 2010.

Y. Y. Wang, I. Haskara, and O. Yaniv, "Quantitative feedback design of air and boost pressure control system for turbocharged diesel engines" Control Engineering Practice, vol. 19, p.626-637, 2011.

V. A. W. Hillier, "Hillier's Fundamentals of Automotive Electronics" Place Published: Stanley Thornes Publishers, 1996.

U. Jürgens, "New product development and production networks: global industrial experience" Place Published: Springer, 2000.

U. Kiencke and L. Nielsen, "Automotive control systems: for engine, driveline, and vehicle" Measurement Science and Technology, vol. 11, p.1828, 2000.

W. J. Cai, W. Ni, M. J. He, and C. Y. Ni, "Normalized decoupling: A new approach for MIMO process control system design" Industrial & Engineering Chemistry Research, vol. 47, p.7347-7356, 2008.

Wall M. E., R. Andreas, and M. R. Luis, "A Practical Approach to Microarray Data Analysis" Place Published: MA: Kluwer, 2003.

W. Tan, H. J. Marquez, and T. Chen, "IMC design for unstable processes with time delays" Journal of Process Control, vol. 13, p.203-213, 2003.

W. W. Pulkrabek, "Engineering fundamentals of the internal combustion engine" Place Published: Pearson Prentice Hall New Jersey, 2004.

Wikipedia, "Electronic control unit" vol. 2012.

Wikipedia, "Powertrain" vol. 2012.

Wikipedia, "Autocorrelation" vol. 2012.

Résumé

Depuis la création des moteurs à combustion interne, les recherches sur les moteurs essence et diesel se sont développées indépendamment. Afin de réduire les temps et les coûts de développement d'un moteur, une ***approche unifiée*** *de conception serait intéressante. Dans ce cadre, le* ***contrôle*** *et la mise au point des* ***moteurs à combustion interne*** *pourrait être elle aussi unifiée. Bien évidemment, ce contrôle doit être stable,* ***robuste*** *vis-à-vis des disparités de fabrication, comme de fonctionnement. Cette thèse porte alors sur une démarche unifiée, pour les moteurs essence comme pour les moteurs diesel, afin d'obtenir un contrôle robuste de la chaîne d'air du moteur. La chaîne d'air du moteur contient les éléments permettant de contrôler la quantité et les proportions d'air et de gaz neutres dans le cylindre (Recirculation des gaz d'échappement, papillon d'admission, turbocompresseur). Cette démarche unifiée de commande, permettant de contrôler les systèmes monovariables, tout comme* ***multivariables non carrés*** *(nombre d'entrées différent du nombre de sorties), contient plusieurs étapes : identification d'un modèle du système, analyse du système permettant d'en déduire une structure de contrôle, synthèse d'un contrôleur autour d'un nominal, vérification de la robustesse en stabilité, tests du contrôle. Le couplage des entrées vers les sorties, les non linéarités sont pris en compte lors de la synthèse du contrôleur. Cette méthode de conception a été validée sur plusieurs applications dont un moteur essence et un moteur diesel. Des résultats expérimentaux sur un banc moteur diesel haute dynamique ont montrés que la commande multivariable permettait de* ***réduire*** *les* ***émissions*** *d'oxydes d'azote.*

Mots clefs: moteurs à combustion interne, chaîne d'air, contrôle moteur, commande robuste, couplage, système MIMO non carré, PID.

Abstract

Since the creation of internal combustion engines, research on gasoline and diesel engines were developed independently. To reduce the time and cost of developing an engine, a unified design approach would be interesting. In this context, control and development of internal combustion engines could also be unified. Obviously, this control must be stable, robust with respect to manufacturing disparities and operating points. This thesis then focuses on a unified approach for gasoline engines as well as diesel engines, to achieve a robust of the air path. The engine air path contains the information needed to control the amount and proportions of air and neutral gases in the cylinder (exhaust gas recirculation, throttle valve, turbocharger). This unified approach to control monovariable systems, as well as non-square multivariable systems (number of inputs different from the number of outputs), consists of several steps: identification of a model of the system, system analysis to deduce a control structure, synthesis of a controller around a nominal model, check robust stability, control tests. The coupling inputs to outputs and nonlinearities are taken into account during the synthesis of the controller. This design method has been validated in several applications including a gasoline engine and a diesel engine. Experimental results on a diesel engine high dynamics test bench have shown that the multivariable control results in lower emissions of nitrogen oxides.

Key words: internal combustion engines, air path, engine control, robust control, coupling, nonsquare MIMO system, PID.

Discipline: Sciences and industrial technologies